IN VITRO RECONSTITUTION OF A RAB ACTIVATION SWITCH

by

Urban Bezeljak

Tuesday 8th September, 2020

A thesis presented to the
Graduate School
of the
Institute of Science and Technology Austria, Klosterneuburg, Austria
in partial fulfillment of the requirements
for the degree of
Doctor of Philosophy

The thesis of Urban Bezeljak, titled *In vitro reconstitution of a Rab activation switch*, is approved by:

Supervisor: Martin Loose, IST Austria, Klosterneuburg, Austria

Signature: _____

Committee Member: Călin C. Guet, IST Austria, Klosterneuburg, Austria

Signature: _____

Committee Member: Jacqueline Cherfils, CNRS and Ecole Normale Supérieure Paris-Saclay, Cachan, France

Signature: _____

Defense Chair: Mario de Bono, IST Austria, Klosterneuburg, Austria

Signature: _____

signed page is on file

IST Austria Thesis, ISSN: 2663-337X

I hereby declare that this thesis is my own work and that it does not contain other people's work without this being so stated; this thesis does not contain my previous work without this being stated, and the bibliography contains all the literature that I used in writing the dissertation.

I declare that this is a true copy of my thesis, including any final revisions, as approved by my thesis committee, and that this thesis has not been submitted for a higher degree to any other university or institution.

I certify that any republication of materials presented in this thesis has been approved by the relevant publishers and co-authors.

Signature: _____

Urban Bezeljak
Tuesday 8th September, 2020
signed page is on file

Abstract

One of the most striking hallmarks of the eukaryotic cell is the presence of intracellular vesicles and organelles. Each of these membrane-enclosed compartments has a distinct composition of lipids and proteins, which is essential for accurate membrane traffic and homeostasis. Interestingly, their biochemical identities are achieved with the help of small GTPases of the Rab family, which cycle between GDP- and GTP-bound forms on the selected membrane surface. While this activity switch is well understood for an individual protein, how Rab GTPases collectively transition between states to generate decisive signal propagation in space and time is unclear. In my PhD thesis, I present *in vitro* reconstitution experiments with theoretical modeling to systematically study a minimal Rab5 activation network from bottom-up. We find that positive feedback based on known molecular interactions gives rise to bistable GTPase activity switching on system's scale. Furthermore, we determine that collective transition near the critical point is intrinsically stochastic and provide evidence that the inactive Rab5 abundance on the membrane can shape the network response. Finally, we demonstrate that collective switching can spread on the lipid bilayer as a traveling activation wave, representing a possible emergent activity pattern in endosomal maturation. Together, our findings reveal new insights into the self-organization properties of signaling networks away from chemical equilibrium. Our work highlights the importance of systematic characterization of biochemical systems in well-defined physiological conditions. This way, we were able to answer long-standing open questions in the field and close the gap between regulatory processes on a molecular scale and emergent responses on system's level.

Acknowledgments

This thesis is the result of experimental work I did during my PhD studies at IST Austria. Importantly, this would not be possible without the generous support of my family, friends, coworkers and collaborators from Saunders and Bieling labs. Foremost, I would like to express my gratitude to Calin, who is the most responsible that I could join IST back in 2015 and Martin, whose trust, mentorship and encouragement made my PhD journey a success. Also, I would like to thank Mario and Jacqueline for kindly accepting their roles on Thesis Committee. My thanks goes to the Loose lab members, BioImaging, Life Science and Nanofabrication Facilities and the wonderful international community at IST for sharing this experience with me. I am leaving Klosterneuburg grateful to have met the most inspiring and enthusiastic friends I will ever have. Furthermore, I would like to acknowledge the Tuma family and Lukas Knaffelsche Privatstiftung in Vienna for supporting my studies since 2018 with the Tuma Scholarship for Slovenian graduate students in Austria. Above all, I am forever grateful to Laura for putting up with me and conquering all the challenges life threw at us during our stay in Austria. Her sacrifices, dedication and love made finishing this thesis possible.

Urban

About the Author

Before joining IST Austria in 2015, Urban Bezeljak completed BSc and MSc studies in Biochemistry at the University of Ljubljana. There, he entered the field of Synthetic Biology and worked on directed protein assembly and designed genetic circuits. At IST, Urban applied his interests in Martin Loose's lab, where he initiated bottom-up examination of Rab GTPase regulation. In his PhD project Urban used *in vitro* reconstitution to observe self-organization properties of Rab5 activation network, which is crucial for normal cell functioning. His results were published in *PNAS* in 2020 and presented at the endocytosis EMBO Workshop and ASCB|EMBO Meeting in 2019. Before defending the Thesis, Urban joined the effort to develop protein-based vaccine platform against SARS CoV-2 at COBIK in Ajdovščina, Slovenia.

List of Publications

1. U. Bezeljak, H. Loya, B. Kaczmarek, T. E. Saunders, and M. Loose, ”Stochastic activation and bistability in a Rab GTPase regulatory network”, *Proceedings of the National Academy of Sciences*, 117(12):6540-6549, 2020.

2. ”Stochastic nucleation events trigger collective Rab GTPase activation”, *in preparation*.

Table of Contents

List of Tables

List of Figures

List of Abbreviations

C. elegans *Caenorhabditis elegans*

E. coli Escherichia coli

S. cerevisiae *Saccharomyces cerevisiae*

S. frugiperda Spodoptera frugiperda

T. ni *Trichoplusia ni*

X. laevis *Xenopus laevis*

ALS amyotrophic lateral sclerosis

BIIC baculovirus-infected insect cells

bp base pair

BSA bovine serum albumin

Ccz1 calcium caffeine zinc sensitivity 1

CDF cumulative distribution function

cDNA coding deoxyribonucleic acid

CDR complementary determining region

DMPE 1,2-dimyristoyl-sn-glycero-3-phosphoethanolamine

DMSO dimethyl sulfoxide

DNA deoxyribonucleic acid

DOGS-NTA 1,2-dioleoyl-sn-glycero-3-[(N-(5-amino-1-carboxypentyl)iminodiacetic acid)-succinyl]

DOPC 1,2-dioleoyl-sn-glycero-3-phosphocholine

DOPE 1,2-dioleoyl-sn-glycero-3-phosphoethanolamine

DOPS 1,2-dioleoyl-sn-glycero-3-phospho-L-serine

EE early endosome

ER endoplasmic reticulum

FRAP fluorescence recovery after photobleaching

GAP GTPase activating protein

GDF GDI dissociation factor

GDI GDP dissociation inhibitor

GDP guanosine 5'-(trihydrogen diphosphate), guanosine diphosphate

GEF guanine nucleotide exchange factor

GGTase geranylgeranyl transferase

GMP-PNP 5'-guanylyl-imidodiphosphate

GMP guanosine-5'-monophosphate, guanosine monophosphate

GndHCl guanidinium chloride

GTP guanosine 5'-(tetrahydrogen triphosphate), guanosine triphosphate

GUV giant unilamellar vesicle

HEPES 2-[4-(2-Hydroxyethyl)-1-piperazinyl]ethanesulfonic acid

IPTG Isopropyl 1-thio-β-D-galactopyranoside

K_d disassociation constant

KOAc potassium acetate

LE late endosome

LECA last eukaryotic common ancestor

mant-GDP 2'/3'-O-(N-methylanthraniloyl)-guanosine-5'-(trihydrogen diphosphate)

MBP maltose binding protein

MLV multilamellar vesicle

Mon1 monensin sensitivity 1

MSD mean square displacement

MT mitochondrion

MW molecular weight

NTA nitrilotriacetic acid

P_i inorganic phosphate

PBS phosphate buffered saline

PCR polymerase chain reaction

PEG polyethylene glycol

PH promoter polyhedrin insect cell promoter

PRA1 Prenylated Rab acceptor 1

RAU relative absorbance unit

rcf relative centrifugal force

RE recycling endosome

REP Rab escort protein

rpm revolutions per minute

RT room temperature

SD standard deviation

SEC-MALS size exclusion chromatography – multi angle light scattering

SEM standard error of the mean

SLB supported lipid bilayer

SrtA sortase A

SUV small unilamellar vesicle

SV secretory vesicle

TCEP 3,3',3"-Phosphinetriyltripropanoic acid, tris(2-carboxyethyl)phosphine

TEV tobacco etch virus

TIRF total internal reflection fluorescence

X-gal 5-bromo-4-chloro-3-indolyl-β-D-galacto-pyranoside

1 Introduction

What sets eukaryotes aside from other domains of life is their internal cellular compartmentalization. How this complexity came about in the evolution of life remains an exciting open question. Nonetheless it seems that a large superfamily of Ras-like small GTPases is intricately linked to the generation of organelles and cellular trafficking in eukaryotes. The discovery of these proteins dates back to the late 1970s, when Ras GTPase was first found (ironically, not in eukaryotes) as an oncogene in Harvey mouse sarcoma retrovirus. This triggered a great interest and human homologues were identified in the following years [Wittinghofer, 2014a].

The Ras-like protein family tree now consists of more than 160 moieties, grouped into six sub-families: Ras (40 members), Rab (67), Rho (27), Arf (29), Ran (1) and Rag (4) [Wittinghofer, 2014a]. These 20-25 kDa proteins share common structural and regulation features. Particularly, they bind guanosine nucleotides GDP and GTP with high affinity and (with exception of Ran) are posttranslationally modified with lipid anchors in order to transition between cytosol and cellular membranes. These two unique properties are reflected in the small GTPase signaling networks, where they function as molecular toggle switches to direct proliferation, cellular motility, gene expression and intracellular trafficking – depending on their localization and nucleotide binding state.

In the past decades, we unraveled the key network components and their regulatory roles using *in vivo* and *in vitro* techniques. By determining the small GTPase crystal structure, we understand guanine nucleotide-induced conformational switching in atomic detail. However, despite all this knowledge, the biologically relevant mechanisms of collective protein behavior on system's level remain unclear. This is mainly due to the complexity of living cells, where extracting mechanistic insights into GTPase regulation is extremely challenging. That is why we still do not know how the identified

molecular interactions fit together in the broader context of cellular signaling. In this work, I present *in vitro* reconstitution of a model Rab signaling network. By employing the method of synthesis [Leduc, 1912], we rebuild the Rab5 activation network form bottom up in order to fully understand the underlying mechanisms of GTPase regulation in a controlled environment under physiological conditions. We demonstrate the composition of a minimal biochemical circuit that is able to generate a bistable switch in Rab5 activation — a prerequisite for decisive and directed cellular signaling. Importantly, our approach uncovers key interactions that generate emergent collective response and modes of its regulation. Together, this work sheds new light on small GTPase signaling and presents new approaches in systematic characterization of biochemical circuits at membrane surface.

Small GTPases, Rab5 activation network and other key concepts are presented in the following chapters. This is followed by description of used materials and experimental methods (Section 3). Finally, I present and discuss results in Section 4.

1.1 Rab small GTPases

1.1.1 Evolution and structure

Rab proteins (Ypts in yeast) constitute the largest protein family of the Ras-like small GTPases, which are key regulators of dynamic processes in the eukaryotic cytoplasm, from organelle maintenance to cytoskeleton motility and vesicular flow. They are localized to distinct cellular membranes (Figure 1.1) and establish large biochemical networks that control unique compartmental functions. As these properties were key to the evolutionary success of eukaryotic cells, it was proposed that the emergence of early eukaryotes was tightly connected with the expansion of small GTPases [Jékely, 2003]. In fact, recent evolutionary studies estimated that the ancient last eukaryotic common ancestor (LECA) possessed at least 20 different Rab proteins over a billion years ago that were – and still are – essential to maintain the complex network of cellular endomembranes [Klöpper *et al.*, 2012; More *et al.*, 2020]. Interestingly, the whole LECA Rab repertoire is not necessary for many present-day eukaryotes, since the budding yeast *Saccharomyces cerevisiae* has 11 Rab family members, representing only 5 out

of 20 LECA Rabs. On the other hand, there are also examples of evolutionary expansion for many Rab families through gene doubling and diversification, resulting in 66 Rabs in humans [Klöpper *et al.*, 2012]. What is more, the Rab origin remains unclear as they do not have structurally similar orthologs in bacteria [Vetter and Wittinghofer, 2001]. Rather, small GTPases are believed to be an invention of the prekaryotic cell, which evolved into eukaryotes [Jékely, 2003].

The Ras (*ra*t *s*arcoma virus) protooncogene was the first discovered small GTPase in the early 1980s [Sweet *et al.*, 1984]. Subsequently, other related members of the protein family were characterized, including Rab (*Ra*s-related in *b*rain) proteins [Touchot *et al.*, 1987]. In humans, there are over 60 Rabs, which are numbered according to the sequential order of their discovery. Evolutionary, Rabs are divided in six large phylogeny groups, based on their sequence similarity across eukarya [Klöpper *et al.*, 2012]. Comparative genomic analysis identified that the Rab family expanded with gene duplication in parallel with increasing membrane trafficking complexity. Thus, the Rab small GTPases are associated with secretion (group I), endolysosomal system (groups II and III), recycling pathways (groups IV and V), and traffic associated with cilia/flagella (group VI) [Klöpper *et al.*, 2012]. There, Rabs localize on the membrane surface and direct vesicular maturation as they transition through characteristic conformational change, associated with nucleotide binding.

Generally, these proteins consist of the nucleotide-binding G domain and a hypervariable carboxyl terminus (Figure 1.2), which contributes to the Rab subfamily diversification and post-translational lipid anchor attachment. The G domain specifically binds to GTP or GDP, but not GMP. It consists of roughly 160 amino acid residues, organized into five α-helices and six β-strands. Structurally, it represents the most abundant P-loop containing nucleotide hydrolase fold [Wittinghofer, 2014a]. There, the guanosine nucleotide is locked into place with nanomolar affinity by a Mg^{2+} ion, N/TKXD motif at the nucleotide base and the P-loop binding of the β- and γ-phosphates. It is the interaction with phosphate groups that elicits conformational changes in flanking protein regions. These mobile elements are called switch I and II as they experience the most prominent changes during nucleotide hydrolysis. There, additional hydrogen bonds with the GTP γ-phosphate stabilize the whole domain, making it more rigid as compared to the GDP-loaded conformation. This mechanism has been described

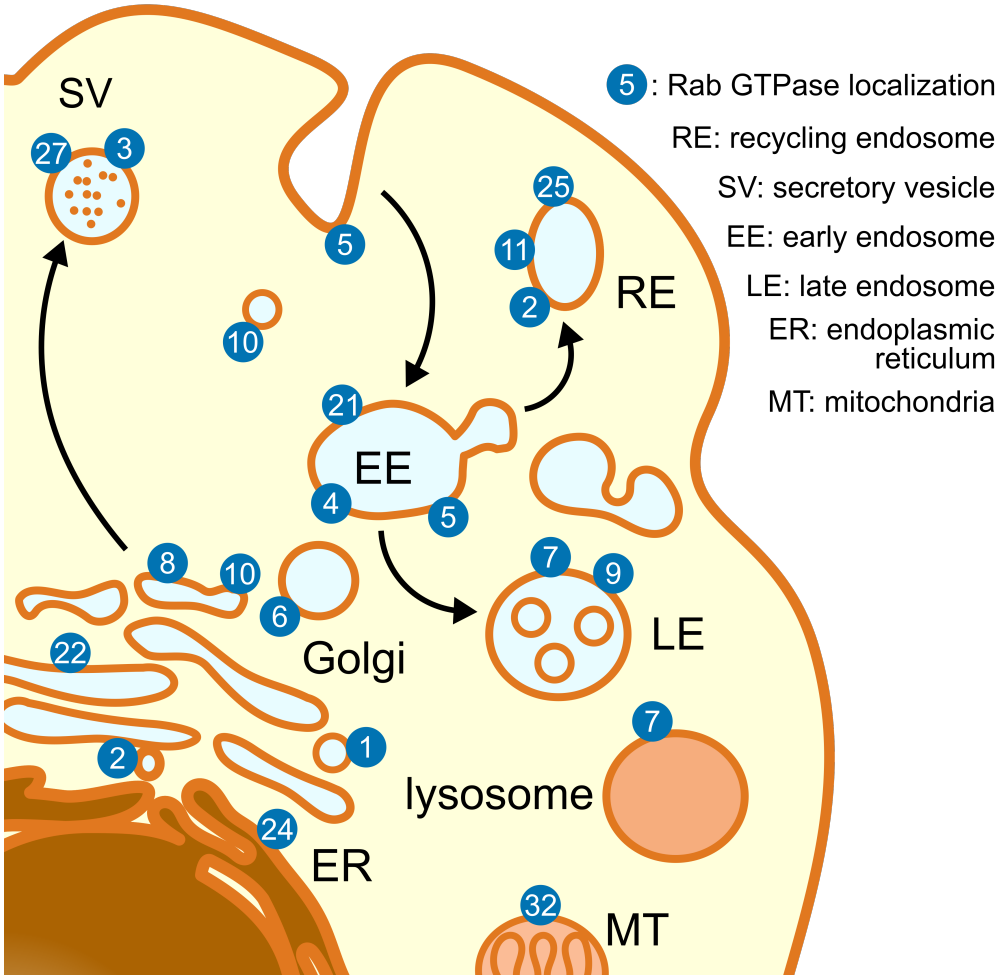

Figure 1.1: **Rabs are eukaryotic organelle markers and organizers.**
Intracellular localization of some Rab GTPases. Rabs localize to distinct cellular membranes, where they control vesicular transport and unique biochemical signature. Biological functions and sets of regulators are presented in Table 1.1. SV: secretory vesicle; RE: recycling endosome; EE: early endosome; LE: late endosome; ER: endoplasmic reticulum; MT: mitochondria. The figure was adapted from excellent existing reviews on Rab GTPases [Stenmark, 2009; Hutagalung and Novick, 2011; Wittinghofer, 2014b]

.

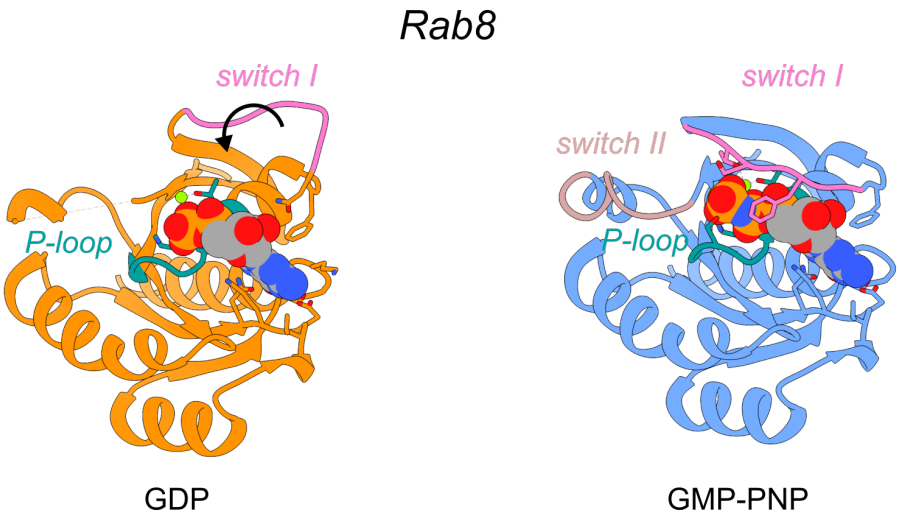

Figure 1.2: **Nucleotide-bound Rab crystal structure.**
Crystal structures of GDP- and non-hydolyzable GTP analog GMP-PNP-bound Rab8. Characteristic nucleotide binding P-loop is indicated in green, the dynamic switch I in pink and switch II in gray. Relaxed switch II region is disordered in the GDP-bound Rab8 and is not visible in the structure. PDB IDs: 4LHV (GDP) and 4LHW (GMP-PNP) [Guo *et al.*, 2013].

as the loaded spring model, where the dissociation of terminal phosphate group after GTP hydrolysis releases the switch region into loose GDP-bound state [Vetter and Wittinghofer, 2001].

The difference in rigidity allows the GTP-loaded Rabs to form interactions with diverse binding partners, called effectors. Strikingly, the effectors are highly Rab-specific, a feature that is yet to be fully appreciated at atomic detail. Nonetheless, it is clear that these proteins can distinguish subtle structural features on Rabs, interacting only with selected GTPases (out of almost 70 in humans). The exposed Rab surface harbors five conserved effector binding amino acid patches that separate these proteins from other Ras-like GTPases (F1-5). Additionally, four exposed regions separate one Rab from another (SF1-4) [Hutagalung and Novick, 2011], enabling specificity in effector interaction. As a result, effectors perform downstream biological functions at precise cellular locations and times, which are determined by the nucleotide bound state of the corresponding Rab.

Another characteristic Rab structural feature is prenylation of one or two C-terminal cysteine residues. This posttranslational modification allows the small GTPases to bind hydrophobic membranes through insertion of their lipid anchors. Consequently,

the Rab signaling potential and localization is related to the bound nucleotide state and is precisely controlled by several groups of regulator proteins, forming the Rab activity cycle.

1.1.2 The Rab GTPase cycle

Rab proteins have emerged as the key orchestrators of intracellular membrane traffic and organelle identity. The eukaryotic cells take advantage of their guanosine nucleotide binding to use them as molecular switches – directing budding, transport, tethering, and fusion of lipid vesicles [Hutagalung and Novick, 2011]. The posttranslational addition of hydrophobic geranylgeranyl chains allows Rabs to bind the membranes by lipid anchoring. However, to ensure spatiotemporal specificity of Rab signaling, the majority of these proteins is kept solubilized in the cytosol by GDP dissociation inhibitor (GDI). This also prevents Rab aggregation in solution by keeping the GTPase anchor chains hidden from the aqueous environment of the cytoplasm. GDI specifically binds Rabs in GDP-state and can actively extract them from the lipid bilayer [Gavriljuk *et al.*, 2013]. Nonetheless, the Rab:GDI complex can dissociate in close proximity of membranes, allowing other regulatory factors to interact with the GTPase. An example are the guanine nucleotide exchange factors (GEFs), which swap the GDP with GTP in Rab binding pocket. This not only prevents GDI re-extraction, but also allows the Rabs to interact with effectors, triggering downstream signaling. Rabs in turn can process the bound GTP to GDP $+$ P_i with their intrinsic GTPase activity [Rybin *et al.*, 1996] or receive help from GTPase activating proteins (GAPs), turning the Rab switch OFF and seizing the signaling cascade. At this point, Rab[GDP] can enter another cycle of GEF-mediated nucleotide exchange or is solubilized to the inactive reservoir by the GDI [Hutagalung and Novick, 2011]. The Rab GTPase cycle is thus propelled by the sequential activity of Rab GEFs, GAPs and GDI (Figure 1.3). As a result, the GTP-loaded Rab molecular switches are said to be active – promoting signaling, while GDP-bound GTPases are inactive. A similar bimodality is also observed in the nucleotide-dependent Rab localization: Rab[GTP] is exclusively membrane-bound and inactive Rab[GDP] is mainly cytosolic due to continuous GDI sequestration.

However, these simple steps do not tell the whole story. Notably, another layer of

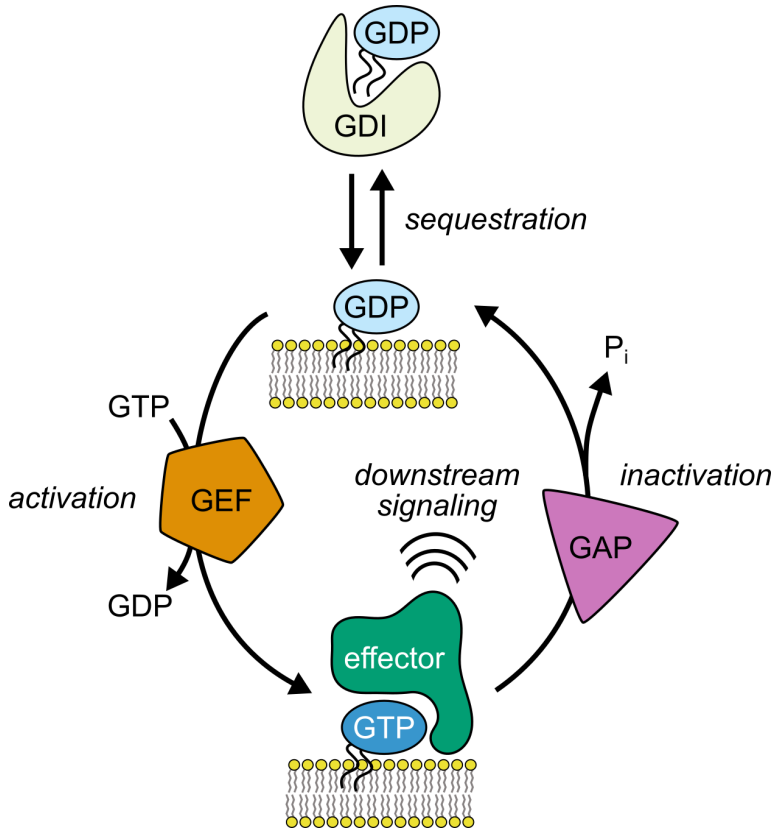

Figure 1.3: **The Rab GTPase cycle.**

In the cytosol, GDP-bound Rab proteins are associated with GDP dissociation inhibitors (GDIs), which shield their hydrophobic isoprenoid tails from the aqueous environment. When this complex dissociates in the equilibrium reaction, the guanine nucleotide exchange factor (GEF) can substitute the Rab-bound GDP for GTP, which prevents the Rab interaction with GDI and enables stable anchoring to the lipid bilayer. There, GTP-bound Rab binds with its cognate effectors that perform specific biological functions. After the induced GTP hydrolysis to GDP by a GTPase activating protein (GAP), the effectors lose their affinity for Rab. The inactive small GTPase gets extracted from the membrane by GDI, closing the Rab cycle.

complexity is added to the Rab cascade by multiple non-enzymatic interactions between the regulators themselves and Rab proteins. These introduce non-linear responses to the whole system, such as ultrasensitivity [Koshland *et al.*, 1982], positive feedback and feed-forward loops [Cherfils and Zeghouf, 2013]. It has been proposed that these regulatory interactions lead to committed Rab signaling and the emergence of higher-order polarized Rab domains with distinct composition on membrane vesicles [Zerial and McBride, 2001; Rivera-Molina and Novick, 2009]. The dynamic non-equilibrium cycling of the small GTPase and its regulators is currently poorly understood and is yet to be confirmed by direct observation. In the next chapters, I will discuss these principles and individual steps in Rab regulatory network in further detail.

1.1.3 Posttranslational modifications

Posttranslational modifications are crucial for Rab small GTPase function and regulation. As these proteins perform their biological roles on intracellular membrane surfaces, they are covalently modified by geranylgeranyl lipid anchor attachment. Moreover, a number of reversible modifications were described that also control small GTPase activity and localization.

Geranylgeranylation

To perform signaling roles on membrane surfaces, the Rab proteins carry one or (more commonly) two isoprenoid geranylgeranyl groups on their C-terminus. The long 20-carbon chains provide the needed hydrophobicity potential for the small GTPase to stably anchor into the phospholipid bilayer and freely diffuse along the surface. In contrast to other Ras-like GTPases, the Rabs do not have a conserved prenylation motif. Rather, they display exposed cysteine residues at their carboxyl ends and require soluble complex formation with Rab escort protein (REP) immediately after translation to undergo geranylgeranylation [Wittinghofer, 2014b]. The REP accessory protein interacts with Rab geranylgeranyl transferase (RabGGTase, GGTase II), which catalyses the prenylation reaction from geranylgeranyl pyrophosphate to the cysteine thiol groups. Peculiarly, only the Rab:REP complex is substrate to GGTase, not the GTPase

alone. Both the GDP- and GTP-bound Rabs are substrates for geranylgeranylation. When the small GTPase is synthesized, it is loaded with either of the two nucleotides and can from a REP-complex independently of the nucleotide state (interaction with GTP-form is 10-times lower, but there is 10-times more GTP in te cell, compensating for the difference) [Wittinghofer, 2014b]. After the GGTase reaction, the Rab:REP complex remains assembled in the cytosol with apparent K_d in the nM range [Pylypenko *et al.*, 2006]. In close proximity of membranes, this complex dissociates in chemical equilibrium, where free anchored Rab can preform its cellular function. Conversely, the GDP- or GTP-bound Rabs can be re-extracted by REP or more efficient GDP-specific GDI.

Carboxymethylation

To ensure sufficient hydrophobicity of the Rabs, harboring only one C-terminal prenylated cysteine, some GTPases are further methylated at their carboxyl ends [Wittinghofer, 2014b]. Indeed, CAAX C-terminal bearing Rabs, where C is cysteine, A is aliphatic residue, and X is any amino acid residue, are postprenylationally cleaved at the AAX peptide and methylated on the terminal α-carboxyl group. The same modification was also shown for CXC-containing Rabs. This modification does not affect proper Rab localization, but it does ensure sufficient GTPase membrane association [Leung *et al.*, 2007].

Phosphorylation

Rab GTPases are reversibly phosphorylated on respective target membranes in order to interfere with solubilization or downstream signaling. The addition of phosphate group introduces steric hindrance to the interaction surface of Rabs and their binding partners. Common modification targets are exposed serine or threonine residues in the switch II region or C-terminal tail. For example, Rab4 is phosphorylated on early endosomes by Cdc2 kinase, which causes its sequestration in the cytosol [Wittinghofer, 2014a]. In contrast, the same modification of Rab1 locks the small GTPase on the lipid bilayer [Shinde and Maddika, 2018]. Similarly, phosphorylation of Rab3, Rab8 and Rab10 at the switch II region causes altered membrane distribution due to prevented

GTPase detachment [Shinde and Maddika, 2018]. Recently, the Parkinson's disease-associated kinase LRRK2 phosphorylation of Rab8 and Rab10 was reported to induce activator-independent membrane accumulation [Gomez *et al.*, 2019].

Other modifications

A number of other posttranslational modifications have been described for subset of Rab proteins. However, a broader significance of some still remains unknown. For instance, mono-ubiquitinated Rab5 was discovered in human cell culture [Shin *et al.*, 2017], where it has an inhibitory effect on downstream signaling. Similar modification regulates Rab11, albeit with opposite effect. Ubiqutination of Rab11 leads to small GTPase activation and increased receptor recycling form early endosomes [Shinde and Maddika, 2018]. Another modification which causes activation is serotonylation, where serotonin attachment to Rab4 triggers platelet excocytosis, while Rab3 and Rab27 promote insulin secretion in pancreatic cells [Shinde and Maddika, 2018]. The constitutive activation is likely caused by transamidation of a catalytic glutamate residue in the nucleotide binding pocket, preventing GTP hydrolysis [Walther *et al.*, 2003].

Also, several pathogens target the host cell vesicular system by modifying Rab small GTPases. For example, *Legionella pneumophila* recruits Rab1 to pathogen-infested vacuoles by adenylylation (AMPylation) in order to maintain stable environment for bacterial growth and division [Oesterlin *et al.*, 2012]. By changing the Rab composition of the phagosome, bacteria can evade entry into degradation pathway [Sherwood and Roy, 2013]. Specifically, Rab1 activation is achieved by inhibiting catalyzed GTP hydrolysis through switch II interaction with regulatory proteins and forcing the GTPase in nucleotide-independent active conformation [Barthelmes *et al.*, 2020]. What is more, this germ catalyses also de-adenylation of modified Rab proteins, fully taking control over their activity state. *L. pneumophila* also induces phosphocholination of Rab1 and Rab35. This time however, the modification locks inactive GTPase on the membrane surface, downregulating its activity [Wittinghofer, 2014a]. Another way to hijack the host's Rab proteins is ADP-ribosylation. For example, pathogens *Listeria monocytogenes* and *Pseudomonas aeruginosa* secrete multidomain enzymes, which modify Rab5 by ADP-ribosylation. This prevents both GEF- and GDI-Rab5 interaction, which locks the inactive GTPase on the membrane and

prevents endosomal maturation towards degratory pathway [Alvarez-Dominguez *et al.*, 2008]. Finally, the typhoid fever-causing *Salmonella enterica* disarms host defenses by cleaving Rab29 in the switch I region with GtgE protease [Sherwood and Roy, 2013; Spano *et al.*, 2011].

1.1.4 Rab effectors and biological function

Despite being the center organizers of internal eukaryote compartmentalization, Rab GTPases do not possess any catalytic activity beyond (poor) GTP hydrolysis that would relate to vesicle trafficking or membrane deformation. Rather, they function as regulatory molecular switches, which specifically recruit diverse group of proteins, called effectors, at just the right time and location. The specificity lies in the exclusive preference of effectors to bind the GTP-conformation of Rab proteins with 0.1-10 µM affinity [Wittinghofer, 2014b]. Thus, GDP-bound Rab proteins are generally regarded as inactive (OFF), while GTP-loaded proteins are active (ON) and can support downstream signaling through effector interaction.

As Rab effectors specifically recognize structural differences between GDP- and GTP-Rab states, they mainly interact with regions that change most during nucleotide exchange and hydrolysis. These include switch I and II regions, along with the ”hydrophobic triad” of aromatic residues in the interswitch loops [Wittinghofer, 2014b]. As Rabs share many similar structural features, it begs the question of how different effectors recognize the right proteins, conferring signaling specificity. As it turns out, there are distinct non-conserved complementary determining regions (CDRs) on the Rab surface, which match the right binding partners [Wittinghofer, 2014b]. Plus, some effectors require additional interactions with the hypervariable C-terminal region or coincidence signals from the surroundings for efficient binding, like phosphoinositides [Mishra *et al.*, 2010].

The nature of recruited effectors directly relates to the biological process a given Rab protein controls. Known Rab effectors include motor proteins and adaptors that direct vesicular transport, vesicle tethers that promote membrane fusion, Rab regulatory proteins that direct downstream cascades and lipid-modification factors, which control membrane composition and identity [Gillingham *et al.*, 2014]. Thus, Rab proteins

are signaling hubs for membrane traffic, protein recycling and organelle biochemical signature. For example, Rab2 and Rab6 interact with over 25 diverse effectors each [Gillingham *et al.*, 2014]. As these two Rabs are localized on the endoplasmic reticulum (ER) and Golgi network, they function as an organizing center in Golgi transport, organelle maintenance and secretory vesicle formation. This role is solely mediated by the GTP-state specific interaction network that preforms coordinated tasks on Rab2/6-decorated membranes.

1.1.5 Rab regulators

Rab signaling potential depends on their nucleotide state. A set of multidomain proteins, called guanine nucleotide exchange factors (GEFs) and GTPase activating proteins (GAPs) regulate the Rab activity (Table 1.1). Furthermore, GDI and GDI dissociation factors (GDFs) are important in small GTPase recycling and localization. The interplay between these regulators determines the Rab signaling in space and time.

Guanine nucleotide exchange factors

GEFs generally activate Rab proteins by promoting GDP nucleotide exchange with GTP in the G domain. To be fair, GEF-catalyzed nucleotide exchange is fully reversible [Vetter and Wittinghofer, 2001]. It is the ratio of relevant nucleotide concentrations in the surrounding medium that determines the reaction direction. As the cellular GDP concentration is 0.03 mM and GTP amount is 10-times higher [Traut, 1994], the GEF-mediated nucleotide exchange usually substitutes GDP with GTP moiety, activating the protein. GEF promotes Rab activation by interacting with switch and nucleotide-binding regions, expelling the GDP nucleotide [Wittinghofer, 2014b].

There are several structurally distinct protein families of Rab GEFs: Vps9, TRAPP, DENN, Sec2 and BLOC3/MC1 heterodimers [Barr and Lambright, 2010; Kiontke *et al.*, 2017]. Members of the Vps9 group regulate endosomal GTPases – Rab5, Rab17, Rab21 and Rab22. Structural studies on Vps9 and TRAPP families show that the catalytic GEF domains contain a conserved aspartate finger, which is inserted in the Rab nucleotide binding pocket. There, it displaces a crucial lysine residue and disrupts the P-loop interaction with GDP phosphate groups and Mg^{2+} [Delprato and Lam-

bright, 2007]. The displaced lysine residue is then stabilized by conserved switch II Rab aspartate or the GEF aspartate finger, which in turn leads to the release of magnesium ion and consequently, the nucleotide. The nucleotide-free GEF:Rab intermediate is finally disassembled by GTP·Mg^{2+} binding in a reverse reaction [Vetter and Wittinghofer, 2001]. GEFs from largest DENN family achieve essentially the same P-loop displacement, albeit without an inserting acidic finger residue. In contrast, they induce the needed Rab conformational changes through switch I and II rearrangement [Cherfils and Zeghouf, 2013; Wittinghofer, 2014b]. Similarly, Sec2 proteins have asymmetric coiled-coil structure, which destabilizes the Rab nucleotide binding through switch I deformation [Barr and Lambright, 2010]. Finally, Hps1:Hps4 (BLOC3) and Mon1:Ccz1 (MC1) GEF complexes constitute a separate group of Rab activators, where the subunits dimerize through longin domains and have substrate-specific nucleotide exchange mechanism [Kiontke *et al.*, 2017].

Structural and functional GEF analysis revealed that their nucleotide exchange activity is often autoregulated through adjacent autoinhibitory and membrane binding domains [Cherfils and Zeghouf, 2013]. For example, the Rab5 GEF Rabex5 is in autoinhibited state in the cytosol, which is relieved by Rab5 and Rabaptin5 effector binding [Zhang *et al.*, 2014]. An autoinhibition mechanism has also been proposed for Rab11 GEF TRAPPII, which is relieved by membrane binding [Thomas and Fromme, 2016]. Finally, Rab GEFs are often involved in feedback regulatory networks, which introduce non-linear and cascading responses to Rab activity switching [Mizuno-Yamasaki *et al.*, 2012]. These emerging concepts will be discussed in greater detail in the following chapters.

What is more, respective GEF organelle localization directly influences Rab membrane targeting as it defines the sites of GTPase activation. This was elegantly demonstrated by mistargeting Rab1, Rab5 and Rab8-specific GEFs to mitochondria, an organelle where these proteins are not found under normal conditions. A *Listeria monocytogenes* mitochondria-localization sequence in combination with rapamycin-inducible heterodimerization system caused GEF mitochondria recruitment, which in turn led to Rab mislocalization to the same membranes [Blümer *et al.*, 2013].

GTPase activating proteins

While the GEF proteins mediate the nucleotide exchange, which results in Rab membrane localization and activation in cells, the GAPs promote GTP hydrolysis to GDP and functional inactivation of Rab molecular switches. Their activity is thought to limit Rab signaling potential in space and time, giving rise to distinct GTPase protein domains on the membrane surface [Zerial and McBride, 2001; Nottingham and Pfeffer, 2009; Franke *et al.*, 2019]. Nonetheless, as the name implies – Rab small GTPases can hydrolyze the GTP to GDP by themselves, albeit with a relatively low efficiency of $\approx 10^{-4}$ s^{-1} reaction rates [Wittinghofer and Vetter, 2011]. For some Rabs this intrinsic enzymatic activity can be viewed as an internal OFF-switch and an additional GAP is not necessary to time the signaling [Rybin *et al.*, 1996]. However, for many dynamic intracellular process the Rab GTPase reaction would take too long. As a consequence, GAPs readily accelerate the GTP hydrolysis reaction by as much as five orders of magnitude [Gavriljuk *et al.*, 2012].

In contrast to structurally diverse GEFs, most Rab GAPs share a common TBC (Tre-2/Cdc16/Bub2) domain [Barr and Lambright, 2010]. There are 44 predicted TBC family members, which negatively regulate Rab activity and are important in GTPase network crosstalk, defining signaling domains in space and time [Frasa *et al.*, 2012]. The catalytic core of these proteins includes conserved amino acid residues, called the arginine and glutamine fingers [Wittinghofer, 2014b]. The GTP hydrolysis in Rabs is initiated by a nucleophylic attack of a non-structural water molecule on the γ-phosphate group. This water molecule is stabilized by a glutamine residue in the switch II region, which is necessary for the intrinsic GTPase activity. The same residue is also often mutated in constitutively active mutants, e.g. Rab5Q80L used in this work, where GTP-loaded Rabs are locked in the ON state [Nottingham and Pfeffer, 2014]. Substituting the glutamine residue, the GAP arginine and glutamine fingers reach in the nucleotide binding pocket and promote GTP to GDP conversion with high efficiency due to a more well-defined active site. Interestingly, also the constitutively active Rab mutants are readily inactivated by GAPs as they provide all the needed molecular interactions for GTP hydrolysis [Gavriljuk *et al.*, 2012].

Like Rab GEFs, GAPs are multisubunit proteins that can be posttranslationally mod-

ified or specifically targeted in space and time. Particularly, GAPs are often recruited by membrane markers and GTPases to act as local inhibitors, defining borders of Rab activation along the lipid bilayer and ensuring temporal GTPase cascades during organelle maturation [Nottingham and Pfeffer, 2009; Frasa *et al.*, 2012]. As global inhibitors, they can minimize the negative effects of stray mis-activated or mis-localized Rabs.

Rab GDP dissociation inhibitors

Rab GDI is soluble cytosolic protein that binds geranylgeranylated Rab proteins and is crucial for Rab delivery and reuptake from the membranes after inactivation. Rab GDIs were discovered as 50-kDa proteins that inhibit GDP dissociation from Rab3 nucleotide binding pockets, which also gave them their name [Sasaki *et al.*, 1990]. These proteins are ubiquitously expressed and are able to recognize the whole 60-odd repertoire of Rab proteins in humans. There are two isoforms of GDI, termed α- and β-, which are 87 % identical and are functionally similar, although they show some tissue specificity [Pfeffer *et al.*, 1995]. In our study, we use the Rab GDI-α isoform.

Early pulse-chase experiments showed that at every given moment, 10-50 % of Rabs are sequestered in the cytosol [Pfeffer *et al.*, 1995]. The majority of these are in tight Rab:GDI complex (Figure 1.4), which is inactive and prevents interactions between Rabs and other regulatory proteins. The GDI interacts with switch and C-terminal regions of Rab, where it provides a hydrophobic grove to accommodate two geranylgeranyl chains, protecting them from the solvent. There, one of the lipid chains is buried in the hydrophobic pocket, while the other is more exposed on the surface, allowing potential interaction with membranes and binding partners. This also explains the mechanism of Rab membrane extraction, where GDI solubilizes GDP- and membrane-bound Rabs by first interacting with their G domain. Then, the isoprenoid chains are sequentially accommodated in the hydrophobic grove and the tight Rab:GDI complex is formed. The opposite sequence of events is also possible in Rab membrane delivery [Pylypenko *et al.*, 2006].

The GDI interacts with both, mono- and di-geranylgeranylated Rabs, with higher affinity for the latter [Pfeffer *et al.*, 1995]. The interaction between GDI and the solu-

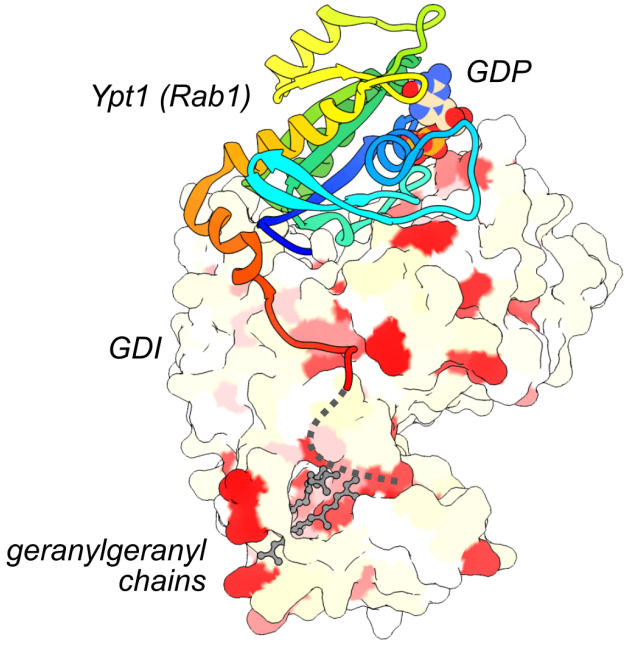

Figure 1.4: **The Rab:GDI crystal structure.**

Crystal structure of yeast Ypt1[GDP] (Rab1 in mammals) in complex with GDI. The Rab structure is shown as rainbow ribbons (N-terminal blue, C-terminal red), GDP is shown as spheres and GDI surface is colored according to hydrophobicity (white to red). Two geranylgeranyl chains are visible in the hydrophobic binding pocket as ball-and-stick model. The hypervariable Rab C-terminus is not visible in the structure, a possible backbone outline is shown in gray. PDB ID: 2BCG [Pylypenko *et al.*, 2006].

ble Rab G domain in GDP state is around 10 µM [Pylypenko *et al.*, 2006], similar to typical Rab[GTP]:effector pairs [Wittinghofer, 2014b]. Additionally, the inclusion of geranylgeranyl lipid chains contribute to low apparent dissociation constant K_d in 10 nM range [Shapiro and Pfeffer, 1995]. Interestingly, the Rab:GDI affinity plummets for at least three orders of magnitude for GTP-bound protein, making the interaction GDP- and prenylation-specific [Wu *et al.*, 2010]. This difference in respective affinities also explains the need for division of labor between GDI and REP, two similar groups of proteins with important distinctions. Firstly, while REP interacts with GDP- and GTP-loaded GTPases with similar efficiency [Wittinghofer, 2014b], the large difference in affinities prevents stable Rab[GTP]:GDI assembly. Secondly, in contrast to REP, which also binds unmodified Rabs with nanomolar affinity [Wu *et al.*, 2007], the GDI interacts with prenylated proteins much more tightly than with GTPase domain alone. This makes GDI thermodynamically much more efficient in Rab membrane extraction than the REP [Pylypenko *et al.*, 2006]. Thus, less abundant REP is particularly well-suited to capture GDP- and GTP-bound Rabs right after ribosomal translation for complex-specific geranylgeranyl-conjugation. Afterwards, Rabs can be delivered to membranes in equilibrium reaction, where REP re-extraction is unfavorable due to low binding energy difference between the G-domain and prenylated Rab tail [Wu *et al.*, 2007]. Conversely, highly expressed GDI is designed to continuously extract inactive Rabs from the lipid bilayer and maintain a constant soluble pool of the GTPases. This ensures specificity in GTPase signaling, efficient Rab turnover and a proof-reading mechanism for mislocalized Rabs. Once GDI-bound, Rabs are thought to continuously exchange between the protein complex and the membranes with $\approx$ 1 min half-life. Once shortly membrane bound, these proteins are substrates for GEF-mediated nucleotide exchange to GTP-state, which prevents GDI re-extraction and promotes effector recruitment [Wu *et al.*, 2010].

GDI dissociation factors

As the measured Rab:GDI association is very tight with K_d in the low nanomolar range, a need for GDI dissociation factors (GDFs) was postulated [Pfeffer *et al.*, 1995]. Apart from the complex breaking, these hypothetical proteins would also ensure proper Rab targeting. Indeed, such factor was detected in isolated endosomal fraction from rat

liver, where a GDF displaced GDI complexes for endosomal Rab5, Rab7 and Rab9 [Dirac-Svejstrup *et al.*, 1997]. Subsequent studies identified the transmembrane 20 kDa prenylated Rab acceptor-1 (PRA1; Yip3 in yeast) as a bona fide GDF for the selected group of Rabs [Sivars *et al.*, 2003]. PRA1 passes the lipid bilayer of Golgi and ER four times and contains an N-terminal soluble domain, which cannot independently mediate Rab release [Lin *et al.*, 2001; Pfeffer and Aivazian, 2004]. Due to instability and hydrophobicity, its structure and GDF mechanism remain unknown. Interaction analysis revealed assemblies with both Rab9 and GDI, so it is assumed that PRA1 recognizes Rab:GDI complex and provides an alternative binding pocket for the Rab prenyl chains. This would then lead to a decrease in Rab:GDI affinity and subsequent release of the assembly. Rab protein could later anchor into the membrane and diffuse away [Pfeffer and Aivazian, 2004]. On the other hand, a GDF could displace the GDI by disrupting the interaction surface with the Rab G domain [Collins, 2003] or preventing GDI re-extraction of the dissociated membrane bound GTPases [Hutt *et al.*, 2000].

Despite other Yip family members in mammals, PRA1 is the only identified GDF so far. Together with few other Yips, PRA1 is involved in Rab-independent Golgi transport [Behnia and Munro, 2005], casting doubt on its central role in Rab:GDI dissociation. What is more, it has been established that a GDF is not required in Rab targeting. Instead, membrane-localized GEFs are sufficient to direct Rab activation on target organelles [Wu *et al.*, 2010]. This was demonstrated also for PRA1-specific Rab5 and Rab7 *in vitro* [Langemeyer *et al.*, 2018] and *in vivo* [Cabrera and Ungermann, 2010; Blümer *et al.*, 2013]. Thus, potential GDFs like PRA1 do not seem to play a major role in Rab delivery and activation. Rather, they likely fine-tune the timely signaling of a Rab subset, together with other molecular cues on the target membranes – like phosphoinositides, ubiquitin, effectors and other GTPases.

Table 1.1: **Table of selected Rabs (Figure 1.1) and their key regulators.** Adapted from [Hutagalung and Novick, 2011; Wittinghofer, 2014b; Müller and Goody, 2017].

GTPase	Group	Process	GEF	GAP
Rab1	I	Golgi transport	TRAPP I	TBC1D20
Rab2	IV	ER to Golgi transport		TBC1D1

(Continued on the next page)

(Continuation)

GTPase	Group	Process	GEF	GAP
Rab3	I	secretory vesicles	DENN:MADD	Rab3GAP
Rab4	IV	recycling from EE		TBC1D11
Rab5	II	EE maturation	Rabex5:Rabaptin5	RabGAP-5
Rab6	V	EE to Golgi transport	Ric1:Rgp1	TBC1D11
Rab7	III	EE to LE and lysosome transition	Mon1:Ccz1	TBC1D2A
Rab8	I	exocytosis	Rabin8	TBC1D1
Rab9	III	LE to Golgi transport	DENND2	
Rab10	I	exocytosis	DENND4	TBC1D1
Rab11	IV	recycling to PM	SH3BP5	TBC1D11
Rab21	II	endosomal transport	Rabex5	TBC1D17
Rab22	II	EE to Golgi transport	Rabex5	TBC1D10B
Rab24	II	autophagosome formation		
Rab25	IV	RE to PM transport		
Rab27	I	exocytosis	DENN:MADD	TBC1D10A
Rab32	III	MT fission	BLOC-3	

1.1.6 Rab misregulation in disease

The role of Rabs as central organizers of intracellular membrane identity and trafficking is also manifested in disease. Their misregulation is associated with a number of human disorders, from bacterial infection to cancer. Luckily, the ensemble of over 60 GTPases also contains Rabs with overlapping function and isoforms, which ensures sufficient redundancy and robustness of basal organelle maintenance.

Bacterial infection

As discussed before (Section 1.1.3), a number of pathogenic bacteria hijack host Rab GTPases to camouflage their presence and evade degradation. For example, *Legionella* and *Salmonella* secrete factors that modify Rab1, Rab35 and Rab29, which

results in cytosolic bacterial vacuoles, where the invaders can safely replicate. They remain hidden behind misregulated Rab markers, which present these bacterial organelles as benign to the host cell [Oesterlin *et al.*, 2012]. Similarly, *Mycobacterium tuberculosis* and *Salmonella* interfere with endosome maturation by disrupting Rab5 and Rab7 signaling [Behnia and Munro, 2005]. Another related example is *Tropheryma whipplei*, the causal agent of fatal Whipple's disease, which likewise targets Rab5 and Rab7 signaling for its survival. It has been proposed that *Listeria monocytogenes* glyceraldehyde-3-phosphate dehydrogenase (GAPDH) Lmo2459 and *Pseudomonas aeruginosa* ExoS can ADP-ribosylate Rab5, locking it on the membrane. This interferes with endosome transition to Rab7-covered late endosomes and subsequent fusion with lysosomes [Stein *et al.*, 2012; Mottola *et al.*, 2014]. The same Rab cascade is manipulated also by *Mycobacterium tuberculosis*, which inhibits Rab5 effector PI3P kinase Vps34 and additionally consumes PI3P, which otherwise serves as a coincidence molecular cue for Rab5 effectors and Rab7 activation [Mottola, 2014]. What is more, *Listeria monocytogenes* activates Rab5 upon cell entry by recruiting GEF RIN1 and later inactivates it with ADP-ribosylation [Mottola, 2014]. Conversely, *Chlamydia pneumonia* disguises its presence by actively recruiting Rab1, Rab4 and Rab11, which are usually associated with Golgi and endocytic recycling [Hutagalung and Novick, 2011].

Neurodegenerative diseases

Neurodegeneration is particularly susceptible to faulty membrane trafficking, which is often caused by defects in Rab signaling. Amyotrophic lateral sclerosis (ALS) or Lou Gehrig's disease is a motor neuron neurodegenerative disorder that is mainly sporadic and progresses with age. In 10 % of patients, it is caused by genetic mutations, often in C9ORF72, which is Rab8 and Rab39 GEF as well as Rab1 effector, regulating autophagy. In ALS and dementia, C9ORF72 defect results in accumulation of characteristic protein aggregates that promote neurodegeneration [Kiral *et al.*, 2018]. A Rab5 GEF Alsin (ALS2) mutation causes ALS 2, a rare juvenile motor neuron disease related to Lou Gehrig's disease. There, defective Rab5 and Rab7 signaling cause increased glutamate receptor degradation, which likely leads to neuronal atrophy [Barnard *et al.*, 2015]. Additionally, disrupted Alsin and Rab5 relocation to mitochondria under oxidative stress can affect neuron survival in ALS, advancing the neuropathology [Hsu *et al.*,

2018].

A number of Rabs are indirectly involved in Parkinson's and Alzheimer's disease. Particularly, onset of Parkinson's has been linked to defects in vesicle-mediated transport [Bonet-Ponce and Cookson, 2019]. In genetic early-onset Parkinson's disease, the Golgi Rab39B is mutated, which results in improper assembly of glutamate receptor AMPA and defective synapses. Furthermore, several Rab GTPases are involved in α-synuclein secretion, the primary agent in amyloid plaque formation in Parkinson's [Kiral *et al.*, 2018]. Furthermore, mutation in Parkinson's disease-associated LRRK2 causes over-phosphorylation of 14 Rab targets, resulting in severe trafficking misregulation in neurons [Bonet-Ponce and Cookson, 2019]. Endosomal Rab4, Rab5, Rab7 and Rab27 are upregulated in Alzheimer's disease, where unbalanced membrane trafficking could lead to insufficient amyloid-β clearance [Kiral *et al.*, 2018].

A neuropathy Charcot-Marie-Tooth type 2B (CMT2B), affecting peripheral nervous system is caused by Rab7 mutations. These target specific effector interactions with molecular motors. Under normal conditions, the coordinated delivery of Rab7-specific late endosomes to the cell body is necessary for neuronal growth factor signaling, which could in turn lead to the observed axonal deterioration in neuropathies like CMT2B [Barnard *et al.*, 2015].

Cancer

Tissue invasion and sustained growth are two of the basic cancer hallmarks [Hanahan and Weinberg, 2011]. Importantly, both are affected by orchestrated Rab signaling in receptor recycling, cell polarity and migration [Mosesson *et al.*, 2008]. Particularly, the aberrant tumor regulation of endocytotic Rabs leads to increased growth factor signaling on plasma membrane an loss of cell-cell and cell-matrix contacts due to faulty internalization of cadherins and integrins, respectively. For example, Rab4 is needed in the fast integrin turnover during metastatic invasion and its effector NDRG1, involved in cadherin recycling, is downregulated in metastatic carcinomas [Mosesson *et al.*, 2008]. Strikingly, Rab25 expression is amplified in half of ovarian and breast cancers, while it is also linked to worse prognosis [Cheng *et al.*, 2004]. Together with Rab11, Rab25 regulates integrin recycling pathway, which could contribute to cancer aggressiveness

[Mosesson *et al.*, 2008]. Similarly, Rab5 upregulation is involved in integrin uptake and focal adhesion disruption, which contributes to metastasis [Mendoza *et al.*, 2014].

Other genetic diseases

Interestingly, GDI has been associated with X-linked intellectual disability [D'Adamo *et al.*, 1998]. Particularly, the loss of GDI-α affected Rab3 recycling, which is important in generation of neuronal secretory vesicles and neurotransmitter release [Chou and Jahn, 2000]. It seems that GDI-β cannot fully rescue the loss of α-isoform during neuronal differentiation and brain development, where Rab-directed endo- and exocytosis play important roles, resulting in intellectual disability of affected patients [D'Adamo *et al.*, 1998].

Similarly, loss of related REP1 protein results in X-linked retinal degradation disease choroideremia as a consequence of insufficient Rab prenylation [Agola *et al.*, 2011]. Retina is particularly susceptible to REP disfunction as related REP2 can compensate for the REP1 deletion in other tissues. Recently, an adenovirus-based gene therapy where intact REP1 gene is transduced into retina completed phase II clinical trial and phase III study is planned in 2020 (trial NCT03496012) [Barnard *et al.*, 2015].

Carpenter syndrome is an intellectual disability disorder, associated with several deformities like skull abnormalities and polydactyly (additional fingers). It is caused by Rab23 mutations that interfere with sonic hedgehog activity during development. Normally, Rab23 negatively regulates sonic hedgehog signaling in embryogenesis by sequestering its transcription factors [Hutagalung and Novick, 2011].

The Rab involvement in complex genetic and infection disorders highlights the need to better understand intricate GTPase signaling on system's level. In the next Chapter, I discuss the main regulatory motifs in Rab signaling, which could be promising targets for the next generation of therapeutic interventions [Agola *et al.*, 2011; Bonet-Ponce and Cookson, 2019].

1.2 Network regulatory motifs in Rab signaling

While the structural mechanisms of Rab conformational switching on molecular scale are well-known, an important aspect of small GTPase signaling remains unexplored. For a long time, it has been clear that sporadic Rab activation on single-protein scale cannot support decisive cellular signaling. Rather, uncoordinated events of nucleotide exchange are filtered-out as background noise in the cytoplasm [Gomez-Uribe *et al.*, 2007; Huang *et al.*, 2016]. Thus, biologically relevant activation of small GTPases is bound to happen on a collective network (system) scale, resulting in spatiotemporal activation domains on membrane surface [Zerial and McBride, 2001; Franke *et al.*, 2019]. To achieve orchestrated regulation of Rab proteins, the cell has to use higher-order regulatory modules, which are encoded in the biochemical network architecture and operate in non-linear regimes [Cherfils and Zeghouf, 2013]. Several distinct Rab domains have been reported *in vivo*, including Rab4, Rab5, Rab7, Rab9 and Rab11 [Pfeffer, 2013]. Furthermore, respective Rab networks are interconnected between themselves and other cascades to mediate trafficking along signaling pathways in space and time [Mizuno-Yamasaki *et al.*, 2012]. A theoretical network topology study revealed that a combination of two interacting GTPase regulatory modules can generate 64 distinct circuits, which support higher-order behaviors like bistable switches, activity overshoots, oscillators and activation waves [Tsyganov *et al.*, 2012]. It is exciting to wonder which of these network motifs exist *in vivo* and whether physiological conditions permit such emergent properties. Disruption of collective GTPase behaviors could likewise contribute to Rab-liked diseases.

1.2.1 Ultrasensitivity

In signal transduction, biochemical networks often generate switch-like collective responses to an incoming signal. When we analyze their steady state response properties, we observe a characteristic sigmoidal relationship, where small changes in input signal generate large differences in system's output (e.g. kinase phosphorylation or Rab GDP-for-GTP nucleotide exchange). We call network responses ultrasensitive when less than 81-fold difference in stimulus leads to an output increase from 10 to 90 % maximal (Figure 1.5). Otherwise, the signaling modules follow regular hyper-

bolic (Michaelian) mass-action response characteristics, which always require 81-fold change in signal input to cover the same output range [Ferrell and Ha, 2014a]. As a consequence, ultrasensitivity is especially important in signal transduction to avoid signal deterioration over multi-step cascades and ensure noise filtering for background input values [Ferrell and Ha, 2014c].

Positive feedback

In positive feedback, and input can indirectly contribute to the network output more than once. Thus, it is a common theme in ultrasensitive signaling modules involved in cell polarization [Altschuler *et al.*, 2008], oocyte maturation [Huang and Ferrell, 1996], cell cycle progression [Pomerening *et al.*, 2003] and Rab regulation [Zerial and McBride, 2001]. An emergent characteristic of positive feedback networks is the threshold input value, which initiates signaling and time lags in systemic response over which the signal accumulates to reach the threshold [Ferrell and Ha, 2014b].

In Rab GTPase regulation, GEFs often directly interact with cognate Rab effectors [Mizuno-Yamasaki *et al.*, 2012; Goryachev and Leda, 2019] – colocalizing with the nucleotide exchange product Rab[GTP]. This potentially creates a positive feedback loop, where GEF:effector complex first activates and then binds Rab[GTP]. The membrane-recruited GEF can then process nucleotide exchange more efficiently as it is localized on the same 2D surface as its substrate [Zerial and McBride, 2001; Mizuno-Yamasaki *et al.*, 2012]. The GEF recruitment positive feedback is thus encoded in the network circuitry, generating membrane-specific active protein domains [Sönnichsen *et al.*, 2000; Zerial and McBride, 2001; Franke *et al.*, 2019]. An extensively studied system with hypothesized positive feedback is the Rab5 activation switch [Lippé *et al.*, 2001], the main theme of this work. Another example includes Sec4 (Rab8)-mediated recruitment of Sec2:Sec15p complex in yeast [Mizuno-Yamasaki *et al.*, 2012]. Despite the long-standing belief that Rab-mediated GEF:effector recruitment can generate positive feedback and cooperative activation dynamics, a direct proof of this concept is still missing.

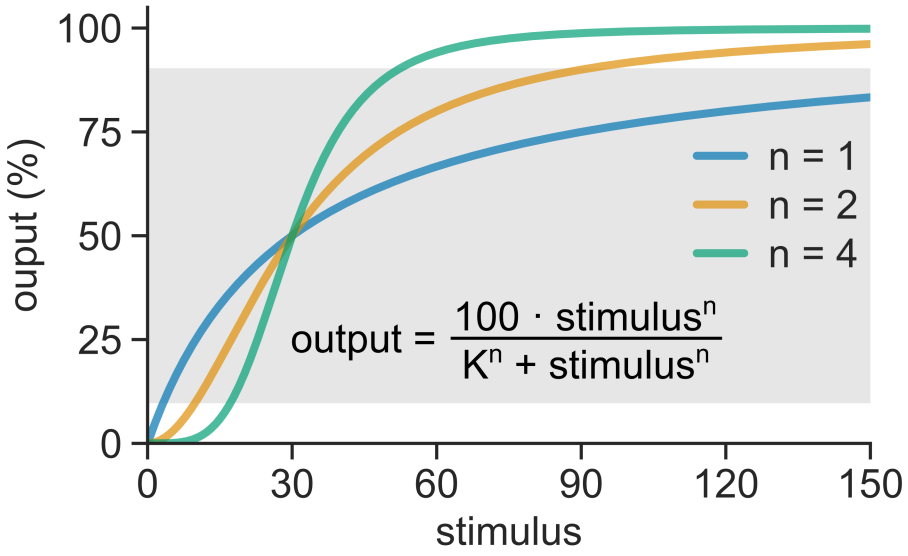

Figure 1.5: **Ultrasensitive networks are more responsive to changes in stimulus concentration.**

Shown are three different network response curves according to the Hill function $output = \frac{100 \cdot stimulus^n}{K^n + stimulus^n}$: a hyperbolic non-ultrasensitive curve for a classical Michaelis-Menten system (Hill coefficient n = 1, blue) and two ultrasensitive sigmoidal curves (n = 2, orange; n = 4, green). For the modeled hyperbolic curve, a 81-fold increase in stimulus is needed to jump from 10 to 90 % of the maximal system response (stimulus increase from 3.33 to 270 arbitrary units, which is out of bounds for clarity). Conversely, for the network with sigmoidal responses just 9-fold (n = 2) and 3-fold increases (n = 4) in stimulus abundance are enough to cover the same signal range. For the ultrasensitive system with n = 2 that corresponds to stimulus concentration change form 10 to 90 units (mind, these are stimulus units, not system output), while even more sensitive network with n = 4 responds from 10 to 90 % of maximum as input increases from 17.3 to 52 arbitrary units. The observed interval between 10 and 90 % of system output is indicated by the gray box; the half-maximum constant K was set to 30.

Bistability

Biochemical systems that possess ultrasensitivity and positive feedback often result in bistability, an all-or-nothing response and likely emergent behavior in Rab cascades [Barr, 2013]. Bistability is particularly useful in cellular signaling as it converts continuous inputs into digital outputs, e.g. ON or OFF collective states for Rab switches. Nevertheless, not every ultrasensitive network is bistable. This depends on specific circuit parameters, where ranges of possible values build parameter landscapes with monostable and bistable system responses [Ferrell and Xiong, 2001]. A monostable system has one stable steady state or an unstable and stable one, towards which it will tend to switch. Conversely, a bistable network has three possible steady states – an unstable and two stable states, between which it can transition, depending on current system parameters [Gardner *et al.*, 2000]. Another property of bistable systems is hysteresis (Figure 1.6) – a form of biological memory where switching from ON to OFF state requires less input as transition from OFF to ON (or vice-versa) [Kramer and Fussenegger, 2005]. Consequently, for a given input near the critical switching point, a hysteretic network can exist in either of the two steady states. The state occupancy will depend on the system history, hence the memory. This is used in differentiation and development to keep cell identities stable even after signal deceases [Ferrell and Xiong, 2001], but it can also be used to maintain Rab signaling domains. In extreme cases, the hysteretic switch is virtually irreversible and the selected state is perpetuated indefinitely [Ferrell and Xiong, 2001], say in organelle identity maintenance.

Inhibitor ultrasensitivity

Cellular signaling often uses stoichiometric inhibitors as noise filters when only a certain threshold amount of signaling molecule leads to decisive cascade initiation. For example, in cell cycle checkpoint progression from G1 to S phase, the cyclin kinase E-Cdk2 is initially inhibited by p21. Only when E-Cdk2 exceeds the critical concentration, the kinase is free to phosphorylate its targets and promote S phase entry [Ferrell and Ha, 2014b]. Similarly, inactive Rabs are in tight GDI complexes with only small proportion available for GEF-mediated nucleotide exchange. It is thus possible that inhibitor ultrasensitivity is inherent to all Rab activation networks. Such biochemi-

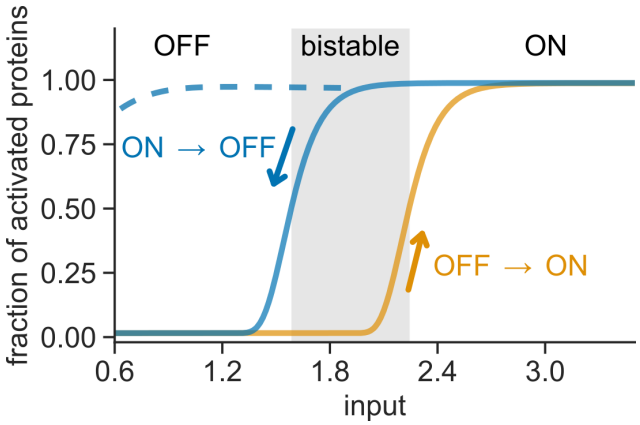

Figure 1.6: **Bistable systems display hysteresis.**
An example of bistable signal-response plot. Depending on the signal amount, the system can either be in ON or OFF states. For inputs between 1.6 and 2.3, the system displays bistability – it can be in both states, depending on its history (the direction of input change). An irreversible ON transition is shown with dashed blue line.

cal systems would exhibit cooperative input-response curves in collective activation. What is more, limiting signaling substrate amounts evokes stochastic effects, which in combination with positive feedback result in bistability. Indeed, stochastic bistability plays a role in bacterial cell fate determination [Lord *et al.*, 2019], as well as in kinase and small GTPase signaling [Bishop and Qian, 2010; Ferrell and Xiong, 2001; Samoilov *et al.*, 2005].

Zero-order ultrasensitivity

The small GTPase spatial cycles counteract the 2nd law of thermodynamics by consuming energy in form of guanine nucleotide conversion [Vartak and Bastiaens, 2010]. Under certain conditions, this activity cycle can be exploited by the cell to generate decisive ”zero-order” ultrasensitive responses [Koshland *et al.*, 1982]. The zero-order ultrasensitivity operates under stringent conditions, where the conversion substrate (e.g. Rab) is in excess over forward- (GEF) and back-reaction (GAP, GTPase) K_ms. There, the activation rate is independent form Rab concentration (hence, zero-order) and only depends on GEF amount. Zero-order ultrasensitivity has been found to describe isocitrate dehydrogenase activity [Goldbeter and Koshland, 1984], glycogen phosphorylase and Erk MAP kinase-mediated transcription regulation [Ferrell and Ha, 2014a]. As the

availability of Rab[GDP] substrate is assumed to be particularly scarce due to GDI continuous extraction and $K_{0.5}$ for GEFs are in the µM range [Chin *et al.*, 2009], the zero order ultrasensitivity is unlikely to be a general mechanism in Rab signaling. Nevertheless, it could be applied in cases where phosphorylation and GDFs generate high local Rab densities on membranes in low mM range [Kuriyan and Eisenberg, 2007]. This could then trigger active nucleation sites and generation of signaling domains.

1.2.2 Feed-forward loops

Individual Rab regulatory modules are connected through feed-forward loops to form cascading signaling pathways that orchestrate membrane flow through organelle maintenance, vesicle formation, trafficking, tethering and fusion. There, small GTPases that regulate successive processes also promote activation or inactivation of adjacent biochemical networks in space and time.

GEF cascades

Distinct Rab proteins regulate consecutive steps in membrane trafficking by recruiting appropriate effector proteins in sequential way. To achieve this coordination in space and time, an active upstream Rab recruits GEF for the downstream acting GTPase as an effector, forming a GEF cascade. For example, the first GEF cascade was identified in yeast, where Golgi Ypt32 (Rab11) recruits GEF for Sec4 (Rab8), a secretory granule Rab. As a consequence, this GEF cascade directly regulates molecular steps in secretory granule budding from the Golgi network by sequential Rab activation on target membrane [Pfeffer, 2013]. Similarly, the Rab5-Rab7 GEF cascade directs early endosome maturation into late endosomes by Rab5 recruitment of a Rab7 GEF [Poteryaev *et al.*, 2010]. The same principle is applied in Golgi Rab33-Rab6 and Rab9-Rab32 cascades [Pfeffer, 2013].

GAP cascades

By the same principle as GEF cascades promote pathway progression, the GAP cascades down-regulate the upstream Rab. In order to achieve spatially and temporally

defined Rab membrane domains, a downstream Rab in turn recruits an upstream Rab-specific GAP. This was demonstrated in yeast ER-to-Golgi exocytosis pathway, where Ypt23 recruits Ypt1-specific GAP, preventing signaling overlap between successive Rabs. As expected, the Ypt1 GAP knock-out strains display membranes with mixed Rab populations and misregulated membrane trafficking [Rivera-Molina and Novick, 2009]. Interestingly, there is some evidence that in Rab5-to-Rab7 transition GEF and GAP cascades could work simultaneously to achieve GTPase conversion. In yeast, an indirect GAP cascade inactivates Rab5 ortholog Vps21 through Ypt7 effector network [Rana *et al.*, 2015]. A similar observation was also confirmed in *C. elegans*, where Rab7-localized TBC-2 GAP acts on Rab5 *in vivo* [Chotard *et al.*, 2010]. However, an equivalent vertebrate regulation network is yet to be confirmed.

1.2.3 Spatiotemporal patterns

The field of system's biology emerged in hopes to reveal underlying mechanisms of molecular self-organization in cell signaling [Karsenti, 2008]. While we cataloged the human genome and continuously reveal protein atomic structure with advanced X-ray and cryo-electron microscopy techniques, a great gap in understanding of biochemical collective coordination in space and time remains [Kholodenko *et al.*, 2010]. The seminal work by Alan Turing [Turing, 1952], which was expanded by Gierer and Meinhardt [Gierer and Meinhardt, 1972], describe spontaneous generation of spatiotemporal patterns in terms of a reaction-diffusion system. For example, the Rab regulation network can be potentially thought as such, where the GEF and GAP interplay alone generates Rab activity patterns on the membrane through nucleotide exchange away form thermodynamic equilibrium. Generally, the simplest system is composed of locally-acting (auto)activator (Rab:effector:GEF complex) and long-range inhibitor (GAP) or depletion of activation substrate (GDI extraction). The respective diffusion coefficients determine the emergent behavior: if the inhibitor diffuses faster than the activator, steady state patterns like gradients, spots and stripes form. Conversely, if the two coefficients are comparable, traveling waves of activation emerge [Tyson *et al.*, 2003]. In Rab signaling, we can imagine that local positive feedback activation leads to situation where transient multifaceted interactions between Rabs, GEF

and effectors significantly reduce components' diffusion, which would result in spot-like domains. On the other hand, in absence of such multivalent complexes, Rab activation waves would spread over the phospholipid bilayer [Tsyganov *et al.*, 2012; Deneke and Di Talia, 2018]. Importantly, these basic chemical patterns are believed to guide living systems in cell (self-)organization and embriogenesis [Kondo and Miura, 2010].

1.2.4 Biological membranes as reaction platforms

A key aspect to Rab signaling is the small GTPase cycling between the membrane and cytosol compartments, which is coupled to the small GTPase activity state. What is more, the energy input in the form of GDP-to-GTP exchange and subsequent hydrolysis of the high energy phosphoanhydride bond makes small GTPase networks operate away from the thermodynamic equilibrium. This opens the door for dynamic self-organization of the network components between the cytosol and membrane surface [Coyle and Lim, 2016; Tan *et al.*, 2020; Karsenti, 2008; Misteli, 2001]. Despite being integral to small GTPase function in *vivo*, many *in vitro* studies omitted phospholipid bilayers from biochemical assays [Lippé *et al.*, 2001; Delprato *et al.*, 2004; Delprato and Lambright, 2007; Nottingham and Pfeffer, 2014], which led to current lack of knowledge in physiological out-of-equilibrium signaling. Importantly, the biological membranes and lipids introduce new concepts in biochemical network regulation as reaction platforms and specific molecular markers.

As lipid-modified Rab GTPases are extremely hydrophobic and prone to immediate aggregation when exposed to aqueous media [Sivars *et al.*, 2005], the regulatory steps of nucleotide exchange and hydrolysis in Rab cycle are impossible in solution. Thus, the membranes provide reaction platforms for coordinated actions of GEFs, GAPs and GDIs. Indeed, it was recently established that geranylgeranylated Rab11 activation is possible only in presence of lipid vesicles [Thomas and Fromme, 2016]. Apart from offering support for hydrophobic Rabs, the membrane biochemical composition also provides additional regulatory signals for Rab networks like phosphoinositide identity [Jean and Kiger, 2012], membrane curvature [Kulakowski *et al.*, 2018] and effector composition [Li *et al.*, 2014]. Additionally, the reduction in dimensional-

ity from 3D to 2D system significantly increases the efficiency of molecular interactions. For example, membrane localization can increase effective local concentration of signaling components for three orders of magnitude compared to solution [Kuriyan and Eisenberg, 2007] and promote productive protein orientations by entropic effects. Consequently, the GEF-mediated nucleotide exchange on Ras and Arf GTPases can be increased for up to 1000-fold on membrane support [Groves and Kuriyan, 2010; Peurois *et al.*, 2018]. Due to these unique synergistic effects on phospholipid bilayers, the widely measured reaction rates of soluble components in *in vitro* assays are likely substantially different *in vivo* [Groves and Kuriyan, 2010]. Indeed, it has been demonstrated that membrane confinement alters dynamics for positive feedback-driven Ras GTPase activation, promoting bistability [Abel *et al.*, 2012].

Besides their influence on emergent properties of Rab circuits, membranes also physically segregate GTPase networks and GEF/GAPs, creating intracellular concentration and function gradients [Kholodenko *et al.*, 2010]. The dynamic boundaries control network crosstalk through proximity and regulatory composition. For instance, Rab1 could be activated on Golgi membrane by GEF TRAPP, which is tethered on COPII coat of the incoming ER vesicle [Barr and Lambright, 2010]. Conversely, Rab5 is activated on early endosomes, where GEF complex Rabex5:Rabaptin5 is located and not on Golgi cisternae, where RabGAP-5 resides. In *C. elegans*, Rab5 is inactivated on late endosomes as both lipid and protein composition change over the course of endosome maturation, recruiting the GAP TBC-2 [Chotard *et al.*, 2010]. Thus, the biological membranes are both necessary and often active players in Rab regulation.

Membrane protein domains

The endosomal system is a complex vesicular meshwork of membrane compartments with different sizes and morphology. Early endosomes are 100-500 nm structures with tubular extensions and late endosomes can span up to 1 µm and contain intraluminal vesicles [Klumperman and Raposo, 2014]. It was shown that distinct Rab domains or clusters populate different features and regulate distinct cellular processes: Rab5 is found on globular parts of early endosomes [Franke *et al.*, 2019; Cezanne *et al.*, 2020] and controls endosomal fusion and maturation. Later, it is replaced by Rab7, which directs lysosomal fusion with late endosomes [Rink *et al.*, 2005]. On the other hand,

Rab4 and Rab11 are involved in endosomal cargo recycling and populate tubular structures, which mature into recycling endosomes [Sönnichsen *et al.*, 2000]. Recently, high resolution imaging revealed 50 nm Rab5 (nano)domains on early endosomes [Franke *et al.*, 2019], which represent distinct signaling platforms for downstream vesicular trafficking events.

This spatial division of labor is achieved by non-linear activation mechanisms and maintained through small GTPase-specific effector ensemble [Zerial and McBride, 2001]. A key component of membrane Rab domain emergence are scaffolding proteins like Rab5 and Rab4 effectors Rabenosyn5 [Jovic *et al.*, 2010] and Rabaptin5 [Kholodenko *et al.*, 2010; Stenmark *et al.*, 1995]. Likely, these interaction partners both organize the domains in time and space, where they maintain stable cluster boundaries [Sönnichsen *et al.*, 2000; Kälin *et al.*, 2015] and facilitate cargo sorting for recycling or degradation pathways [Solinger *et al.*, 2020]. Crucially, Rabaptin5 ensures positive feedback in Rab5 activation through Rabex5 recruitment, a Rab5-specific GEF [Lippé *et al.*, 2001]. Particularly, the GEF and effector association is a common small GTPase regulatory mechanism that triggers symmetry breaking and results in self-organized protein clusters on membrane supports [Barr, 2013; Pfeffer, 2013; Halatek *et al.*, 2018]. Besides Rabs, the membrane protein (nano)domains are also a common theme in Ras [Wittinghofer, 2014a; Lee *et al.*, 2019] and Rho [Altschuler *et al.*, 2008; Rapali *et al.*, 2017; Remorino *et al.*, 2017] small GTPase signaling. Besides, they are believed to regulate Arf1-mediated vesicular trafficking in the trans-Golgi network [Stalder and Antonny, 2013; Nagano *et al.*, 2019]. The self-organized small GTPase membrane domains ensure robust signal transmission by recruiting a large number of relevant effector proteins at specific cellular locations [Wittinghofer, 2014a].

1.3 Rab5

Rab5 is a 24 kDa regulator of the vesicular trafficking and is cycling between the plasma membrane, early endosomes (EE) and the cytoplasm [Chavrier *et al.*, 1990]. A quarter of century ago, it has been identified to promote endocytic vesicle fusion and regulate endocytosis [Gorvel *et al.*, 1991; Bucci *et al.*, 1992]. In it's active state, Rab5 is orchestrating the endocytic pathway by recruiting specific effector and regulator proteins

[Christoforidis *et al.*, 1999] in a spatiotemporally distinct manner. Interestingly, Rab5 has one of the highest GTPase activities in Ras-like GTPases, which is on the order of $t_{1/2} \approx$ 5-15 min [Stenmark *et al.*, 1994; Rybin *et al.*, 1996; Simon *et al.*, 1996a], fitting with the estimated endosome budding and maturation time scales [Rybin *et al.*, 1996; Simon *et al.*, 1996a; Rink *et al.*, 2005]. Thus, it was proposed that Rab5 GTP hydrolysis is an internal timer for Rab5 function [Rybin *et al.*, 1996]. The GTPase activity is reduced by 100-fold in constitutively active Q79L mutant (equivalent to Q80L in *X. laevis* that was used in this work) [Stenmark *et al.*, 1994]. On the contrary, S34N mutant binds GDP with high affinity and prevents nucleotide exchange, generating a constitutively inactive GTPase [Stenmark *et al.*, 1994].

The human genome encodes three Rab5 isoforms, denoted Rab5A, B and C, which are expressed in all tissues [Chen *et al.*, 2014]. They are functionally redundant [Zeigerer *et al.*, 2012] and ensure high robustness of the endosomal network. Nevertheless, Rab5A has been recently observed to preferentially mediate epidermal growth factor receptor trafficking, while Rab5C is primarily involved in cell motility [Chen *et al.*, 2014]. In this work, I take the Rab5A as the canonical isoform and refer to it as ”Rab5”.

1.3.1 Cellular function

The Rab5 interactome consists of over 30 effectors, ranging from membrane tethers, motor proteins, vesicle docking and fusion machinery, phosphatidylinositol kinase and downstream Rab activators [Christoforidis *et al.*, 1999; Gillingham *et al.*, 2014]. The spatiotemporal coordination of Rab5 activation and effector availability leads to formation of clathrin-coated vesicles, [McLauchlan *et al.*, 1998], clathrin coat disassembly [Semerdjieva *et al.*, 2008], endosomal flux along the microtubules [Nielsen *et al.*, 1999], tethering [Murray *et al.*, 2016] and fusion of endosomes [Gorvel *et al.*, 1991], EE maturation and final conversion to late endosomes [Poteryaev *et al.*, 2010], all depending on the identity of Rab5 interaction partners. Given the large number of cellular functions, it is no surprise that RNAi Rab5 knock-down in mice leads to disruption of the whole endo-lysosomal system, highlighting Rab5 as a principle factor in endosomal biogenesis and maintenance [Zeigerer *et al.*, 2012].

As Rab5 activity is linked with distinct steps in the intracellular vesicle trafficking, dynamic domains of Rab5-associated protein complexes with unique transient compositions exist on the membrane [Franke *et al.*, 2019]. These then direct the EE through subsequent steps in the endocytic pathway [Zerial and McBride, 2001], emerging from the interaction-driven protein self-organization.

1.3.2 Rab5 GEF: Rabex5

There are as may as six different GEFs that have been reported to act on Rab5 in different pathways [Chen *et al.*, 2014; Hsu *et al.*, 2018]. Nonetheless, the Vps9 family GEF Rabex5 is the main endosomal Rab5 activator [Horiuchi *et al.*, 1997]. It has roughly 60 kDa and is composed of two N-terminal ubiquitin (Ub)-binding domains, a helical bundle, the catalytic Vps9 domain, C-terminal coiled-coil and a proline-rich region [Delprato and Lambright, 2007].

Interestingly, Rabex5 forms a complex with Rabaptin5 (from Greek *apto* – to touch and *Rab5*, Figure 1.7A), a Rab5 effector [Horiuchi *et al.*, 1997]. Nucleotide exchange assays revealed that Rabex5 is three times more active on soluble Rab5 when in Rabaptin5 complex, compared with GEF alone (rates on membrane support are not known) [Lippé *et al.*, 2001]. This implies that free Rabex5 is in auto-inhibited state, which is released upon Rabaptin5 and Rab5 binding. Indeed, a truncation analysis identified an inhibitory motif in the C-terminal coiled-coil region, which is involved in Rabaptin5 interaction and partly covers Rab5 binding surface [Delprato and Lambright, 2007]. A recent study suggests an additional inhibitory role of Ub-binding domains and adjacent linker region [Lauer *et al.*, 2019]. It is likely that both binding events contribute to release of auto-inhibition, further expanding the allosteric Rabex5 self-regulation, which is relieved in EE-specific chemical environment. Despite this, the measured catalytic rate of nucleotide exchange on soluble Rab5 is relatively slow compared to other GEFs [Delprato *et al.*, 2004], suggesting that membrane support is needed for efficient cooperative GTPase activation. Along with Rab5, Rabex5 also activates related Rab21 and Rab22 [Delprato *et al.*, 2004].

As Rab membrane targeting largely depends on GEF localization, it is important to explore many ways of Rabex5 recruitment to endosomal membranes. Monoubiq-

uitination is a common molecular tag, marking transmembrane cargo for sorting into endocytic pathway. As Rabex5 N-terminal Ub-binding domains interact with mono-Ub ($K_d \approx 30$ µM), it is believed that tagged sorting cargo recruits Rabex5 and releases its auto-inhibition, promoting Rab5 activation for downstream signaling specifically on EE [Lee *et al.*, 2006; Lauer *et al.*, 2019]. Furthermore, Ub is also involved in regulated Rabex5 detachment from EEs. The GEF has Ub-ligase activity, which promotes auto-ubiquitination and release to cytosol [Mattera and Bonifacino, 2008]. Negatively charged lipids [Zhu *et al.*, 2007] and Rab22[GTP] [Zhu *et al.*, 2009] are additional cues that contribute to endosome-specific Rabex5 recruitment. The GEF can be also brought to the endosomes indirectly, by the means of Rabaptin5. It has been long thought that Rabaptin5 recognizes pre-existing active Rab5 to shuttle Rabex5 on EEs, giving rise to stable Rab5 domains. However, Rabaptin5 is also Rab4 effector, raising the possibility that Rab4 activation precedes and triggers Rab5 nucleotide exchange [Kälin *et al.*, 2015].

Other Rab5 GEFs

Apart from Rabex5, which is by far the most characterized Rab5 GEF, the GTPase is also activated by other Vps9 domain exchange factors, ensuring function-specific signaling and robustness of the endo-lysosomal system through redundancy. For instance, Alsin (ALS2) is Rab5 GEF, which is defective in juvenile amyotrophic lateral sclerosis (ALS) and was found to activate Rab5 on endosomes and – interestingly – mitochondria under oxidative stress, where it triggers anti-apoptotic mechanisms [Topp *et al.*, 2004; Hsu *et al.*, 2018]. In contrast, GAPVD1 (also RME6, GAPex5) is localized on the plasma membrane, where it regulates receptor endocytic uptake and activates Rab5 on clathrin-coated pits or vesicles [Sato *et al.*, 2005; Su *et al.*, 2007; Semerdjieva *et al.*, 2008]. Similarly, Rin1, -2 and -3 couple Ras GTPase activation with Rab5 nucleotide exchange to induce endocytosis of selected peripheral proteins and receptors. They all bind active Ras, which relieves auto-inhibited Vps9 domain, promoting Rab5 signaling [Tall *et al.*, 2001; Kimura *et al.*, 2006; Kajiho *et al.*, 2003]. Interestingly, Rin2 and Rin3 have also been shown to bind Rab5[GTP], potentially merging the functions of Rabex5:Rabaptin5 complex in a single polypeptide chain [Kajiho *et al.*, 2003]. Nonetheless, in contrast to Rabex5, the regulatory interaction networks of these

GEFs remain largely unknown, which limits our understanding of GEF-specific Rab5 activation mechanisms.

1.3.3 Rab5 GAP: RabGAP-5

Rab5 has a reasonably high intrinsic GTP hydrolysis rate [Simon *et al.*, 1996a], which probably makes GAPs less crucial in its spatiotemporal cycling [Barr and Lambright, 2010]. Despite, RN-tre and RabGAP-5 (also RUTBC3, SGSM3 and CIP85) are two Rab5-specific GAPs, which might regulate distinct Rab5 signaling cascades in space and time [Pfeffer, 2005]. Of the two, RabGAP-5 has higher GTPase promoting activity and can localize to EEs through interactions with cargo proteins [Haas *et al.*, 2005]. It is a 85 kDa protein, consisting of C-termainal RUN and SH3 domains that are important in its localization and a TBC catalytic domain, which enhances Rab5 GTPase activity by 3-fold [Haas *et al.*, 2005]. Thus, it is regarded as the primary Rab5 GAP, which regulates the amount of endosomal tethering and fusion.

1.3.4 Rab5 activation signaling network

The composition of a minimal Rab5 activation network is still unknown. For example, the need for a GDF, cross-linking effectors or GAP have not been tested in physiological setting. Here, I propose that the minimal biochemical module, which results in collective Rab5 activation is composed solely of inactive Rab5:GDI, the Rabex5:Rabaptin5 GEF complex and a membrane support. It is believed that membrane-localized Rabex5 promotes non-linear positive feedback by directly interacting with Rabaptin5, which in turn binds active Rab5 and allosterically upregulates Rabex5. This indirect positive feedback arises from the network circuitry (Figure 1.7B) and could be the basis for ultrasensitive or bistable behavior, which is necessary for collective GTPase activation [Barr, 2013]. These inherent properties would be harnessed by the cell to precisely regulate the emergence of Rab5 active domains and reliably maintain their composition over the EE maturation process, which takes 5-20 min [Wenzel *et al.*, 2018].

Taking a closer look at the prevailing model, the cooperative Rabex5:Rabaptin5 complex drives the positive feedback of Rab5 activation as more GEF moieties are

recruited to the sites with active Rab5, in turn promoting more nucleotide exchange [Lippe *et al.*, 2001; Del Conte-Zerial *et al.*, 2008; Zhu *et al.*, 2010]. Accordingly, the activation is believed to first progress at a basal rate, where the initial active Rab5 population is established and Rabex:Rabaptin5 is not yet fully engaged in the ternary complex [Zhu *et al.*, 2010]. However, with increasing Rab5[GTP] density the positive feedback loop eventually forms. Then, the activation of free Rab5 out-competes GDI re-extraction, progressing at an increasing rate and resulting in collective activation with a dense Rab5 membrane patch. These sites are then signaling hubs for GTPase effectors and downstream events [Zerial and McBride, 2001]. Unfortunately, the Rab5 cascade has been hitherto observed only in the complex environment of cells or cellular extracts [Lippe *et al.*, 2001; Rink *et al.*, 2005; Poteryaev *et al.*, 2010; Zhu *et al.*, 2010; Wenzel *et al.*, 2018], where a direct readout of network state is impossible. As a consequence, the proposed Rab5 activation mechanism is still debated [Kälin *et al.*, 2015; Kälin *et al.*, 2016].

1.3.5 Rab cascade to Rab7 activation

The unique properties of Rab signaling also allow for sequential coupling of small GTPases. In a Rab cascade or conversion, an active Rab recruits the downstream-acting GEF, initiating subsequent pathway steps [Mizuno-Yamasaki *et al.*, 2012]. A well-studied example is the Rab5-Rab7 conversion at early to late endosome transition [Poteryaev *et al.*, 2010; Kinchen and Ravichandran, 2010]. There, active Rab5 interacts with Mon1:Ccz1, which is a Rab7 GEF [Kinchen and Ravichandran, 2010; Langemeyer *et al.*, 2020]. Furthermore, Mon1 has been shown to displace the Rab5 GEF Rabex5, facilitating the transition from Rab5 to Rab7 positive endosomes [Poteryaev *et al.*, 2010]. At the same time, Rab5 recruits PI3P kinase Vps34 – generating PI3P lipids that also recruit Mon1. Thus, the exact timing of Rab5-Rab7 switch depends on the balance between Rab5:Rabaptin5:Rabex5 positive- and Rab5:Mon1:Ccz1 negative feedback [Vartak and Bastiaens, 2010], which is likely tipped by PI3P or related coincidence signal. This sequential interplay between the GTPases represents a well preserved regulatory mechanism [Mizuno-Yamasaki *et al.*, 2012], which the cells use to coordinate Rab activities. Nonetheless, the proposed link between the spatiotem-

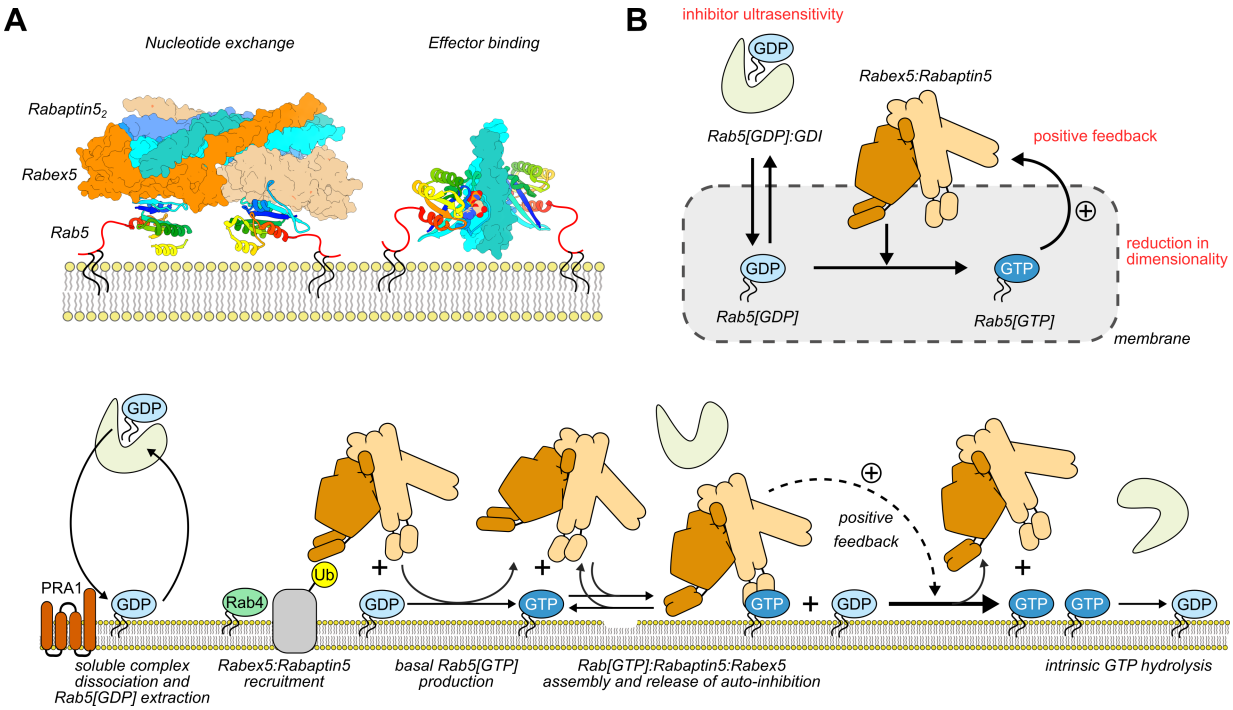

Figure 1.7: **Minimal Rab5 activation network.**

(A) Crystal structure of Rab5:Rabex5:Rabaptin5 and Rab5:Rabaptin5 complexes with membrane representation. Left: The asymmetric unit of ternary complex during nucleotide exchange contains a dimer supercomplex, where nucleotide-free Rab5 is bound by Rabex5 and Rabaptin5 dimer fragments. Rabex5 N-terminal domains and Rabaptin5 Rab5 binding domains (RBD) are not visible. PDB ID: 4Q9U [Zhang *et al.*, 2014]. Right: Rabaptin5 fragment forms a coiled-coil dimer, which can cross-link two Rab5[GMP-PNP]. The Rab5 hypervariable region and geranylgeranyl chain representations were drawn by hand. PDB ID: 1TU3 [Zhu *et al.*, 2004]. **(B)** Model of minimal Rab5 activation network. Top: simple circuit with possible sources of non-linear regulation in red. Bottom: possible events in network switching. Rabex5:Rabaptin5 is first localized to early endosome membrane, where it activates Rab5 at basal rate. After assembly of Rab5[GTP]:Rabaptin5:Rabex5 complex, positive feedback enhances Rab5 activation. Finally, intrinsic Rab5 GTPase hydrolyses GTP and Rab5 is extracted by GDI.

poral dynamics of Rab5 activation and Rab7 recruitment is yet to be mechanistically confirmed and characterized. *In vitro* reconstitution offers a possible approach to elucidate biochemical network properties using physiological conditions in well-defined experimental setting [Liu and Fletcher, 2009; Langemeyer *et al.*, 2020].

1.4 *In vitro* reconstitution

The living cell is a wonderful self-organized system with over $9{\cdot}10^9$ moving parts [Sims and Allbritton, 2007]. Naturally, there is no hope of understanding the intricate workings of the whole cell at once, but we can re-build individual biochemical networks from bottom-up and dissect their function one by one [Fletcher, 2016]. This is the main motivation of the booming field of bottom-up synthetic biology, which relies on *in vitro* reconstitution to understand living processes by rebuilding them under controlled conditions with purified components. The modular nature of cellular organization [Hartwell *et al.*, 1999; Rives and Galitski, 2003] permits reconstitution of individual signaling networks that are composed of just a few biological parts. This way, it is possible to examine and understand mechanistic details of living systems, which otherwise remain obscured in intact cells. The final goal of bottom-up synthetic biology is the reconstitution of a fully functional living cell from characterized parts – bridging the divide between living and non-living matter [Göpfrich *et al.*, 2018].

The term *synthetic biology* dates back over a century when Stéphane Leduc published La Biologie Synthétique (The Synthetic Biology) in 1912 [Leduc, 1912]. In his work, Leduc recognizes that the natural world is governed by physical and chemical laws, which can be harnessed experimentally to understand processes like development and growth. He proposed to use the method of synthesis in order to re-assemble living systems from bottom up – a notion that is nicely captured in Richard Feynman's quote "That which I cannot create, I do not understand." and is now known as *in vitro* reconstitution. The reconstruction of cellular networks combines expertise from cellular and molecular biology, biochemistry, biophysics and mathematical modeling to advance the pure reductionist approach of looking at individual components in isolation as has been done in classical biochemical studies. By assembling known components together and inspecting the biological network as a single functioning unit, important

lessons on underlying mechanisms can be learned. At the same time, emergent behavior – where the network's response cannot be predicted from the characteristics of its constituents – can be revealed under defined conditions *in vitro* [Ganzinger and Schwille, 2019]. Of course, there are obvious caveats to the investigation of re-built and engineered circuits. The synthetic *in vitro* reconstitution cannot match the biological context and conditions *in vivo*, but it can offer a useful platform to build mathematical models, which help us better understand living processes [Fletcher, 2011]. What is more, the defined and controlled conditions in an *in vitro* reconstitution study allow direct application of simulation-based hypotheses, which is often not possible in *in vivo* experiments. This way we can develop detailed mechanistic insights and dispel alternative interpretations of complex biological phenomena [Fletcher, 2011].

Early on, reconstitution studies focused on cytoskeleton and molecular motors. For example, Szent-Györgyi and Staub identified the biochemical components of actomyosin fibers and reconstituted muscle contraction with ATP *in vitro* in 1940s [Liu and Fletcher, 2009]. This seminal work eventually led to cell-free investigation of cytoskeleton polymerization and reconstitution of self-organizing actomyosin structures like contractile rings, asters and active mesh-like networks [Backouche *et al.*, 2006]. Moreover, biochemical in vitro reconstitution was crucial in discovery of microtubule polymerization and dynamic instability in 1980s [Mitchison and Kirschner, 1984], which is the underlying mechanism of microtubule organization in cell division and morphogenesis. This lay the foundations to *in vitro* reconstitution of the mitotic spindle [Nguyen *et al.*, 2014] from *Xenopus* cell extracts that lead to unparalleled biochemical and biophysical investigation of cell division machinery. On the other hand, reconstitution of organelle transport from cell lysates along microtubules *in vitro* lead to the discovery of kinesin motor proteins [Vale *et al.*, 1985], demonstrating the power of combining bottom-up and top-down experimental approaches. This discovery in combination with the adoption of fluorescent labeling and total internal reflection fluorescence (TIRF) microscopy opened up new avenues in real-time and single-molecule investigation of reconstituted systems [Vale *et al.*, 1996]. Recently, this technique was utilized to confirm the hypothesized mRNA transport on kinesin motors along microtubule tracks *in vitro* [Baumann *et al.*, 2020] and the dynamic shrinkage and growth of microtubules was determined down to nanometer and sub-second resolution using microfluidic flow

chambers [Duellberg *et al.*, 2016]. This versatile microfluidic technology now drives the production of artificial cellular compartments and endomembrane systems [Göpfrich *et al.*, 2018] *in vitro*. For example, microtubule asters were rebuilt in water-in-oil droplets form purified tubulin and kinesin motors to examine self-organization of active networks in confined cell-like compartments [Juniper *et al.*, 2018]. While both actin, myosin and tubulin were first identified *in vivo* and characterized *in vitro*, it was the reconstitution experiments that eventually lead to conceptual advances and the appreciation of self-organization principles in cytoskeleton cell biology. It turns out that exact protein ratios, boundary conditions and confinement greatly influence the state of biochemical systems – a notion that was fully revealed only by outlining the parameter landscapes through *in vitro* reconstitution [Ganzinger and Schwille, 2019].

Outside the cytoskeleton field, with the advances in recombinant protein purification [Kalinin *et al.*, 2001; Wu *et al.*, 2010; Huang *et al.*, 2019] and imaging, the membrane-localized processes became particularly well-suited for *in vitro* reconstitution of larger signaling networks [Fletcher, 2016]. The traditional biochemical test tube experiments typically describe the average behavior of the reconstituted system, without the important spatial information. On the other hand, light microscopy methods allow direct examination of system's spatial organization in real time [Liu and Fletcher, 2009] – capturing dynamic phenomena in cell signaling like protein recruitment, redistribution and pattern formation on membrane surface [Loose and Schwille, 2009; Loose *et al.*, 2011], bilayer deformation [Ganzinger and Schwille, 2019], phase separation [Alberti *et al.*, 2019] and nanodomain formation [Janosi *et al.*, 2012]. The biomimetic membranes like large/giant unilamellar vesicles (LUV and GUVs) and supported lipid bilayers (SLBs) are readily available [Ganzinger and Schwille, 2019] and allow direct high signal-to-noise activity readouts with fluorescent microscopy. Particularly, SLB can be prepared by fusing synthetic vesicles on clean microscopy coverslips. In combination with TIRF microscopy the labeled purified proteins can be visualized down to single molecule level on the flat 2D SLB surface [Nguyen *et al.*, 2015]. This precise control over experimental conditions and membrane binding-sensitive readout allows detailed biophysical examination of reconstituted reaction-diffusion systems on membrane support. For example, by controlling the composition of biochemical networks on SLB, self-organized emergent behavior was characterized in bacterial polarity [Loose

et al., 2008] and division machinery [Loose and Mitchison, 2014], cytoskeleton dynamics [Köster *et al.*, 2016], ESCRT-III membrane deformation [Chiaruttini *et al.*, 2015] and clathrin coat assembly [Saleem *et al.*, 2015], dynamin vesicle fission [Pucadyil and Schmid, 2008], T-cell receptor signaling [Su *et al.*, 2016], immunological synapse assembly [Mossman, 2005] and phosphatidylinositol phosphate lipid cycles [Hansen *et al.*, 2019]. Particularly, reconstitution of bacterial polarity machinery revealed that the simple MinD-MinE interaction network self-organizes into stunning periodic traveling waves on the SLB [Loose *et al.*, 2008]. On the other hand, a colossal reconstitution of T-cell receptor signaling and downstream actin filament assembly with 12 purified protein components highlighted the importance of phase separation in signal generation and transmission on the plasma membrane [Su *et al.*, 2016]. Similarly to the presented examples, small GTPase regulation also requires membrane support. As such, it is particularly well suited for *in vitro* reconstitution studies.

1.4.1 Reconstituting small GTPase signaling

Despite the interest in *in vitro* examination of small GTPase signaling and regulation, the posttranslational lipid modifications, which make proteins insoluble in aqueous buffers and complicate the purification of native forms greatly hindered the adoption and progress of systemic reconstitution studies. As a consequence, the GTPase regulators GEFs and GAPs were characterized exclusively on bacterially expressed Ras-like proteins (without lipid anchors). This also means that the role of biological membranes and solubilization factors like REP and GDI still remains under-explored. What is more, the known GEF and GAP activities were determined in chemical equilibrium, without the dynamic state transitions of small GTPases through GTP consumption [Haas *et al.*, 2005; Yoshimura *et al.*, 2010; Langemeyer *et al.*, 2014; Kiontke *et al.*, 2017]. Consequently, emergent and biologically-relevant out-of-equilibrium properties of small GTPase regulation are yet to be determined. To bridge this gap, the underlying regulatory mechanisms were deduced indirectly by correlating the *in vitro* findings with *in vivo* localization and deletion effects on cell physiology.

Another experimental work-around to the lipid anchor-associated complications was the small GTPase membrane immobilization through recombinant His-tag fusion and

use of Ni^{2+}-NTA conjugated synthetic lipids. This way, the effect of reduction in dimensionality and spatiotemporal dynamics became apparent [Peurois *et al.*, 2017; Coyle and Lim, 2016; Iversen *et al.*, 2014; Huang *et al.*, 2019]. However, while simplifying the experimental setup and revealing effector recruitment as a readout function, the immobilized proteins are not sequestered by GDI and allowed to cycle between the solution and lipid bilayer – missing on two basic hallmarks of GTPase networks. We can only assume that the dynamic out-of-equilibrium network responses are vastly different when the small GTPases are allowed to transition between the 2D membrane surface and the 3D medium.

Only recently full-length lipid modified Arfs [Stalder *et al.*, 2011] and Rabs [Thomas and Fromme, 2016; Thomas *et al.*, 2019; Langemeyer *et al.*, 2018; Langemeyer *et al.*, 2020] were included in *in vitro* reconstitution. Importantly, these studies identified the lipid bilayer as a crucial component in lipid-modified small GTPase signaling, where spatiotemporal GEF recruitment triggers GTPase activation. What is more, GEF recruitment by active GTPase can initiate positive feedback loop, resulting in fast and robust acttivation dynamics [Stalder and Antonny, 2013]. Yet, a systemic reconstitution of the full out-of-equilibrium GTPase cycling network under physiological conditions is still missing.

In vitro reconstitution using purified components and cell lysates played a major role also in Rab5 activation network discovery and characterization. In 1990s, the main actors of endocytic membrane fusion machinery were identified: Rab5, GDI, Rabex5 and Rabaptin5 [Horiuchi *et al.*, 1997; Lippé *et al.*, 2001]. These early reconstitution studies focused on the functional roles of protein components in endosomal system, resulting in reconstitution of vesicle fusion [Ohya *et al.*, 2009] and tethering [Murray *et al.*, 2016]. What is more, reconstitution of endosomal fusion with partly purified components identified Rabaptin5-mediated Rabex5 recruitment as a possible mechanism in Rab5 activation positive feedback and Rab membrane domain assembly [Zerial and McBride, 2001], which were recently imaged *in vivo* [Franke *et al.*, 2019]. Based on these breakthroughs, we can hypothesize on the biochemical composition of a minimal signaling module, which is suited further *in vitro* examinations (see Section 1.3.4). During the preparation of this thesis, exciting *in vitro* reconstitution studies looked at Rab5 [Cezanne *et al.*, 2020] and Rab7 [Langemeyer *et al.*, 2020] activations. By reconstitut-

ing Rab5 activation network on silica beads, Cezanne *et al.* confirm the composition of a minimal Rab5 activation network and observe that the endosomal lipids can promote emergence of Rab nanoclusters [Cezanne *et al.*, 2020]. Using a similar *in vitro* reconstitution platform, Langemeyer *et al.* identify the Rab7 GEF complex Mon1:Ccz1 as a Rab5 effector that could initiate the Rab5-Rab7 cascade in early- to late endosome maturation [Langemeyer *et al.*, 2020]. Nonetheless, the mechanistic details of Rab activation and the existence of positive feedback remained unaddressed. Consequently, a systematic *in vitro* reconstitution of a Rab5 activation network could answer these pressing questions and open new avenues for downstream Rab7 regulation.

This work focuses on *in vitro* reconstitution of a minimal Rab5 activation network using full length components. By systematically investigating the dynamic system switching on the SLB, we are able to evaluate network regulatory motifs (including positive feedback) and build a mathematical model, which can reliably predict network behavior under different conditions.

2 Aims and open questions

Great advances in imaging and molecular biology techniques in recent years allowed us to track Rab5 localization and activity in living cells [Rink *et al.*, 2005; Kitano *et al.*, 2008; Li *et al.*, 2015; He *et al.*, 2017; Wenzel *et al.*, 2018]. As a consequence, we have a fairly good understanding of the processes and binding partners Rab5 is involved with. What is more, Rab5 has been identified as the principal organizer of the whole endo-lysosomal compartmental network [Zeigerer *et al.*, 2012], where it directly interacts with over 30 effectors in its active GTP-bound state [Christoforidis *et al.*, 1999]. However, the traditional *in vivo* approaches are unable to assay the underlying mechanisms in GTPase regulation due to the overwhelming complexity and unclear functional readouts in cells. That is why a systematic characterization of Rab5 activation network using pure components under controlled conditions is needed. In order to ensure physiological relevance of the synthetic experimental system a bottom-up network reconstitution with full length and posttranslationally modified components is needed.

In this thesis, I use *in vitro* reconstitution to apply systemic analysis on Rab5 activation switch network. Although Rab5 discovery dates back to 1990 [Chavrier *et al.*, 1990], a series of open questions remain regarding its regulation and network composition. Principally, the *in vitro* use of non-prenylated small GTPases has prevented the evaluation of GDI-bound Rab activation. Consequently, the role of biological membranes in Rab activity cycling and self-organization remains unknown. It is believed that the proposed positive feedback in Rab5 activation is critical for the generation of membrane-bound Rab domains that serve as signaling hubs in the generation, fusion and maturation of endosomes [Zerial and McBride, 2001; Franke *et al.*, 2019; Cezanne *et al.*, 2020]. Nonetheless, this positive feedback and spatial self-organization

have not been directly demonstrated. Here, I address these open questions by using native purified components in combination with glass supported lipid bilayer and surface-sensitive fluorescence microscopy:

1. *The composition of a minimal Rab5 activation network remains unknown.* Naively, one would expect that Rab5:GDI and Rabex5 represent the minimal system, which supports Rab5 activation. However, the GDI-mediated sequestration of inactive GTPases raises concern whether GEF alone can mediate sufficient nucleotide exchange to achieve biologically relevant high-density protein domains on the bilayer. So far, the Rabex5 nucleotide exchange activity was characterized only on bacterially expressed Rab5 without lipid modifications [Delprato and Lambright, 2007; Langemeyer *et al.*, 2014]. Using prenylated Rab5 as substrate, GDI markedly inhibits activation by Rabex5:Rabaptin5 complex [Horiuchi *et al.*, 1997]. This inhibition was relieved with isolated clathrin-coated vesicles, suggesting that an additional factor like GDF is needed for efficient nucleotide exchange on Rab5:GDI. PRA1 was identified as possible candidate [Sivars *et al.*, 2003] and was also included in previous *in vitro* functional assays [Ohya *et al.*, 2009]. The need for GDF in Rab activation was since disputed *in vivo* [Blümer *et al.*, 2013], adding to the uncertainty. My aim is to evaluate the necessity of PRA1 and Rabaptin5 in Rab5:GDI activation and potentially identify additional factors, which are needed for robust network activity switching.

2. *The role of membrane in Rab signaling remains unexplored.* For similar Rho and Arf small GTPases, a substantial increase in GEF activity on membrane support is observed [Peurois *et al.*, 2018]. Thus, membranes play an active and possibly necessary role in small GTPase regulation by providing coincident molecular signals and a reaction platform for lipidated proteins. I investigate the role of biological membranes in Rab5 regulation by reconstituting the activation network on SLB, which can be modified in lipid composition and protein decoration.

3. *Does the GEF complex recruitment lead to positive feedback and cooperativity in Rab5 activation?* Since the observation that Rab5 GEF Rabex5 forms a complex with effector Rabaptin5, a positive feedback loop in GTPase activation was proposed [Horiuchi *et al.*, 1997; Lippé *et al.*, 2001; Zerial and McBride, 2001] and

widely accepted [Mizuno-Yamasaki *et al.*, 2012]. Nevertheless, a cooperative response in Rab5 switching, which could support such claims, was not demonstrated. Additionally, Rab5-mediated Rabex5:Rabaptin5 endosome recruitment might not contribute to Rab5 activation at all [Kälin *et al.*, 2015]. Consequently, we cannot know whether GEF recruitment results in positive feedback or if it only contributes to co-localization. Using purified components and systematic parameter titration, I am able to uncover the underlying ultrasensitivity in Rab5 activation and identify some if its mechanisms.

4. *Rab5 activation on a system level has not been characterized.* So far, the Rab molecular switch was determined only on atomic scale, while emergent network behavior remains unknown. Accordingly, a description of signal input-output relationship in Rab regulation is still missing. Using *in vitro* reconstitution, I aim to observe network response profile and determine possible tuning parameters [Coyle, 2016]. This information will be valuable to understand Rab regulation also in cellular context, where multiple factors can modulate signaling cascades in space and time.

5. *Collective activation in space and time has not been directly observed.* Finally, I would like to determine whether the reconstituted network architecture supports emergent Turing-like spatial patters [Gierer and Meinhardt, 1972] without pre-existing cues. For example, Rho GTPase membrane polarization and signaling wave propagation is important in cell morphology, motility and division [Altschuler *et al.*, 2008; Tan *et al.*, 2020]. Therefore, it would be interesting to know if such collective behaviors are also possible for Rab regulatory circuits.

By addressing these questions, our work significantly contributes to the understanding of Rab5 and GTPase regulatory networks in general. Hitherto the small GTPase *in vitro* reconstitution studies relied on truncated mutants and non-physiological membrane immobilization of key network components [Iversen *et al.*, 2014; Coyle and Lim, 2016]. This was largely due to the difficulties associated with low yields and purification of full-length and lipid-modified proteins. Consequently, this prevented a detailed examination of Rabs and other Ras-related small GTPases under native cycling conditions, where proteins are allowed to transition between the solution and lipid bilayer

with GDP/GTP exchange. In the presented work we were able to observe collective self-organization of a small GTPase network *in vitro* for the first time by using full length purified proteins with native posttranslational modifications, including Rab geranylgeranylation. This is the first systematic examination of the parameter landscape in a Rab regulatory network under controlled physiological conditions. Importantly, the techniques and identified system properties can be further applied to other biochemical circuits, particularly the Ras, Arf and Rho small GTPase regulatory networks.

The following chapters present detailed descriptions of methods and experimental results, which can serve as a foundation for *in vitro* studies on the expanded Rab5 regulatome and crosstalk with other signaling pathways like Rab4, Rab7 and Arf1. The key network properties, which are identified in synthetic biomimetic systems like the one presented for Rab5 here, should later be confirmed under more complex conditions. For example, the *Xenopus* egg cell extracts [Nguyen *et al.*, 2015] are readily available and provide the unique environment and factors of cellular cytoplasm. Finally, the consistency and significance of observed emergent GTPase collective behavior should be confirmed *in vivo*. Excitingly, the recent years have offered great advances in genetic editing, single particle tracking, super resolution and cryo-electron microscopy that promise to open new avenues in system's biology, where the principles of bottom-up *in vitro* reconstitution could be applied to examination of living cells in real time.

3 Experimental methods

3.1 Materials

Table 3.1: **Table of key reagents and resources.**

Material	Source	Identifier
Bacterial strains		
E. coli BL21(DE3)	New England BioLabs	C2527
E. coli BL21(DE3)-RIL [pRK793]	Addgene	8827
E. coli DH10EMBacY	F. Garzoni (EMBL Grenoble)	/
E. coli DH5α	Thermo Fisher Scientific	18265017
Insect cell strains		
HighFive	Thermo Fisher Scientific	B85502
Sf9	Oxford Expression Technologies	600100
Reagents		
2-mercaptoethanol	Sigma Aldrich	M6250-100ML
Biorad Protein Assay Dye	Biorad	5000006
catalase	Sigma Aldrich	C40
CF488A maleimide	Sigma Aldrich	SCJ4600016-1UMOL
CHAPS hydrate	Sigma Aldrich	C3023-5G
CLPETGG peptide	Biomatik	/

(Continued on the next page)

(Continuation)

Material	Source	Identifier
cOmplete Protease Inhibitor Cocktail	Roche	5056489001
D-desthiobiotin	Sigma Aldrich	D1411-500MG
DiD	Sigma Aldrich	D7757
DiO	Sigma Aldrich	D4292
DMPE-PEG2000	Avanti Polar lipids	880150C
DNase I	Thermo Fisher Scientific	90083
DOGS-NTA	Avanti Polar lipids	790404C
DOPC	Avanti Polar lipids	850375C
DOPS	Avanti Polar lipids	840035C
DTT	Sigma Aldrich	D5545, D0632
ESF 921 serum free insect media	Expression Systems	500304
Express Five SFM (1X)	Thermo Fisher Scientific	10486-025
GDP	Sigma Aldrich	G7127
glucose oxidase	SERVA	22778.01
glycerol	Sigma Aldrich	G5516-1L
GMPPNP	Jena Bioscience	NU-401-10
GTP	Jena Bioscience	NU-1012-1G
HisPur Ni-NTA resin	Thermo Fisher Scientific	88221
hydrogen peroxide (H_2O_2)	Sigma Aldrich	216763-500ML-M
IGEPAL CA-630	Sigma Aldrich	I8896-50ML
imidazole	Sigma Aldrich	I2399
Insect GeneJuice	Merck Millipore	71259-3
IPTG	Bartelt	6.259 683
L-Glutamine	Thermo Fisher Scientific	25030024
mant-GDP	Jena Bioscience	NU-204S
methyl-β-cyclodextrin	Sigma Aldrich	332615
Phusion HF DNA polymerase	New England BioLabs	M0530S
Pierce BCA Protein Assay Kit	Thermo Fisher Scientific	23227

(Continued on the next page)

(Continuation)

Material	Source	Identifier
PMSF	Sigma Aldrich	P7626
potassium acetate (KOAc)	Sigma Aldrich	P1190-500G
Protino Ni-IDA Resin	Macherey Nagel	745210.3
Q5 HF DNA polymerase	New England BioLabs	M0491S
sodium chloride (NaCl)	Sigma Aldrich	S3014
sulfo-Cy5 (sCy5)-maleimide	Lumiprobe	23380
sulfuric acid (H_2SO_4)	Merck Millipore	1007311000
Taq DNA ligase	New England BioLabs	M0208L
TCEP	Sigma Aldrich	C4706
Triton X-100	Sigma Aldrich	X100-100ML
Trolox	Sigma Aldrich	238813
Consumables		
Amicon Ultra-2 concentrators	Millipore	Z740164-24EA
black 384-well NBS microplate	Corning	3820
coverslips 24×50 mm, no. 1.5H	Marienfeld	107222
LiposoFast 100 nm membrane	Sigma Aldrich	Z373419-50EA
Norland optical adhesive 63	APM Technica	284239
PCR tubes (reaction chambers)	Biozym Scientific	710920
PD10 desalting columns	GE Healthcare	GE17-0851-01l
Pur-a-dialyzer dialysis kit	Sigma Aldrich	purg60010-1kt
sticky-Slide VI 0.4	ibidi	80608
Vivaspin 20 concentrators	Sartorious	Z614599
Zeba desalt spin columns	Thermo Fisher Scientific	PIER89882
Purification columns		
HiLoad 16/600 Superdex 200 PG	GE Healthcare	28989335
HiLoad 16/600 Superdex 75 PG	GE Healthcare	28989333
MonoQ 5/50 GL	GE Healthcare	17516601
StrepTrap HP 1 mL	GE Healthcare	28907546
StrepTrap HP 5 mL	GE Healthcare	28907547

(Continued on the next page)

(Continuation)

Material	Source	Identifier
Superdex 200 Increase 10/300	GE Healthcare	28990944
Superdex 75 Increase 10/300	GE Healthcare	29148721
Plasmids		
pet30b-7M SrtA	Addgene	51141
pRK793	Addgene	8827

3.2 Cell cultures

3.2.1 Bacterial cultures

For routine molecular cloning techniques and glycerol stock preparation, we used DH5α *E. coli* strain. Conversely, BL21(DE3) *E. coli* was used for bacterial cell expression of recombinant proteins. To generate recombinant bacmids, we used DH10EMBacY bacterial strain. Unless specified differently, *E. coli* cells were grown at 37 ℃ in LB medium or on LB-agar plates, supplemented with the corresponding antibiotic. For recombinant protein expression, we routinely used rich Terrific broth (TB) medium.

3.2.2 Insect cell cultures

For baculovirus preparation and Rab protein expression, Sf9 *S. frugiperda* insect cell culture was used. Alternatively, the *T. ni* HighFive insect cell strain was used for expression of some proteins. The insect cell suspension cultures were grown at 27 ℃ and 127 rpm. The Sf9 cells were grown in ESF 921 (Expression Systems) culture medium, supplemented with 1:100 penicillin and streptomycin (Sigma) dilution. The HighFive cells were grown in Express Five SFM (Gibco) medium, supplemented with 16 mM L-glutamine (Gibco). The Sf9 cells were split to $0.5 \cdot 10^6$/mL in fresh medium up to 30th passage and maintained at 4-6$\cdot 10^6$/mL maximum density with $>$ 90 % viability. Similarly, the HighFive cells were split to $0.3 \cdot 10^6$/mL and let to grow until 2-4$\cdot 10^6$/mL density.

3.3 Molecular cloning

3.3.1 Competent *E. coli* cell preparation

We prepared chemically competent *E. coli* cells by harvesting a growing bacterial culture in the early log phase with OD_{600} 0.3-0.4. Cells were later washed with ice cold 0.1 M $CaCl_2$ and finally frozen in 0.1 M $CaCl_2$ and 15 % glycerol with liquid nitrogen. Aliquots of chemically competent bacteria were stored at –80 °C.

3.3.2 *E. coli* transformation

Competent DH5α and BL21(DE3) *E. coli* cells were transformed with plasmid DNA using heat shock method. First, frozen competent cell aliquots were thawed on ice for 10 min. DNA was then added and the suspension was left on ice for 20 min. To generate heat shock, the cells were incubated at 42 °C for 45 seconds and returned to ice for 2 min. Next, 1 mL SOC medium was added to the cell suspension and cells were incubated at 37 °C for 1 hour with shaking. The transformed bacteria were finally collected by centrifugation at 12,000 rcf for 30 s and spread on a LB-agar plate, supplemented with the appropriate antibiotic. The agar plates were incubated at 37 °C overnight, at which point distinct bacterial colonies developed. Similarly, the chemically competent DH10EMBacY cells were transformed with heat shock and left to recover in 1 mL SOC at 37 °C for 4 h to ensure sufficient expression of the antibiotic resistance genes. We spread the transformed DH10EMBacY culture on BAC plates (LB-agar + 10 µg/mL tetracyclin, 50 µg/mL kanamycin, 7 µg/mL gentamycin, 100 µg/mL X-gal, 40 µg/ml IPTG) and incubated the plates in dark at 37 °C for up to 2 days.

3.3.3 Sf9 transfection

Sf9 cells were transected with recombinant bacmid DNA using liposome-based Insect GeneJuice (Merck Millipore) reagent. First, Sf9 cells were seeded at $0.8 \cdot 10^6$ into a 6-well cell culture plate and left to adhere for 1 h. To prepare the transfection mixture, 5 µg of recombinant bacmid DNA were diluted in 100 µL of antibiotic-free ESF 921 medium and mixed dropwise with 10 µL Insect GeneJuice in 100 µL medium. The transfection

mixture was incubated for 20 min at room temperate before continuing to the next step. Before transfection, the adhered Sf9 cells were washed with antibiotic-free ESF 921 medium. The transfection mixture was diluted in 1 mL of growth medium and spread dropwise on washed cells. The transfection reaction was left to proceed at 27 ℃ for 4 h. At that point, the growth medium with transfection reagent was replaced with 3 mL of ESF 921 medium, supplemented with penicillin and streptomycin. The adherent transfected cells were incubated in the 6-well plates at 27 ℃ until V0 recombinant baculovirus harvest, usually 3-5 days post-transfection. We could observe YFP reporter gene expression from pFL or pFastBac bacmid backbone under inverted widefield microscope with LED or mercury fluorescent lamp to confirm successful transfection and baculovirus production.

3.3.4 Polymerase chain reaction

The polymerase chain reaction (PCR) was run using the peqSTAR(PEQLAB) thermo cycler. Depending on the needs, we used either a high fidelity DNA polymerase or a mix of robust Taq and Deep Vent polymerases (New England BioLabs). Particularly, the high-fidelity DNA polymerase Q5 was used for preparation of DNA fragments in molecular cloning, according to the manufacturer's protocol. We used OneTaq blend of DNA polymerases for colony PCR and recombinant bacmid quality checks.

3.3.5 Isothermal assembly

Recombinant DNA plasmids were prepared using Gibson isothermal assembly cloning technique [Gibson *et al.*, 2009]. To this end, we used a Gibson reaction mastermix, which we prepared ourselves. To prepare the 1.33× mastermix, 320 µL of 5× isothermal reaction buffer (25 % PEG-8000, 500 mM Tris-HCl pH 7.5, 50 mM $MgCl_2$, 50 mM DTT, 1 mM dNTPs, 5 mM NAD) were supplemented with 1.2 µL 10 U μL^{-1} T5 exonuclease (Biozym), 160 uL 40 U μL^{-1} Taq ligase (New England BioLabs), 20 µL 2 U μL^{-1} Phusion DNA polymerase (New England BioLabs) and 700 µ Milli-Q water. This reaction mastermix was then aliquoted in 15 µL and stored at –20 ℃ for up to a year. For the isothermal DNA assembly, 5 uL of DNA fragments (50-100 ng each) were mixed

with 15 µL 1.33× mastermix on ice and incubated at 50 ℃ for 45 min. The reaction mixture was then used to transform DH5α competent cells.

3.3.6 DNA fragment preparation

Double stranded DNA fragments for isothermal assembly reactions were either ordered as synthetic pieces of DNA (”gBlocks”) or obtained with PCR. In general, DNA fragments were designed to have 25-35 bp overlap to ensure robust DNA assembly.

Nucleotide sequences

Details on key DNA constructs are given in Table 3.2 below. For Rab5 regulatory networks components, we used *Xenopus laevis* orthologues, which should be most active at room temperature and can be potentially coupled with *X. laevis* egg cell extract experiments.

Table 3.2: **Table of DNA construct properties.**

Name	Fusion	Modification	Backbone	UniProt ID
GDI	(5’): His_6-TEV	/	pFastBac	Q642Q8
His_{10}-Ub	(5’): His_{10}-3C	/	pCoofy18	Q6GQF3
PRA1	(5’): TwinStrep-TEV-G_4	/	pET28a	Q640E6
Rab5(Q80L)-His_{10}	(5’): TwinStrep-TEV-G_4, (3’): His_{10}	Q80L	pET28a	/
Rab5-His_{10}	(5’): TwinStrep-TEV-G_4, (3’): His_{10}	/	pET28a	/
Rab5A	(5’): TwinStrep-TEV-G_4	/	pFL	A0A1L8FRH6
Rab5B	(5’): His_6-TEV-G_4	/	pFL	A0A1L8HHX1
Rabaptin5	(5’): TwinStrep-TEV	/	pFL	A0A1L8H8K4
Rabex5	(5’): TEV	/	pFL	Q4V7X1
Rabex5 (D314A)	(5’): TEV	D314A	pFL	/
RabGAP-5	(5’): TwinStrep-3C	/	pFL	A6H8I2

(Continued on the next page)

(Continuation)

Name	Fusion	Modification	Backbone	UniProt ID
Δ_{RBD}Rabaptin5	(5'): TwinStrep-TEV	Δ(217-319), Δ(807-854)	pFL	/
ΔRabex5	(5'): His_6-TEV-G_4	Δ(1-131)	pFastBac	/

3.3.7 DNA purification

Recombinant DNA was purified from E. coli using established techniques.

Plasmid purification

Plasmid DNA was routinely purified from transformed *E. coli* DH5α using E.Z.N.A. spin column plasmid miniprep kit (Omega Bio-tek) according to the manufacturer's recommendations.

Bacmid purification

A single white colony from BAC agar plate was grown in LB medium with 50 µg/mL kanamycin, 7 µg/mL gentamicin and 10 µg/mL tetracycline overnight. The overnight culture was pelleted by centrifugation at 4,000 rcf for 10 min. The cell pellet was then resuspended in home-made Qiagen P1 buffer (50 mM Tris-HCl pH 8.0, 10 mM EDTA, 100 µg/mL RNase A) and lysed with P2 buffer (200 mM NaOH, 1 % SDS). After 5 min, the lysis was neutralized with N3 Qiagen buffer (4.2 M GndHCl, 0.9 M KOAc, pH 4.8). The suspension was placed on ice for 10 min and centrifuged at 16,000 rcf for 10 min. The supernatant was then incubated with isopropanol for 30 min on ice and centrifuged at 16,000 rcf for 15 min. The precipitated bacmid DNA in the pellet was later washed with 70 % ethanol and centrifuged for 10 min at 16,000 rcf. This step was repeated twice. The ethanol solution was finally removed and the pellet was dried. The bacmid DNA was resuspended in Milli-Q water and stored at 4 °C.

3.3.8 Baculovirus preparation

DNA fragments of recombinant proteins were cloned into pFL [Fitzgerald *et al.*, 2006] or pFastBacHTc plasmid backbones and transformed into DH5α *E. coli*. Next, the expression cassettes were integrated into recombinant bacmid backbones by Tn7 transposition in DH10EMBacY strain. To that end, DH10EMBacY were transformed with pFL plasmids and white colonies from BAC plates were isolated after two days incubation in dark at 37 °C. The recombinant bacmids were isolated using home-made Qiagen Kit buffers according to protocol described in Section 3.3.7 and success of transposition was assayed by PCR using M13 primer pair. Isolated bacmids were used to transfect adherent Sf9 insect cell culture using Insect GeneJuice (Merck Millipore) reagent according to the manufacturer's recommendations. We harvested the V0 baculovirus supernatants 3-5 days after transfection, depending on fluorescence intensity of expressed YFP. 2 mL of V0 virus was used to infect 50 mL Sf9 culture seeded at $1{\cdot}10^6$ cells/mL. Three days after infection, V1 baculovirus stock was harvested by centrifugation at 1,000 rcf for 5 min and stored in dark at 4 °C. V1 virus stock supernatant was later used for infection of recombinant protein expression culture or baculovirus-infected insect cells stock generation.

3.3.9 Glycerol stocks

Glycerol stocks were prepared by mixing a fresh overnight LB media culture of transformed DH5α or DH10EMBacY with 50 % glycerol solution in 1:1 ratio. The cell suspension was then frozen in liquid nitrogen and stored at –80 °C.

3.3.10 Baculovirus-infected insect cells stocks

Baculovirus-infected insect cells (BIICs) stocks were generated from V1-infected Sf9 cell cultures. The infected cells were grown at 27 °C and 127 rpm for 2-3 days before being centrifuged at 1,000 rcf for 10 min, depending on the YFP reporter expression. We harvested the cells before the YFP expression plateaued at maximum intensity. Generally, pellets from 100 mL of cell culture were resuspended in 10 mL of freezing solution containing ESF 921 medium with 10 mg/mL BSA and 10 v/v % DMSO. A 1 mL

cell suspension aliquots were then placed at –20 °C for at least 1 hour, before being stored at –80 °C. A 1 mL BIIC aliquot was subsequently used to infect 400 mL of Sf9 or HighFive cell culture at $1.0 \cdot 10^6$/mL. When the insect cells were infected with BIIC, the recombinant protein expression usually took one day more compared to cells infected with baculovirus supernatant.

3.4 Biomimetic membranes

To reconstitute Rab signaling networks *in vitro*, we used synthetic biomimetic bilayers with defined lipid compositions. Specifically, we used small unilamellar vesicles (SUVs) and supported lipid bilayers (SLBs) as substrates for Rab activation.

3.4.1 Small unilamellar vesicles

Synthetic lipids were ordered as chloroform solutions at Avanti Polar lipids. Phosphoinositides were purchased as lyophilized powder and dissolved in 1:2:0.8 chloroform:methanol:water solution. Lipid stock solutions were covered with argon gas and stored at –20 °C. Small unilamellar vesicles (SUVs) were prepared by mixing the desired lipid composition in glass vials. We used 79.9 % DOPC, 20 % DOPS and 0.1 % DMPE-PEG2000. Next, lipids were dried under nitrogen gas stream and remaining organic solvents were evaporated under vacuum for at least 1 hour. Then, the dried lipids were hydrated in Vesicle buffer (20 mM HEPES-KOH pH 7.4, 150 mM KOAc) to 0.5 mM lipid concentration to produce multilamellar vesicle (MLV) suspension with vortexing. Finally, SUVs were obtained by passing the MLV solution through 5 freeze-thaw cycles in liquid nitrogen and extrusion with 100 nm pore size polycarbonate membrane 21-times (LiposoFast, Avestin). The SUV suspension was stored in the fridge for up to 5 days.

3.4.2 Coverslip treatment and reaction chamber immobilization

We used 24×50 mm coverslips (no. 1.5H, Marienfeld) in our fluorescence microscopy assays with SLB. First, coverslips were cleaned by 1 h incubation in piranha solution (1:3 volume ratio of 30 % H_2O_2, Sigma Aldrich and 98 % H_2SO_4, Merck) and extensive

washing in Milli-Q grade water. The cleaned coverslips were stored in Milli-Q water for up to two weeks. Immediately before use, the coverslips were dried and further cleaned in Zepto B (Diener electronic) plasma oven for 10 min at 30 W under 1 NL/h air flow. We immobilized the microscopy reaction chambers by attaching a cut PCR tube on the cleaned coverslip glass using ultraviolet glue (Norland optical adhesive 63) under 365 nm UV light for 5-10 min. The attached reaction chambers were then ready for SLB preparation.

3.4.3 Supported lipid bilayer preparation

To mimic the intracellular membranes, we prepared supported lipid bilayers (SLBs) on high precision microscope slides (no. 1.5H). The SLBs are made by bursting SUVs with defined composition on clean glass. In this study, we used 79.9 % DOPC, 20 % DOPS, 0.1 % DMPE-PEG2000 and varying amounts of DOGS-NTA[Ni^{2+}] lipids (Avanti Polar Lipids). For the experiments with DOGS-NTA, we decreased the ratio of DOPC proportionally. The produced SUVs were stored at 4 ℃ for up to 5 days. Similarly, we used DOGS-NTA SUVs within 2 days since production. The SLB was formed in immobilized plastic reaction chambers on a clean glass surface by inducing fusion of the SUVs with 3.33 mM $CaCl_2$. The SLBs were left to form for at least 45 min at 37 ℃. Later, the unfused vesicles were washed away with Vesicle buffer, Milli-Q water and reaction buffer.

3.5 Protein expression

3.5.1 Bacterial protein expression

We used bacterial expression systems for routine production of smaller recombinant proteins that do not require posttranslational modifications. We used BL21(DE3) *E. coli* strain in TB medium.

His_{10}-Ub

Ubiquitin cDNA from *X. laevis* was inserted downstream from His_{10} tag and 3C HRV protease site in a pCoofy18 plasmid backbone [Scholz *et al.*, 2013]. The recombinant protein was expressed in BL21(DE3) cells after dilution of an overnight LB culture to OD_{600} 0.05 in TB medium and recovery to OD_{600} 0.8 at 37 °C. The transgene expression was then induced with 0.5 mM IPTG and continued at 30 °C for 5 h. We later harvested the cells and washed them in 1× PBS. The cells were finally pelleted at 4,000 rcf for 10 min and frozen in N_2(l) before storage at –80 °C.

Rab5, Rab5-His_{10}, Rab5Q80L-His_{10}

Unprenylated Rab5A and related mutant proteins from *X. laevis* were expressed in *E. coli* BL21(DE3) from kanamycin resistance-bearing pET28a vector under lacO-regulated T7 promoter. The Rab5 protein was expressed as an N-terminal TwinStrep fusion with a TEV protease cleavage site and Gly_4 linker preceding the Ala2 of Rab5. First, 50 mL of LB broth were inoculated with a colony of transformed BL21(DE3) cells and incubated at 200 rpm and 30 °C overnight. On the following day, 2 L of pre-warmed TB medium were inoculated with the overnight culture to OD_{600} = 0.02 and incubated at 37 °C and 200 rpm. The protein expression was induced at OD_{600} = 0.8 with 0.5 mM IPTG and left to proceed at 30 °C and 200 rpm for 4 h. Finally, cells were harvested by centrifugation at 5,000 rcf for 20 min at 4 °C and resuspended in PBS. After 15 min centrifugation at 4,000 rcf and 4 °C, cell pellet was frozen in liquid nitrogen and stored at –80 °C.

PRA1 expression

X. laevis PRA1 is a transmembrane protein, which was cloned in a pET28a backbone downstream of a TwinStrep purification tag and TEV protease recognition site. Of note, a His_6-SUMO fusion in pTB146 vector backbone failed to express a functional full length protein. An overnight culture of transformed BL21(DE3) cells was used to inoculate TB medium to OD_{600} 0.05 and left to reach OD_{600} 0.8. The PRA1 expression was induced with 0.5 mM IPTG and proceeded at 30 °C for 4 h. We harvested the

cells by centrifugation at 4,000 rcf for 20 min and washed the pellets with 1× PBS. For convenience, we prepared smaller bacterial cell aliquots for later purification as the PRA1 protein could only be used fresh in reconstitution assays. The cells were finally pelleted at 4,000 rcf for 10 min and snap frozen in liquid nitrogen. The frozen pellets were stored at –80 °C.

SrtA 7M expression

Sortase A 7M mutant [Hirakawa *et al.*, 2015] from *Staphylococcus aureus* was obtained on Addgene #51141. The gene is cloned in a pET30b plasmid as a His_6 fusion. An overnight LB culture of transformed BL21(DE3) cells was first diluted to OD_{600} 0.05 in TB medium and incubated at 37 °C until OD_{600} reached 0.6-0.8. SrtA 7M expression was induced with 0.5 mM IPTG and continued at 37 °C for 4 h. The bacterial cells were then harvested by centrifugation at 5,000 rcf and washed with 1× PBS. Finally, the cells were pelleted and frozen in N_2(l) before storage at –80 °C.

TEV(S219V) protease expression

The S219V mutant of tobacco etch virus (TEV) protease with enhanced activity and less self-cleavage [Kapust *et al.*, 2001] was obtained from Addgene (#8827) as pRK793-transformed bacterial strain BL21(DE3)-RIL. The protease was expressed as a self-cleaving MBP fusion from pMal-C2, which revealed a His_6 purification tag. An overnight LB-culture was diluted to OD_{600} 0.05 in TB medium. We expanded the bacterial culture at 37 °Cand induced protein expression at OD_{600} 0.6-0.8 with 0.5 mM IPTG. The expression continued at 30 °C for 3 h to prevent inactivation of the protease due to self-processing. Next, we harvested and washed the cells with 1× PBS before pelleting at 4,000 rcf and freezing in liquid nitrogen.

3.5.2 Insect cell protein expression

To ensure eukarya-specific posttranslational modifications, proteins used in *in vitro* reconstitution assays were mainly expressed using insect cell expression system. We

used either *S. frugiperda* Sf9 or *T. ni* HighFive expression strains, depending on the transgenic protein yield.

GDI expression

We expressed GDI in insect cells to ensure proper folding of the expressed proteins. *X. laevis* RabGDIα cDNA was inserted as a His_6 fusion downstream of a TEV protease recognition site in pFastBac plasmid. The recombinant protein was expressed in High-Five or Sf9 insect cells for 3 or 4 days after baculovirus or BIIC infection, respectively. The expressing cells were infected at $1.0{\cdot}10^6$/mL and grown at 27 ℃ and 127 rpm. Insect cells were later harvested by centrifugation at 1,000 rcf for 10 min and washed with 1× PBS. Finally, the cells were pelleted at 1,000 rcf for 10 min and snap frozen in liquid nitrogen before storage at –80 ℃.

Rab5A expression

For efficient purification of expressed proteins, we included a TwinStrep purification tag with TEV protease cleavage site and Gly_4 linker upstream of codon-optimized *X. laevis* Rab5A cDNA. Rab5 was expressed in Sf9 insect cell system, as production in HighFive resulted in less post-transitionally modified protein. Briefly, a $1.0{\cdot}10^6$ cells/mL Sf9 culture was infected with baculovirus supernatant in 1:100 volume ratio or BIIC. We incubated the infected cells at 27 ℃for 3 to 4 days post-infection at 127 rpm. We harvested the cells at 1,000 rcf for 10 min and washed them with 1× PBS prior to pelleting at 1,000 rcf for 10 min. Finally, insect cell pellets were snap frozen in liquid nitrogen and stored at –80 ℃.

Rab5B expression

The Rab5B isoform, which lacks the geranylgeranylated C-terminal cysteins, was cloned downstream from His_6 and TEV processing site in a pFL vector backbone. Rab5B was expressed in Sf9 insect cells, where $1.0{\cdot}10^6$ cells/mL Sf9 culture was infected with baculovirus supernatant in 1:100 volume ratio. We incubated the infected cells at 27 ℃for 3 days at 127 rpm. We harvested the cells at 1,000 rcf for 10 min and washed

them with 1× PBS before to pelleting at the same settings. Finally, the cell pellets were frozen in liquid nitrogen and stored at –80 °C.

Rabaptin5 expression

Full length Rabaptin5 was expressed from pFL expression cassette in HighFive insect cells as a TwinStrep-TEV fusion. We infected insect cells at $1.0 \cdot 10^6$ cells/mL with harvested baculovirus supernatant in 1:100 ratio. The protein production was left to continue at 27 °C and 127 rpm for three days. The cells were then harvested at 1,000 rpm for 10 min and washed with 1× PBS. Finally, we pelleted the cells and froze them in N_2(l) before storage at –80 °C.

Rabex5:Rabaptin5, ΔRabex5:Rabaptin5, Rabex5:Δ_{RBD}Rabaptin5 and Rabex5(D314A):Rabaptin5 expression

The *X. laevis* Rabex5 and Rabaptin5 variants were expressed from a bicistronic pFL vector. Rabex5 expression was under p10 constitutive promoter control on the (–) strand and a TwinStrep fusion of Rabaptin5 was transcribed downstream from PH promoter. A HighFive or Sf9 insect cell culture was infected either by 1:100 baculovirus supernatant dilution or BIIC. We kept the expressing cells at 27 °C and 127 rpm for three days before harvesting the cells at 1,000 rcf for 10 min. We then washed the cells with 1× PBS and froze the cell pellets after 10 min 1,000 rcf centrifugation in liquid nitrogen. The insect cell pellets were kept at –80 °C until purification.

ΔRabex5 expression

The deletion mutant ΔRabex5 was cloned into pFastBac plasmid as His_6 fusion downstream from a TEV cleavage site. The recombinant protein was expressed in HighFive cells for 3 days at 27 °Cand 127 rpm after infection with baculovirus suspension in 1:100 ratio. We harvested the cells by centrifugation at 1,000 rcf for 10 min and washed them with 1×nPBS. The cells were then pelleted at the same setting and frozen in liquid nitrogen. The frozen cell pellets were kept at –80 °C.

RabGAP-5 expression

RabGAP-5 (SGSM3) from *X. laevis* was inserted into pFL expression cassette as a TwinStrep-3C fusion. The recombinant protein was expressed in HighFive insect cells for 3 days at 27 °C after infection with harvested baculovirus suspension in 1:100 ratio. We harvested the insect cells by centrifugation at 1,000 rcf for 10 min and wash the cells before pelleting and freezing in liquid nitrogen. The cell pellets were stored at –80 °C.

3.6 Protein purification

We used a combination of affinity purification, size-exclusion and ion-exchange chromatography to prepare pure protein components. Amino acid sequences of isolated constructs are listed in Appendix A.1.

3.6.1 GDI purification

X. laevis RabGDI was cloned as a His6-(linker)-TEV-GDI construct in a pFastBac vector. The protein was expressed in Sf9 insect cell culture at 27 °C for 3 days after baculovirus infection. The harvested cell pellets were kept at –80 °C and thawed on the day of purification. The pellets were suspended in Lysis/Wash buffer (20 mM HEPES-NaOH pH 8.0, 500 mM NaCl, 5 mM 2-mercaptoethanol, 10 vol% glycerol) and supplemented with cOmplete EDTA-free protease inhibitor cocktail (Roche), 2.5 U/mL DNase I (Thermo Fisher Scientific) and 1 mM PMSF (Sigma Aldrich). We lysed insect cells using a glass douncer and 1 % IGEPAL CA-630 (Sigma Aldrich). The lysate supernatant was incubated with Protino Ni-IDA (Macherey Nagel) affinity resin after 45 min centrifugation at 60,000 rcf. After extensive washing of the affinity resin, we eluted the purified proteins with 150 mM imidazole in Lysis/Wash buffer. Next, we performed buffer exchange to the Lysis/Wash buffer using a PD-10 desalting column (GE Healthcare). The purification tag was later cleaved off with TEV(S219V) protease (pRK793; Addgene #8827) [Kapust *et al.*, 2001], which was removed by passing the solution over HisPur Ni-NTA resin (Thermo Fisher Scientific). Finally, the purified samples were con-

centrated on Vivaspin 20 concentrators (Sartorius), aliquoted and snap frozen in liquid nitrogen before storage at –80 °C.

3.6.2 His_{10}-Ub purification

X. laevis ubiquitin was cloned as a His_{10} fusion downstream from HRV 3C protease recognition site in a pCoofy18 expression plasmid [Scholz *et al.*, 2013]. The recombinant protein was expressed in BL21(DE3) cells at 30 °Cfor 5 h. First, the frozen cell pellets were thawed and resuspended in Lysis/Wash buffer (50 mM HEPES-NaOH pH 8.0, 500 mM NaCl, 5 mM 2-mercaptoethanol, 10 vol% glycerol), supplemented with cOmplete EDTA-free protease inhibitor cocktail. The resuspended cells were then lysed using a cell disruptor (CF2, Constant Systems Ltd.) and 2.5 U/mL DNase I was added to the suspension. The lysate was cleared by centrifugation at 60,000 rcf and 4 °Cfor 45 min. The collected supernatant was then incubated with 0.5 g of Protino-IDA affinity resin and loaded on a purification column under gravity flow. The column was washed extensively with Lysis/Wash buffer and the purified proteins were eluted with 150 mM imidazole. Finally, the elution buffer was exchanged back to Lysis/Wash buffer using PD-10 desalting columns and the aliquoted samples were snap frozen in liquid nitrogen for storage at –80 °C.

3.6.3 PRA1 purification

PRA1 was expressed for 4 h at 30 °C as TwinStrep-(linker)-TEV-Gly4-PRA1 fusion in BL21(DE3) cells from a pET28a plasmid backbone. First, the cell pellets were resuspended in Lysis buffer (20 mM HEPES-KOH pH 7.8, 300 mM KOAc, 5 mM 2-mercaptoethanol, 10 vol% glycerol), supplemented with cOmplete EDTA-free protease inhibitor cocktail. The cells were lysed using cell disruptor and 1 mM PMSF, 2.5 U/mL DNase I and 5 % Triton X-100 detergent (Sigma Aldrich) were added to the lysate. The transmembrane PRA1 was extracted with the detergent during 1 h incubation at 4 °C with mixing. We isolated the soluble fraction with 45 min centrifugation at 60,000 rcf and 4 °C. The supernatant was then loaded on StrepTrap HP affinity column (GE Healtcare), equilibrated with Purification buffer (20 mM HEPES-KOH pH 7.8, 300 mM KOAc, 5 mM 2-mercaptoethanol, 10 vol% glycerol, 0.1 % Triton X-100) and the bound

proteins were eluted with 2.5 mM D-desthiobiotin (Sigma Aldrich). The pooled fractions were digested with TEV(S219V) protease overnight. The PRA1-detergent complexes were finally purified on Superdex 200 chromatography column (GE Healthcare). PRA1 suspension was stored at 4 ℃ for up to 5 days as freezing abolished the PRA1 activity. To produce PRA1-containing SLBs, 5 mM lipids with 79.9 % DOPC, 20 % DOPS and 0.1 % DMPE-PEG2000 (Avanti Polar Lipids) were dried under constant Nitrogen flow. Then, the lipids were hydrated in 100 µL Vesicle buffer (20 mM HEPES-KOH pH 7.4, 150 mM KOAc) with 20 mM Triton X-100. The purified PRA1 was added to the lipid suspension at 1 µM and the solution was incubated at room temperature for 10 min. We removed the detergent by chelation with 40 mM methyl-β-cyclodextrin (Sigma Aldrich) in Vesicle buffer, which was added to the suspension in 1:1 volume ratio. After 5 min incubation, the PRA1-lipid suspension was diluted to 0.5 mM and used to produce glass-supported membranes.

3.6.4 Rab5A purification

A TwinStrep purification tag with TEV protease cleavage site and a Gly_4 linker was fused to codon-optimized *X. laevis* Rab5A. The non-prenylated GTPase was expressed in BL21(DE3) cells. Then, the cell pellets were resuspended in Rab purification buffer (20 mM HEPES-KOH pH 7.4, 150 mM KOAc, 1 mM $MgCl_2$, 1 mM DTT, 10 vol% glycerol), supplemented with cOmplete EDTA-free protease inhibitor cocktail. The cells were later lysed using cell disruptor and 1 mM PMSF and 2.5 U/mL DNase I were added to the suspension. Next, we centrifuged the sample at 60,000 rcf for 45 min and 4 ℃. The supernatant was then loaded on StrepTrap HP affinity column, equilibrated with Rab purification buffer and the bound proteins were eluted with 2.5 mM D-desthiobiotin. We removed the purification peptide with TEV(S219V) protease digestion overnight at 4 ℃, which was later removed with Ni^{2+}-NTA resin (HisPur, Thermo Fisher Scientific). The protein was finally isolated with size exclusion chromatography on Superdex 75 column, equilibrated with Rab purification buffer. Rab5 aliquots were stored at –80 ℃until use.

To prepare the native geranylgenanyl-Rab5, we used the baculovirus expression system. The genetic construct was cloned into pFL plasmid backbone and expressed

in Sf9 cells for 72 h at 27 °C. Notably, expression in alternative HighFive insect cell strain resulted in lower levels of posttranslationally modified protein product. Rab5 was purified from insect cell pellets according to previously published protocol [Horiuchi *et al.*, 1995; Peter *et al.*, 1995], with some modifications. First, the pellets were resuspended in Rab purification buffer (20 mM HEPES-KOH pH 7.4, 150 mM KOAc, 1 mM MgCl2, 1 mM DTT and 10 vol% glycerol), supplemented with cOmplete EDTA-free protease inhibitor cocktail tablets, 2.5 U/mL DNase I and 1 mM PMSF. The cells were lysed by douncing and ten 1 s pulses of tip sonication with 3 s pauses. We isolated the prenylated Rab5 from the membrane fraction, which was collected by ultracentrifugation at 150,000 rcf for 30 min at 4 °C. We then resuspended the membrane fraction in Rab purification buffer, supplemented with 0.6 % CHAPS (Sigma Aldrich) and 100 µM GDP (Sigma Aldrich) (extraction buffer). The membrane-bound proteins were solubilized during 2 h incubation at 4 °C with agitation. The soluble fraction with extracted Rab5 was isolated by another ultracentrifugation at 150,000 rcf for 30 min at 4 °C. We loaded the supernatant on StrepTrap HP column in extraction buffer and bound proteins were eluted with 2.5 mM D-desthiobiotin. Next, the purification tag was cleaved with TEV(S219V) protease overnight. For fluorescent labeling, we used the sortagging method [Guimaraes *et al.*, 2013] with 10 µM Srt7M (Addgene #51141) [Hirakawa *et al.*, 2015] and 0.3 mM maleimide dye-CLPETGG peptide. For GEF activity assay, the unlabeled Rab5 was loaded with mant-GDP (Jena Bioscience) by 1 h incubation at 37 °C in presence of 2 mM EDTA and 20-times molar excess of the labeled nucleotide. The reaction was then quenched with 5 mM $MgCl_2$ and the buffer was exchanged back to extraction buffer using Zeba spin columns (Thermo Fisher Scientific). The Rab5:GDI complex was assembled by dialyzing the purified components in 1:2 molar ratio against the Rab purification buffer with 0.1 % CHAPS. If necessary, the dialyzed samples were concentrated on Amicon Ultra-2 filter units (Millipore). Finally, the complex was loaded on Superdex 75 size exclusion column (GE Healthcare) equilibrated with Rab purification buffer without any detergent. This separated the Rab5:GDI complex from individual components, the TEV protease, SrtA and unused labeled peptide. The peak fractions containing the Rab5:GDI complex were subsequently pooled and frozen in liquid nitrogen before storage at −80 °C.

3.6.5 Rab5B purification

Similarly to Rab5A, the recombinant Rab5B was purified from insect cells according to previously published protocol [Horiuchi *et al.*, 1995; Peter *et al.*, 1995] (see above), without sortase labeling and GDI complexation.

3.6.6 Rab5Q80L-His_{10} purification

Unprenylated Rab5Q80L-His_{10} from *X. laevis* was expressed in *E. coli* BL21(DE3) bacterial strain from pET28a vector. The protein was cloned as TwinStrep-(linker)-TEV-Gly_4-Rab5Q80L-His_{10} fusion. The frozen bacterial pellets were thawed on ice and resuspended in Lysis/Wash buffer (50 mM HEPES-NaOH pH 8.0, 500 mM NaCl, 5 mM 2-mercaptoethanol, 10 vol% glycerol). To prevent non-specific protease digestion, cOmplete EDTA-free protease inhibitor cocktail tablets and 1 mM PMSF were added to the cell suspension. Next, the recombinant cells were lysed using cell disruption and centrifuged at 60,000 rcf for 45 min at 4 °C. The protein was purified using Protino Ni-IDA affinity resin and eluted in Lysis/Wash buffer with 150 mM imidazole. After buffer exchange on PD-10 columns to MonoQ A buffer (50 mM Tris-HCl pH 8.8, 1 mM DTT), the protein was digested with TEV(S219V) protease at 4 °C overnight. Digested Rab5Q80L-His_{10} and the protease were separated with ion exchange on Mono Q column (GE Healthcare) with MonoQ B buffer (50 mM Tris-HCl pH 8.8, 1 mM DTT, 1 M NaCl). Next, the buffer was exchanged to Rab buffer (20 mM HEPES-KOH pH 7.4, 150 mM KOAc, 1 mM $MgCl_2$, 1 mM DTT) and Rab5Q80L-His_{10} was loaded with GTP in presence of 5 mM EDTA and 1 mM GTP for 4 h at room temperature. The reaction was finally quenched with 10 mM $MgCl_2$ and the buffer was exchanged back to Rab buffer using PD-10 columns. Aliquoted samples were then snap frozen in liquid nitrogen and stored at –80 °C.

3.6.7 Rabex5:Rabaptin5 purification

The Rabex5:Rabaptin5 GEF complex was expressed in HighFive insect cell culture from bicistronic pFL bacmid expression cassette for 3 days. Rabex5 was cloned downstream of p10 promoter as a (linker)-TEV-Gly_4-Rabex5 fusion and TwinStrep-(linker)-

TEV-Rabaptin5 expression was under PH promoter control. The harvested cell pellets were resuspended in StrepTrap buffer (50 mM Tris-HCl pH 8.0, 150 mM NaCl, 0.5 mM EDTA, 5 mM 2-mercaptoethanol), supplemented with cOmplete EDTA-free protease inhibitor cocktail, 2.5 U/mL DNase I and 1 mM PMSF. The cells were lysed by douncing and 10 bursts of tip sonication for 1 s with 3 s pause in between. We ultracentrifuged the lysate at 150,000 rcf for 30 min and loaded the supernatant on StrepTrap HP affinity column. The purified complexes were eluted with 2.5 mM D-desthiobiotin and digested with TEV(S219V) protease. Next, the samples were concentrated on Amicon Ultra-2 cassettes and run on Superdex 200 gel filtration column to isolate the digested GEF complexes. The pooled fractions were further concentrated, aliquoted and snap frozen in liquid nitrogen for –80 ℃ storage. The same protocol was also used for **Rabaptin5**, **∆Rabex5**, **∆Rabex5:Rabaptin5** and **Rabex5:Δ_{RBD}Rabaptin5** purification. Importantly, purification of full length Rabex5 resulted in aggregation when not in complex with Rabaptin5. For the fluorescently labeled Rabex5:sCy5-Rabaptin5 complex, Rabex5 was expressed without an N-terminal linker as fluorescent labeling disrupted the Rabex5 catalytic activity. The sortagging reaction was performed after Rabaptin5 digestion with TEV protease.

3.6.8 RabGAP-5 purification

Sf9 insect cells were used to express TwinStrep-(linker)-3C-RabGAP-5 construct for 72 h at 27 ℃. We used StrepTrap buffer (50 mM Tris-HCl pH 8.0, 150 mM NaCl, 0.5 mM EDTA, 5 mM 2-mercaptoethanol), supplemented with cOmplete EDTA-free protease inhibitor cocktail to resuspend the cell pellets. The cells were lysed by douncing and 1 % IGEPAL CA-630 detergent solubilization for 10 min on ice. Later, the lysate was ultracentrifuged at 150,000 rcf for 30 min at 4 ℃. The supernatant was then loaded on StrepTrap HP affinity column and bound proteins were eluted with 2.5 mM D-desthiobiotin. The pooled fractions were digested with HRV 3C protease overnight and the samples were run on Superdex 200 size exclusion column to separate the RabGAP-5 and 3C protease. We finally pooled the RabGAP-5 fractions, which were snap frozen in liquid nitrogen and stored at –80 ℃.

3.6.9 SrtA 7M purification

The Ca^{2+}-independent mutant 7M of *S. aureus* SrtA was expressed as a His_6-tag fusion in BL21(DE3) cells. The frozen cell pellets were first thawed in Protino Lysis/Wash buffer (20 mM HEPES-NaOH pH 8.0, 500 nM NaCl, 5 mM 2-mercaptoethanol, 10 vol% glycerol). Then, we added 2.5 U/mL DNase I and 1 mM PMSF before lysis in cell disruptor. We cleared the lysates by centrifugation for 45 min at 60,000 rcf at 4 ℃and collected the supernatants. To isolate the expressed proteins, we incubated the soluble lysate fraction with 0.5 g of Protino-IDA resin per 50 mL for 2 h at 4 ℃with agitation. Next, we washed the affinity resin with Protino Lysis/Wash buffer using gravity flow and finally eluted the bound proteins with 150 mM imidazole. The buffer was exchanged back to 20 mM HEPES-NaOH pH 8.0, 500 nM NaCl, 5 mM 2-mercaptoethanol, 10 vol% glycerol and sample aliquites were snap frozen in liquid nitrogen before storage at –80 ℃.

3.6.10 TEV(S219V) protease purification

Enhanced TEV(S219V) protease mutant was expressed as His_6 mutant in BL21(DE3)-RIL cells. The pellets were resuspendend in Protino Lysis/Wash buffer (20 mM HEPES-NaOH pH 8.0, 500 mM NaCl, 5 mM 2-mercaptoethanol, 10 vol% glycerol). Only 2.5 U/mL DNase I was added to the suspension to prevent inhibition of the protease. We lysed the cells in cell disruptor and isolated the soluble fraction by centrifuging the samples for 45 min at 60,000 rcf at 4 ℃. We incubated the supernatants with Protino-IDA affinity resin for 2 h at 4 ℃ with agitation. We isolated the expressed proteases in batch using gravity flow. The affinity resin was first washed extensively with Protino Wash/Lysis buffer before elution with 150 mM imidazole. The buffer was then exchanged to Storage buffer (20 mM HEPES-NaOH pH 8.0, 0.5 mM EDTA, 1 mM DTT, 100 mM NaCl, 25 vol% glycerol) on PD-10 desalting columns. The isolated and purified samples were then snap frozen in liquid nitrogen and stored at –80 ℃.

3.7 Protein fluorescent labeling

After purification of transgenic proteins and subsequent digestion with TEV(S219V) protease, the proteins were labeled N-terminally with Sortagging method [Popp *et al.*, 2007] using calcium-independent mutant of *S. aureus* sortase A enzyme (SrtA7M) [Hirakawa *et al.*, 2015]. First, lyophillized synthetic CLPETGG peptide (Biomatik) was dissolved in Vesicle buffer (20 mM HEPES-KOH pH 7.4, 150 mM KOAc) with 0.2 M TCEP to 50 mM final concentration. In the next step, maleimide-conjugated synthetic fluorescent dye (sulfo-Cy5-maleimide [sCy5-maleimide] or CF488A-maleimide) in DMSO was added to the peptide in 3-times molar excess and left to react at room temperature overnight, protected from ambient light. We quenched the peptide labeling reaction with 1.5 M 2-mercaptoethanol. Labeled peptides were frozen in liquid nitrogen and stored at –80 °C. In the sortagging reaction, the purified protein was mixed with 10 µM SrtA7M and 0.3 mM labeled peptide. The reaction was then incubated for at least 5 hours at 4 °C in dark. Unreacted peptide, dye and SrtA7M were finally removed from the protein sample with size exclusion chromatography.

3.8 Guanine nucleotide exchange factor assay

Activity assays of purified GEFs were performed in 96- or 384-well plates (black non-binding surface microplate, Corining). First, Rab proteins were loaded with mant-GDP by 1 h incubation at 37 °C in presence of 2 mM EDTA and 20-times molar excess of the labeled nucleotide during purification or before the assay for soluble proteins. The exchange reaction was then quenched with 5 mM $MgCl_2$ and the buffer was exchanged to the reaction buffer using desalting columns. On the day of the experiment, 250 nM Rab5[mant-GDP]:GDI, Rabex5:Rabaptin5 and 500 µM SUVs were added to the microplate and incubated in reaction buffer (20 mM HEPES-KOH pH 7.4, 150 mM KOAc, 1 mM $MgCl_2$, 1 mM DTT) for 10 min. The measurements of mant-GDP fluorescence were performed on Biotek Synergy H1 plate reader (excitation 355 nm, emission 450 nm). After acquiring the baseline fluorescence for 40 min, the GEF exchange reaction was induced by injecting GTP to the wells at 1 mM final concentration. Finally, to determine observed exchange rates k_{obs}, the measured time courses were fitted with a

monoexponential function:

$$I(t) = A \cdot e^{-k_{obs}t} + B$$

where *I(t)* is the measured fluorescence intensity at time *t*. The catalytic efficiency k_{cat}/K_m was obtained from the slope of a linear fit to k_{obs}([GEF]) plot, where k_{obs} is the observed exchange rate at the given Rabex5:Rabaptin5 molar concentration [GEF] and k_0 is the intrinsic Rab5 nucleotide exchange rate.

$$k_{obs} = k_{cat}/K_m \cdot [GEF] + k_0$$

3.9 Fluorescence microscopy

The reconstituted biochemical reactions were observed in real time using labeled purified protein components and fluorescence microscopy. We used confocal laser scanning microscopy and surface-sensitive total internal reflection fluorescence (TIRF) microscopy.

3.9.1 Confocal microscopy

Confocal imaging was done on a Zeiss LSM 700 inverted microscope, equipped with air Plan-APOCHROMAT 10×/NA 0.45, water Plan-APOCHROMAT 40×/NA 1.3 and oil immersion Plan-APOCHROMAT 63×/NA 1.4 objective.

3.9.2 Total internal reflection fluorescence microscopy

TIRF microscopy experiments were done on *(i)* Zeiss Axio Observer.Z1 inverted microscope with Visitron iLas2 illumination module (GATACA), Zeiss Deffinite Focus 2 and Plan-APOCHROMAT 63×/NA 1.46 immersion objective and *(ii)* inverted Olympus IX83 with Cellˆ TIRF system and Olympus Uapo N 100×/NA 1.49 oil objective. Imaging on the Zeiss system was performed on two Photometrics Evolve-EM 512 D EMCCD cameras. Conversely, the Olympus stand was equipped with water-cooed Hamamatsu C9100-13 EMCCD camera. On both systems, the imaging was done with 200 EM camera gain and 30 ms exposure time with varying laser intensities unless stated otherwise.

3.10 Rab5 activation reconstitution assays on the SLB

For the *in vitro* reconstitution assays on the SLBs, the purified and fluorescently labeled proteins were incubated in the immobilized reaction chamber with glass supported membrane in Rab reaction buffer (20 mM HEPES-KOH pH 7.4, 150 mM KOAc, 1 mM $MgCl_2$, 1 mM DTT, 50 µM GDP), supplemented with 0.5 mM GTP in 30 µL total volume. We used surface-sensitive TIRF microscopy to specifically visualize membrane binding of labeled components. For that, we set the focal plane at the SLB with $<$ 100 nm penetration depth of the evanescent excitation field. We recorded the fluorescence signal in 30 s intervals for at least 10 min after equilibration of the reconstituted system to obtain stable baseline intensity. Then, we injected GEF in 20 µL Rab reaction buffer and mixed the contents of the reaction chamber to initiate the nucleotide exchange (50 µL total volume). We continued the recording in 30 s intervals until the fluorescence signal reached steady state. For the hysteresis assay, we first injected 10 µL 80 nM Rabex5:Rabaptin5 and allowed the activation reaction to plateau. We induced switching back to the basal state by addition of 10 µL RabGAP-5 to a final concentration of 500 or 2000 µM. In cases where no increase in signal was detected after at least 150 min post-induction, the recording was stopped and the activation delay time was deemed to be $>$ 150 min. Additionally, we recorded the camera noise by closing the microscope shutter and collecting the detector readout for 50 frames.

3.11 Chromium microgrid pattern preparation

The microgrid pattern was designed by Bryan Wu during his rotation project in the Loose lab. The chromium deposition protocol was developed with the IST Austria nanofabrication facility (J. Merrin, I. Prieto Gonzalez) by using E-beam photolithography with metal etching [Schweizer *et al.*, 2012] . The grid design included several 50$\times$50 arrays with different compartment numbers (1-25$\times$25) and metal wall thickness (1-32 µm). Briefly, the high-precision glass slides were first cleaned with piranha solution for 2 min and rinsed with MQ water. Next, the slides were dipped in isopropanol and dried with compressed air before chromium deposition with evaporation in a high vacuum Plassys. We spin-coated a thick (500 nm) PMMA 950K A4 resist layer at 2,000 rpm for

60 s and baked the slides at 180 °C for 5 min on a hotplate. Then, the design was used to guide the E-beam in Raith EBPG 5150 tool at 100 keV. We then developed the E-beam traced resist with isopropanol and methyl isobutyl ketone to remove the protective layer. The exposed chromium was then etched with $HClO_4$ and $(NH_4)_2[Ce(NO_3)_6]$ for 90 s at room temperature. Finally, the remaining photoresist was washed away with acetone. The chromium wall height was 50 nm.

The SLB was prepared as described before. To prevent non-specific protein binding to the exposed metal, we passivated the surface with 0.125 µM BSA for 15 min at room temperature after washing the reaction chambers with Vesicle buffer and MQ. The unbound BSA was removed with three successive wash steps with reaction buffer. We tracked the activation progression on Zeiss Axio Observer.Z1 inverted microscope with Visitron iLas2 TIRF illumination with 63× objective and 1.6× optovar magnification. We used 100 EM camera gain and 30 ms exposure with varying laser intensity for imaging. The patterned coverslips were recycled several times by washing the used chambers with MQ and isopropanol to remove the reaction components. The glued reaction chambers were removed with acetone and bath sonication. Finally, the exposed glass was cleaned with piranha solution for 2-5 min immediately before the next use.

3.12 Rab5 extraction assay under flow

To perform GDI Rab5 extraction assay from the SLB, we glued a 6-channel sticky-slide VI 0.4 chamber (ibidi) on a clean coverslip. Next, we washed the chambers with 1× PBS and formed the SLB by incubating 0.5 µM SUVs with 3.33 mM $CaCl_2$ for 45 min at room temperature. Next, we washed the chambers with 5 mL 1× PBS, supplemented with 2 mg/mL β-casein and exchanged the solution for the Rab reaction buffer, supplemented with 2 mg/mL β-casein. To achieve Rab5:GDI disassociation, we incubated 100 nM sCy5-Rab5:GDI with 20 nM ΔRabex5:Rabaptin5 and 0.5 mM GTP for 20 min. We washed the chambers with 0.5 mL reaction buffer with β-casein and incubated the membrane-bound sCy5-Rab5 with 5 mM EDTA and 0.5 mM GDP or GMP-PNP for 1 h to load the GTPase with the selected nucleotide. We then washed the chambers with reaction buffer and performed the extraction assay. GDI was injected into the flow chamber under constant flow (5 or 10 µL/s) in reaction buffer with β-

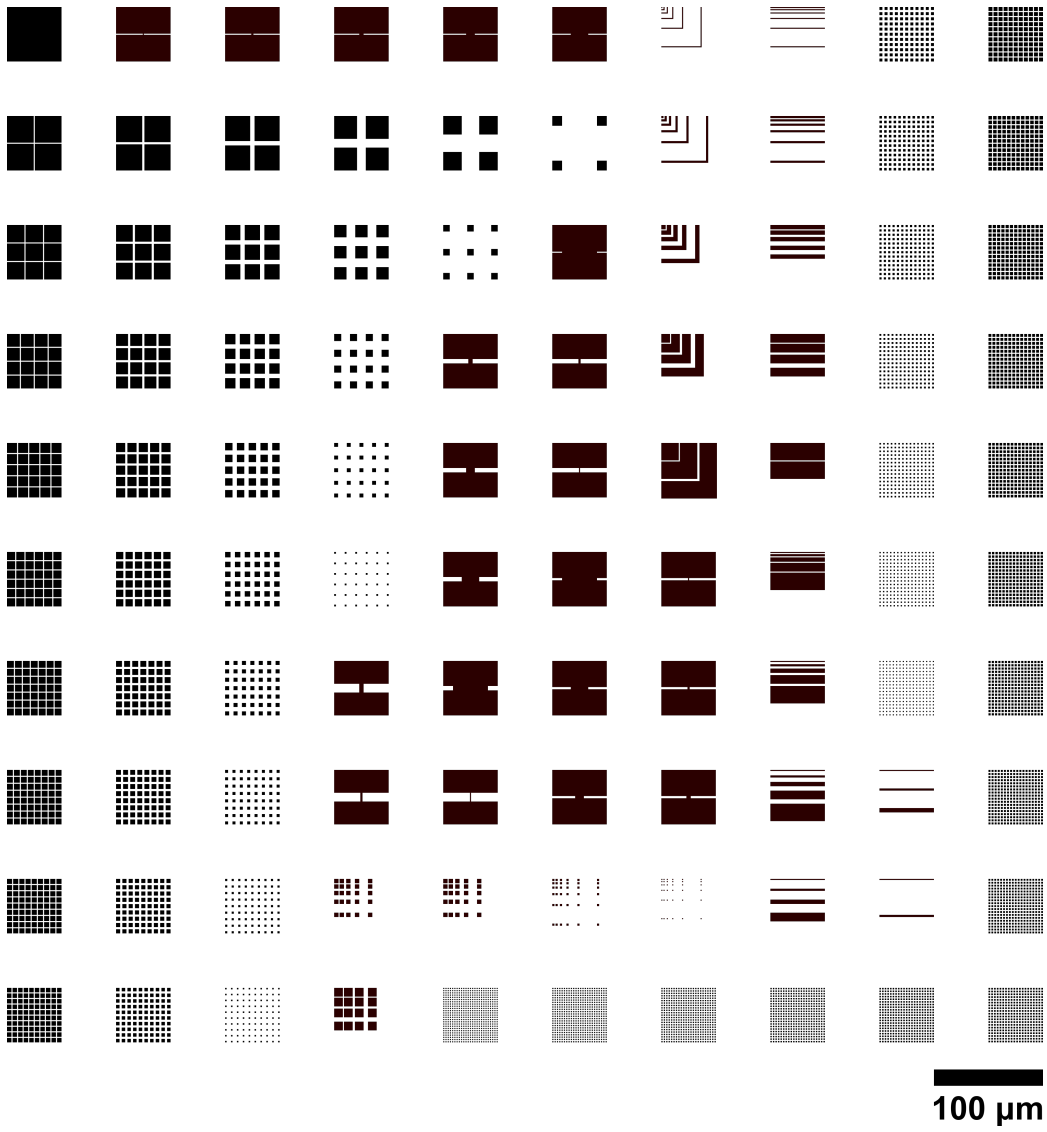

Figure 3.1: **The chromium microgrid design.**

The microgrid design was used to guide the E-beam for photoresist removal on chromium-covered glass coverslips. It included several grid designs, lines and channels. The microgrid was designed by Bryan Wu.

casein and oxigen scavengers (60 mM D-glucose, 1.25 mg/ml glucose oxidase, 0.2 mg/ml catalase). The Rab5 fluorescence signal at the SLB was monitored by TIRF microscopy on a Nikon Eclipse Ti inverted microscope equipped with iLas2 illumination module, 60×/NA 1.49 Apo-TIRF objective and Evolve 512 Delta EMCCD camera. To obtain Rab5 extraction rates k_{obs}, a monoexponential was fitted to the fluorescence intensity time traces after GDI injection under flow:

$$I(t) = A \cdot e^{-k_{obs}t} + B$$

where *I(t)* is the measured mean fluorescence intensity of the frame at time *t*, *A* is the amplitude and *B* is the function offset. The Rab5:GDI half-extraction constant $K_{0.5}$ and the maximum Rab5 extraction rates k_{max} were determined from hyperbolic fit:

$$k_{obs}([GDI]) = \frac{k_{max}[GDI]}{K_{0.5} + [GDI]}$$

3.13 Microscopy data analysis

The collected microscopy data was analyzed using Fiji ImageJ 1.52i package. The membrane localization of the selected fluorescently labeled component was determined by measuring the mean fluorescence intensity at the SLB and subtracting the recorded camera noise value for each collected frame. The point of GEF addition was set as t = 0. To obtain the time of inflection T_i and maximum growth rate k_{max}, we fitted a Gompertz function [Tjørve and Tjørve, 2017] to the subtracted fluorescence intensity values between the GEF addition and the onset of steady state:

$$I(t) = B + (A - B)\exp(-\exp(-e \cdot k_{max}(t - T_i)))$$

where *I(t)* is the measured fluorescence intensity at time *t*, *A* and *B* are the upper and lower fit asymptotes, respectively, k_{max} is the relative maximum signal growth rate and T_i is the temporal delay to reach k_{max} after GEF addition. For the reactions where no signal increase was observed after 150 min post-GEF addition, the activation delay T_i was taken to be $>$ 150 min and the k_{max} was set to 0. To normalize the data, we divided the fluorescence intensities by the upper fitted asymptote *A*. The traces that

did not result in collective activation were normalized by dividing the signal intensities with the mean of upper asymptotes *A* at the corresponding microscope setup. The normalized fluorescence intensities were used to group independent replicates. This way, we obtained the mean intensity traces and standard deviations (SD) for selected conditions. Similarly, the fold change in fluorescence signal was calculated by taking the upper asymptote value *A* and dividing it with the mean value of the baseline signal before GEF injection.

3.14 Single particle tracking

For single particle tracking, we used CF488A-Rab5:GDI, supplemented with small amounts of sCy5-Rab5:GDI. The particle diffusion of sCy5-Rab5 on the SLB was captured using the Zeiss Axio Observer.Z1 inverted microscope with Visitron iLas2 illumination module. We used 100 % 640 nm laser power, 30 ms exposure time, 300 EM-CCD camera gain and 100 ms acquisition interval. To capture single particles landing on the SLB before nucleotide exchange, we incubated the glass supported membrane with 500 nM CF488A-Rab5:GDI, 2 µM µGDI, 50 µM GDP, 500 µM GTP and ca. 1 nM sCy5:GDI. To limit the effects of photobleaching, we also included an oxygen scavenging system with 60 mM D-glucose, 0.1 mg/ml glucose oxidase (SERVA), 0.32 mg/ml catalase (Sigma Aldrich) and 2 mM Trolox (Sigma Aldrich). We built the particle trajectories using the TrackMate ImageJ plugin v.3.7.0 [Tinevez *et al.*, 2017]. We used simple LAP tracker with 0.7 µm particle diameter, 15 threshold value with median filter, signal-to-noise ratio $>$ 0.6, 2 µm maximum linking distance and up to 2 frame gap with 3 µm closing distance to account for fluorophore blinking. To image particles after the nucleotide exchange with GTP or GMP-PNP, we first triggered the Rab5 activation by injecting 200 nM Rabex5:Rabaptin5 into 500 nM CF488A-Rab5:GDI, 2 µM GDI, 50 µM GDP, 500 µM GTP/GMP-PNP and ca. 50 fM sCy5:GDI mixture. We followed the progression of collective activation by measuring the CF488A-Rab5 fluorescence intensity at the SLB. When the reaction reached steady state, we supplemented the sample with fresh oxygen scavengers and imaged sCy5-Rab5 particles with 100 % 640 nm laser power, 30 ms exposure, 300 EM gain and 100 ms acquisition interval. The TrackMate trajectories were built with simple LAP tracker, 0.7 µm particle diameter, 15 threshold

value with median filter, signal-to-noise ratio $>$ 0.6, 1 µm maximum linking distance and at most 2 frame gap with 1.5 µm closing distance. For GMP-PNP-bound sCy5-Rab5, $=<$0.8 µm and $=<$ 1.2µm distances were used to link particles and close up to 2 frame gaps, respectively. We analyzed only trajectories with 3 spots or longer. To calculate the membrane residence lifetimes for sCy5-Rab5[GDP] τ^{GDP}, we fitted a monoexponential function to the logarithmic probability density values in a trajectory duration histogram:

$$\ln p(t) = \ln A - \frac{t}{\tau}$$

where $\ln$ is natural logarithm, *p(t)* is the trajectory probability density at a given duration *t* and τ is the mean lifetime. Conversely, a two-exponential function was better at fitting the sCy5-Rab5[GTP/GMP-PNP] trajectory histogram. This gave us $\tau_1^{GTP/GMP-PNP}$, $\tau_2^{GTP/GMP-PNP}$ and amplitudes A_1 and A_2.

$$\ln p(t) = \ln \left(A_1 \cdot e^{-t/\tau_1} + A_2 \cdot e^{-t/\tau_2}\right)$$

We excluded the rare stuck particles from the analysis by limiting the fitting range up to the 98th percentile of the trajectory duration distribution. The calculated lifetimes are not corrected for photobleaching and thus represent a lower estimate of the actual membrane residence lifetimes.

3.15 Particle deflection angle determination

We calculated the deflection angles θ from particle trajectory vectors at each successive frame [Burov *et al.*, 2013]:

$$\cos\theta(t) = \frac{\vec{v}(t) \cdot \vec{v}(t+1)}{\|\vec{v}(t)\|\|\vec{v}(t+1)\|}$$

where $\vec{v}$ represents the vector connecting two adjacent particle positions.

3.16 Mean square displacement analysis

The single particle mean square displacement (MSD) was performed using the MATLAB @msdanalyzer script [Tarantino *et al.*, 2014]. Individual trajectories from several independent experiments were pooled and the diffusion coefficients were calculated from the linear part of the weighted MSD curve (10 % of track lengths).

3.17 Activation wave velocity

Activation waves were observed several minutes after 80 nM Rabex5:Rabaptin5 injection to 500 nM CF488A-Rab5:GDI, 2 µM GDI, 50 µM GDP, 500 µM GTP and 50 nM RabGAP-5. The collected time series were first corrected for uneven illumination profile. To this end, we prepared glass supported membrane, doped with 0.25 µg/mL fluorescent DiO tracer (Sigma Aldrich) to determine the TIRF illumination profile across the field of view. We analyzed the acquired images using ImageJ 1.52i. First, we generated an illumination profile reference image by gaussian filtering of the DiO-labeled SLB snapshot with ImageJ FFT Bandpass Filter. We then divided the wave time series with the illumination reference to produce corrected images. These images were used to construct a kymograph along a line across the field of view. Finally, we estimated the activation wave velocity from the slope of the kymograph fluorescence profile.

3.18 Fluorescence recovery after photobleaching

Fluorescence recovery after photobleaching (FRAP) was used to estimate the protein turnover at the SLB after nucleotide exchange. A reaction composed of 500 nM CF488A-Rab5:GDI, 2 µM GDI, 50 µM GDP, 500 µM GTP or GMP-PNP and 80 nM Rabex5:Rabaptin5 was let to reach steady state. We then exposed a central area of roughly 20×20 µm to high-power 488 nm laser for 3-5 ms/px. The FRAP was then monitored in 1 s intervals until the fluorescence intensity reached a new steady state. We determined the fluorescence intensities of a center 3×3 px square to minimize the effects of lateral diffusion in the bleached area. To determine the protein exchange rate, we fitted a monoexponential function to the normalized intensity profile:

$$I(t) = A \cdot (1 - e^{-k_{ex}t}) + B$$

where *I(t)* is the normalized fluorescence intensity at time *t* and k_{ex} is the protein exchange rate. We normalized the fluorescence intensity by first subtracting the camera noise from the bleached 3×3 px square intensity profile. Then, we corrected the fluorescence recovery series for photobleaching during imaging by dividing the subtracted intensities with fluorescence signal outside the bleached area. Finally, the corrected fluorescence profiles were normalized to the mean intensity of 10 pre-bleach frames.

3.19 Size exclusion chromatography–multi angle light scattering

The oligomeric state of the purified Rabex5:Rabaptin5 sample was analyzed with size exclusion chromatography–multi angle light scattering (SEC-MALS). A 100 µL sample at 1.0 mg/mL in 50 mM Tris-HCl pH 7.5, 150 mM KCl, 5 mM $MgCl_2$, 2 mM TCEP and 10 vol% glycerol was run in duplicate on Superdex 200 Increase 10/300 column at 0.5 mL/min and 35 °C. We used OMNISEC RESOLVE for sample separation and the REVEAL module (Malvern Instruments) for multi angle light scattering and refractive index detection. Prior to the runs, the samples were stored at 6 °C in the autosampler. The recorded data were analyzed using the OMNISEC v10.41 software package.

3.20 Mathematical modeling

The mathematical model of the minimal Rab5 switching network was prepared in close collaboration with Timothy E. Saunders of the Mechanobiology Institute at National University of Singapore (MBI-NUS) and Hrushikesh Loya of Indian Institute of Technology (IIT) Bombay while visiting the Saunders lab. Particularly, Hrushikesh Loya derived the ordinary differential equations (ODE) and ran both deterministic and stochastic simulations based on proposed set of reactions:

$$Rab5[GDP] : GDI \underset{k_2}{\overset{k_1}{\rightleftharpoons}} Rab5[GDP] + GDI \tag{3.1}$$

$$Rab5[GTP] \xrightarrow{k_3} Rab5[GDP] \tag{3.2}$$

$$Rab5[GDP] + RR \xrightarrow{k_4} Rab5[GTP] + RR \tag{3.3}$$

$$Rab5[GTP] + RR \underset{k_6}{\overset{k_5}{\rightleftharpoons}} Rab5[GTP] : RR \tag{3.4}$$

$$Rab5[GDP] + Rab5[GTP] : RR \xrightarrow{k_7} 2Rab5[GTP] + RR \tag{3.5}$$

where RR denotes the Rabex5:Rabaptin5 complex and k_n is the reaction rate parameter (Table 3.3). We derived the modeled reactions based on characterized molecular interactions [Stenmark *et al.*, 1995; Lippé *et al.*, 2001; Delprato and Lambright, 2007; Zhu *et al.*, 2010; Zhang *et al.*, 2014]. We assume that Rab5:GDI complex must first dissociate in order for the GEF to promote nucleotide exchange. The exchange itself can happen at basal level (Reaction 3.3) or through positive feedback (Reaction 3.5). There, the k_7 parameter aggregates possible contributions from active Rab5 positive feedback, the complex unbinding, reduction in dimensionality, substrate proximity [Groves and Kuriyan, 2010], release of auto-inhibition [Delprato and Lambright, 2007] and oligomerization of the ternary complex [Zhang *et al.*, 2014].

For solving the set of ODE, we assume that the system is well-mixed. The above reaction scheme was solved using numerical integration with the ODE solver in SimBiology toolbox (MATLAB) and with a stochastic ODE solver using the Biosimulator.jl package [Landeros *et al.*, 2018] in Julia. All stochastic simulations start with 500 particles of Rab5[GDP]:GDI and varying concentrations of RR and GDI (based on the experiments). All other reaction species have zero particles at the start of the experiment. The relative magnitude of the stochastic fluctuations depends on the local particle number.

Table 3.3: **Table of the model reaction parameters.**

Parameter	Value	Notes
k_1	1.2·10^{-1} s^{-1}	Fitted from estimated $K_d = k1/k2$ = 6 µM [Pylypenko *et al.*, 2006] (Figure 4.8).
k_2	2.25·10^{5} M^{-1} s^{-1}	
k_3	5.25·10^{-4} s^{-1}	Fitted from k = 0.0006 s^{-1} [Simon *et al.*, 1996b].

(Continued on the next page)

(Continuation)

Parameter	Value	Notes
k_4	$5{\cdot}10^4$ M^{-1} s^{-1}	Fitted from $k = 2.5{\cdot}10^4$ M^{-1} s^{-1} [Lippé *et al.*, 2001].
k_5	$2.875{\cdot}10^4$ M^{-1} s^{-1}	Fitted from estimated $K_d = k5/k6 = 50$ µM [Zhu *et al.*, 2010].
k_6	$8{\cdot}10^{-2}$ s^{-1}	
k_7	$1{\cdot}10^8$ M^{-1} s^{-1}	Fitted from $k = 7.5{\cdot}10^4$ M^{-1} s^{-1} [Lippé *et al.*, 2001].

3.21 Spatial stochastic model

Spatial stochastic model was implemented in Smoldyn 2.61 simulator [Andrews *et al.*, 2010]. Smoldyn is a particle-based stochastic engine, which simulates reaction-diffusion systems within the biophysical framework of von Smoluchowski. At each time step, the modeled molecules are allowed to diffuse, bounce or interact with a certain probability. This way, we can better understand ways confinement can influence Rab5 activation and how nucleation events can trigger collective GTPase activation. The model configuration files are available on IST Austria Git repository: https://git.ist.ac.at/urban.bezeljak/rab5-spatial-stochastic-model.

The model simulated single molecule interactions in a 4×4×0.2 µm box in 50 ms time steps and included the following set of reactions:

$$Rab5[GDP] : GDI_{sol} \underset{k_2}{\overset{k_1}{\rightleftharpoons}} Rab5[GDP]_{sol} + GDI_{sol} \tag{3.6}$$

$$Rab5[GDP]_{sol} \xrightarrow{k_{rab}} Rab5[GDP]_{mem} \tag{3.7}$$

$$Rab5[GDP]_{mem} + GDI_{sol} \xrightarrow{k_8} Rab5[GDP] : GDI_{sol} \tag{3.8}$$

$$Rab5[GTP]_{mem} \xrightarrow{k_3} Rab5[GDP]_{mem} \tag{3.9}$$

$$Rab5[GDP]_{mem} + RR_{sol} \xrightarrow{k_4} Rab5[GTP]_{mem} + RR_{sol} \tag{3.10}$$

$$RR_{sol} \underset{k_{rrOFF}}{\overset{k_{rrON}}{\rightleftharpoons}} RR_{mem} \tag{3.11}$$

$$Rab5[GDP]_{mem} + RR_{mem} \xrightarrow{k_4} Rab5[GTP]_{mem} + RR_{mem} \tag{3.12}$$

$$Rab5[GTP]_{mem} + RR_{sol} \underset{k_6}{\overset{k_5}{\rightleftharpoons}} Rab5[GTP] : RR_{mem} \tag{3.13}$$

$$Rab5[GTP]_{mem} + RR_{mem} \underset{k_6}{\overset{k_5}{\rightleftharpoons}} Rab5[GTP] : RR_{mem} \tag{3.14}$$

$$Rab5[GDP]_{mem} + Rab5[GTP] : RR_{mem} \xrightarrow{k_7} Rab5[GTP] : RR_{mem} + Rab5[GTP]_{mem} \tag{3.15}$$

The model parameters were estimated to reproduce the observed system responses in *in vitro* reconstitution assays. The modeled number of molecules approximates the expected particle number in the simulated volume of 3.2 μm^3. The simulation initiated with soluble Rab5[GDP]:GDI and GDI above a membrane surface, which was compartmentalized in grids or unbounded. To approximate grid compartments the membrane=bound molecules were bouncing off the grid walls, while the unbounded membrane included periodic walls (diffusing particle passes trough the wall, but enters back at the opposite wall). The initial system was left to equilibrate for 1 min of simulation time. At that point, Rabex5:Rabaptin5 molecules were included in the simulation and Rab5 activation reaction could progress. We assumed the nucleotides are in constant stoichiometric excess and were not explicitly modeled. To limit the effect of substrate depletion in the early stages of collective switching, we kept the number of Rab5[GDP]:GDI and GDI constant during the first 500 activation events. After that, the reactants in the simulated volume were consumed. The simulation parameters were:

Table 3.4: **Table of the spatial stochastic model parameters.**Smoldyn takes the concentration parameters in units of particles per μm^3, which have to re-calculated from molar concentrations listed below.

Parameter	Value	Notes
k_1	0.01 s^{-1}	Rab5:GDI dissociation rate; K_d = 250 nM.
k_2	$4{\cdot}10^4$ M^{-1} s^{-1}	Rab5:GDI association rate.
k_3	$5{\cdot}10^{-4}$ s^{-1}	Intrinsic GTPase activity.
k_4	$2{\cdot}10^3$ M^{-1} s^{-1}	Basal GEF activation rate.
k_5	$2{\cdot}10^4$ M^{-1} s^{-1}	Rab5[GTP]:GEF complex association rate; K_d = 5 μM.

(Continued on the next page)

(Continuation)

Parameter	Value	Notes
k_6	0.1 s^{-1}	Rab5[GTP]:GEF complex dissociation rate.
k_7	$6{\cdot}10^6$ M^{-1} s^{-1}	Positive feedback activation rate.
k_8	$8{\cdot}10^4$ M^{-1} s^{-1}	GDI Rab5 extraction rate.
k_{rab}	10 µm s^{-1}	Rab5[GDP] membrane adsorption.
k_{rrON}	0.01 µm s^{-1}	GEF membrane adsorption.
k_{rrOFF}	1 s^{-1}	GEF membrane desorption.
$N_{Rab5[GDP]:GDI}$	1000	Initial number of Rab5[GDP]:GDI. The number of particles per 3.2 μm^3 corresponds to the molar concentration in nM·2.
N_{GDI}	4000	Initial number of GDI.
N_{GEF}	variable	Initial number of Rabex5:Rabaptin5 (RR).
D_{sol}	10 μm^2 s^{-1}	Diffusion coefficient of soluble components.
D_{mem}	0.3 μm^2 s^{-1}	Diffusion coefficient of membrane-bound components.

4 Results and discussion

In this work, we take the Rab5 regulatory network as a model small GTPase biochemical system to study self-organization principles in cellular signaling. We identify that small GTPase activity switching is well-understood on structural level, whereas relevant concepts in network state transitions are still missing. In living systems, signal transduction happens on ensemble level, where pools of proteins collectively switch to generate signaling potential. This potential results in non-diluted directional message propagation along the signaling cascade [Koshland *et al.*, 1982]. This must apply also to small GTPase circuits, where Rabs direct membrane flow [Cherfils and Zeghouf, 2013] and were proposed to encode positive and negative feedback loops [Mizuno-Yamasaki *et al.*, 2012]. Here, we use *in vitro* reconstitution to tackle open questions in system behavior of a minimal Rab activation network. The learned lessons can be applied also to other Rab modules and small GTPases in general.

The majority of presented results in Chapters 4.1-4.7 were included in publication "Stochastic activation and bistability in a Rab GTPase regulatory network" in *PNAS* (2020) [Bezeljak *et al.*, 2020]. Parts of Chapter 4.5 and Chapters 4.8-4.9 will be presented in upcoming publications.

4.1 Purification of the network components

We hypothesized that the Rab5 minimal regulation network is composed of Rab5:-GDI and Rabex5:Rabaptin5 complexes. As these include large protein components like Rabaptin5 (100 kDa) and posttranslationally modified Rab5, we produced these recombinant proteins using baculovirus expression system in eukaryotic insect cells [Fitzgerald *et al.*, 2006]. Conversely, we used bacterial cell expression for smaller pro-

teins that do not require posttranslational processing. All recombinant proteins were from African clawed frog *Xenopus laevis*, which lives in aquatic environments of sub-Saharan Africa. We reasoned that these proteins would be most active at room temperature that was normally used in our *in vitro* assays. To ensure high yield and purity, we constructed recombinant fusions with polyhistidine- or TwinStrep [Schmidt *et al.*, 2013] affinity peptides upstream from specific protease cleavage recognition sites to produce native-like proteins. By combining affinity and size exclusion chromatography, we were able to obtain highly pure protein components that were used in *in vitro* reconstitution assays (Figure 4.1A-F). Of the isolated proteins, we expressed the components of Rab5:GDI and GEF complexes in insect cells, along with the 90 kDa RabGAP-5. On the other hand, we could reliably isolate non-lipidated Rab5 and the transmembrane PRA1 from transformed *E. coli* cells.

There were recent reports showing that Rabex5:Rabaptin5 complex exists in 1:1 stoichiometric ratio [Lauer *et al.*, 2019], which is in contrast to the established model, where Rabaptin5 forms a homodimer colied-coil to build a 1:2 Rabex5:Rabaptin5 assembly [Lippé *et al.*, 2001; Zhang *et al.*, 2014]. To characterize the purified *Xenopus* GEF complex, we performed size exclusion chromatography with multi angle light scattering (SEC-MALS) (Figure 4.1G). Surprisingly, our data suggests that the Rabex5:Rabaptin5 complex exists as a 2:2 heterodimer of 320 kDa, which is in equilibrium with higher-order structures of 2000 kDa. The 2:2 stoichiometry was recently also confirmed for human Rabex5:Rabaptin5 complex [Cezanne *et al.*, 2020; Lauer *et al.*, 2019]. The broad range of observed and reported structures could be explained by species-, concentration- and buffer-specific dynamic assemblies of Rabex5 GEF and Rabaptin5. Nonetheless, we used the measured 2:2 complex as a reference for molar concentration determination and theoretical modeling.

The full length Rabex5:Rabaptin5 GEF complex was expressed from a bicistronic bacmid expression cassette and formed spontaneously in baculovirus-infected insect cells. On the other hand, we had to achieve Rab5:GDI complexation after isolating the respective components. To this end, we followed the established protocol of Rab solubilization in detergent with subsequent GDI incubation and gradual detergent reduction below the critical micelle concentration [Horiuchi *et al.*, 1995; Peter *et al.*, 1995]. We observed complex formation on size-exclusion chromatogram only with the full length

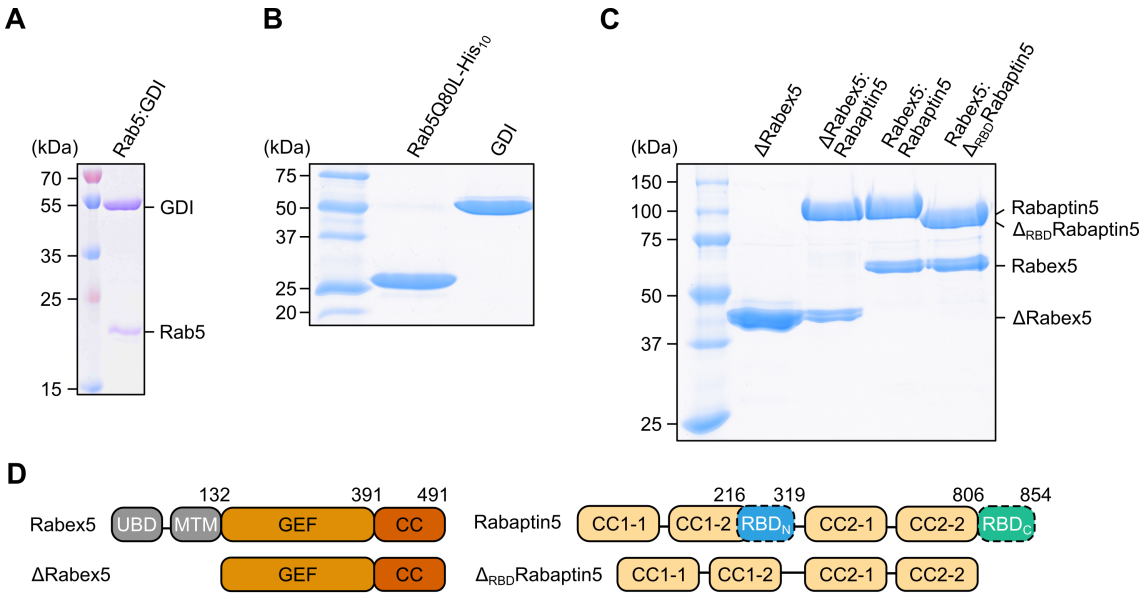

	Peak 1	Peak 2	Peak 3
retention volume (mL)	7.87 ± 0.01	8.54 ± 0.01	8.78 ± 0.01
Mw (kDa)	73740 ± 8296	1990 ± 73	323 ± 4
Frac. of sample (%)	0.8 ± 0.4	21.8 ± 1.4	77.4 ± 1.8

Figure 4.1: *(Continued on the next page)*

X. laevis Rab5A isoform (Figure 4.2). A C-terminally truncated Rab5B, which lacks the posttranslationally modified cysteine residues did not interact with GDI – indicated by two distinct elution peaks.

Preparing the native Rab5:GDI complex is crucial to investigate nucleotide exchange and membrane binding of prenylated small GTPase. Currently, there is a great lack of knowledge in Rab:GDI regulation due to the difficult handling of native proteins. Furthermore, early *in vitro* studies suggested that the tight Rab5:GDI association effectively inhibits the GEF-mediated nucleotide exchange [Horiuchi *et al.*, 1997]. This lead to the prevailing assumption that an additional GDI dissociation fac-

Figure 4.1: **Purified protein components used in *in vitro* reconstitution assays.**
(A) Purified *X. laevis* Rab5:GDI complex. The expected molecular weights were 23.7 and 50.8 kDa for Rab5A and RabGDI, respectively. **(B)** Rab5Q80L-His_{10} and RabGDI. The expected molecular weights were 24.7 kDa for Rab5Q80L-His_{10} and 50.8 kDa for RabGDI, respectively. **(C)** The purified GEF complexes. Expected molecular weights for monomeric components: 42.0 kDa, 57.1 kDa, 81.1 and 99.2 kDa for ΔRabex5, full length Rabex5, Δ_{RBD}Rabaptin5 and Rabaptin5, respectively. **(D)** Schematic domain representations of full length- and Rabex5, Rabaptin5 deletion mutants. UBD: ubiquitin binding domain; MTM: membrane targeting motif; GEF: GEF domain; CC: coiled-coil region; RBD: Rab5 binding domain. **(E)** Purified PRA1 in 0.1 % Triton X-100. The PRA1 had expected molecular weight of 21.3 kDa. **(F)** RabGAP-5 (SGSM3) with expected molecular weight 86.1 kDa. **(G)** SEC-MALS characterization of purified Rabex5:Rabaptin5 complex. The sample was run in duplicate and produced three peaks. The first peak ($<$ 1 % of total sample) are protein aggregates, the second peak represents higher-order oligomers with average molecular weight 1990 kDa (22 %) and the third peak is 2:2 Rabex5:Rabaptin5 heterodimer with average molecular weight 323 kDa. The expected molecular weight of a 2:2 complex is 313 kDa. The second peak with corresponding apparent molecular weight of 1990 kDa could represent a hexamer of 2:2 heterodimer GEF complexes.

tor is needed in the minimal regulatory Rab network [Dirac-Svejstrup *et al.*, 1997; Sivars *et al.*, 2003]. Clearly, a systematic study of the purified native components under physiological conditions is needed. In the following sections we assay individual biochemical components on collective, system's scale using biomimetic membranes as a reaction substrate to unravel the self-organization properties and construct a model of the minimal Rab5 activation circuit.

4.2 Characterization of the guanine nucleotide exchange factor complex

In order to test the nucleotide exchange activity of the purified Rabex5:Rabaptin5 complex, we loaded soluble Rab5 with fluorescent GDP analog mant-GDP. We performed a nucleotide release assay by monitoring intensity change in fluorescence signal as a readout of GEF's catalytic activity. There, mant-GDP is exchanged with non-labeled

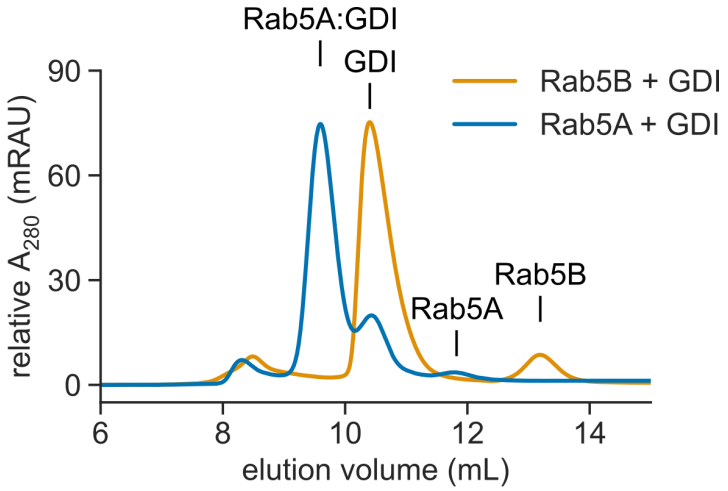

Figure 4.2: **The purified full length Rab5A forms a stable complex with GDI.**
Elution chromatogram of Rab5A and Rab5B with GDI, respectively, after isolation form Sf9 insect cell culture and overnight complexation. The isolated samples were loaded on Superdex75 Increase 10/300 column and separated by size. The first peak at 8.3 mL corresponds to the column void volume with aggregates and $>$ 100 kDa contaminants. The Rab5A:GDI complex elutes at 9.6 mL (estimated MW 75 kDa), the free GDI at 10.4 mL (51 kDa), non-complexed singly- or un-prenylated Rab5A at 11.8 (24 kDa) and Rab5B at 13.2 mL (20 kDa). The chromatograms were offset to 0 mRAU at 6 mL and normalized to the same area under curve in the range from 6 to 16 mL for clarity.

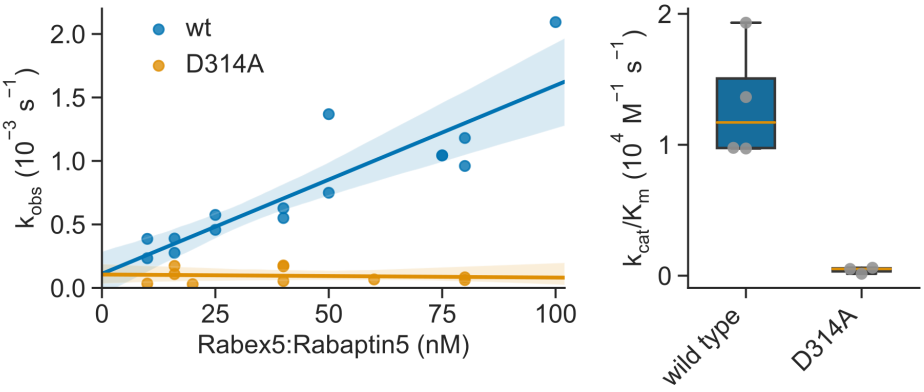

Figure 4.3: **Purified GEF complex is active *in vitro*.**
Left: The observed nucleotide exchange rates of wild type and Rabex5(D314A):Rabaptin5 complex on soluble Rab5. Shaded area represents 95 % CI. Right: Catalytic efficiency of the purified GEF complexes on soluble Rab5. The determined Rabex5:Rabaptin5 catalytic efficiency was $1.3 \pm 0.5 \cdot 10^4$ M^{-1} s^{-1}.

GTP in Rab5 nucleotide binding pocket, which leads to a decrease in mant fluorescence as the fluorophore changes its chemical environment. We assayed the full length wild type Rabex5:Rabaptin5 and the inactivated mutant Rabex5(D314):Rabaptin5 as a negative control (Figure 4.3).

Similarly, to test the nucleotide exchange activity on prenylated Rab5A (hereafter referred to as "Rab5" unless explicitly stated) in complex with GDI, we loaded the small GTPase with mant-GDP and preformed the GEF assay as before. Interestingly, we observe GEF-mediated nucleotide exchange only in presence of small unilamellar vesicles (SUVs) with catalytic efficiency (k_{cat}/K_m) of $1.0 \pm 0.6 \cdot 10^4$ M^{-1} s^{-1} (Figure 4.4), comparable to the value for soluble Rab5B.

This exchange rate is about three times lower than previously determined Rabex5 activity on *soluble* Rab5 [Delprato *et al.*, 2004; Langemeyer *et al.*, 2014] and almost an order of magnitude less than reported values for fully active Rabex5:Rabaptin5 complex [Delprato and Lambright, 2007]. Lower vales could be attributed to species-specific variability and experimental conditions. Importantly, these vales were previously measured on bacterially expressed Rab5 in absence of GDI from different organism sources. In contrast, our Rab5:GDI k_{cat}/K_m values are the first measurements on native complex under more physiological conditions. Here, we show that the Rabex5:Rabaptin5 GEF complex can activate Rab5 even when associated with GDI.

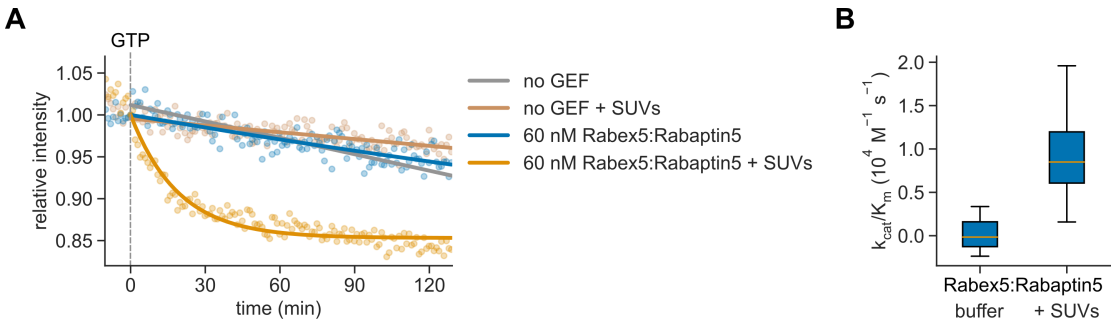

Figure 4.4: **Membranes are necessary for Rab5:GDI activation.**

(A) Kinetic traces of Rabex5:Rabaptin5 activity assay on Rab5:GDI. The 250 nM mant-GDP loaded Rab5:GDI complexes were incubated with 60 nM Rabex5:Rabaptin5 in presence or absence of SUVs. The Rab5 activation reaction was monitored by relative change in intrinsic mant-GDP fluorescence after nucleotide exchange with non-labeled GTP, which was injected at t = 0. The GEF-mediated nucleotide exchange proceeds only in presence of 500 nM SUVs, signified by marked exponential decrease in signal intensity. In experiments without the GEF (no GEF), we incubated the Rab5[mant-GDP]:GDI with reaction buffer. Points are means from three independent experiments; solid lines are linear and monoexponential fits for buffer control and experiments with Rabex5:Rabaptin5, respectively. **(B)** Catalytic efficiency of the purified GEF complex on Rab5:GDI in reaction buffer (n = 3) and in buffer, supplemented with SUVs as reaction substrates (n = 4). The determined Rabex5:Rabaptin5 catalytic efficiency in presence of membranes was $1.0 \pm 0.6 \cdot 10^4$ M^{-1} s^{-1}.

Importantly, this is possible only in presence of biological membranes like the SUVs [Thomas and Fromme, 2016].

This finding highlights the crucial role of biological membranes in small GTPase signaling. For the first time, we identify the lipid bilayer as a necessary component of the minimal Rab5 activation network. In order to further investigate the non-equilibrium dynamics of the reconstituted biochemical system, we combine site-specific fluorescent labeling of the purified protein components with glass-supported lipid bilayers (SLBs) and total internal reflection fluorescent (TIRF) microscopy [Loose and Schwille, 2009; Nguyen *et al.*, 2015].

4.3 *In vitro* reconstitution of the Rab5 activation network on supported lipid bilayer

The Rab GTPase signaling depends on nucleotide cycling, where Rab proteins transition between the lipid bilayer and the cytosol as a consequence of non-equilibrium GEF- and GAP-mediated nucleotide exchange and hydrolysis, respectively. Crucially, this is coupled with Rab[GDP] membrane extraction and solubilization by the GDI to ensure nucleotide-specific distribution of the small GTPase between the solution (GDP-; inactive state) and the phospholipid bilayer (GTP-; active state) [Cherfils and Zeghouf, 2013]. To observe this dynamic transition of labeled Rab5 in real time, we use surface-sensitive TIRF microscopy and glass coverslip-supported membranes (Figure 4.5) in our *in vitro* reconstitution assays.

4.3.1 Rab5 binds the supported membrane after nucleotide exchange

In these assays, we use N-terminally fluorescently labeled geranylgeranylated Rab5 in native complex with GDI. We measure the fluorescence intensity at the SLB focal plane as a direct readout of Rab5 membrane binding. Furthermore, to mimic the physiological conditions, we include GTP in 10-times excess over GDP [Traut, 1994; Goody and Hofmann-Goody, 2002; Goody, 2014] and the GDI in 5-fold molar excess

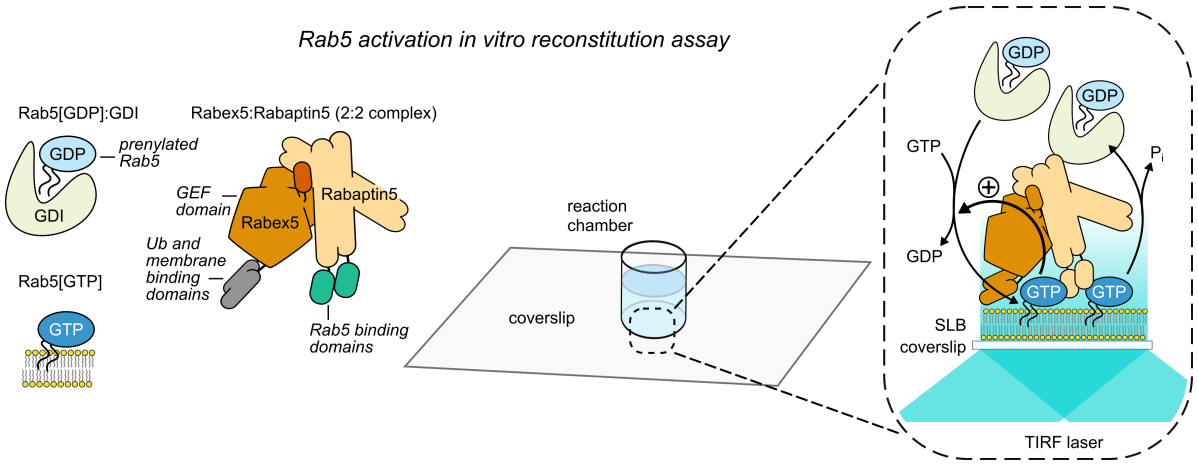

Figure 4.5: **Schematic of Rab5 activation reconstitution assay on a SLB.**
In our *in vitro* experimental platform, the fluorescently labeled prenylated Rab5 in GDI complex was incubated with GTP in 10-fold excess over GDP in a reaction chamber above the SLB. To ensure nucleotide-specific membrane localization, we keep GDI in 5-fold stoichiometric excess over Rab5. We induce the nucleotide exchange by injecting the Rabex5:Rabaptin5 GEF complex, which was reported to form a positive feedback loop of Rab5 activation (+) [Zerial and McBride, 2001]. The resulting Rab5 membrane localization is monitored by TIRF microscopy.

over Rab5 [Pfeffer *et al.*, 1995; Lippé *et al.*, 2001], respectively. Generally, we incubate 500 nM CF488A-Rab5[GDP]:GDI with 2 µM GDI, 50 µM GDP and 0.5 mM GTP in a plastic chamber with reaction buffer and cover glass-supported membrane. Under these conditions, we observe a low and steady background fluorescence from the inactive GTPase:GDI complex (Figure 4.6). Then injecting 200 nM of the Rabex5:Rabaptin5 complex triggers the GEF-mediated nucleotide exchange and CF488A-Rab5 SLB localization, which manifests as a characteristic sigmoidal increase in fluorescence intensity. The signal continues to accumulate across the whole field of view for several minutes and plateaus after 40 min. By fitting the Gompertz function [Tjørve and Tjørve, 2017] to time courses, we determine the maximum rate of the signal increase k_{max} and the corresponding temporal delay T_i at the sigmoid inflection point.

Interestingly, switching the order of component addition influences the Rab5 activation properties. When we incubated sCy5-Rab5:GDI with Rabex5:Rabaptin5 in presence of excess GDI and induced the GTPase activation with GTP addition, we observed and initial overshoot of Rab5 intensity as a result of burst in sCy5-Rab5 membrane binding (Figure 4.7). In absence of excess GDI, the system switched to active

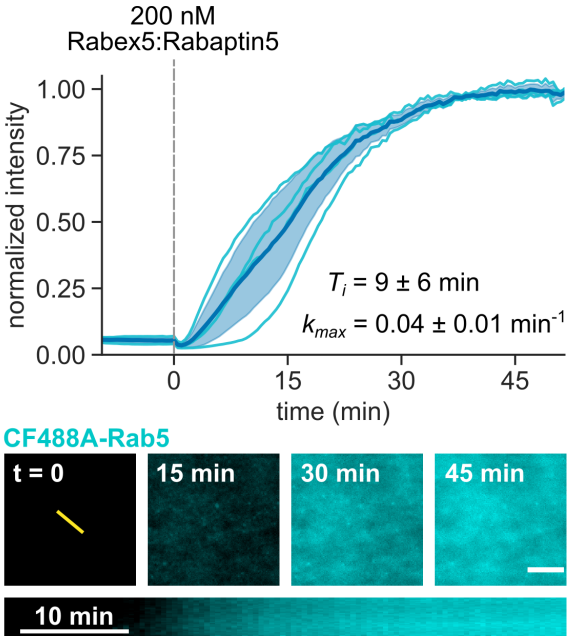

Figure 4.6: **The GEF complex induces Rab5 membrane localization.**

Top panel: addition of Rabex5:Rabaptin5 triggers nucleotide exchange by CF488A-Rab5, which can be followed by an increase of fluorescence intensity on the membrane surface. The reaction composition was 500 nM CF488A-Rab5:GDI, 2 µM GDI and 200 nM Rabex5:Rabaptin5. Solid blue line is mean normalized intensity and individual traces are shown in cyan, shaded area corresponds to ± SD (n = 4). Bottom: micrographs of CF488A-Rab5 binding to the SLB after addition of 200 nM GEF complex and corresponding kymograph (below) taken along the yellow line. Scale bar = 5 µm.

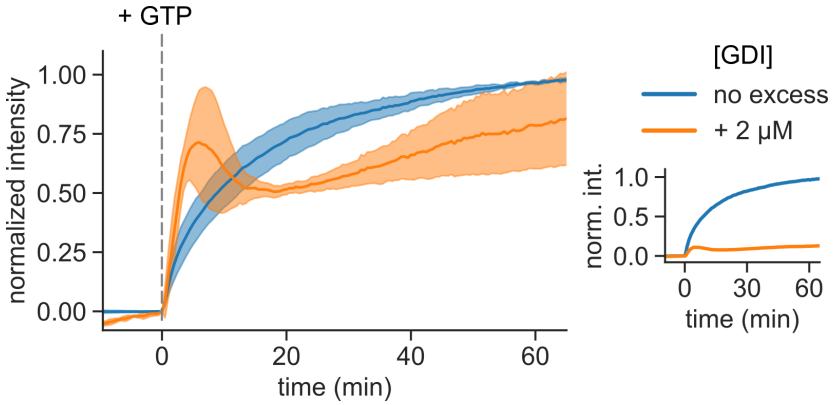

Figure 4.7: **Rab5:GDI activation with GTP induces an overshoot.**
Induction of Rab5 activation with GTP is different in presence or absence of excess GDI. In these experiments 500 nM sCy5-Rab5:GDI and 100 nM Rabex5:Rabaptin5 was incubated in presence (blue curve) or absence of 2 µM free GDI excess (orange curve) for at least 10 min. The GTPase activation was then induced with addition of 0.5 mM GTP from 25 mM stock at t = 0. Both reaction compositions immediately initiated Rab5 activation, which was contained after 5 min in presence of excess GDI to produce and overshoot and reach steady state, which was at 10-15 % of the mean maximal intensity in GDI excess absence (inset). The solid lines are mean normalized intensities, shaded areas correspond to ± SD (n = 5). The mean intensity trace with GDI excess in inset was scaled by dividing the measured sCy5 fluorescence values with average maximum intensities in experiments without free GDI.

state immediately and reached steady state that was 10-fold higher than in presence of 2 µM GDI. This discrepancy compared to the activation induction with GEF (Figure 4.6) is likely explained by the inefficient mixing of GTP when added to the reaction chamber in great stoichiometric excess. Also, incubating Rab5:GDI with the GEF complex could prime the reconstituted system for faster Rab5 activation through transient Rabex5:Rabaptin5 membrane binding and Rabex5:Rab5[GDP] interaction. Consequently, the spikes in GTP concentration can trigger the primed system to immediately switch and produce an overshoot, which is soon contained by the inhibitory effect of GDI and GTP concentration equilibration. Without the GDI excess, the induced system is allowed to reach the maximum steady state value of active Rab5. Since the cellular concentration of GTP is virtually constant we focused our further *in vitro* experiments on Rabex5:Rabaptin5 addition. This experimental setup is less prone to mixing artifacts and also mimics the physiological GEF recruitment on endosomes.

4.3.2 GDI extracts inactive Rab5 from the supported membrane

Out-of-equilibrium GTPase cycling depends on both, the GEF-catalyzed nucleotide exchange and re-extraction of inactivated proteins from the membrane surface after GTP hydrolysis. Using the SLB as a membrane substrate, we successfully demonstrated Rab5 activation through stable bilayer binding after GEF nucleotide exchange (Figure 4.6). However, characterizing the reverse reaction of Rab re-extraction requires a flow chamber to decouple the two halves of the Rab cycle. To this end, we prepared the SLB in flow channels and sequentially activated sCy5-labeled Rab5 with GTP to achieve membrane binding, followed by EDTA-induced GDP-loading of the lipid-anchored GTPase. Finally, we injected GDI under constant flow to extract sCy5-Rab5[GDP] and prevent re-binding events. Using this setup, we confirm the nucleotide specificity of GDI extraction by loading Rab5 with non-hydrolyzable GTP analog GMP-PNP. The fluorescence signal of the GMP-PNP-loaded GTPase remained unchanged after GDI addition (Figure 4.8B). In contrast, GDP-loaded Rab5 was efficiently extracted from the SLB with 2 µM GDI within a minute after injection (Figure 4.8C). These contrasting observations further confirm the model where Rab GTPase can bind the lipid bilayer irrespective of its nucleotide state. It is only the continuous extraction of the inactive proteins by GDI that controls the distribution of GTP and GDP-bound proteins between the membranes and solution [Wu *et al.*, 2010]. Furthermore, if we assume that Rab5 extraction by the GDI coincides with Rab5:GDI complex formation, we observe the association (half-extraction) constant $K_{0.5}$ = 6 µM (Figure 4.8D). The determined constant is in good agreement with previously reported values for the yeast Ypt7(Rab7):GDI interaction [Pylypenko *et al.*, 2006]. What is more, the linear range (0-1.25 µM GDI) association rate constant is 0.08 s^{-1} μM^{-1}, which would correspond to 250 nM dissociation constant K_d if we account for previously reported dissociation rate constant 0.02 s^{-1} [Wu *et al.*, 2010; Oesterlin *et al.*, 2012]. Surprisingly, this estimated value is one to two orders of magnitude higher than previously thought [Shapiro and Pfeffer, 1995; Wu *et al.*, 2010].

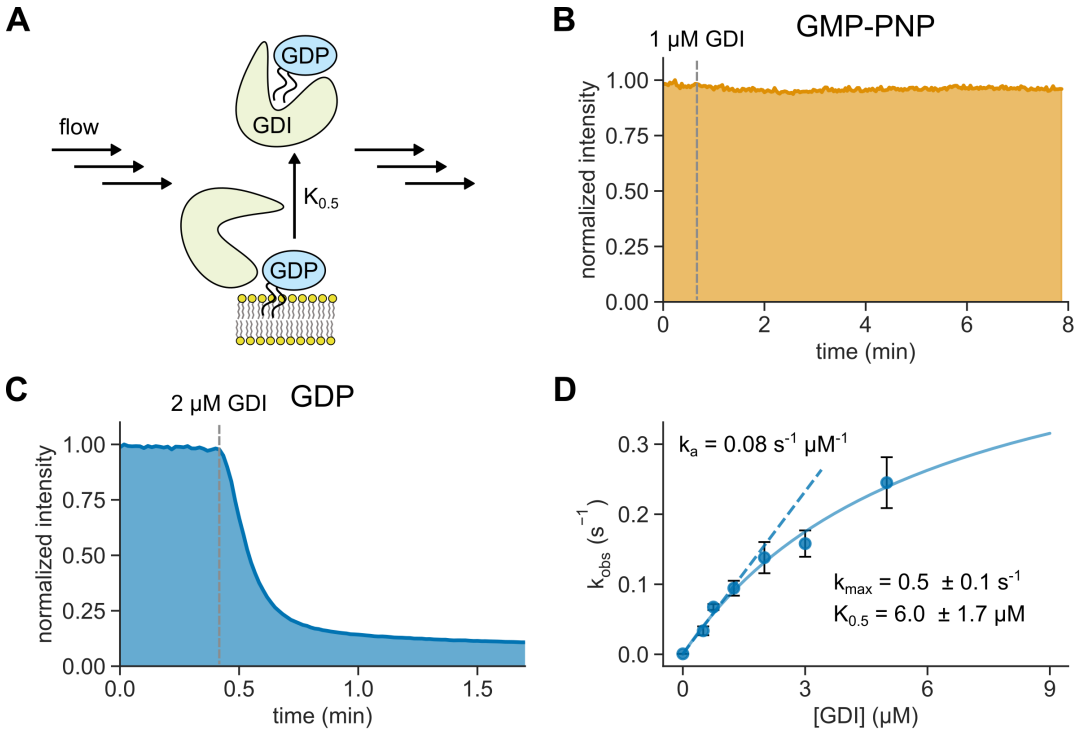

Figure 4.8: **GDI extracts inactive Rab5 from the SLB.**

(A) Illustration of Rab5[GDP] extraction. **(B)** GDI cannot extract GMP-PNP-loaded Rab5 from the SLB. 100 nM sCy5-Rab5:GDI was first activated with 20 nM ΔRabex5:Rabaptin5 and loaded with GMP-PNP in 5 mM EDTA. 1 μM GDI under 5 μL/s flow did not extract the GTPase from the SLB. **(C)** GDI efficiently extracts GDP-loaded Rab5 from the SLB. We used ΔRabex5:Rabaptin5 to first activate 100 nM sCy5-Rab5:GDI. 5 mM EDTA was later used to load the SLB-bound GTPase with GDP and 2 μM GDI was flowed though the reaction chamber at 10 μL/s. **(D)** The GDI sCy5-Rab5 extraction rate titration curve. Solid line is hyperbolic function fit, dashed line is linear fit to interval [0, 1.25] μM GDI, points are means from 3 independent experiments and error bars are ± SD.

4.3.3 Network components collectively redistribute to the membrane surface

Presumably, the traced CF488A-Rab5 fluorescence increase at the SLB (Figure 4.6) corresponds to a system-scale emergent collective switching after GEF-mediated nucleotide exchange, resulting in Rab5 polarization to the membrane surface [Altschuler *et al.*, 2008]. The coordinated GTPase state transition at an ensemble level is relevant for decisive downstream signaling [Heinrich *et al.*, 2002; Ferrell and Ha, 2014c; Huang *et al.*, 2019]. This is in contrast to sparse and sporadic nucleotide exchange as an expected consequence of Rab sequestration by the GDI [Collins, 2003]. The rare non-coordinated Rab activation would be filtered out as noise in the cytosol and could not trigger downstream cascades [Huang *et al.*, 2016]. To determine the extent of network polarization, we visualized the relative localizations of specific protein components before and after Rab5 activation. This was achieved by taking a series of micrographs along the Z-axis using a laser scanning confocal microscope (Figure 4.9). Comparing relative distributions of the labeled components in the reaction chamber, we observe the collective Rab5 transition from soluble- to membrane-bound state in the 3rd dimension. Interestingly, based on initial fluorescence intensity there exists a fraction of membrane-bound proteins even before the GTP addition. We assume that this Rab5 population contributes to the measured basal signal in the TIRF assay and is available substrate for catalyzed nucleotide exchange [Wu *et al.*, 2010]. After the exchange, there is a dramatic polarization in Rab5 and GEF localizations. Both network components redistribute towards the SLB-plane in agreement with Rab5[GTP]-specific effector recruitment of the Rabex5:Rabaptin5. At the active steady state, the reaction solution is locally depleted of soluble components, highlighting the coordinated network's response as a whole.

The network switching between the OFF- and ON-states can thus be interpreted by GTPase polarization with increase in Rab5 membrane density and reduced exchange with cytosol. In the OFF-state, low-density inactive Rab5 is continuously cycling between the membrane and soluble GDI complex. Conversely, after collective transition to ON-state, active Rab5 forms dense membrane-bound protein domain, which is resistant to GDI extraction. This dynamics can be captured by fluorescence recovery

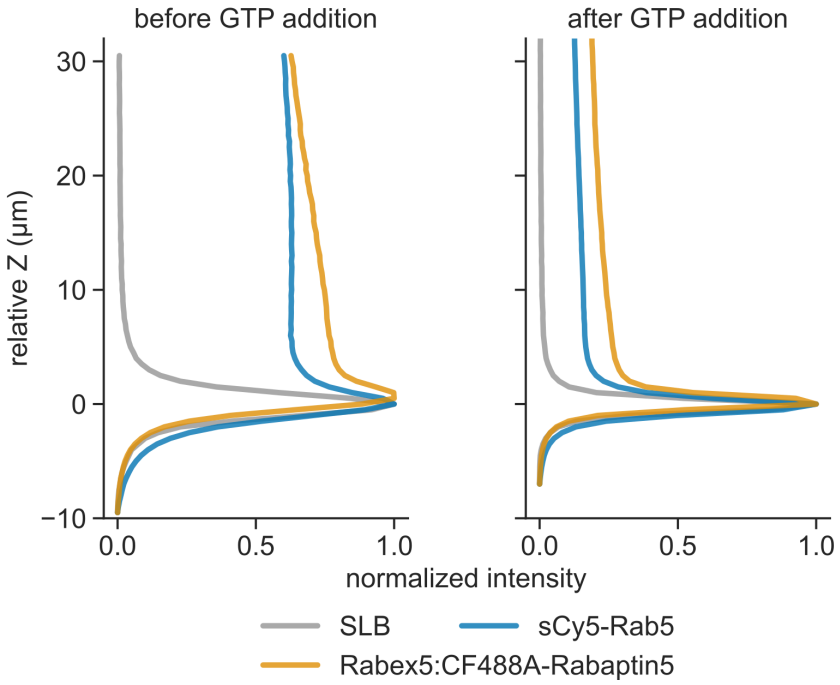

Figure 4.9: **Labeled components localize to the lipid bilayer after Rab5 activation.**
A Z-stack of the reaction chamber before and after system activation reveal relative distribution of labeled components. The reconstituted system was composed of 500 nM sCy5-Rab5:GDI, 2 µM GDI and 200 nM Rabex5:CF488A-Rabaptin5 in presence of DOPE-RhodB labeled SLB. The nucleotide exchange reaction is induced by GTP addition to 0.5 mM and left to reach steady state. The slices along the Z axis were aquired in 0.5 µm steps on a laser scanning confocal microscope. The traces represent fluorescence intensity normalized to the maximal measured signal in respective channel.

after bleaching (FRAP) before and after system switching (Figure 4.10). In GDP-bound state, the bleached population is rapidly exchanged with non-bleached proteins at k_{off} = 0.12 s^{-1}, which is in good agreement with the 2 µM GDI extraction rate under flow (Figure 4.8). On the other hand, the photobleached GTP- or GMP-PNP-bound GTPase population recovers only slowly through lateral diffusion and ongoing GEF activation when the nucleotide exchange reaction was let to reach steady state. This is indicative of a densely-packed protein domain on the SLB after collective Rab5 activation with GTP or the non-hydrolyzable analog GMP-PNP.

These results fit with the proposed GEF complex recruitment hypothesis, which drives a positive feedback loop of GTPase activation, resulting in active Rab5 membrane patches [Lippé *et al.*, 2001; Zerial and McBride, 2001; Zhang *et al.*, 2014; Franke *et al.*, 2019]. Despite the great interest, this non-linear regulation was not successfully demonstrated on system's level due to the intrinsic complexity of a living cell. Conversely, our *in vitro* reconstitution approach is particularly well suited to systematically probe the network's input-output responses under different controlled conditions – uncovering intrinsic system properties.

4.4 Rab5 activation is ultrasensitive and stochastic

Positive feedback loop through the effector Rabaptin5 and associated GEF Rabex5 has been postulated to drive Rab5 activation for over two decades [Lippé *et al.*, 2001; Zerial and McBride, 2001; Zhang *et al.*, 2014; Horiuchi *et al.*, 1997]. Utilizing *in vitro* reconstitution, we aimed to test this long-standing hypothesis by determining the system's response to an increasing input signal, i.e. the GEF concentration (Figure 4.11A). Generally, non-linear activation mechanisms like positive feedback give rise to sigmoidal signal-response curves [Barr, 2013] with Hill coefficient $n > 1$, signifying cooperativity (or ultrasensitivity). In these cases a system's response from 10 % to 90 % of the maximum happens over < 81-fold increase of the incoming signal [Koshland *et al.*, 1982]. Strikingly, we found that the GEF titration resulted in an ultrasensitive two-state response profile of Rab5 activation. While there is no activation at GEF concentrations below 20 nM even 150 minutes after Rabex5:Rabaptin5 injection (orange circles, Figure 4.11B), we see a 10- to 80-fold increase in Rab5 signal on the membrane

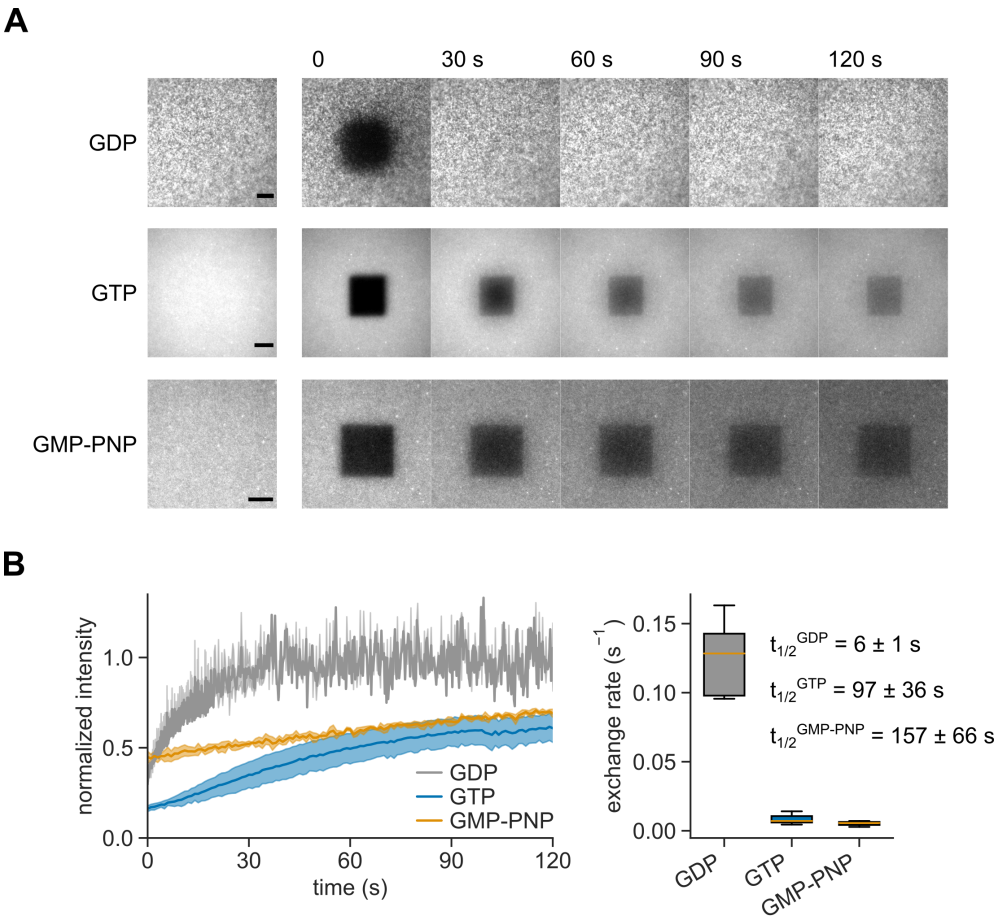

Figure 4.10: **Active Rab5 forms dense protein domain on the SLB.**

(A) FRAP sequences for SLB-bound CF488A-Rab5 at steady state before activation (GDP) and after nucleotide exchange with GTP and GMP-PNP. Area of roughly 20×20 µm was bleached by exposing each pixel to high-power 488 nm laser for 3-5 ms. The activation reaction was triggered with 80 nM Rabex5:Rabaptin5. After bleaching, the GTP- and GMP-PNP-bound Rab5 reached new steady state of fluorescence intensity after ca. 2 min. The scale bar corresponds to 10 µm. **(B)** The recovery profiles, observed exchange rates and half-times of GDP- (n = 8), GTP- (n = 6) and GMP-PNP-loaded Rab5 (n = 3). The calculated half-times are mean ± SD.

with higher concentrations of the GEF. The abrupt transition to collective ON state at critical GEF concentration is also accompanied by large variance in fold change, a sign of emergent stochastic bistability [Qian, 2012]. Overall, this system property strongly supports a non-linear Rab5 activation mechanism.

By analyzing the respective time courses, we observe that the traces are similar in shape. However, high GEF complex concentrations (400 nM) give rise to an immediate increase in Rab5 fluorescence intensity, while the switching is delayed for up to 2 hours at intermediate GEF concentrations (Figure 4.11C). Interestingly, the temporal delays needed to reach activation inflection increase linearly with the inverse of GEF complex concentrations (Figure 4.11C, inset), which supports stochastic triggering of the collective GTPase transition [Zheng *et al.*, 2011; Borri *et al.*, 2020]. By plotting k_{max} against the increasing GEF concentration, we found that nucleotide exchange showed high non-linearity (Figure 4.11D) with a critical GEF concentration around 28 nM, where we observed significant variations between the response curves. There, some measurements had no significant response, while others resulted in fast Rab5 activation dynamics. Higher GEF concentrations allowed for rapid Rab5 membrane accumulation, where the determined rates gradually increased, in agreement with a general positive feedback model [Ferrell and Xiong, 2001]. Interestingly, the OFF-state remained stable for several hours after 8 nM GEF addition (Figure 4.12). This is typical for systems with two stable steady states, where sub-threshold input signal cannot induce collective switching.

Next, we constructed a model of the minimal reaction network to better understand the dynamic response curves and the origin of observed activation delays. The model is composed of expected molecular reactions, which includes cooperative activation due to a direct interaction of Rab5[GTP] with its GEF complex (Figure 5.1, Methods 3.20). We constructed a set of ODEs and solved the model both deterministically and stochastically using the Gillespie algorithm to incorporate biochemical noise in the reactions (Figure 4.13A). Interestingly, the stochastic solver produces similar dynamics and time delays to those observed experimentally (Figure 4.11B-D, 4.13B-D). In the absence of stochasticity, the predicted response curves deviated from the experiments, where *(i)* at early times the intensity profiles were not flat, unlike measured experimentally; *(ii)* the time courses for intermediate [GEF] were not sigmoidal in shape and *(iii)*

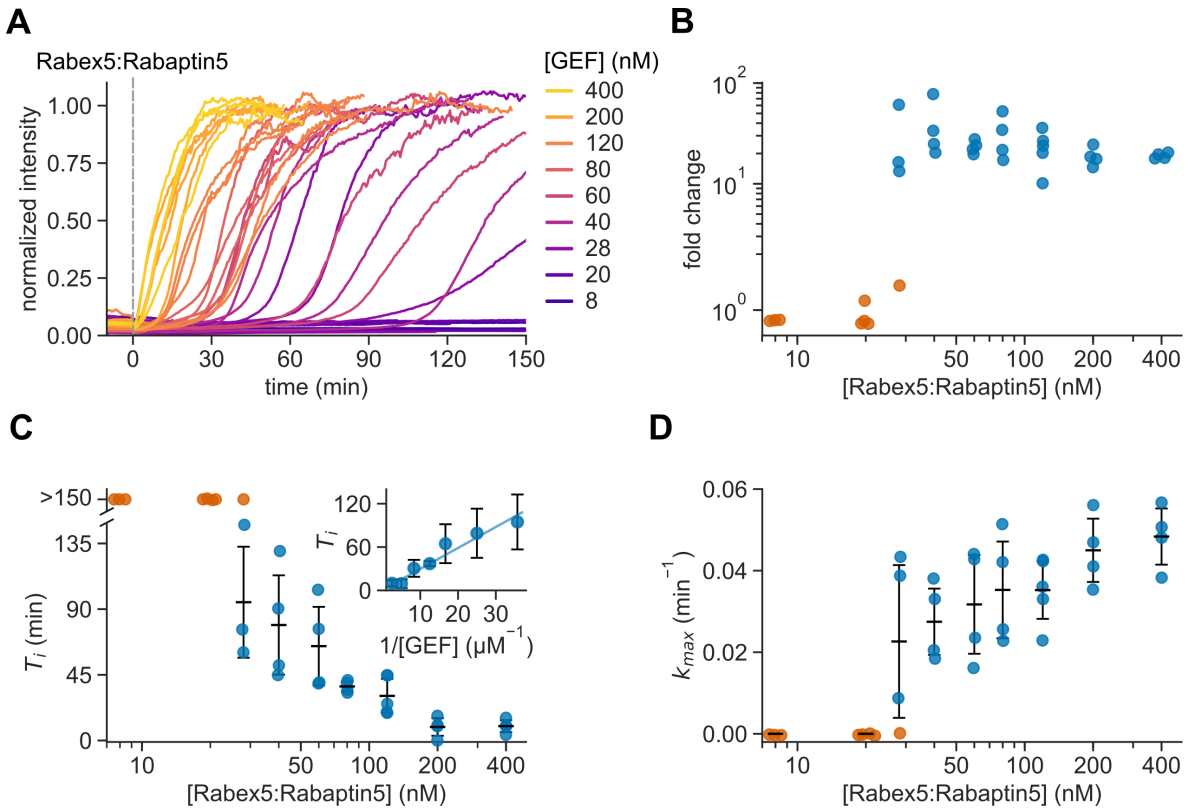

Figure 4.11: **Rab5 activation is ultrasensitive.**

(A) Rab5 intensity traces obtained at increasing Rabex5:Rabaptin5 concentrations. **(B)** Rab5:GDI-Rabex5:Rabaptin5 activation response curve. The fold change was calculated by dividing the fluorescence intensity at steady state with the average signal 10 min before GEF addition. **(C)** Activation delay T_i decreases with higher Rabex5:Rabaptin5 concentration. Inset: temporal delays linearly increase with 1/[GEF]. Where no detectable activation was observed within 150 min, the T_is are denoted as $>$ 150 min and shown in orange. Error bars are $\pm$ SD. **(D)** Relative maximum rates k_{max} against the GEF complex concentration also reveal cooperativity of Rab5 activation. Without detectable system switching within 150 min, the activation rate was determined to be 0 and the corresponding points are depicted in orange. Error bars are means $\pm$ SD.

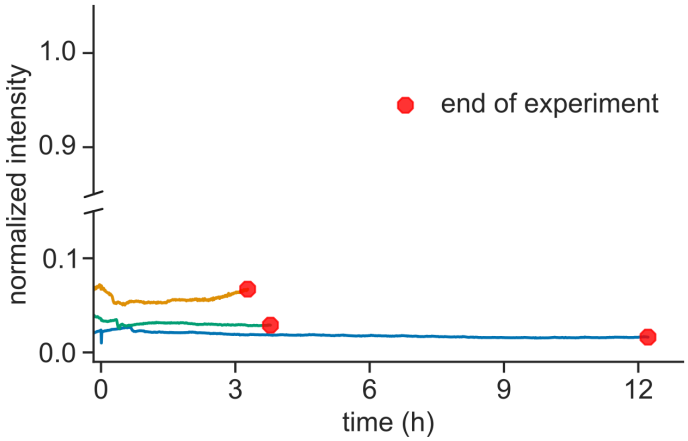

Figure 4.12: **Low amounts of Rabex5:Rabaptin5 fail to trigger collective switching even after 12 hours.**

Prolonged kinetic traces of Rab5:GDI with 8 nM Rabex5:Rabaptin5. CF488A-Rab5[GDP]:GDI was incubated with GDI, GTP and 10-times lower amount of GDP in an immobilized reaction chamber above glass supported membrane. After 10 min, 8 nM Rabex5:Rabaptin5 was injected and CF488A-Rab5 fluorescence signal was tracked with TIRF microscopy at the SLB focal plane in 30 s intervals. Final concentrations were: 500 nM CF488A-Rab5:GDI, 2 µM GDI, 0.5 mM GTP, 0.05 mM GDP and 8 nM Rabex5:Rabaptin5. To compare the traces with others, we normalized the fluorescence measurements to the mean activation steady state values on the respective microscope setup.

near the critical Rab5 concentration ($\approx$ 30 nM), the model cannot replicate the variation in switching times. For highest and lowest GEF concentrations, both types of solutions are in close agreement. Together, our experimental and theoretical results provide clear indication for positive feedback within a minimal Rab activation network, which is sufficient to generate switch-like, ultrasensitive behavior. Furthermore, stochasticity is relevant for the system response near the critical switching concentration.

Despite, there is a number of cooperative activation mechanisms that can result in similar behavior besides the positive feedback loop. For example, Rabex5 is expressed in an auto-inhibited conformation, which can be released by Rabaptin5 or ubiquitin binding [Delprato and Lambright, 2007; Zhang *et al.*, 2014; Lauer *et al.*, 2019]. Furthermore, a cascading nucleation of higher-order GEF supercomplexes could also result in ultrasensitivity [Zhang *et al.*, 2014]. To elucidate the mechanism of cooperative collective Rab5 switching, we prepared a number of GEF complex deletion mutants to assay the key molecular interactions.

4.5 Positive feedback of Rab5 activation depends on GEF recruitment

The GEF titration revealed non-linear collective Rab5 activation, but did not answer open questions on the underlying mechanisms. Earlier structural and biochemistry studies reported several possible molecular interactions that could contribute to the cooperative Rab5 activation by Rabex5:Rabaptin5 complex *in vivo*. Firstly, as the Rabex5:Rabaptin5 consists of a GEF and effector assembly, membrane recruitment by active Rab5 could drive positive feedback in nucleotide exchange [Lippé *et al.*, 2001]. Secondly, the Rabex5 binding to Rabaptin5, Rab5 and ubiquitin induces allosteric conformational change in the GEF, which displaces auto-inhibitory elements to enhance catalytic activity [Delprato and Lambright, 2007; Zhang *et al.*, 2014; Lauer *et al.*, 2019]. Thirdly, Rabaptin5 forms higher order homodimer coiled-coil structures [Zhu *et al.*, 2004; Zhang *et al.*, 2014], which could promote nucleation sites of positive feedback [Arosio *et al.*, 2015] and even phase separation through multivalent transient interactions [Banani *et al.*, 2017]. Apart from Rab5, the GEF complex could also be actively

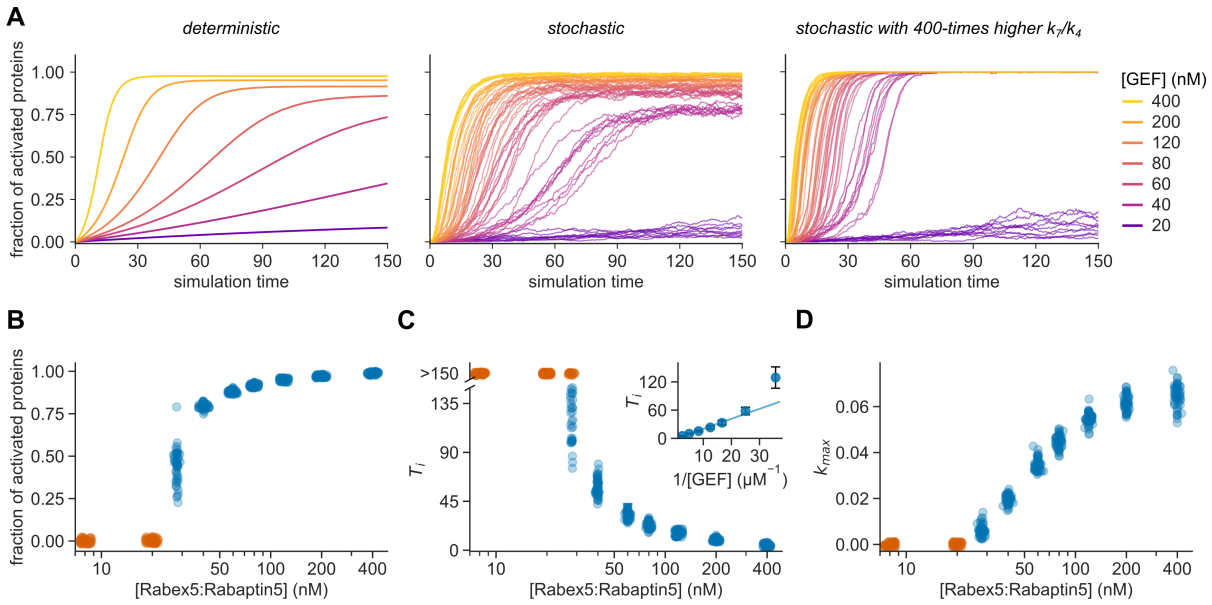

Figure 4.13: **Rab5 activation is stochastic.**

(A) Simulation results of Rab5 activation model. Only by running the stochastic simulations, we could observe the characteristic delays in activation and sigmoidal reaction profiles near the critical GEF concentration (see Figure 4.11A). At high GEF concentrations, the stochastic and deterministic solutions are comparable, in agreement with diminished stochastic effects. Increasing the k_7/k_4 ratio (i.e. greater positive feedback effect) reduces the temporal delay and increases rates of collective switching. Under these conditions, the critical GEF concentration is maintained above 20 nM. The stochastic simulations were run 50-times per condition. Depicted are 10 random runs per given GEF concentration. Parameters in middle panel capture the experimental results best and were used in all following model runs. **(B-D)** Signal fold change, temporal delays and relative maximum rates from the stochastic simulations in panel A, middle. We ran 50 individual stochastic simulations per condition. The simulations were performed by Hrushikesh Loya.

recruited to the early endosomes (EEs) by an independent mechanism during vesicle maturation process. Namely, Rabex5 consists of a positively charged N-terminal helical bundle [Zhu *et al.*, 2007] and ubiquitin-binding domains[Mattera and Bonifacino, 2008; Penengo *et al.*, 2006; Lee *et al.*, 2006]. Importantly, both structures could pick up on dynamic EE-specific molecular cues to localize the GEF on the bilayer surface, enhancing Rab5 nucleotide exchange. Furthermore, Rabaptin5 can be recruited by Rab4 in a feed-forward loop to drive Rab5 activation *in vivo* [Kälin *et al.*, 2015]. Inside the complex cellular environment, all of the observed mechanisms could contribute to Rab5 activation on EE to a different extent. Thus, identification of the basic Rab5 collective activation mechanism is needed in a minimal biochemical network.

4.5.1 GEF recruitment is necessary for collective Rab5 activation

The longest standing theory is the Rab5-mediated GEF recruitment [Lippé *et al.*, 2001; Zerial and McBride, 2001]. This proposed mechanism depends on Rab5[GTP]:Rabaptin5 interaction, which brings associated Rabex5 on the membrane surface to efficiently promote Rab activation. We set of to test this hypothesis by assaying a set of GEF complex deletion mutants (Figures 4.1D, 4.14A) in the GEF activity assay with soluble Rab5 and SLB-based *in vitro* reconstitution with native prenylated Rab5:GDI.

First, we prepared Rabex5 and Rabaptin5 deletion mutants to specifically test the influence of GEF membrane binding (ΔRabex5) and effector recruitment by Rab5-[GTP] (Δ_{RBD}Rabaptin5) in GTPase activation. All assayed GEF complex deletion mutants were catalytically active on mant-GDP loaded soluble Rab5 (i.e. unprenylated), in absence of membranes and GDI (Figure 4.14B). We used the full length Rabex5:Rabaptin5 and inactive Rabex5D314:Rabaptin5 [Langemeyer *et al.*, 2014] as positive and negative control, respectively. In agreement with previous studies [Lippé *et al.*, 2001; Delprato *et al.*, 2004; Delprato and Lambright, 2007; Zhang *et al.*, 2014], ΔRabex5 alone was slightly less active as Rabex5:Rabaptin5 due to the auto-inhibitory C-terminal coiled-coil region, which is displaced in complex with Rabaptin5. Conversely, the ΔRabex5:Rabaptin5 exhibited the highest nucleotide exchange efficiency, which fits well with recent reports on allosteric inhibitory effects of N-terminal Rabex5 domains [Lauer *et al.*, 2019]. Thus, this GEF complex represents the fully active GEF

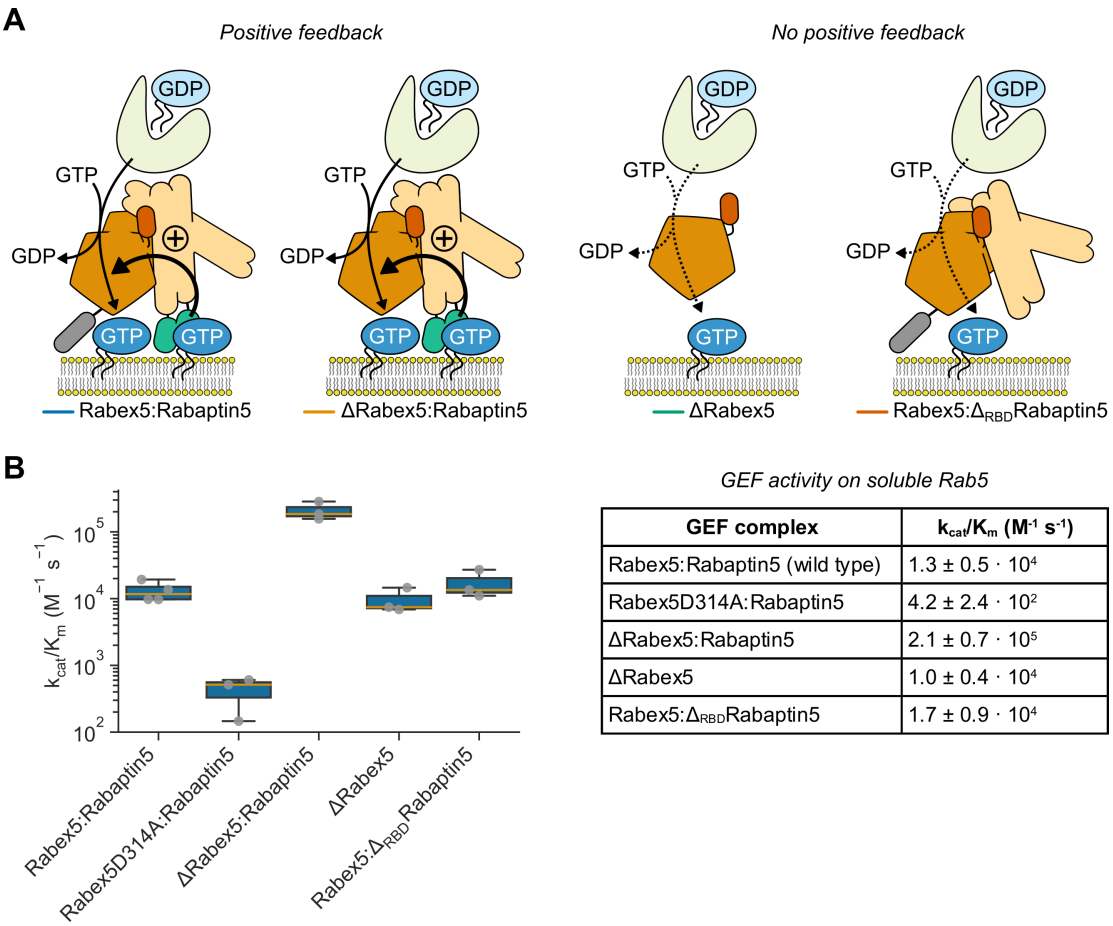

GEF activity on soluble Rab5

GEF complex	k_{cat}/K_m (M^{-1} s^{-1})
Rabex5:Rabaptin5 (wild type)	$1.3 \pm 0.5 \cdot 10^4$
Rabex5D314A:Rabaptin5	$4.2 \pm 2.4 \cdot 10^2$
ΔRabex5:Rabaptin5	$2.1 \pm 0.7 \cdot 10^5$
ΔRabex5	$1.0 \pm 0.4 \cdot 10^4$
Rabex5:Δ_{RBD}Rabaptin5	$1.7 \pm 0.9 \cdot 10^4$

Figure 4.14: **Nucleotide exchange efficiency of GEF complex variants.**

(A) Schematic representation of GEF complex deletion mutants. According to the GEF recruitment hypothesis, the positive feedback originates from a direct interaction between Rabex5:Rabaptin5 and Rab5[GTP]. We assayed Rabex5 lacking the membrane and Ub-binding domains ΔRabex5 in complex with Rabaptin5 or alone and Δ_{RBD}Rabaptin5 lacking Rab5 interaction domains in Rabex5 complex. Of note, the full length Rabex5 aggregated during purification and was not included in the assay. **(B)** The GEF complex deletion mutants are active on soluble Rab5. Bacterially expressed Rab5 was loaded with mant-GDP and the nucleotide exchange efficiency k_{cat}/K_m at 37 °C was determined for GEF complex variants, which were used in this study. Rabex5D314A is a catalytically inactive GEF mutant [Langemeyer *et al.*, 2014] and serves as a negative control. The calculated k_{cat}/K_m are means ± SD.

complex mutant.

Next, we compared these results with the ability of GEF complexes to trigger collective GTPase switching in the reconstitution assay with lipidated Rab5:GDI and SLBs. By measuring the fluorescence intensity change as a consequence of collective CF488A-Rab5 activation, we see a clear dependence on Rab5:Rabaptin5 interaction (Figure 4.15). Only the full length Rabex5:Rabpatin5 and ΔRabex5:Rabaptin5 could trigger full Rab5 activation. This also suggests that the Rabex5 N-terminal membrane binding motifs are not crucial for successful switching *in vitro* because ΔRabex5:Rabaptin5 is as effective in Rab5 activation as the wild type. Conversely, ΔRabex5 alone and Rabex5:Δ_{RBD}Rabaptin5 did not support collective activation. With these two deletion mutants, a direct GEF complex:Rab5[GTP] interaction is not possible, either because of Rab5 binding domains deletion(Δ_{RBD}Rabaptin5) or the lack of Rabaptin5 altogether. Strikingly, the same dependence on direct Rab5:GEF interaction is reproduced also in stochastic model simulations (Figure 4.15C). There, basal GTPase activation is still possible, but it similarly does not lead to system state switching. Altogether, these results demonstrate that the formation of ternary Rab5:GEF effector complex is absolutely necessary to achieve collective Rab5 activation. This also confirms the positive feedback hypothesis of GEF recruitment, which was proposed almost two decades ago [Lippé *et al.*, 2001; Zerial and McBride, 2001]. Furthermore, we demonstrate that nucleotide exchange activity on soluble Rab5 (Figure 4.14B) does not necessary mirror a GEF's ability to achieve biologically relevant collective GTPase switching in presence of GDI-bound and lipid modified Rab proteins (Figure 4.15A).

Taking advantage of our *in vitro* reconstitution approach, we were able to visualize temporal recruitment of labeled network components during Rab5 activation with 200 nM GEF (Figure 4.15B). Using dual-color imaging, we detect both CF488A-Rab5 and Rabex5:sCy5-Rabaptin5 signal increase. What is more, the two traces take similar shapes, further confirming that Rabex5:Rabaptin5 is retained on the membrane by active Rab5[GTP] to engage in the positive feedback loop. Under these conditions, the mean delay times for Rab5 collective switching were 23.3 $\pm$ 4.6 min, with Rabex5:Rabaptin5 signal reaching the inflection point 5.8 min later, 29.1 $\pm$ 5.0 min after injection. This is also captured in our stochastic model (Figure 4.15D) [Zhu *et al.*, 2010]. The observed delay in GTPase and GEF signals suggests that efficient Rabex5:Rabaptin5

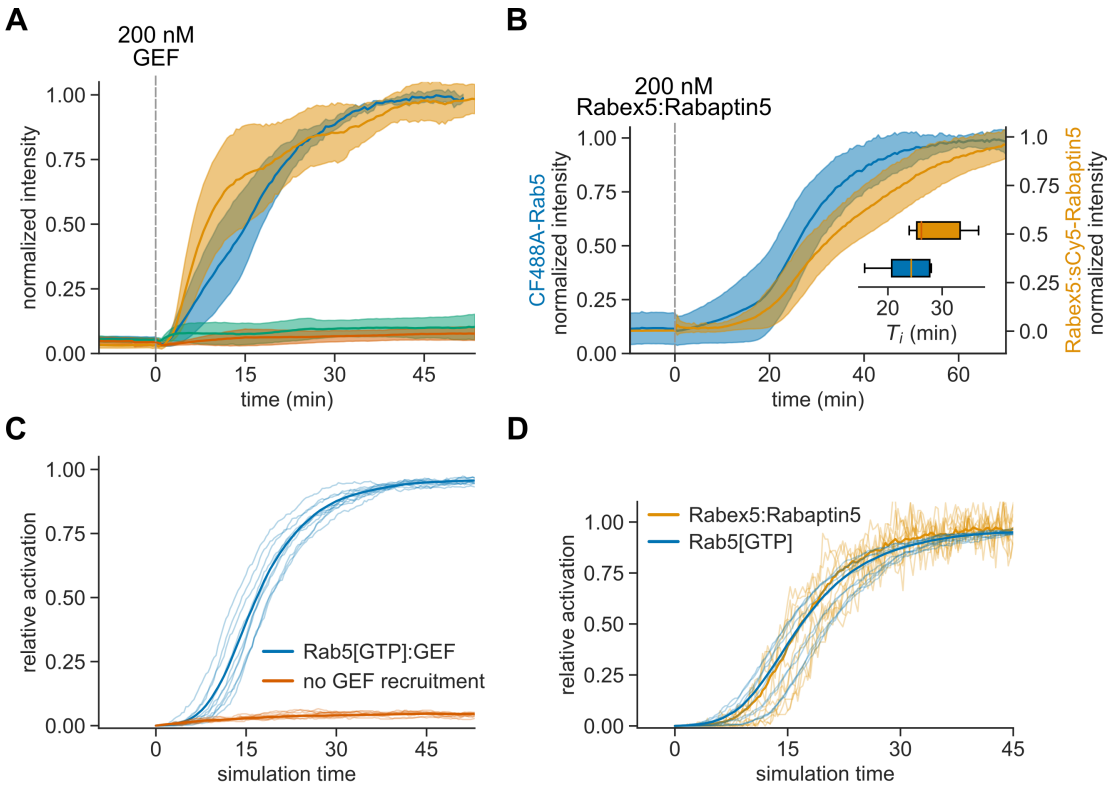

Figure 4.15: **GEF recruitment supports collective Rab5 switching.**

(A) Fluorescence intensity traces obtained from experiments schematically depicted in Figure 4.14A. 200 nM of GEF complexes were used to induce collective Rab5 switching. The initial reaction composition was 500 nM CF488A-Rab5:GDI, 2 µM GDI and 0.5 mM GTP in Rab reaction buffer. Solid lines are mean normalized intensities, shaded areas are SD (Rabex5:Rabaptin5, ΔRabex5:Rabaptin5 n = 4; ΔRabex5, Rabex5:Δ_{RBD}Rabaptin5 n = 3). **(B)** Kinetic traces of CF488A-Rab5 and Rabex5:sCy5-Rabaptin5 during activation. 500 nM CF488A-Rab5:GDI, 2 µM GDI and 0.5 mM GTP were first incubated in reaction chamber with SLB. Rab5 activation was triggered with 1:1 mixture of labeled Rabex5:sCy5-Rabaptin5 and wild type Rabex5:Rabaptin5 at 200 nM. Solid line is mean relative normalized fluorescence intensity, shaded area is SD (n = 5). Inset: T_i for CF488A-Rab5 (blue) and Rabex5:sCy5-Rabaptin5 (orange). **(C-D)** Stochastic model simulations with and without Rabex5:Rabaptin5:Rab5[GTP] complex formation ($k5$, $k6$ = 0) (C) and Rab5, Rabex5:Rabaptin5 membrane binding (D) for 200 Rabex5:Rabaptin5 particles. Average curves from 50 individual runs are depicted in bold with 10 random traces per condition. The simulations were performed by Hrushikesh Loya.

membrane localization depends on a critical Rab5[GTP] density, which can support the transition from basal nucleotide exchange activity of freely-diffusing GEF complex to the cooperative positive feedback that requires Rab5[GTP]:Rabaptin5:Rabex5 ternary complex [Zhu *et al.*, 2010; Jilkine *et al.*, 2011]. The characteristic delays in Rab5 collective switching (Figure 4.11C) are thus indicative of positive feedback engagement after slow Rab5[GTP] accumulation to a critical level with intermediate GEF amounts.

4.5.2 Active Rab5 triggers positive feedback

If Rabex5:Rabaptin5 membrane retention by active Rab5 triggers positive feedback, we would expect reduced temporal delays and more efficient activation when there is Rab5[GTP] present on the bilayer prior to GEF injection. We answered this hypothesis by immobilizing a GTP-loaded and GTPase deficient Rab5Q80L-His_{10} mutant on DOGS-NTA[Ni^{2+}]-containing SLB before Rab5:GDI activation (Figure 4.16A). We find that the delays to reach inflection point (T_i) are significantly reduced with increased DOGS-NTA concentration (Figure 4.16B). We assume this correlates with higher density of immobilized Rab5Q80L-His_{10}, which can recruit Rabex5:Rabaptin5 immediately after addition to form the positive feedback. With 5 % DOGS-NTA, the collective switching progressed immediately at maximum rate, while it took 6 min to reach similar rate with 2 % DOGS-NTA. This is still three times quicker than experiments done on membranes without DOGS-NTA and in presence of soluble Rab5Q80L-His_{10}. Overall, the reaction progressed even faster than activation with 400 nM GEF without the immobilized mutant GTPase (Figure 4.11A), confirming the key role of active Rab5 in the formation of positive feedback.

These experiments demonstrate the important role of GEF recruitment and the resulting positive feedback in collective Rab5 activation. In a minimal network composed of Rab5:GDI complex and Rabex5:Rabaptin5, the small GTPase alone can provide the deciding molecular cue for GEF membrane localization and feedback initiation. Nonetheless, alternative factors can also retain the GEF complex on EE and promote more efficient Rab5 activation with reduction in reaction dimensionality.

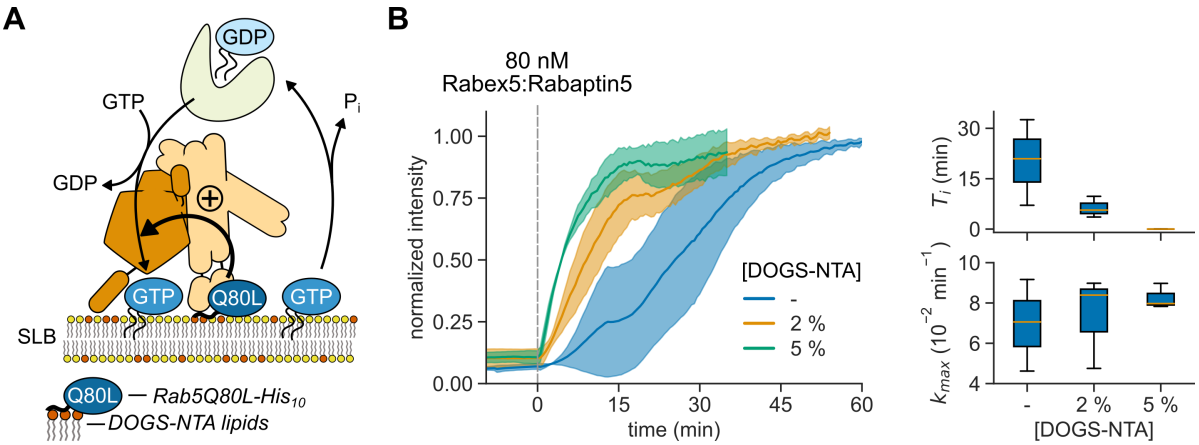

Figure 4.16: **Pre-seeded Rab5Q80L initiates positive feedback.**

(A) Schematic of the reconstitution experiment with pre-activated SLB-immobilized Rab5Q80L-His_{10}[GTP]. The His_{10} peptide anchors the GTP-loaded mutants on the supported membrane with DOGS-NTA[Ni^{2+}], where histidine residues chelate Ni^{2+} ions. Consequently, Rabex5:Rabaptin5 is immediately retained on the membrane surface and Rab5 activation positive feedback is formed. **(B)** Collective switching is faster with pre-activated Rab5. Left: Rab5 switching time courses in presence of 500 nM Rab5Q80L-His_{10} with increasing DOGS-NTA lipid concentration in the SLB. The GTP-loaded Rab5Q80L-His_{10} was first incubated on the SLB with 500 nM CF488A-Rab5:GDI, 2 µM GDI and 0.5 mM GTP. We induced the nucleotide exchange with 80 nM Rabex5:Rabaptin5. Solid line is mean normalized fluorescence intensity over time, shaded area is mean ± SD (n = 3). Right: corresponding time delays T_i and relative maximum rates k_{max}.

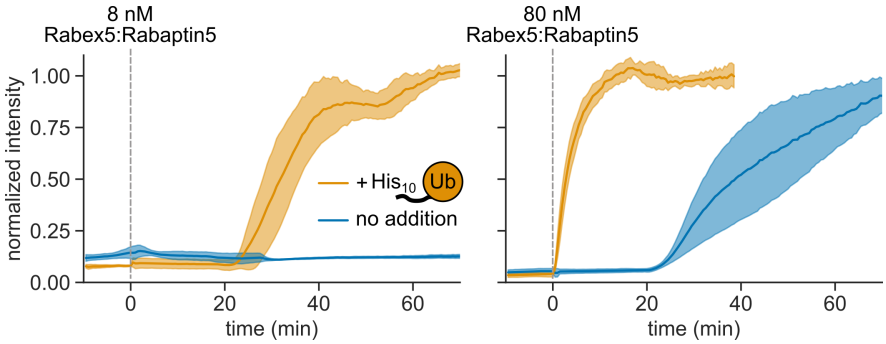

Figure 4.17: **Ubiquitin promotes collective Rab5 activation.**
Time courses of Rab5 activation on 2 % DOGS-NTA containing SLB in presence or absence of His_{10}-tagged mono-ubiquitin. The SLB was incubated with 500 nM CF488A-Rab5:GDI, 2 µM GDI, 0.5 mM GTP (blue traces) and 500 nM His_{10}-Ub (orange). Network switching was induced with either 8- (left) or 80 nM Rabex5:Rabaptin5 (right). Solid lines are means (8 nM GEF (+ Ub) n = 3; 8 nM GEF (- Ub) n = 3; 80 nM GEF n = 5) with $\pm$ SD according to the shaded area.

4.5.3 Ubiquitin can promote Rab5 activation by GEF recruitment

Transmembrane proteins on plasma membrane and in the Golgi network are targeted towards the endosome system, where there are trafficked to the recycling or degradation pathways. Particularly, receptor proteins undergo mono-ubiquitination on the cytosolic domains, which promotes vesicle budding, internalization and early endosome maturation [Hicke, 2001; Di Fiore *et al.*, 2003]. This molecular label is also recognized by Rabex5 N-terminal domains [Lee *et al.*, 2006], which could promote Rab5 activation without pre-existing Rab5[GTP] pool on the EE surface. We set off to evaluate this hypothesis by binding His_{10}-Ub to the SLB surface by DOGS-NTA[Ni^{2+}] chelation and inducing Rab5 activation with full length Rabex5:Rabaptin5 (Figure 4.17).

In a minimal network, GEF concentrations below 20 nM cannot promote Rab5 switching (Figure 4.11). Still, when we bind Ub to the membrane surface, Rab5 successfully switches even with 8 nM Rabex5:Rabaptin5. In fact, the observed switching delay with 8 nM GEF and Ub is comparable to the effect of 10-fold higher GEF concentration without Ub. At higher Rabex5:Rabaptin5 amounts, Ub mimics the pre-activated Rab5 effect as it triggers immediate collective activation on the SLB. Thus, Ub can initiate Rab5-independent GEF recruitment to substantially enhance the likelihood of Rab5 activation with physiological amounts of Rabex5:Rabaptin5 complex [Lippé *et al.*, 2001]. This significant effect raises the question whether Ub-mediated

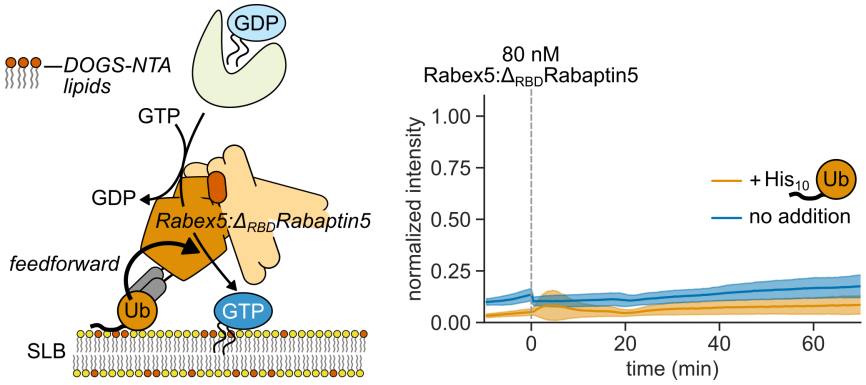

Figure 4.18: **Ubiquitin cannot bypass positive feedback.**
Left: schematic representation of Ub feed-forward experiments. To prevent the formation of positive feedback loop, we used Rabex5:Δ_{RBD}Rabaptin5 deletion mutant, which cannot interact with active Rab5. Alas, the membrane-bound Ub can independently recruit the mutant GEF, triggering a feed-forward loop to promote Rab5 activation. Right: time courses of Rab5 incubation with Rabex5:Δ_{RBD}Rabaptin5 deletion mutant on 2 % DOGS-NTA SLB in presence or absence of His$_{10}$-Ub. The SLB was incubated with 500 nM CF488A-Rab5:GDI, 2 µM GDI, 0.5 mM GTP (blue; n = 3) and 500 nM His$_{10}$-Ub (orange; n = 4). 80 nM Rabex5:Δ_{RBD}Rabaptin5 was added to induce Rab5 activation. Solid lines are means with $\pm$ SD in the shaded area. Individual fluorescence traces were normalized to average active steady state values for wild type GEF + Ub on respective microscope systems (Figure 4.17).

GEF recruitment can bypass the positive feedback of Rab5 activation altogether. The reported release of auto-inhibition [Lauer *et al.*, 2019] could provide the necessary non-linear response profile, triggering network. In fact, a Rab5-independent Ub- and Rab4 feedforward mechanism has been proposed as an alternative model to the positive feedback of GEF recruitment in Rab5 activation [Kälin *et al.*, 2015]. To distinguish between the two control mechanisms, we used the Rab5 binding-deficient mutant Rabex5:Δ_{RBD}Rabaptin5 in concert with His$_{10}$-Ub SLB immobilization (Figure 4.18).

Surprisingly, we did not observe collective Rab5 switching despite Ub membrane immobilization and induction with 80 nM Rabex5:Δ_{RBD}Rabaptin5. This underscores the importance of Rab5[GTP]:Rabaptin5 interaction, which ensures GEF co-localization and allosteric activation [Zhang *et al.*, 2014], resulting in non-linear positive feedback and collective Rab5 activation. On the other hand, despite its allosteric effects [Lauer *et al.*, 2019], the ubiquitin GEF recruitment alone cannot form a feed-forward loop above the critical threshold, imposed by GDI sequestration. Rather, ubiquitinated cargo

acts synergistically with the Rabex5:Rabaptin5-mediated positive feedback to drastically speed up Rab5 activation. This mechanism could also be used by the cell to localize Rab5 activation specifically on EE. There, Rabex5:Rabaptin5 recruitment factors like Ub [Lee *et al.*, 2006], negatively charged lipids [Delprato *et al.*, 2004] and Rab4 [Kälin *et al.*, 2015] drastically reduce the critical GEF amount and enable rapid engagement of Rab5-driven positive feedback, which is a hallmark of the minimal signaling network. In turn, this keeps the probability of off-target switching low. Recently, it has been reported that small population of Rab5 undergoes mono-ubiquitination, which interferes with Rabaptin5 effector binding [Shin *et al.*, 2017]. The role of this modification remains unclear, however it could serve as a cut-off switch for the positive feedback.

4.6 Rab5[GDP] availability tunes collective switching

Clearly, active Rab5 can direct collective system switching by promoting Rabex5:Rabaptin5 mediated positive feedback. What about inactive Rab5? The GDP-bound Rab5 is largely solubilized in a tight GDI complex, which is not a direct substrate for nucleotide exchange. In fact, it is thought that a small population of membrane-bound and GDI-free small GTPase is available for GEF interaction [Wu *et al.*, 2010]. However, Rabs and GDI form a tight association in µM to nM range [Pylypenko *et al.*, 2006]. Consequently, the disassociated, yet inactive membrane Rab pool has not been observed in a dynamic equilibrium with the sequestered fraction. By using bright synthetic fluorescent dyes and TIRF microscopy, we could observe individual Rab5 particles landing and diffusing on the SLB, before being re-extracted by the GDI.

4.6.1 TIRF microscopy detects increase in single Rab5 molecule number after collective switching

One of important Rab small GTPase distinctions is their C-terminal geranylgeranylation. These lipid anchors make the modified proteins extremely hydrophobic, which explains their high membrane affinity in the nanomolar range [Shahinian and Silvius, 1995; Pylypenko *et al.*, 2006]. On the other hand, prenylated Rab proteins are insoluble

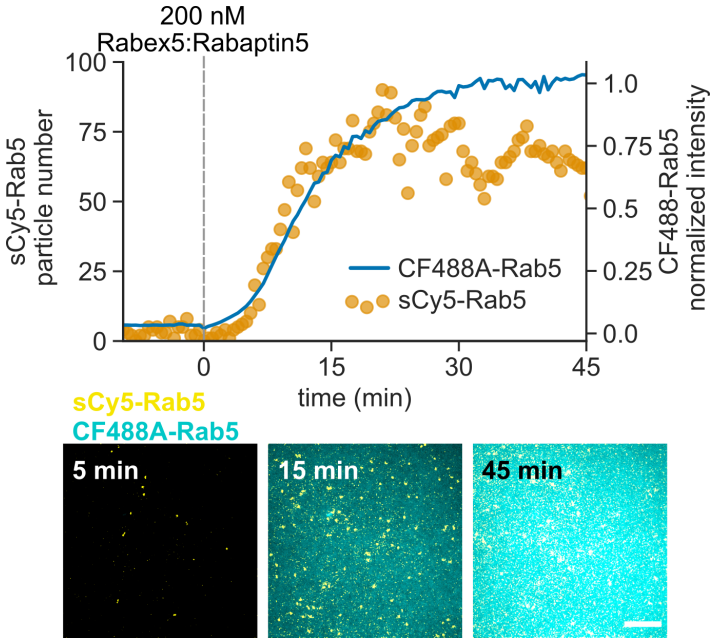

Figure 4.19: **Rab5 activation at single particle and collective scale.**
Top: sCy5-Rab5 molecule counts per frame and collective CF488A-Rab5 activation. Reaction mixture composed of 500 nM CF488A-Rab5:GDI, 2 µM GDI and 0.5 mM GTP was doped with ca. 50 fM sCy5-Rab5:GDI and left to equilibrate. Then, we triggered the nucleotide exchange by injecting 200 nM Rabex5:Rabaptin5 into the reaction chamber and tracked the GTPase switching with dual color imaging. Bottom: snapshots of the activation reaction. sCy5- and CF488A-Rab5 are depicted in yellow and cyan, respectively. Scale bar is 10 µm.

in aqueous solutions, which would limit their regulation and localization. The eukaryotic cell solves this problem with GDI, a Rab solubility factor that continuously extracts and sequesters inactive GTPases. Nonetheless, the tight Rab:GDI complex introduces an additional problem for Rab cycling as it blocks GEF binding surface on the G domain. Thus, it has been proposed that Rab:GDI complex is in chemical equilibrium with membrane bound Rab[GDP] ($K_d \approx 10^{-8}$ M [Pylypenko *et al.*, 2006]), which is available for GTP nucleotide exchange, preventing GDI re-extraction [Wu *et al.*, 2010]. Due to low estimated abundance and lack of reliable probes, this inactive Rab population in a GDI-bound equilibrium was hitherto not observed *in vivo* or *in vitro*. The combination of bright fluorescent labels and surface-sensitive TIRF microscopy allows us to image single Rab5 particles on the SLB in parallel with the bulk GTPase ensemble, representing the collective system state (Figure 4.19).

Using highly diluted (ca. 10^4-times) sCy5-Rab5:GDI in combination with bulk CF488A-

labeled complex, we detect individual SLB-bound Rab5 molecules (0-6 per frame) as bright fluorescent dots with an apparent point spread function diameter of 0.7 µm even before GEF addition. Over the course of Rab5 activation, the sCy5-particle counts increase over 10-times in agreement with the overall bulk fluorescence readout in CF-488A channel. Based on the single molecule counts and the dilution ratio, we estimate the number of membrane bound Rab5 to rise from 20 to 200 μm^{-2} over the course of the experiment. To our knowledge, this represents the first direct demonstration that there exists a dynamic equilibrium between GDI- and membrane-bound Rab[GDP] proteins. As a consequence of GEF nucleotide exchange, the membrane-bound fraction becomes enriched and remains stably anchored for prolonged duration of time. We evaluated the characteristic SLB lifetimes of Rab5 in GDP- and GTP-states using high speed acquisition and molecule trajectory tracking.

4.6.2 Rab5 particles display distinct membrane dwell times before and after activation

To estimate the nucleotide-dependent membrane dwell times of Rab5, we doped CF488A-Rab5:GDI with two distinct sCy5-Rab5:GDI dilutions and performed TIRF imaging at 100 ms intervals before and after activation (Figures 4.20A and B). For sCy5-Rab5[GDP] imaging, we used 1 nM sCy5-Rab5:GDI with 500 nM CF488A-Rab5:GDI, 2 µM GDI, 50 µM GDP and 500 µM GTP. Conversely, for single molecule tracking after GTP and GMP-PNP exchange, the reaction mixture contained 50 fM sCy5-Rab5:GDI, a 10^4-fold dilution compared to the bulk CF488A-Rab5. As before, we could easily detect single sCy5-Rab5[GDP] proteins that landed on the membrane surface and shortly diffused around, before GDI extraction. On the other hand, GTP-bound particles were visible for much longer durations. In this case, the observation was severely affected by photobleaching. We built the corresponding diffusion trajectories using the TrackMate ImageJ plugin [Tinevez *et al.*, 2017] and analyzed their deflection angles (Figure 4.20C), mean square displacement (MSD) (Figure 4.20D) and average lifetimes for tracks that were at least three frames long (Figure 4.20E). Particularly,the distribution of trajectory angles indicates the effect of protein density on the diffusion characteristics of SLB-bound molecules [Burov *et al.*, 2013; Lee *et al.*, 2019]. As discussed before, the

protein density increases for 10-fold over the course of collective switching (from ca. 20 to 200 Rab5 molecules per μm^2, see Section 4.6.1). For a free-diffusing molecule, we expect an even distribution of changes in direction, while a densely-packed bilayer would result in higher number of acute angles. Indeed, we observe more sharp particle deflection angles after the GTP nucleotide exchange, when the membrane is decorated with active Rab5 (Figure 4.10). Similarly, the MSD measures the extent of particle diffusion. There, a linear increase in weighted MSD mean represents Brownian motion, a quadratic curve would mean directed motion, while asymptotic behavior reveals confined diffusion. Interestingly, both GDP- and GTP-bound Rab5 particles experience spatial confinement in motion for longer tracks ($>$ 1 s for Rab5[GDP] and $>$ 5 s for Rab5[GTP]). This is likely the consequence of long-lived stuck particles or aggregates – particularly for $\Delta t > 15$ s, which are resistant to GDI-extraction, and increased protein density on the membrane surface. The calculated diffusion coefficient of inactive Rab5[GDP] was 2 $\mu m^2/s$, typical for a lipidated protein [Bement *et al.*, 2006; Kulakowski *et al.*, 2018; Chung *et al.*, 2018], and the activated GTPase diffused with 0.4 $\mu m^2/s$, in agreement with Ras mobility in active GTPase domains [Lee *et al.*, 2019].

The track duration frequency plot reveals two distinct particle populations. Interestingly, an abundant short-lived fraction is detected before and after nucleotide exchange, while the long-lasting one is found only after activation. Thus, the short-lived population represents inactive Rab5, which is in continuous equilibrium between the SLB and GDI complex. As a consequence of perpetual cycling, this fraction is present both before and after GEF addition. Conversely, Rabex5:Rabaptin5 GEF can swap the GDP for GTP on these particles and lock them on the membrane, signified by the longer trajectories after GEF addition. By fitting mono- and two-exponential functions to the obtained track duration histograms, we calculated the mean Rab5 membrane lifetimes of the distinct populations. The inactive Rab5 displays 0.8 $\pm$ 0.4 s mean lifetime (τ^{GDP}) before being re-extracted by the GDI. This is similar to 0.7 $\pm$ 0.3 s of the short-lived component ($\tau_1{}^{GTP}$) after GEF activation. Furthermore, the longer-lived fraction after nucleotide exchange had 10-fold longer lifetime, 7.4 $\pm$ 3.2 s. Importantly, these values are not corrected for photobleaching and thus represent lower-bound estimates. Likely, the short lived inactive population is not affected by the photon damage and its half-life depends mostly on GDI sequestration. To evaluate the photobleaching effect

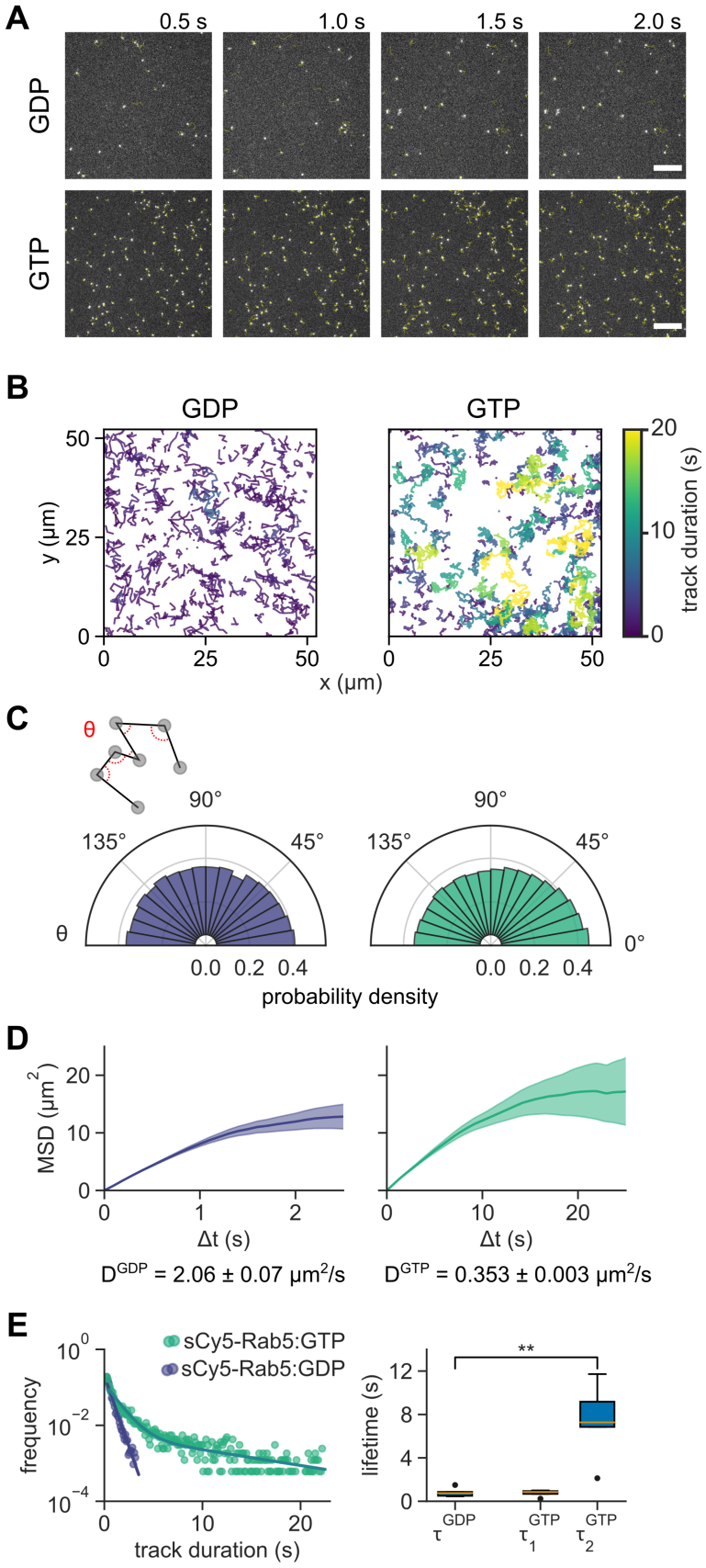

Figure 4.20: *(Continued on the next page)*

Figure 4.20: **Single particle trajectories reveal GDP- and GTP-bound SLB species.** **(A)** TIRF micrographs of diffusing sCy5-Rab5 particles before (GDP) and after (GTP) activation. We included an oxygen scavenging system to limit signal loss due to photobleaching. The reaction composition were as follows: 500 nM CF488A-Rab5:GDI, 2 µM GDI, 0.5 mM GTP, ca. 1 nM sCy5:GDI for GDP- and 50 fM for GTP state, 60 mM D-glucose, 0.1 mg/ml glucose oxidase, 0.32 mg/ml catalase, 2 mM Trolox. For the GTP-bound Rab5, the trajectories were captured after the activation reaction with 200 nM Rabex5:Rabaptin5 reached steady state in CF488A channel. Single particle trajectories are depicted in yellow with 20 frame depth (2 s), scale bar is 10 µm. **(B)** 500 tracks of membrane-bound sCy5-Rab5, colored according to their durations. **(C)** The probability density histogram of measured particle deflection angles (θ). Bins are 10°. 37,280 and 111,665 angles from 5 independent experiments were calculated for GDP- and GTP-bound particles, respectively. **(D)** Particle mean square displacement (MSD) for increasing time steps. Solid line is the weighted mean with SEM in shaded area. We analyzed 4,131 and 3090 trajectories from 5 independent experiments, respectively. The diffusion coefficients D with 95 % confidence intervals were calculated from the linear regime (10 % of track lengths). **(E)** Frequency plot identifies two populations with distinct lifetimes. The track durations present a monoexponential decay with lifetime τ^{GDP} before activation and two-exponential decay with lifetimes ${\tau_1}^{GTP}$ and ${\tau_2}^{GTP}$, respectively (n = 5).

on active Rab5, we compared the measured lifetimes with GMP-PNP loaded GTPase, which does not cycle and is permanently bound to the membrane (Figure 4.21). Interestingly, we detect a high proportion of acute particle deflection angles, highlighting the increased membrane protein density with prevented GTPase extraction. This also resulted in lower diffusion constant and constrained MSD motion. In terms of particle lifetimes, the GTP- and GMP-PNP bound Rabs display comparable values of 1 and 8 s for short- and long-lived GTPase fractions, which suggests that the obtained dwell times are limited by the accumulated fluorophore bleaching and represent the lower bound estimate.

Using single molecule imaging, we demonstrated the existence of inactive small GTPase membrane pool. In principle, this population is a convenient tuning parameter for the cell to orchestrate Rab signaling in space and time as it represents the relevant switching reactant. We put this assumption to the test by adjusting the composition of the reconstituted network.

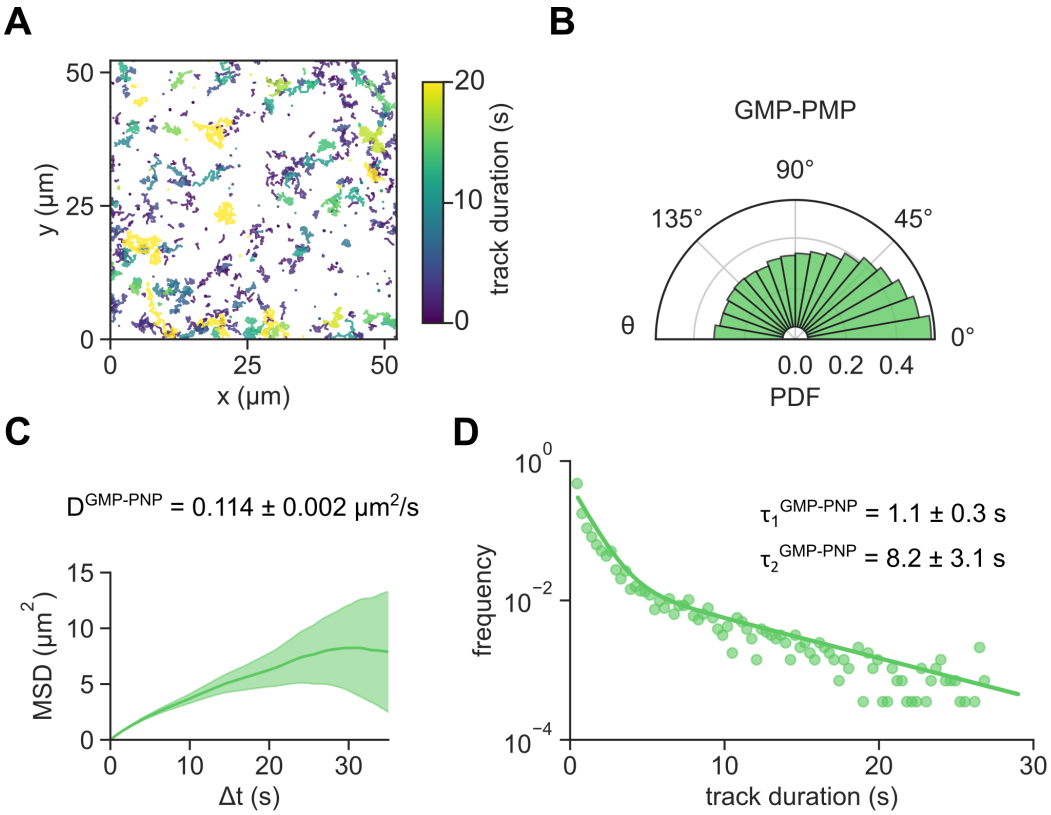

Figure 4.21: **GMP-PNP bound Rab5 displays dense membrane population with distinct lifetimes.**

(A) Single particle trajectories for activated sCy5-Rab5[GMP-PNP] in steady state. Before acquisition, CF488A-Rab5:GDI, doped with sCy5-Rab5:GDI, was activated with Rabex5:Rabaptin5 in presence of GMP-PNP. The reaction contained 500 nM CF488A-Rab5:GDI, 2 µM GDI, 0.5 mM GTP, ca. 50 fM sCy5-Rab5:GDI, 60 mM D-glucose, 0.1 mg/ml glucose oxidase, 0.32 mg/ml catalase, 2 mM Trolox. Shown are 1000 trajectories, which are color-coded for their duration. **(B)** Particle deflection angle distribution. Bin size is 10° for 153,579 angles from 3 independent experiments. **(C)** Mean square displacement (MSD) for GMP-PNP substituted sCy5-Rab5 at increasing time steps. Solid line is the weighted mean with SEM in shaded area. We analyzed 4,424 trajectories from 3 independent experiments. The diffusion coefficient D with 95 % confidence interval was calculated from the linear regime (10 % of track lengths).**(D)** Frequency plot for sCy5-Rab5[GMP-PNP] trajectory duration from three independent experiments. Noted are mean lifetimes ± SD (n = 3) for the tracked particles according to a two-exponential decay fit.

4.6.3 Inactive Rab5 population tunes the network response

It is assumed that the inactive and membrane bound Rab population undergoes nucleotide exchange during activation. As a consequence, the relative abundance of this small GTPase fraction is sensitive to the equilibrium with GDI-bound pool. This can be regulated with the amount of GDI and phosphorylation of either moieties [Steele-Mortimer *et al.*, 1993; Shinde and Maddika, 2016]. Additionally, the equilibrium is also target of pathogenic bacteria to promote cell invasion [Oesterlin *et al.*, 2012]. We directed the balance of Rab5:GDI equilibrium by changing the amount of free GDI in the minimal Rab5 activation network (Figure 4.22A). As predicted, we can tune the system's response by changing this parameter both *in vitro* and *in silico* (Figure 4.22B).

Notably, when we did not include GDI in stoichiometric excess, a marked increase in basal fluorescence level was observed. This is in agreement with shifted CF488A-Rab5:GDI dissociation equilibrium, where more Rab5 could redistribute to the SLB. Accordingly, with more available substrate the critical active GTPase density for positive feedback engagement was reached soon after GEF addition, which resulted in fast collective switching. In turn, the initial fluorescence levels at the membrane decreased with more GDI in the reaction mixture and delays towards full-blown activation progressively increased. The maximal observed rates of activation likewise dropped with GDI in high excess, demonstrating the importance of Rabex5 substrate availability for collective Rab5 activation. Another way to disrupt the Rab5:GDI equilibrium is by inhibiting the complex re-formation, either by reversible covalent modifications, tight binding partners [Oesterlin *et al.*, 2012; Sivars *et al.*, 2003] or non-hydrolyzable GTP analogues like GMP-PNP. By substituting GTP with GMP-PNP, we induced fast collective Rab5:GDI switching even in presence of 2 µM GDI. This surprising result suggests that relatively high intrinsic Rab5 GTP hydrolysis rate [Simon *et al.*, 1996a; Rybin *et al.*, 1996] plays an important role in characteristic population switching delays. By preventing the Rab5 self-inactivation and GDI extraction, the positive feedback formed substantially sooner, which is also recapitulated in the stochastic model.

Similarly, a family of GDI dissociation factors (GDFs) was proposed to help inactive Rab membrane anchoring. So far, the only characterized GDF is PRA1, a transmembrane protein, which can perturb the Rab:GDI equilibrium either by disrupting the com-

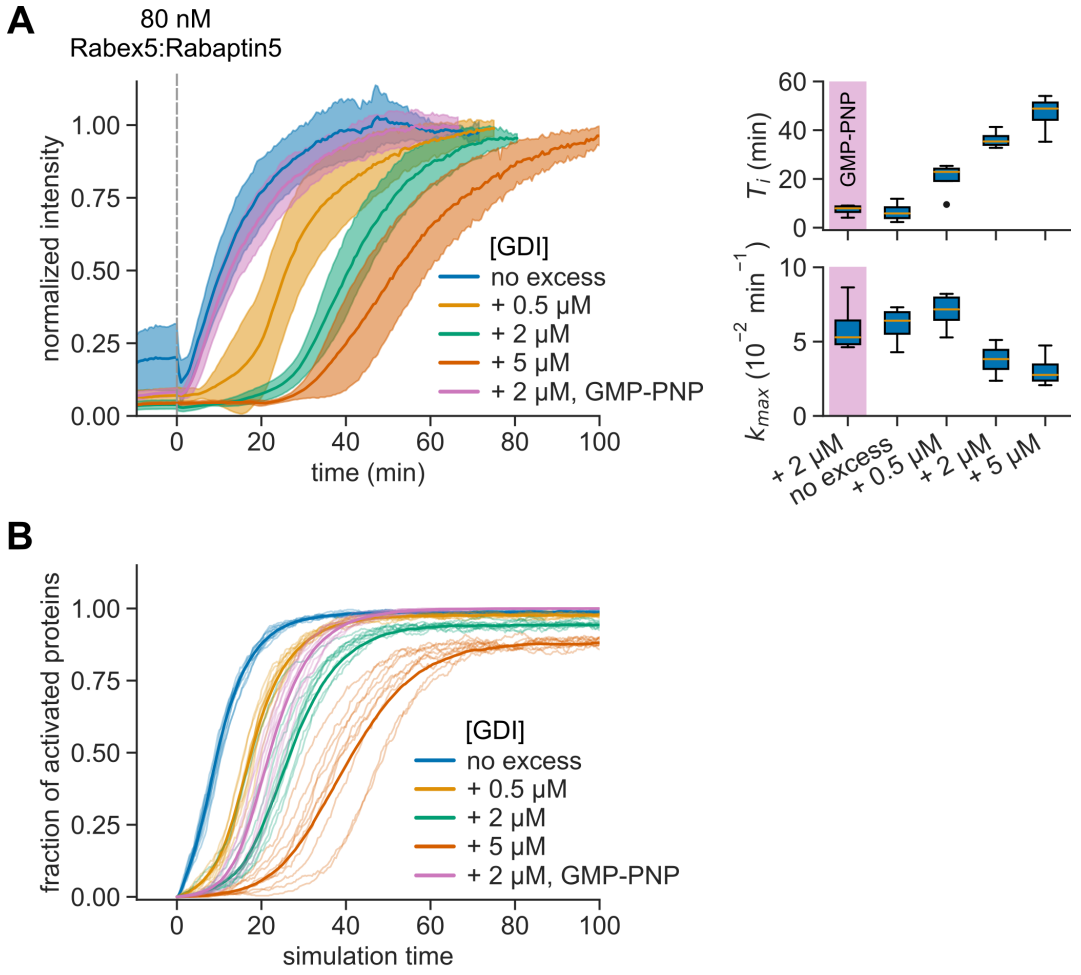

Figure 4.22: **GDI controls collective Rab5 switching.**

(A) Time courses of Rab5 activation with varying free GDI amounts and GMP-PNP. We included 500 nM CF488A-Rab5:GDI, GDI, 0.5 mM GTP or GMP-PNP and 80 nM Rabex5:Rabaptn5 in the final reaction composition. Left: solid lines are mean normalized intensities over time, shaded areas correspond to SD (n = 3). Right: corresponding activation delays T_i and relative maximum rates k_{max}. **(B)** Stochastic simulations of the model for varying initial amounts of GDI excess (0–2000 particle number). Shown are curves from 10 random runs per condition, the mean line from 50 runs is depicted bold. The simulations were performed by Hrushikesh Loya.

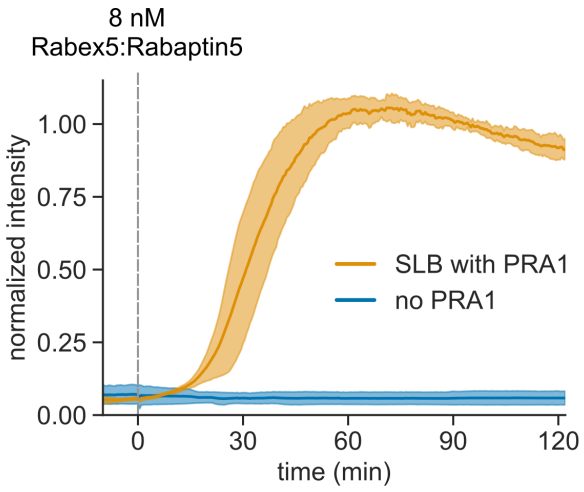

Figure 4.23: **PRA1 promotes Rab5 switching.**
Intensity traces of Rab5 activation on SLB with and without PRA1. 500 nM CF488A-Rab5:GDI, 2 µM GDI and 0.5 mM GTP were incubated on SLB with and without incorporated PRA1 (see Methods 3.6.3 for details). We induced Rab5 switching with 8 nM Rabex5:Rabaptin5. Solid lines are mean normalized fluorescence intensities, shaded areas correspond to SD (n = 3). Presented results were obtained by Beata Kaczmarek.

plex [Sivars *et al.*, 2003] or preventing the Rab re-extraction by binding either of the two partners [Hutt *et al.*, 2000]. To this end, we incorporated PRA1 in the supported membrane and performed Rab5 activation reaction with limiting amount of Rabex5:Rabaptin5. If PRA1 can shift the Rab5:GDI equilibrium towards Rab5 membrane binding, we would expect Rab5 collective switching even with low GEF input.

Agreeably, inclusion of PRA1 into the lipid bilayer enabled the system to transition into active state even with 8 nM Rabex5:Rabaptin5, far below the established threshold around 30 nM for bare membranes. Furthermore, we did not observe an increase in basal CF488A-Rab5 fluorescence levels, implying that PRA1 might affect the Rab5:GDI complex by increasing its dissociation rate constant, rather than inhibiting re-extraction, which would manifest in inactive Rab5 membrane accumulation.

Finally, we turned our attention towards the last Rab cycle regulator – the GTPase activating protein (GAP). These proteins catalyze GTP hydrolysis to turn the Rabs back to OFF state, where they are readily solubilized by GDI. What is more, the combination of locally-driven activator like a recruited GEF and global inhibitor was shown to produce spatial Turing patterns [Turing, 1952; Gierer and Meinhardt, 1972] and activation waves [Deneke and Di Talia, 2018].

4.7 Spatial patterns emerge under global inhibition

GAPs are a group of protein families that inactivate target Rab proteins by increasing their GTP hydrolysis potential. As a consequence, they regulate Rab signaling by limiting cascades in space and time. Interestingly, Rab5 has unusually high intrinsic GTPase activity, which lead to the assumption that an additional factor is not needed to maintain Rab5 signaling within physiologically relevant durations [Rybin *et al.*, 1996]. Nonetheless, a Rab5-specific GAP RabGAP-5 (also SGSM3, RUTBC3 and CIP85) has been identified [Haas *et al.*, 2005]. This cytoplasmic protein is mainly localized to the Golgi network and can accelerate Rab5 GTP hydrolysis for 3-5 fold. Still, its cellular function in Rab regulation remains uncertain as RabGAP-5 is also involved in Rab-distinct tumor suppression [Lee *et al.*, 2004], while another study did not detect Rab5 GAP activity *in vitro* [Itoh *et al.*, 2006]. Despite, a *C. elegans* homolog TBC-2 has been determined to interact with downstream-acting Rab7 [Chotard *et al.*, 2010], where it could induce the Rab5-Rab7 switch in early to late endosome maturation [Rink *et al.*, 2005; Del Conte-Zerial *et al.*, 2008]. To better understand the architecture of our reconstituted network, we tested what effect the GAP-mediated increase in Rab5 GTP hydrolysis rate has on collective GTPase activation.

4.7.1 RabGAP-5 inhibits collective Rab5 switching

GAPs like RabGAP-5 promote GTP hydrolysis in the nucleotide binding pocked of Rab GTPases. Consequently, they inhibit the GTP-dependent downstream signaling and enable Rab[GDP] membrane extraction by the GDI. We reasoned that the GAP addition to the reconstituted Rab5 signaling will increase the GTPase cycling between the SLB and solution. To this end, we preformed FRAP experiments in presence and absence of 50 nM RabGAP-5 and determined the CF488A-Rab5 exchange (recovery) rate in the center of bleached area after the activated system reached steady state (Figure 4.24). Surprisingly, we did not detect any differences in the FRAP recovery rates, suggesting that Rab5 cycling in collectively activated state is not dominated by GTP hydrolysis. Rather, under these conditions the effect of GEF-mediated positive feedback in Rab5 activation can buffer the increase in GTP hydrolysis by the GAP. Also, including 50 nM GAP in Rab5 switching reaction does not significantly influence

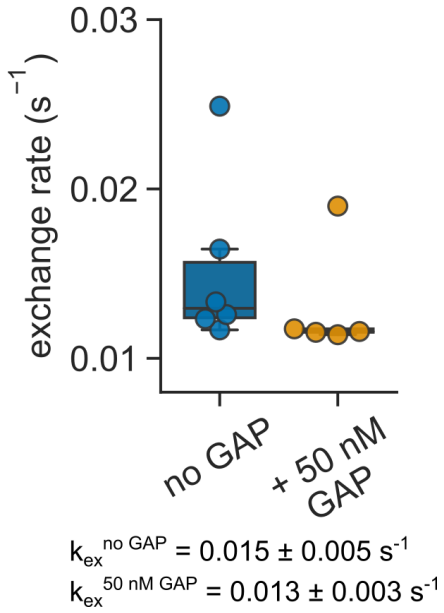

Figure 4.24: **50 nM GAP does not increase Rab5 cycling rate.**
Rab5 FRAP recovery rates in presence and absence of RabGAP-5. The reaction chamber above SLB contained 500 nM CF488A-Rab5:GDI, 2 µM GDI, 50 nM RabGAP-5 and 0.5 mM GTP. The GTPase switching was induced with 80 nM Rabex5:Rabaptin5. When the reaction reached active steady state we bleached a 20×20 µm square with 100 % 488 nm laser output. The recovery after photobleaching in the center 3×3 pixels was monitored in 1 s intervals and the Rab5 exchange rate was determined by fitting a linear function to the logarithm of normalized fluorescence values, which were corrected for photobleaching. The calculated exchange rates are means ± SD (no GAP n = 6, + 50 nM GAP n = 5).

the amount of Rab5[GDP] that could be sequestered by GDI. The Rabex5:Rabaptin5 nucleotide exchange reaction and lateral diffusion are likely the main contributors to the observed exchange rates under both experimental conditions. Next, we set off to determine the reconstituted system response to increasing amounts of GAP to better understand the role of RabGAP-5 in Rab5 regulation. We assumed that further increasing the RabGAP-5 concentration in our reconstituted network should dramatically affect collective Rab5 activation dynamics.

To elucidate the system's response to GAP perturbation, we performed a GAP titration by including progressively higher RabGAP-5 amounts in the minimal Rab5 activation network (Figure 4.25A). We can instantly see that 500 nM GAP completely suppressed the collective switching with 80 nM GEF, while lower amounts had mixed effects. RabGAP-5 does not interfere with the maximal observed rate of collective

switching for concentrations less than 250 nM. It does however contribute to an increased variability in the onset of state transition for the intermediate GAP amounts. This suggests that RabGAP-5 is not directly involved in the minimal Rab5 positive feedback network, but acts as a tuning factor. RabGAP-5 regulates the system's response by limiting the availability of Rab5[GTP] as the GEF positive feedback binding substrate. This in turn manifests as an increased variability (and stochasticity) in switching delay times and complete inhibition of Rab5 activation at very high GAP concentrations. Interestingly, we also observe reliable network outcomes for both low or high GAP concentrations. There, Rab5 pool collectively switches with 80 nM Rabex5:Rabaptin5 (0 and 50 nM GAP, blue circles) or remains in inactive state (500 nM GAP, orange circles). For 100- and 250 nM GAP, we see mixed system behavior with some reactions reaching active state and some remaining switched OFF at the same parameter conditions. This is a characteristic of bistable biochemical systems, a common network architecture that ensures committed cellular signaling in gene transcription [Gardner *et al.*, 2000], cell polarity [Altschuler *et al.*, 2008] and cell cycle progression [Pomerening *et al.*, 2003]. Another distinct feature of bistable systems is hysteresis – network memory where the switching occurs at different input values, depending on the intended direction of the transition [Kramer and Fussenegger, 2005].

4.7.2 Rab5 switching displays hysteresis

A necessary prerequisite for a bistable biochemical system is a source of non-linear response, e.g. positive feedback [Ferrell and Ha, 2014b], reciprocal repression [Gardner *et al.*, 2000] or competitive binding [Lebar *et al.*, 2014]. Furthermore, the main distinction between a highly cooperative and a bistable network is the existence of hysteresis. By building a GEF response diagram we already demonstrated the non-linearity in Rab5 activation (Figure 4.11). Now, to evaluate whether the observed bimodal distribution of system's responses to GAP also manifests in hysteresis, we performed Rab5 switching experiments in the opposite direction, from active back to inactive state (Figure 4.26). To this end, we first induced Rab5 activation with 80 nM GEF without GAP to reach stable ON state. We then injected either 0.5 or 2 µM RabGAP-5 and observed decrease in membrane-bound Rab5 signal. We set the 10-fold difference in signal

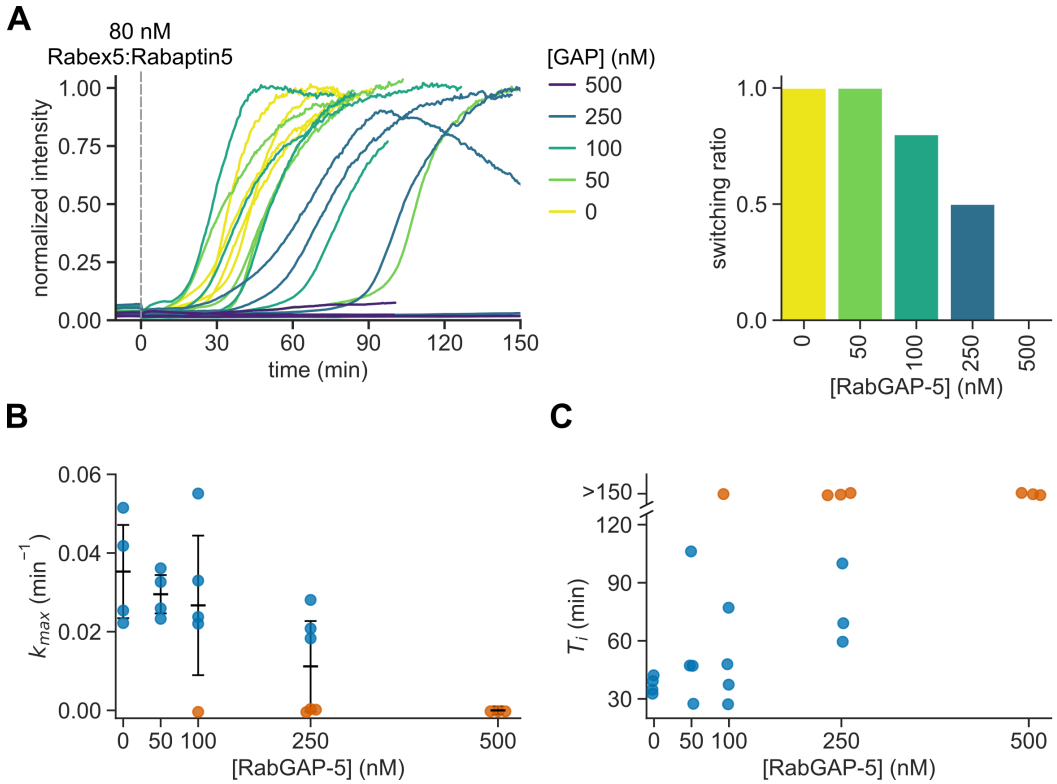

Figure 4.25: **GAP prevents Rab5 activation at high concentration.**

(A) Shown are time courses at increasing GAP concentrations (left) and the observed ratio of successful activations for a given condition (right). We included full length RabGAP-5 in the initial reaction mixture of 500 nM CF488A-Rab5:GDI, 2 µM GDI and 0.5 mM GTP. After equilibration, we induced nucleotide exchange with 80 nM Rabex5:Rabaptin5 injection. **(B)** RabGAP-5 effect on the observed maximal rates of activation k_{max}. Experiments that did not result in Rab5 activation within 150 min after induction are denoted in orange. Mean is represented by line, errors are ± SD. **(C)** Delays to collective switching with increasing GAP concentration. Orange are experiments that failed to switch. Presented results were partly obtained by Beata Kaczmarek.

over background levels as threshold to distinguish between ON and OFF states. This way, we can observe the bistable distribution of system's response profiles. At 500 nM GAP, we see no activation when switching from OFF $\rightarrow$ ON. In contrast, the same GAP amount is not sufficient to force the system back to low Rab5 activation levels when initiating ON $\rightarrow$ OFF transition. Only by adding 2 µM RabGAP-5 we were able to see Rab5 signal dipping below 10-fold background value, confirming inherent hysteresis in Rab5 switching. Thus, the reconstituted Rab5 activation network is bistable over a broad range of GAP concentrations, from 100 nM to 500 nM. This network feature is in line with similar kinase-based systems [Pomerening *et al.*, 2003] and sheds new light on Rab5 regulation. As we observed complete inactivation only at unphysiologically high GAP concentrations, it is clear that Rab5 signaling requires additional factors to prevent continuous propagation of the positive feedback. Two such mechanisms could be Rabex5:Rabaptin5 displacement factors like the Mon1:Ccz1 complex [Poteryaev *et al.*, 2010], mono-Ub [Shin *et al.*, 2017] or active GAP recruitment [Chotard *et al.*, 2010], which is yet to be confirmed in vertebrates.

The combined properties of reaction-diffusion systems like Rab5 activation network, positive feedback and bistability can trigger the formation of chemical waves [Deneke and Di Talia, 2018]. There, an active particle can diffuse in its immediate neighborhood and propagate activation of more molecules in an emergent traveling wave. We discuss the formation of this spatial reaction pattern in the next section.

4.7.3 Rab5 activation spreads in a traveling wave

By including 50 nM RabGAP-5 in the Rab5 activation network, we did not detect a substantial effect on switching parameters k_{max} and T_i. However, we often spotted regions of high active Rab5 density, which spread across the field of view as a bistable chemical wave, which finally settled the system in a fully active state after several tens of minutes (Figure 4.27). Overall, we observed this activation spatiotemporal pattern in 9 out of 13 experiments; in 3 cases no obvious waves were noticed during activation, while in one experiment no switching occurred.

The activation wave spread as a distinct front across the membrane at nearly constant velocity of 5 µm/min, triggering collective switching at its edges. In the bright

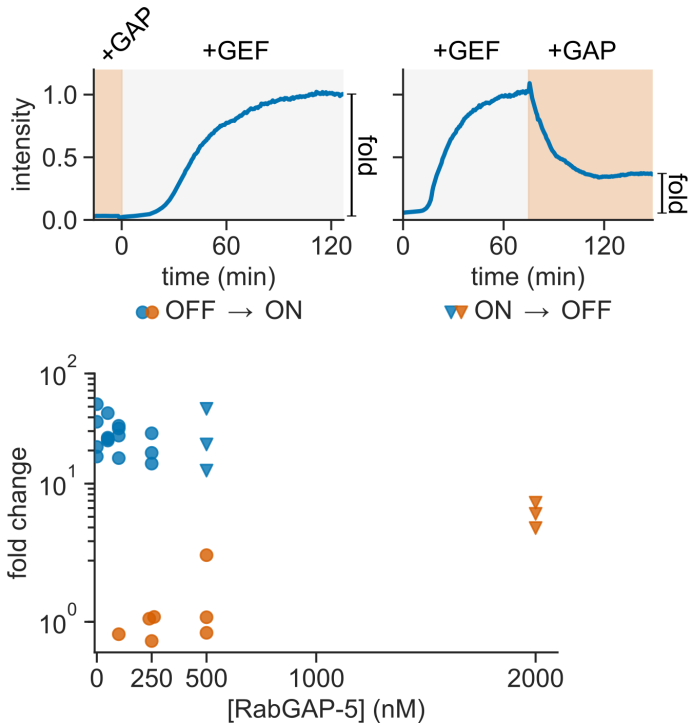

Figure 4.26: **Collective Rab5 transition is bistable.**

Top: time courses for OFF → ON (100 nM GAP) and ON → OFF switching (2 µM GAP). Colored background indicate the addition of either GAP or GEF to the reaction chamber. Bottom: hysteretic GAP titration response plot. The fold change was calculated by dividing the fluorescence intensity at steady state with the average fluorescence signal 10 min before GEF addition. For ON → OFF switching, the system first reached active state (ON) with 80 nM GEF. Then, RabGAP-5 was added and the reaction was followed until the system reached a new steady state (OFF). In both switching regimes, the reaction network was composed of 500 nM CF488A-Rab5:GDI, 2 µM GDI, 0.5 mM GTP and varying amounts of RabGAP-5. Rab5 activation was triggered with 80 nM Rabex5:Rabaptin5. Points for OFF → ON switching correspond to the time courses shown in Figure 4.25. Data points with final fold signal increase < 10 are depicted in orange.

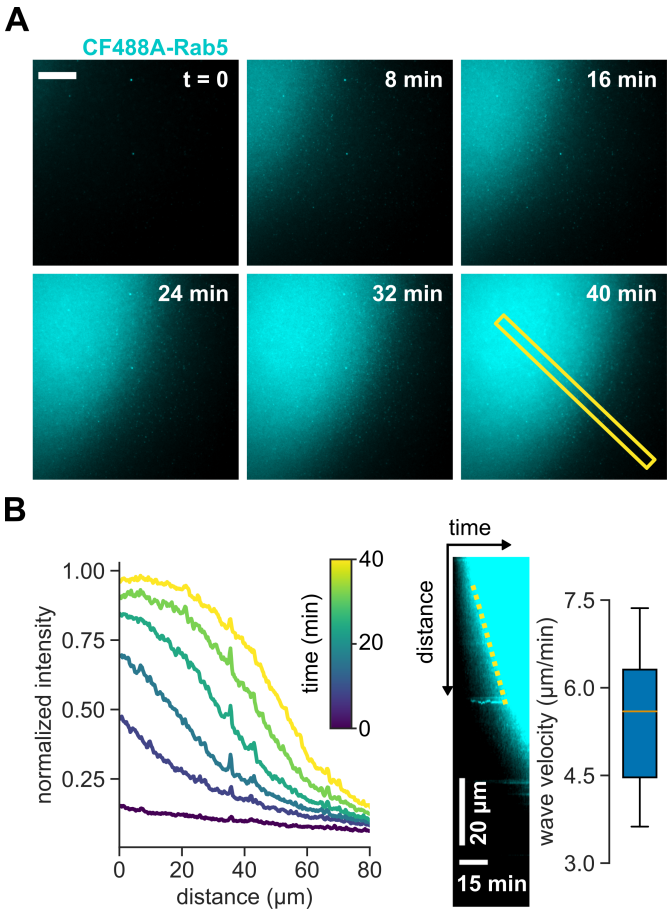

Figure 4.27: **Rab5 activation wave on SLB.**

(A) Rab5 activation wave spreading across the SLB. Scale bar is 20 µm. Times indicate relative duration after start of image sequence acquisition, not time after addition of GEF complex. **(B)** Left: fluorescence intensity profile and kymograph of the indicated area in (A). Right: measured mean wave velocity. Wave velocity was determined from the slope of fluorescence increase in generated kymographs (n = 6).

areas, the reaction progressed towards the active steady state as indicated by the intensity profiles. This spontaneous pattern formation is in agreement with general principles of self-organization in living systems and likely forms the basis of small GTPase membrane (nano)clusters and domains. It is thought that distinct clusters of active Rab proteins direct endosomal recycling [Sönnichsen *et al.*, 2000; Franke *et al.*, 2019], Ras signaling [Lee *et al.*, 2019], cell migration through actin polymerization on Rac1 domains [Remorino *et al.*, 2017] and yeast bud formation with Cdc42 polarization [Altschuler *et al.*, 2008; Goehring and Grill, 2013; Goryachev and Leda, 2017]. What is more, theoretical analysis supports the idea of GTPase pattern formation through amplification of a local increase in active protein density and coupled cytosolic concentration gradients. As seen in Figure 4.27, this eventually results in stable GTPase attachment and detachment zones [Halatek *et al.*, 2018]. When the substrate (Rab5), activator (Rabex5:Rabaptin5) and inhibitor (RabGAP-5) share similar diffusion constants, traveling waves can form in simple biochemical networks [Tyson *et al.*, 2003].

Here, the emergence of activation wave is triggered by stochastic fluctuations in active Rab5 membrane density. When the critical value is passed, positive feedback loop of Rabex5:Rabaptin5 recruitment can form and the transition to active state can self-propagate along the SLB through lateral diffusion (attachment zone). Nonetheless, the reaction spread is contained by continuous global RabGAP-5 inhibition and GDI extraction, which maintains the active Rab5 density in surrounding regions low (detachment zone). As a consequence, the activation wave is a tug-of-war between the GEF and GAP, where both regulators act upon Rab5[GTP] population. We also believe that the collective Rab5 activation spreads as a wave even in absence of GAP, but at much higher rates – likely from several sources on the membrane at once. This then creates the impression of uniform fluorescence increase as seen in Figure 4.6. Only by slowing down the progression of diffusing reaction with RabGAP-5, we were able to appreciate this fundamental propagation mechanism. By using chemical waves to trigger collective Rab activation, the cell can efficiently cover the $\approx$100 nm endosomes [Klumperman and Raposo, 2014] and contain the spread of active Rab5 patches with e.g. GAP inhibitory boundaries, producing membrane protein domains.

4.8 Rab5 activation as a random nucleation process

The collective Rab5 state transition likely spreads across the 2D membrane surface as a chemical wave from one – or several – positive feedback nucleation events. To visualize individual nucleation reactions, we compartmentalized the reaction-diffusion network on a micropatterned SLB array (Figure 4.28A). To this end, we prepared 50 nm-tall chromium grids on glass coverslips using E-beam photolitography [Schweizer *et al.*, 2012]. As the SLB cannot form on metal, the grids partition the $\approx$ 6 nm-thick supported membrane into isolated corrals [Groves, 1997]. This prevents lipid and protein exchange by lateral diffusion between the neighboring compartments. This way, the positive-feedback reactions, stemming from a single nucleation event, are contained in respective array compartments.

4.8.1 Rab5 activation switch is a Poisson point process

On a 22$\times$22 array, we effectively observed up to 484 Rab5 activation reactions with 200 nM GEF in parallel (Figure 4.28B). To visualize the segregated bilayer, we prepared SLB with intercalated fluorescent membrane tracer DiD, which does not interfere with CF488A-Rab5 signal. In the experiment, we see a moderate decrease in DiD intensity over time as the laser-induced photodamage accumulates and lateral fluorophore exchange is prevented. In the GTPase channel, we see individual CF488A-Rab5 activation reactions triggering for more than 120 min, before the steady state is reached (Figure 4.28C). Under these conditions, 464 out of 484 compartments switched to the active Rab5 state, signified by bright GTPase fluorescence signal. Interestingly, we can describe the microarray experiment as a Poisson process [Gallager, 2013], where the observable collective activations are random events that happen at T_i epochs.

Statistically, a Poisson process is signified by gamma distribution of activation epochs (delays T_i) and an exponential distribution of interactivation times $\Delta T_i = T_i(t+1) - T_i(t)$, where $T_i(t)$ and $T_i(t+1)$ are temporal delays of activation reactions happening one after the other in distinct compartments [Gallager, 2013]. Indeed, the characteristic distribution functions describe the reconstituted system behavior with great accuracy (Figure 4.28D). Characterizing the individual reactions, we see that the activation reaction parameters T_i and k_{max} are distributed according to gamma and Gaussian distributions,

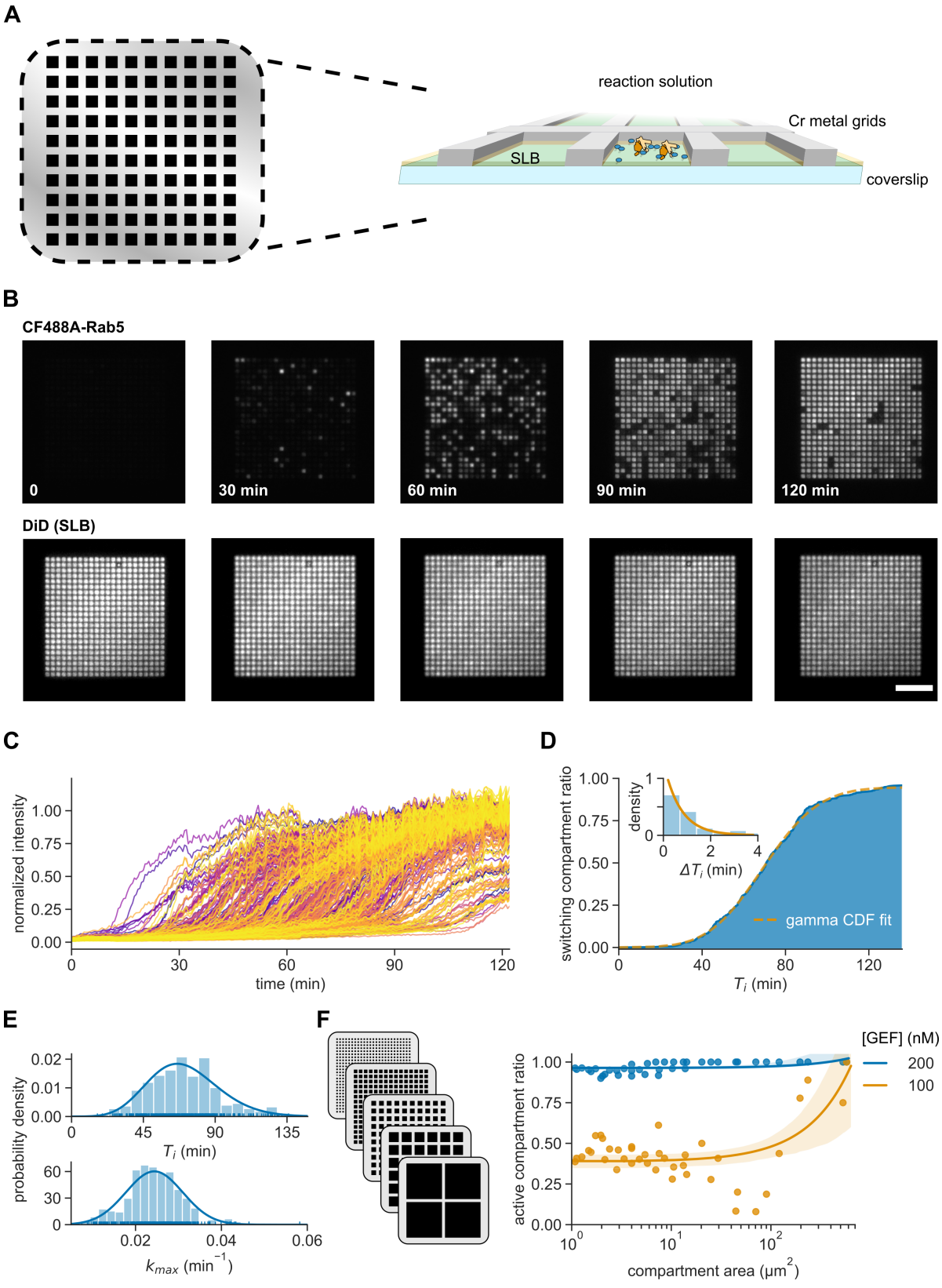

Figure 4.28: *(Continued on the next page)*

Figure 4.28: **Rab5 activation is a stochastic Poisson process.**
(A) Schematic representation of a chromium micropatterned array on glass coverslip with SLB compartments. The 50 nm-tall chromium microgrids, which were produced with E-beam photolitography, partitioned the SLB into spatially isolated compartments. **(B)** Micrographs of Rab5 activation on a 22×22 array. The reaction was composed of 500 nM CF488A-Rab5:GDI, 2 µM GDI, 0.5 mM GTP and 200 nM Rabex5:Rabaptin5, which was added at t = 0. Top: CF488A-Rab5 channel; bottom: DiD-labeled SLB channel. Scale bar is 15 µm. **(C)** Individual switching reactions. **(D)** Ratio of compartments that underwent collective Rab5 activation as a function of temporal delays T_i with fitted gamma cumulative distribution function (CDF). Inset: distribution of interactivation times in terms of ΔT_i with fitted exponential function. **(E)** Density histograms of temporal delays T_i and maximal rates k_{max} for active compartments with fitted gamma- and normal distributions, respectively. **(F)** The ratio of active compartments at steady state for different grid dimensions and GEF concentrations. Fitted are linear regression curves with 95 % confidence intervals in shaded area.

respectively (Figure 4.28E). The observed k_{max} reaction rate mean at $2.4 \cdot 10^{-2}$ min^{-1} is 2-times lower than what we observed on continuous SLB, suggesting that the introduced reaction boundaries slightly shifted the parameter landscape.

Finally, we characterized the end-point states for 40 different grid configurations with varying compartment areas at steady state (Figure 4.28F). There, the microgrids offer binary statistical trials for positive feedback nucleation events. Therefore, the observed ratio of active compartments can be approximated as the switching probability per given compartment area. Taking into account only arrays with $\geq$225 compartments (area 1.1-5.8 μm^2), we get the extrapolated collective switching probabilities of 0.45 $\pm$ 0.04 and 0.94 $\pm$ 0.01 μm^{-2} for reactions with 100 and 200 nM Rabex5:Rabaptin5, respectively. These values represent the likelihood for a productive nucleation event per 1 μm^2 of membrane before the system reaches steady state, which depends on the GEF concentration in the reconstituted system. To better understand this relationship, a larger set of GEF concentrations needs to be screened.

To sum up, the triggering of collective Rab5 activation happens as a Poisson process on the bilayer surface with distinct probability that is proportional to the GEF amount. Consequently, this statistical model describes the positive feedback nucleation on SLB microgrids as stochastic, independent and memoryless – the hallmarks

of a Poisson processes. Thus, an individual collective Rab5 activation happens randomly due to local protein density fluctuations and does not influence the likelihood of other compartments switching to the active state. *In vivo*, the Rab5 activation happens on a nascent endosome with 30 nm diameter and 3 μm^2 surface [Huotari and Helenius, 2011]. There, the collective switching will depend on many more factors like the temporal and compartment-specific GEF concentration and other environmental factors like lipid composition, GAPs and GDFs.

4.8.2 Rabex5:Rabaptin5 is retained on the membrane during the collective Rab5 activation

We used the same approach with compartmentalized glass-supported bilayer to assay GEF localization during the positive feedback initiation of Rab5 activation. Our previous results suggest that stochastic nucleation events of Rab5[GTP]:Rabaptin5:Rabex5 ternary complex formation trigger positive feedback of Rab5 activation and GEF recruitment. Despite the known crystal structure of Rab5:Rabaptin5:Rabex5 fragments [Zhang *et al.*, 2014], the full-length GEF complex was not yet captured in direct co-localization with active Rab5 clusters. We hypothesized that the Rabex5:Rabaptin5 complex continuously probes the negatively-charged membrane (20 % $DOPS^-$ in the SLB composition) and activates available Rab5[GDP] at a basal level, but is stably retained only after the critical Rab5[GTP] density is reached [Zhu *et al.*, 2010]. Then, the activation reaction is propelled by the positive feedback of enhanced GEF recruitment and collective GTPase switching ensues. Importantly, all these events correlate with the amount of membrane-bound GEF complexes.

To capture single complexes of the fluorescent Rabex5:sCy5-Rabaptin5, we used a 1:20 dilution ratio with the non-labeled GEF. We assayed Rab5 activation in presence of 100 nM GEF, which led to GTPase collective state switching in 186 out of 400 compartments on a 20×20 microarray (Figure 4.29A). The steady state was reached after 140 min of observation (ca. 150 min after GEF injection), with first Rab5 transitions happening at 2 min mark. Strikingly, GEF particles localized to these compartments in high numbers, while the inactive compartments were only rarely visited. Furthermore, observing a Rabex5:Rabaptin5 particle for a prolonged amount of time was an

excellent predictor of Rab5 switching in the respective compartment, which resulted in further accumulation of sCy5-labeled proteins through positive feedback. Interestingly, the number of tagged GEF particles peaked during the abrupt increase of Rab5 signal and subsided as the reaction approached steady state, which could also be a consequence of photobleaching.

Like before, the Rab activation on microgrids represented a Poisson process with gamma and exponential distributions of activation delays and interactivation times (Figure 4.29B). Looking closer at individual active compartments, we can correlate the Rabex5:sCy5-Rabaptin5 fluorescence intensity with the progression of individual reactions (Figure 4.29C). We see that the GEF signal abruptly increases together with the progression of Rab5 activation. After the Rabex5:sCy5-Rabaptin5 signal peaks, the GEF particle number per compartment steadily decreases, while the Rab5 signal remains stable. What is more, for the selected examples, the Rabex5:sCy5-Rabaptin5 signal reaches maximum slightly after the inflection point of activation reaction and just before the steady state onset. On average, the mean time difference $\Delta()$t between CF488A-Rab5 T_i and the peak in GEF signal is 5.6 $\pm$ 5.3 min (Figure 4.29D, n = 124), which is in agreement with the 5.8 min delay in Rab5 and GEF membrane recruitment that was observed on a continuous SLB (Figure 4.15B). Taking advantage of the *in vitro* reconstitution assay, we wanted to know if a high GEF recruitment at the reaction inflection point ΔT_i correlates with higher activation rate k_{max}. We measured the mean Rabex5:sCy5-Rabaptin5 fluorescence intensity at $T_i \pm 2$ min (window size = 5 time points) and compared it with the fitted k_{max} (Figure 4.29E). We see that there is only weak correlation between GEF membrane binding and the rate of Rab5 switching (Pearson correlation coefficient r = 0.2), which could be attributed to the noisy single molecule data and the fact that Rab5 activation and GEF recruitment time courses are offset by 5-6 min. What is more, the detected Rabex5:sCy5-Rabaptin5 molecules are not necessarily forming active ternary complexes with Rab5. The GEF complex particles can bind the negatively charged SLB surface independently of Rab5 [Zhu *et al.*, 2007] and could form non-productive complexes with Rab5, similar to Ras activator Son of Sevenless (SOS) [Huang *et al.*, 2019], which has to allosterically transition over several conformations to escape the auto-inhibited state. Intriguingly, the full length Rabex5 is also expressed in auto-inhibited conformation, with Rabaptin5, Rab5 [Zhang

et al., 2014] and ubiquitin [Lauer *et al.*, 2019] acting on different interaction surfaces to release it.

Finally, we wanted to estimate the number of GEF molecules during Rab5 collective activation. By observing several single Rabex5:sCy5-Rabaptin5 binding events, we determined the average associated change in fluorescence is 500 $\pm$ 350 RFU per compartment (n = 59). Knowing this, we can roughly determine the number of GEF protein complexes during different stages of GTPase activation reaction. The mean sCy5 signal during positive feedback ($T_i \pm 2$ min) is 3590 RFU and the average background intensity is 1526. Thus, we could expect 4 labeled particles and several tens of unlabeled Rabex5:Rabaptin5 GEF (1:20 dilution of sCy5-labeled Rabex5:Rabaptin5) in the Rab5 nucleation cluster at T_i, while the mean measured GEF peak value is 4741, corresponding to 6 GEF molecules. Looking closely at two examples of compartments (Figure 4.29F; reactions 5 and 6 in 4.29A), where the system did not collectively switch (reaction 5) or reach steady state (reaction 6) during the observation period, we can see how the detected GEF binding/unbinding events ($\triangle/\triangledown$) relate to the Rab5 fluorescence intensity. Surprisingly, low Rab5 signal can oscillate near the background levels as the system responds to basal GEF recruitment that fails to engage further positive feedback (reaction 5). There, Rabex5:sCy5-Rabaptin5 unbinding happens too soon to activate sufficient amount of available Rab5[GDP] and collective Rab5 switching does not happen. In reaction 6, we spotted very few binding events of labeled Rabex5:Rabaptin5 before 130 min and the Rab5 signal remained low. However, an increased number of GEF molecules was recruited to the respective compartment after 130 min, which resulted in rapid increase of Rab5 fluorescence and further influx of Rabex5:sCy5-Rabaptin5 through late positive feedback engagement. Unfortunately, the experimental acquisition ended before Reaction 6 could reach full activation.

The experiments on microfabricated grids gave us a new insight into collective Rab5 activation events. Firstly, by laterally dividing the membrane substrate, we demonstrated that the Rab5 regulation network constitutes a bistable reaction-diffusion system, which stochastically transitions to the active state from local self-organized nucleation domains on the bilayer. Secondly, we confirmed Rabex5:Rabaptin5 colocalization and recruitment during the Rab5 activation. Based on our preliminary observations, we believe that collective switching is triggered when the local density of membrane- and

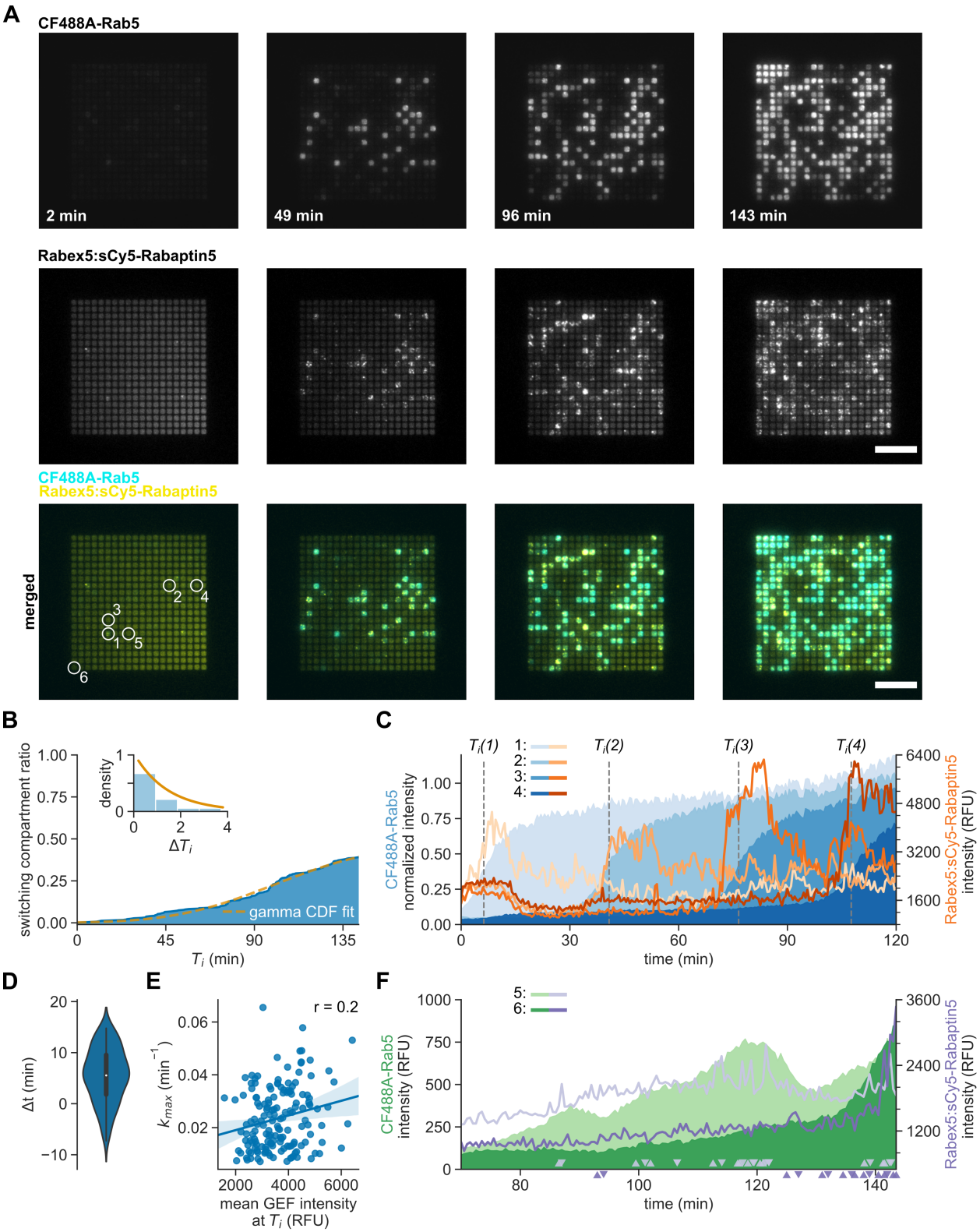

Figure 4.29: *(Continued on the next page)*

Figure 4.29: **Rabex5:Rabaptin5 membrane retention coincides with collective Rab5 activation**

(A) Micrographs of CF488A-Rab5 and diluted Rabex5:sCy5-Rabaptin5 during GTPase activation with 100 nM GEF on 20×20 microgrid (compartment area 2.4 µm^2). Times denote the duration of imaging and do not relate to the point of GEF injection, which was 8 min before. The reaction included 500 nM CF488A-Rab5, 2 µM GDI, 0.5 mM GTP and 100 nM Rabex5:Rabaptin5, doped with near-single particle imaging dilution of Rabex5:sCy5-Rabaptin (ca. 5 nM). Scale bar is 15 µm. 1-6: selected reactions in compartments, which are included in panels (C) and (E). **(B)** Ratio of switching compartments at inflection times T_i with fitted scaled gamma CDF. Inset: distribution of interactivation times ΔT_i with exponential function fit. **(C)** Examples of activation timecourses from indicated compartments 1-4 in (A). The normalized CF488A-Rab5 signal evolutions are presented as filled blue areas and the Rabex5:sCy5-Rabaptin5 fluorescence signals are shown in orange. The inflection points are indicated by dashed gray lines. A single GEF complex particle has mean intensity of 500 $\pm$ 350 RFU (SD; n = 59). **(D)** Violin plot of Δt, which are time differences between the inflection point T_i of CF488A-Rab5 activation and the maximal value of Rabex5:sCy5-Rabaptin5 signal in each respective compartment. The mean Δt is 5.6 $\pm$ 5.3 min (SD; n = 124). We smoothed the Rabex5:sCy5-Rabaptin5 signal by calculating the rolling mean fluorescence intensities with window size 5 to reduce artifacts from the signal noise. **(E)** Relation between the measured maximal activity rate k_{max} and the mean GEF signal intensity at the inflection point $T_i \pm 2$ min. A linear function with 95 % confidence interval in shaded area is fitted to all reactions, which reached T_i within the observation period. **(F)** Examples of reactions 5 & 6 in (A), which did not switch to the active Rab5 state during imaging. The CF488A-Rab5 signal is presented in RFU as filled green areas and the Rabex5:sCy5-Rabaptin5 signal is depicted purple. Detected GEF particle membrane binding and unbinding events are indicated by $\triangle$ and $\bigtriangledown$, respectively. A single GEF complex particle has mean intensity of 500 $\pm$ 350 RFU (SD; n = 59).

Rab[GTP]-bound GEFs is at least few tens of molecules per µm^2. Clearly, further experimental repetitions and a broader scan of the parameter landscape has to be implemented to confirm these conclusions and expand our knowledge of the GTPase regulatory networks.

This approach also opens exciting avenues in answering another long standing question: ”How is the organelle-specific targeting of Rab GTPases achieved?”. We

could mimic the diverse organelle compositions by probing custom protein and lipid cues in parallel. Assaying the roles of Rab4, Ub-cargo, PI3P and PRA1 would help us understand how the regulatory network directs Rab5 activation exclusively on the endosomal system [Blümer *et al.*, 2013]. To further investigate the mechanism of Rab5 nucleation and the role of boundary conditions, we lastly implemented a spatial stochastic model of the reconstituted biochemical network.

4.9 Spatial stochastic model of Rab5 activation

In vitro reconstitution experiments of Rab5 activation on glass-supported lipid bilayer revealed that direct interaction between active Rab5[GTP] and Rabex5:Rabaptin5 GEF complex generates non-linear network responses on a collective scale. What is more, assays on compartmentalized SLB confirm that system-wide collective Rab5 activation is triggered by local positive feedback reaction nucleation events, which happen stochastically and independently over the duration of experiment. The Rab5 activation assays on SLB corral grids revealed that the likelihood of collective activation generally increases on a larger compartment area (Figure 4.28F). This is in line with the assumption that we are more likely to detect positive feedback nucleation events if we observe larger stretches of membrane. Consequently, there must be stringent mechanisms that prevent non-specific Rab5 activation on large membrane surfaces *in vivo* – like the plasma membrane or the Golgi apparatus. Unique niches where collective GTPase activation is possible could be constituted by GEF recruitment [Mattera and Bonifacino, 2008; Blümer *et al.*, 2013], effector targeting [Jongsma *et al.*, 2020], lipid composition and GAP localization [Müller *et al.*, 2020]. On the other hand, some bistable biochemical networks can also sense geometrical boundary conditions. For example, reconstitutions of similar phosphoinositide lipid kinase-phosphatase networks discovered stochastic geometry sensing as an intrinsic systemic property, which influences the system state depending on the membrane compartment size [Hansen *et al.*, 2019]. To discover whether the reconstituted minimal Rab5 activation network possesses similar geometry sensing properties, we implemented a spatial stochastic model based on Smoldyn particle simulator [Andrews *et al.*, 2010]. Using this model, we could observe how the simulated molecules interact with different boundary conditions and make con-

clusions whether the predicted interaction network could potentially target collective Rab5 activation to smaller organelles like the endosomes.

The spatial model captured the main features of Rab5 activation circuit: *(i)* Rab5-[GDP] was sequestered by GDI in 4×4×0.2 µm box above the membrane; *(ii)* Rab5:-GDI could dissociate and free Rab5 would adsorb to the membrane surface, where it could be re-extracted by the GDI; *(iii)* Rabex5:Rabaptin5 could activate free Rab5 molecules at a basal rate from the solution or while transiently interacting with the bilayer; *(iv)* active Rab5 could bind Rabex5:Rabaptin5 and form ternary membrane-bound complex with greatly enhanced nucleotide exchange activity; *(v)* Rab5 had intrinsic GTPase activity to hydrolyze GTP to GDP (see Section 3.21 for list of reactions and parameters). We first compared the simulated Rab5 activation on a unbounded membrane or 5×5 grid that prevented lateral diffusion (Figure 4.30A-D). To model unbounded SLB surface, we created periodic side walls in the simulated box. There, laterally diffusing molecules are returned back to the system at the opposite side and do not encounter any bounds. On the other hand, the 5×5 grid introduced rigid walls on membrane surface that compartmentalized membrane-bound molecules similarly to the metal microgrid *in vitro*.

We see that in both cases the system collectively switched to the active state for GEF concentrations above 10 nM, with comparable dynamics and bistability to the experimental assays (Figure 4.11A, 4.28B-D) and computational stochastic model (Figure 4.13). Particularly, the simulated grid introduced boundary conditions, which limited the collective activation to respective compartments. Generally, the simulated reaction networks with periodic boundaries reached the steady state faster and in shorter simulation time than the corresponding examples with membrane grids. Interestingly, this difference was noted also in reconstitution experiments, where reactions on continuous SLB progressed twice as fast as reactions on membrane corrals (Figures 4.11D and 4.28E). To understand why this was the case, we first visualized the cumulative counts of positive feedback reactions in 3 min intervals for the 6 simulation runs at different GEF amounts (Figure 4.30E and F). This way, we can see when the positive feedback activation peaks for each parameter condition. For simulations with high GEF concentrations, the positive feedback reactions are most common at the activation inflection point. Furthermore, we see that the number of positive feedback reactions is lower with

compartmentalized membrane compared to the unbounded surface, which could explain the slower activation dynamics in the former case. At the same time, we wanted to determine the average number of nucleotide exchange reactions an activated GTPase catalyzes when in complex with Rabex5:Rabaptin5. This is given by the mean positive feedback processivity factor (Figure 4.30G), which is slightly higher for the unbounded simulations. Likely, the compartmentalized membrane limits the availability of reaction substrate Rab[GDP], which results in slower switching dynamics both *in silico* and *in vitro*. Finally, we calculated the ratio of active compartments at the end of simulations for increasing GEF concentrations (Figure 4.30H). The switching ratios reveal bistability with critical transition point between 10 and 20 nM GEF. Above this threshold, at least 7 and up to 18 of 25 compartments were switched ON (when the active Rab5 density was above 20 Rab5[GTP]/μm^2).

Identifying the critical GEF concentration between 10 and 20 nM, we focused on the effects of membrane area on compartment switching ratio for these two amounts. To this end, we simulated Rab5 activation in the same $4\times4\times0.2$ µm box, but with different grid configurations – from 5×5 grid to 1×1 enclosed membrane (Figure 4.31A). Consequently, we observed collective Rab5 switching on compartment areas ranging from 0.64 to 16 μm^2. In agreement with *in vitro* experiments (Figure 4.28F), we observed more switching events for 10 nM GEF as the compartment size increased (Figure 4.31B). Similarly, the mean active compartment ratio increased for simulations with 20 nM Rabex5:Rabaptin5 according to the compartment area based on 6 individual runs per condition (Figure 4.31C). These results suggest that we are more likely to observe randomly distributed positive feedback nucleation events on a larger membrane surface. At the same time, the modeled protein network does not have intrinsic stochastic geometry sensing properties like the one in lipid kinase-phosphatase system [Hansen *et al.*, 2019]. This is even more evident from the heatmap of compartment activation ratios for increasing Rabex5:Rabaptin5 amounts from 5 to 25 nM (Figure 4.32). In this parameter scan, we detected GTPase activation for all simulated reaction compositions above 5 nM GEF under the right conditions. Particularly, higher amounts of GEF could trigger collective switching on 16 μm^2 enclosed membrane (1×1 grid) with increasing efficiency. Conversely, the GTPase activation was progressively less likely to occur on smaller corrals.

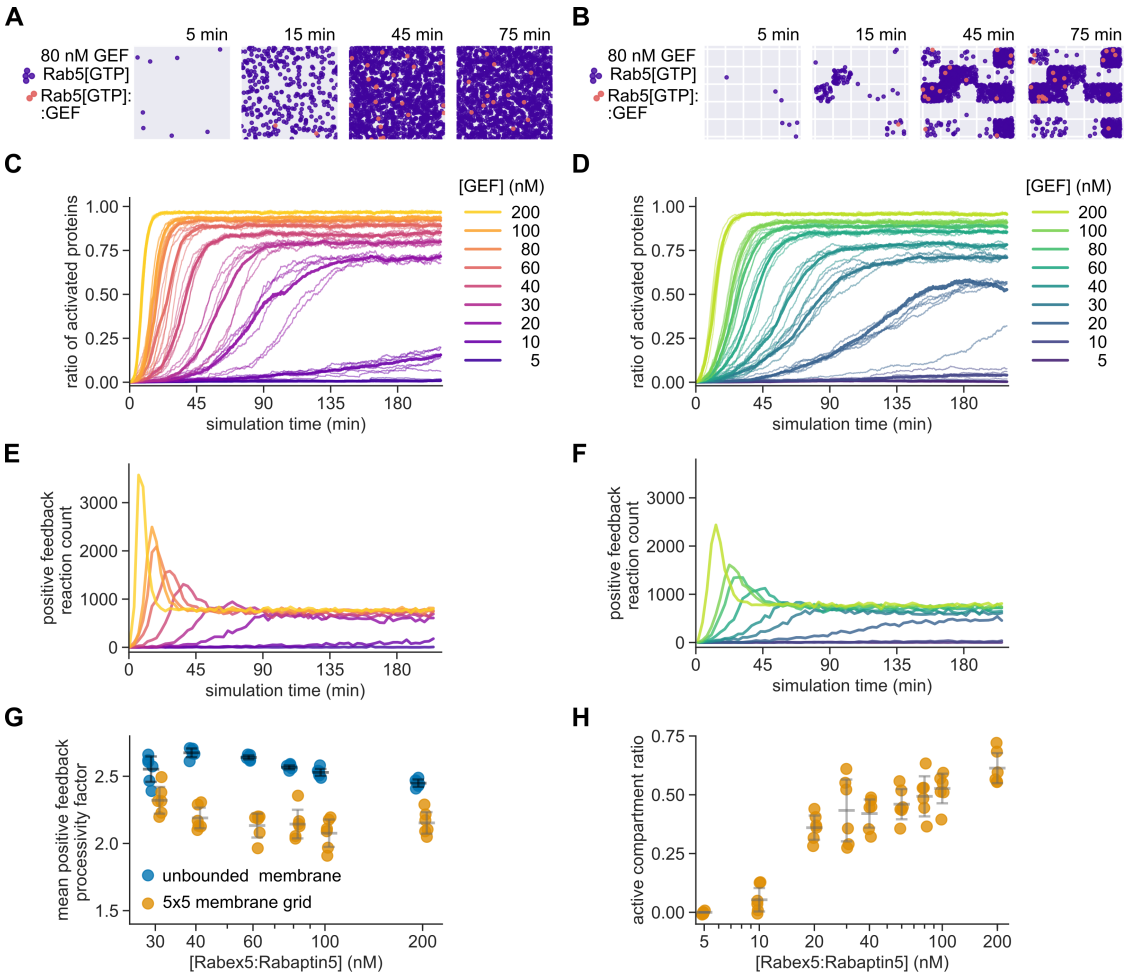

Figure 4.30: **System bounds affect Rab5 activation *in silico*.**

(A-B) Membrane snapshots of Rab5[GTP] and Rab5[GTP]:Rabaptin5:Rabex5 molecules in a spatial stochastic simulation. The Rab5 activation network was simulated in a 4×4×0.2 µm box with periodic lateral walls (A) or rigid 5×5 grid on the membrane surface (B). This either produces virtually unbounded system (A), where particles can freely diffuse outside and enter again at the opposite side or bounce off the rigid grid walls (B). In the example, 160 GEF particles, which is equivalent to 80 nM, were used to induce Rab5 activation. **(C-D)** Time evolution of Rab5 activation simulations. (C) Time courses of active Rab5 molecule ratio in laterally unbounded example with increasing GEF concentration. (D) Rab5 activation for GEF titration on a 5×5 membrane grid. For each condition, 6 simulations were run and the mean is shown in bold. **(E-F)** Cumulative number of positive feedback reactions in 3 min intervals for unbounded (E) and 5×5 grid simulations (F; n = 6). **(G)** Mean positive feedback processivity factor for unbounded (blue) and 5×5 grid. The mean processivity factor is the average number of Rab5 molecules that a given Rab5[GTP]:GEF complex activates. **(H)** Active compartment ratio at the end of stochastic simulations on 5×5 grid. The threshold value for active compartments was set as 20 Rab5[GTP]/µm^2.

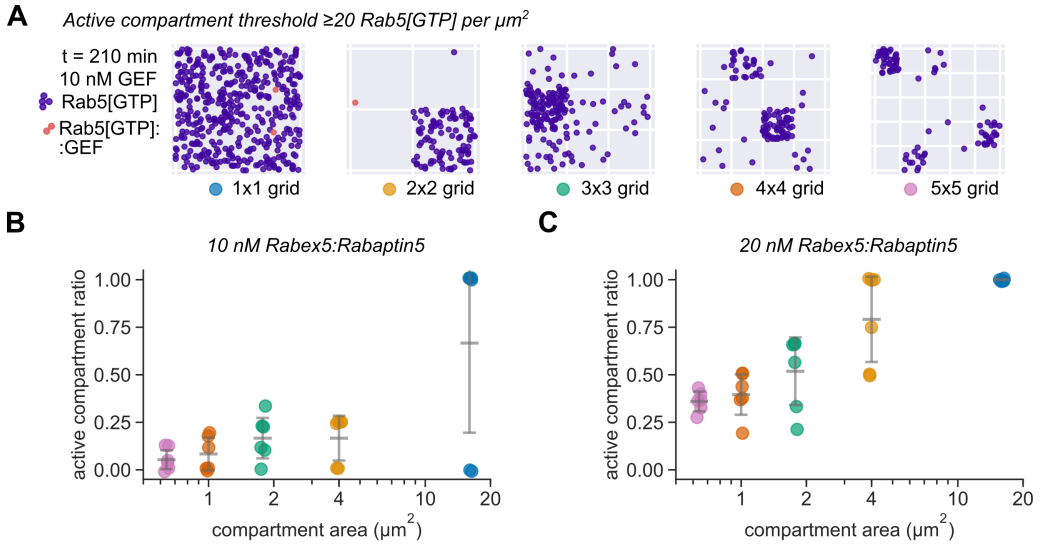

Figure 4.31: **Rab5 switching probability depends on boundary conditions.**
(A) End point snapshots of active Rab5 molecules on membrane with different grid configurations. **(B-C)** Ratios of activated compartments for different grid configurations. (B) Switching ratios with 10 nM GEF. (C) Active compartments with 20 nM GEF. Active compartment threshold was set at 20 Rab[GTP]/μm^2. We ran 6 simulations for a given condition.

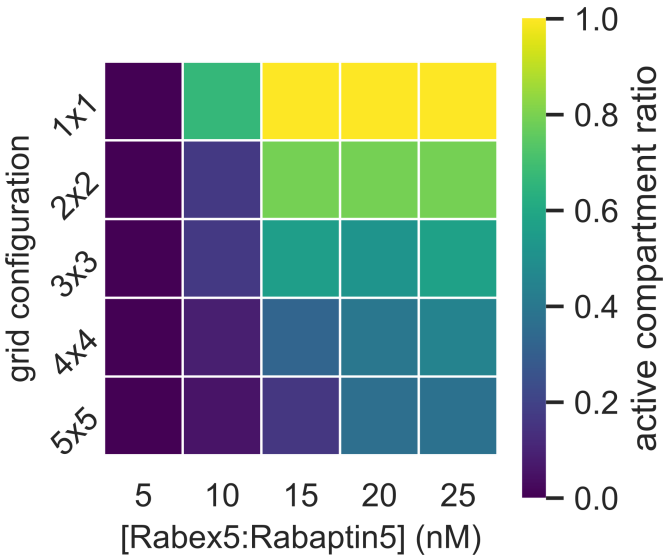

Figure 4.32: **Rab5 activation probability increases with compartment size.**
Heatmap of mean active compartment ratio for different grid configurations and increasing Rabex5:Rabaptin5 concentration. We ran spatial stochastic simulations on different membrane grids with GEF concentration between 5 and 25 nM. The compartment areas ranged from 16 μm^2 (1×1) to 0.64 μm^2 (5×5). We determined the mean active compartment ratio from 6 individual runs per condition. The active compartment threshold was ≥20 Rab5[GTP]/μm^2.

In summary, the spatial stochastic model closely replicated the observed systemic behavior of reconstituted Rab5 activation network and was used to explore effects of boundary conditions on collective Rab5 switching. We conclude that the results of spatial simulations based on hypothesized protein interactions from the literature [Lippé *et al.*, 2001; Delprato and Lambright, 2007; Zhang *et al.*, 2014] and our *in vitro* assays do not support intrinsic geometry sensing properties in the minimal activation circuit. Likely, the spatial specificity of collective Rab5 activity switching is ensured through specific targeting of Rabex5 [Blümer *et al.*, 2013; Zhu *et al.*, 2007; Mattera and Bonifacino, 2008; Zhu *et al.*, 2009] and Rabaptin5 [Kälin *et al.*, 2015] on early endosomal surface and GAP activity on other organelles [Haas *et al.*, 2005]. Nonetheless, it will be interesting to confirm these model results under physiological conditions and explore whether other biophysical cues like membrane curvature [Kirsten *et al.*, 2013] contribute to Rab5 activation.

5 Conclusions

Rab proteins are the main membrane identity determinants in eukaryotes. Specifically, our cells regulate their GTPase cycle to accurately orchestrate vesicular trafficking in space and time. Despite our understanding of the GTPase cycle in atomic detail [Vetter and Wittinghofer, 2001], we do not know how the nucleotide conversion is related to ensemble dynamics of protein pools that results in the complexity of e.g endosomal maturation, let alone cellular signaling as a whole. Answering these challenges are the emerging fields of synthetic [Csete and Doyle, 2002] and systems biology [Kitano, 2002]. Using engineering approaches and purified basic components, it is now possible to build signaling modules in defined physiological conditions from bottom-up and observe self-organized properties of reconstituted assemblies. In this work, we rebuild Rab5 activation network to answer longstanding questions of coordinated small GTPase emergent behavior and the underlying regulation mechanisms.

Recently, *in vitro* reconstitution techniques were used to elucidate Ras small GTPase signaling [Coyle and Lim, 2016; Iversen *et al.*, 2014; Huang *et al.*, 2016; Huang *et al.*, 2019]. These studies revealed new regulatory aspects and highlighted the importance of systematic bottom-up approach to better understand design principles that are wired in biochemical networks [Coyle, 2016]. Nonetheless, the crucial network components were hitherto non-physiologically attached to the reaction surface, which prevented system evaluation under cycling conditions away from chemical equilibrium. In contrast, we used native full length components in combination with glass-supported lipid bilayer, specific fluorescent labeling and TIRF microscopy to shed light at Rab regulation from single molecule to protein ensemble level. A similar approach was recently used to reconstitute Rab5 nanodomain formation on SLB-covered silica beads [Cezanne *et al.*, 2020].

Using our *in vitro* reconstitution approach we show:

1. Biological phospholipid membranes are necessary components of prenylated Rab activation networks.

2. The minimal Rab5 collective activation network is composed of Rab5:GDI and Rabex5:Rabaptin5 complexes, where biological membranes act as two dimensional reaction substrates. The membranes accommodate prenylated Rab GTPases and enable formation of non-linear positive feedback in Rab5 activation.

3. Collective Rab5 activation requires full length Rabex5:Rabaptin5 complex. The GEF component alone or Rab5 binding-deficient Rabaptin5 mutant cannot trigger system switching as they fail to form a positive feedback loop. The formation of active Rab5-driven positive feedback through GEF recruitment is necessary for collective GTPase switching and cannot be rescued by non-specific Rabex5 recruitment by mono-ubiquitin.

4. Rab5 activation by Rabex5:Rabaptin5 is ultrasensitive and bistable. The ultrasensitivity in collective Rab5 activation is achieved by the positive feedback in GEF recruitment to the membrane by active Rab5. Bistabilty becomes apparent with inclusion of RabGAP-5, where the reconstitution of collective Rab5 state switching exhibits hysteresis.

5. Inactive Rab5 is present on the membrane surface and provides a tuning parameter for coordinated system switching.

6. Molecular cues on membrane surface like ubiquitin, PRA1 and active Rab5 can promote decisive and fast Rab5 activation through feed-forward loops. Nonetheless, ubiquitin cannot rescue the collective switching with positive feedback deficient GEF complex mutant.

7. RabGAP-5 acts as a global inhibitor and enables formation of Rab5 activation waves on membrane surface at intermediate concentrations. The emergent spatial pattern self-organizes from the concurrent actions of GEF positive feedback activation and GAP global inactivation.

8. Collective Rab5 activation is stochastic and spreads laterally from self-organized active Rab5 clusters on the membrane. It can be described as a Poisson nucleation process.

So far, the composition of a minimal Rab5 activation network remained uncharacterized due to the overwhelming complexity of the cell, which was the only assay system for posttranslationally modified GTPases. Here, we identify biological membranes, along with Rab5:GDI and Rabex5:Rabaptin5 as the necessary components for collective Rab5 switching (Figure 5.1). This basic composition was also confirmed by Cezanne et al., which observed prenylated Rab5 activation on SLB-decorated silica beads [Cezanne *et al.*, 2020]. Despite its simplicity, this biochemical network encodes non-linear regulation mechanisms like *stoichiometric inhibition* and *positive feedback* through its unique biophysical properties and molecular interactions. The stoichiometric inhibition is delivered by the action of GDI, which maintains a limiting supply of available Rab5[GDP] on the membrane surface. As a consequence, the reconstituted system is very sensitive to the changes in Rab5 activation state after Rabex5:Rabaptin5 nucleotide exchange. This change in local Rab5[GTP] concentration is also sensed by the Rabex5:Rabaptin5, introducing a positive feedback loop that drives Rab5 activation on a collective scale across the whole membrane surface. Furthermore, the lipid bilayer not only offers a 2D support for the reaction constituents, it can also present additional molecular cues, which shift the parameter landscape to facilitate bistable switching. Here, we explored roles of pre-activated Rab5, PRA1 GDF and mono-ubiquitin. However, there are additional factors that have been proposed to influence Rab5 activation, including the endosomal lipid composition with phosphoinositide PIP3 [Cezanne *et al.*, 2020], Rab4 [Kälin *et al.*, 2015], Rab22 [Zhu *et al.*, 2009] and Arf1 [Nagano *et al.*, 2019]. Together, this manifests in stochastic and ultrasensitive responses to signal inputs on a collective, system's, level. By utilizing key deletion mutants – equivalent to severing wiring in an electronic circuit – we deduce that collective ON-switching is possible only through active Rab5-mediated GEF complex interaction and is not rescued by an alternative non-specific recruitment mechanism. Consequently, the non-linear GTPase collective activity switching does not depend solely on membrane co-localization, but requires specific Rab5:Rabaptin5:Rabex5 interaction. The transient formation of the ternary complex both forms a positive feedback loop and releases Rabex5 auto-

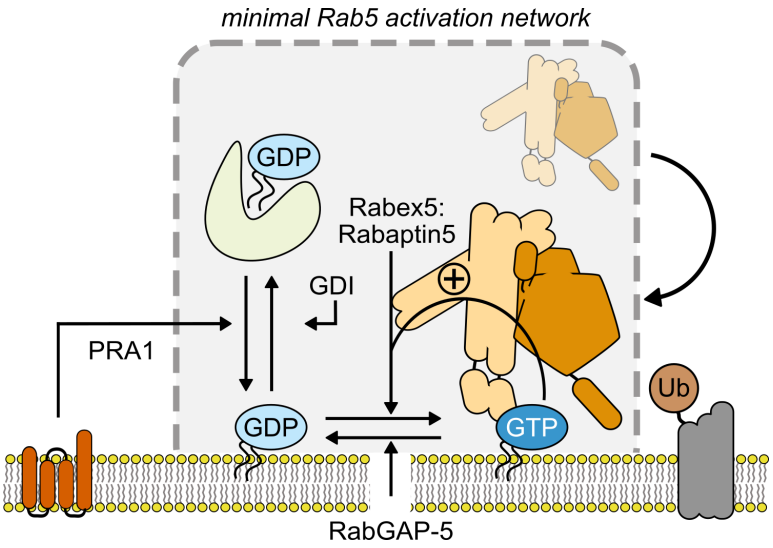

Figure 5.1: **Model of reconstituted Rab5 activation network.**
The minimal Rab5 activation networks consists of lipid bilayer, Rab5:GDI and Rabex5:Rabaptin5 complexes. This signaling module acts as a stochastic collective GTPase switch that can transition between high-density Rab5 domains on the membrane and inactive soluble Rab5:GDI pool. The eukaryotic cell tunes this network by controlling the amount of free Rab5-[GDP] with PRA1 or phosphoregulation, GAP-mediated GTP hydrolysis and GEF recruitment by mono-ubiquitinated cargo, Rab4, Arf1 and organelle-specific lipid composition. The additional level of regulation ensures correct localization, amplitude and duration of Rab5 signaling.

inhibition, resulting in fully active GEF complex, which fuels the system-wide response. We believe that the observed collective Rab activation is biologically relevant as basal non-coordinated GTPase activations would be lost in the cellular noise [Huang *et al.*, 2016].

What is more, by capturing single molecule snapshots in real time, we demonstrate that short-lived inactive Rab5 is present on the lipid bilayer as it dissociates from GDI complex in equilibrium reaction. The relative availability of this molecular species is a likely control parameter *in vivo*, where it could be tuned by the extended network components like GDF PRA1, GAP RabGAP-5 and PKCε kinase [Ong *et al.*, 2014]. These factors can shift the critical GEF concentration for Rab switching in concert with local chemical environment at the target membrane. There, the unique lipid and protein composition can ensure specific Rab5 activation through GEF localization and reduced stochastic effects. Possible Rabex5:Rabaptin5 localization factors are Rab4, Arf1, mono-ubiquitinated transmembrane cargo and PI3P.

Finally, inclusion of a GAP in our reconstituted network revealed bistability and self-organized pattern formation of Rab5 activation on system scale. We observe hysteresis in Rab5 collective switching where a much higher GAP concentration is needed to turn the system from active state back to inactive than it is to prevent switching from an initially inactive state. This insight bridged the gap between apparent bimodality of the GTPase nucleotide exchange switch on the molecular scale with higher-order state transition of the whole protein ensemble. Here, it is the network architecture that enables emergent and coordinated collective switching, manifesting in spreading activation waves. In these self-organized protein patters the intrinsic stochasticity of the Rab5 system generates local concentration gradients of active Rab5, which are maintained by the positive feedback of GEF recruitment and stabilized with global inhibitory effect of the GAP. This basic network property could be used by the cell to establish spatial boundaries in sub-organelle small GTPase localization and maintain protein membrane domains, which are the main signaling platforms for Rab [Zerial and McBride, 2001], Arf [Stalder and Antonny, 2013], Ras [Wittinghofer, 2014a] and Rho small GTPase networks [Rapali *et al.*, 2017].

Despite the exciting findings presented in this thesis, the *in vitro* reconstitution approach still has some drawbacks. By examining Rab5 activation in well-defined synthetic conditions, we could disentangle underlying network properties like non-linear positive feedback and stochastic bistabilty. Furthermore, we examined what roles do individual components play in Rab5 activity switching under assayed conditions. Nonetheless, we cannot easily extrapolate our findings to situation *in vivo*. The crosstalk and broader cellular context likely contribute to unique parameter conditions, which cannot be replicated *in vitro*. To bridge this gap, it would be exciting to reconstitute the characterized minimal activation network in *Xenopus* egg extract [Nguyen *et al.*, 2015], which closely resembles cytoplasmic environment. Replicating the observed system behavior in a more complex setting *in vitro* and eventually *in vivo* would provide additional aspects of Rab5 signaling and small GTPase regulation in general. Importantly, the constructionist *in vitro* approach presented here and future research on more complex systems will open new avenues in understanding the integrated small GTPase signaling that orchestrates the inner ticking of our cells.

5.1 Potential for future research

To sum up, our work addresses long-standing assumptions in Rab and small GTPase signaling in general. By using *in vitro* reconstitution, we identify common regulatory mechanisms that ensure specificity and tunability in Rab signal transduction. Nonetheless, our approach opens new avenues in small GTPase network exploration. Particularly, we prepared metal micropatterned glass coverslips that allow detailed and high-throughput investigation of boundary conditions in the reconstituted Rab5 activation network. For example, in Figures 4.28, 4.31 and 4.32 we present preliminary experimental and computational data on stochastic Rab5 transition using different sizes and shapes of SLB membrane substrates. This investigation is especially interesting since a conceptually similar kinase-based bistable system was shown to demonstrate stochastic geometry sensing – an intrinsic network property, which allows the cell to generate distinct membrane domains through physical confinement [Hansen *et al.*, 2019]. On the other hand, our initial results do not suggest that Rab5 network would exhibit emergent geometry sensing properties. Nevertheless, a further investigation into GTPase activity switching in different confinement conditions would be an important contribution to the *in vitro* reconstitution and small GTPase fields.

Similarly, the micropatterned grid design already contains L-shaped compartments and divisions with slits (Figure 3.1) that are aimed at investigation of Rab5 activation wave propagation in presence of RabGAP-5. A similar strategy of *in vitro* reconstitution already contributed to our understanding of Min wave propagation under different geometries [Schweizer *et al.*, 2012]. We would be interested to see how spatial perturbation influences the self-organized protein patterns and if it can induce emergence of new system shapes like periodic waves, stationary domains or standing waves. According to the picket fence model of lateral membrane organization *in vivo*, the cytoskeleton, lipid rafts and transmembrane proteins introduce physical boundaries [Jacobson *et al.*, 2019] that are mimicked by the grid design. It is possible that these structures and lateral confinement could influence Rab5 self-organization on collective scale. Taking advantage of the well-defined reconstituted network and unique microgrid design could be the first step toward a systematic analysis of small GTPase domain interaction with geometric boundaries.

Another geometrical aspect, which could influence Rab5 activation and is suitable for *in vitro* reconstitution, is membrane curvature sensing. The structure-dependent curvature sensing is well established in Arf signaling [Drin and Antonny, 2010] and has also been proposed for Rabs [Kirsten *et al.*, 2013; Kulakowski *et al.*, 2018]. Nevertheless, there is no conclusive evidence that Rabs or their regulators would be selective for membrane shape. It would be exciting to determine how the described Rab5-Rabex5:Rabaptin5 regulatory module responds to different membrane topologies *in vitro*. Possibly, Rab5 activation network intrinsically prefers membranes that resemble curved early endosomes and clathrin-coated vesicles. To our knowledge, these organelles are the primary locations of Rab5 activation *in vivo*. By extension, the 60-odd Rab ensemble in humans could ensure localization specificity by also sensing the bilayer curvature – e.g. relatively flat plasma membrane or round secretory vesicles would accumulate different repertoires of Rabs, GEFs and GAPs. For example, we could compare Rab5 switching on flat SLB as was shown here with network reconstitution on round silica beads or giant unilamellar vesicles (GUVs). These biomimetic membranes can be precisely manipulated with optical tweezers to probe a wide variety of topologies [Ambroggio *et al.*, 2010].

The presented *in vitro* reconstitution platform can be readily utilized to determine the role of complex membrane composition in Rab5 signaling. As has been demonstrated recently, the endosomal lipid composition could play a role in Rab5 nanodomain self-organization [Cezanne *et al.*, 2020]. Our experimental approach is especially well-suited to tackle this open question by using defined synthetic lipids in SLB preparation that more closely resemble physiological conditions *in vivo*. Possibly, the complex lipid mixture could undergo phase separation and form lipids rafts, which would accumulate different amounts of network components and influence their diffusion coefficients. Both of these factors could impact the likelihood of Rab5 activation. Particularly, the Rabex5 membrane targeting motif, Rab5 C-terminal hypervariable region could and geranyl-geranyl anchors could be sensitive towards lipid composition and mobility. On the other hand, a future study should also focus on endosomal protein composition that steers Rab5 activation. Here, we extended the minimal activation network by including PRA1, pre-activated Rab5 and ubiquitin in our assay. We expect that these location-specific molecular cues direct Rab5 activation towards early endosomes by

lowering the necessary GEF threshold for collective GTPase transition. Likewise, we could test relative contributions of additional protein factors like Rab4, Rab22 and Arf1. Excitingly, we could produce unique compartment compositions by combining optogenetic patterning of the SLB [Bhagawati *et al.*, 2010] and chromium microgrids[1]. This would allow us to simulate location-specific Rab activation *in vitro* by controlling protein make-up of the SLB surface. Also, by taking advantage of light-induced oligomerization, we could trigger active Rab5 nucleation [Nguyen *et al.*, 2016] at specific locations and observe early stages of protein pattern formation and positive feedback propagation in real time. I believe that joining advanced imaging techniques with direct light perturbation of the reconstituted network would present a new experimental platform, which would advance our understanding of small GTPase signaling in general.

The basic structure of Rab5 activation network also opens new exciting questions regarding the properties of interactions between its components. Here, we demonstrated positive feedback by GEF recruitment, which results in collective Rab5 switching to the activated GTP-bound state. What is more, introducing globally-acting RabGAP-5 triggered the formation of a traveling activation front across the supported membrane. Despite this interesting finding, RabGAP-5 cellular role in Rab5 regulation is not precisely known. Possibly, RabGAP-5 *in vivo* does not act as global inhibitor but is rather recruited to the bilayer similarly to the Rabex5:Rabaptin5 complex. This raises an interesting idea of simultaneous or sequential action of GEF positive- and GAP negative feedback in Rab5 activation. We could test this hypothetical biochemical circuit by assembling a GAP fusion protein that would combine the RabGAP-5 TBC catalytic domain with Rab5[GTP]-binding region of a Rab5 effector, e.g. C_2H_2 domain of EEA1 [Mishra *et al.*, 2010]. Potentially, the opposing feedback loops could give raise to more complex emergent properties like oscillations and Turing patterns [Tyson *et al.*, 2003; Turing, 1952]. Despite the lack of knowledge, it would be interesting to conceptually examine principles of feedback and self-organization of Rab small GTPase networks in further detail. The lessons learned *in vitro* could soon be applied to newly discovered GAP localization and recruitment factors as has been shown for RabGAP-5 *C. elegans* homolog TBC-2 that binds Rab7, a downstream GTPase from Rab5 [Chotard *et al.*, 2010].

[1] Idea developed by M. Loose and L. Kowalski.

Finally, characterization of Rab5 activation and development of the *in vitro* reconstitution assay opens the possibility to examine Rab5 crosstalk with other small GTPase networks. Among others, Rab4 has been proposed to initiate Rab5 activation through Rabaptin5-mediated feed-forward loop [Kälin *et al.*, 2015]. By coupling Rab4 activation with Rab5 switching, we could test the feed-forward hypothesis and resolve an interesting open question in Rab5 signaling. Similarly, Rabaptin5 mediates tethering of trans-Golgi cargo to endosomal compartment through interaction with Arf1 effector GGA1 [Mattera *et al.*, 2003; Kawasaki *et al.*, 2005]. What is more, Arf1 was recently shown to recruit Rabex5 ortholog to trans-Golgi in yeast [Nagano *et al.*, 2019]. For the first time, we could demonstrate the Arf1-mediated Rabex5:Rabaptin5 recruitment using our established SLB-based reconstitution approach. Last but not least, the Rab5-Rab7 cascade is the main regulatory event in endosomal maturation from sorting compartments in early endosomes to the degradation pathway in late endosomes [Rink *et al.*, 2005; Poteryaev *et al.*, 2010; Kinchen and Ravichandran, 2010; Huotari and Helenius, 2011; Langemeyer *et al.*, 2020]. There, the Mon1:Ccz1 complex acts as Rab5 effector and Rab7 GEF, paving the way for Rab cascade. Moreover, Mon1:Ccz1 also displaces Rabex5 from endosome surface, potentially acting as a cut-out switch for Rabex5:Rabaptin5 positive feedback in Rab5 activation. Recently, Bulli/RMC1 was identified as additional regulator of Mon1:Ccz1-mediated Rab5-Rab7 transition [Langemeyer *et al.*, 2020; Dehnen *et al.*, 2020]. As the list of network components for the Rab5-Rab7 cascade grows, we can reconstitute the GTPase transition switch *in vitro* to fully understand the proposed mechanisms and characterize the minimal functional network. To achieve the full cascade *in vitro*, we would need to better understand the temporal and spatial requirements of Rab5 and Rab7 activation. Plus, the early-to-late endosomal transition is also defined by parallel PI3P accumulation through Vps34 – another Rab5 effector, which could be necessary to mimic or reconstitute as well. This is an extremely ambitious task that would greatly advance our knowledge of input-output relationships in Rab GTPase signaling circuits.

Summing up all potential future research directions, I encourage the eager reader to consider taking the full advantage of our *in vitro* reconstitution technique presented here. Only by re-building biochemical networks from bottom-up, we can better understand how these circuits function to interpret incoming signals and transmitting

the message to downstream cascades. This inevitably closes the gap in mechanistic knowledge between the small GTPase orchestration on molecular and system's scales, which is the ultimate goal of bottom-up synthetic and systems biology. Good luck!

Bibliography

[Abel *et al.*, 2012] Steven M. Abel, Jeroen P. Roose, Jay T. Groves, Arthur Weiss, and Arup K. Chakraborty, "The Membrane Environment Can Promote or Suppress Bistability in Cell Signaling Networks," *The Journal of Physical Chemistry B*, 116(11):3630–3640, mar 2012.

[Agola *et al.*, 2011] J. O. Agola, P. A. Jim, H. H. Ward, S. Basuray, and A. Wandinger-Ness, "Rab GTPases as regulators of endocytosis, targets of disease and therapeutic opportunities.," *Clinical genetics*, 80(4):305–18, oct 2011.

[Alberti *et al.*, 2019] Simon Alberti, Amy Gladfelter, and Tanja Mittag, "Considerations and Challenges in Studying Liquid-Liquid Phase Separation and Biomolecular Condensates," *Cell*, 176(3):419–434, 2019.

[Altschuler *et al.*, 2008] Steven J Altschuler, Sigurd B Angenent, Yanqin Wang, and Lani F Wu, "On the spontaneous emergence of cell polarity.," *Nature*, 454(7206):886–9, aug 2008.

[Alvarez-Dominguez *et al.*, 2008] Carmen Alvarez-Dominguez, Fidel Madrazo-Toca, Lorena Fernandez-Prieto, Joël Vandekerckhove, Eduardo Pareja, Raquel Tobes, Maria Teresa Gomez-Lopez, Elida Del Cerro-Vadillo, Manuel Fresno, Francisco Leyva-Cobián, and Eugenio Carrasco-Marín, "Characterization of a Listeria monocytogenes Protein Interfering with Rab5a," *Traffic*, 9(3):325–337, mar 2008.

[Ambroggio *et al.*, 2010] Ernesto Ambroggio, Benoît Sorre, Patricia Bassereau, Bruno Goud, Jean-Baptiste Manneville, and Bruno Antonny, "ArfGAP1 generates an Arf1 gradient on continuous lipid membranes displaying flat and curved regions," *The EMBO Journal*, 29(2):292–303, jan 2010.

[Andrews *et al.*, 2010] Steven S. Andrews, Nathan J. Addy, Roger Brent, and Adam P. Arkin, "Detailed simulations of cell biology with Smoldyn 2.1.," *PLoS computational biology*, 6(3):e1000705, mar 2010.

[Arosio *et al.*, 2015] Paolo Arosio, Tuomas P J Knowles, and Sara Linse, "On the lag phase in amyloid fibril formation.," *Physical chemistry chemical physics : PCCP*, 17(12):7606–18, mar 2015.

[Backouche *et al.*, 2006] F. Backouche, L. Haviv, D. Groswasser, and A. Bernheim-Groswasser, "Active gels: dynamics of patterning and self-organization," *Physical Biology*, 3(4):264–273, dec 2006.

[Banani *et al.*, 2017] Salman F. Banani, Hyun O. Lee, Anthony A. Hyman, and Michael K. Rosen, "Biomolecular condensates: organizers of cellular biochemistry," *Nature Reviews Molecular Cell Biology*, 2017.

[Barnard *et al.*, 2015] Alun R. Barnard, Markus Groppe, and Robert E. Maclaren, "Gene therapy for choroideremia using an adeno-associated viral (AAV) vector," *Cold Spring Harbor Perspectives in Medicine*, 5(3):1–14, 2015.

[Barr and Lambright, 2010] Francis Barr and David G. Lambright, "Rab GEFs and GAPs," *Current Opinion in Cell Biology*, 22(4):461–470, 2010.

[Barr, 2013] Francis A. Barr, "Rab GTPases and membrane identity: Causal or inconsequential?," *The Journal of Cell Biology*, 202(2):191–199, jul 2013.

[Barthelmes *et al.*, 2020] Katja Barthelmes, Evelyn Ramcke, Hyun-seo Kang, Michael Sattler, and Aymelt Itzen, "Conformational control of small GTPases by AMPylation," *Proceedings of the National Academy of Sciences*, page 201917549, mar 2020.

[Baumann *et al.*, 2020] Sebastian Baumann, Artem Komissarov, Maria Gili, Verena Ruprecht, Stefan Wieser, and Sebastian P. Maurer, "A reconstituted mammalian APC-kinesin complex selectively transports defined packages of axonal mRNAs," *Science Advances*, 6(11):eaaz1588, mar 2020.

[Behnia and Munro, 2005] Rudy Behnia and Sean Munro, "Organelle identity and the signposts for membrane traffic.," *Nature*, 438(7068):597–604, 2005.

[Bement *et al.*, 2006] William M. Bement, Ann L. Miller, and George Von Dassow, "Rho GTPase activity zones and transient contractile arrays," *BioEssays*, 28(10):983–993, 2006.

[Bezeljak *et al.*, 2020] Urban Bezeljak, Hrushikesh Loya, Beata Kaczmarek, Timothy E Saunders, and Martin Loose, "Stochastic activation and bistability in a Rab GTPase regulatory network.," *Proceedings of the National Academy of Sciences of the United States of America*, 117(12):6540–6549, mar 2020.

[Bhagawati *et al.*, 2010] Maniraj Bhagawati, Suman Lata, Robert Tampé, and Jacob Piehler, "Native laser lithography of his-tagged proteins by uncaging of multivalent chelators," *Journal of the American Chemical Society*, 132(17):5932–5933, 2010.

[Bishop and Qian, 2010] Lisa M. Bishop and Hong Qian, "Stochastic bistability and bifurcation in a mesoscopic signaling system with autocatalytic kinase," *Biophysical Journal*, 98(1):1–11, 2010.

[Blümer *et al.*, 2013] Julia Blümer, Juliana Rey, Leif Dehmelt, Tomáš Maze, Yao Wen Wu, Philippe Bastiaens, Roger S. Goody, and Aymelt Itzen, "RabGEFs are a major determinant for specific Rab membrane targeting," *Journal of Cell Biology*, 200(3):287–300, 2013.

[Bonet-Ponce and Cookson, 2019] Luis Bonet-Ponce and Mark R. Cookson, "The role of Rab GTPases in the pathobiology of Parkinson' disease," *Current Opinion in Cell Biology*, 59:73–80, 2019.

[Borri *et al.*, 2020] Alessandro Borri, Pasquale Palumbo, and Abhyudai Singh, "Time Delays in a Genetic Positive-Feedback Circuit," *IEEE Control Systems Letters*, 4(1):163–168, jan 2020.

[Bucci *et al.*, 1992] C Bucci, R G Parton, I H Mather, H Stunnenberg, K Simons, B Hoflack, and M Zerial, "The small GTPase rab5 functions as a regulatory factor in the early endocytic pathway.," *Cell*, 70(5):715–28, sep 1992.

[Burov *et al.*, 2013] Stanislav Burov, S. M. A. Tabei, Toan Huynh, Michael P. Murrell, Louis H. Philipson, Stuart A. Rice, Margaret L. Gardel, Norbert F. Scherer, and

Aaron R. Dinner, "Distribution of directional change as a signature of complex dynamics," *Proceedings of the National Academy of Sciences*, 110(49):19689–19694, dec 2013.

[Cabrera and Ungermann, 2010] Margarita Cabrera and Christian Ungermann, "Guiding endosomal maturation," *Cell*, 141(3):404–406, 2010.

[Cezanne *et al.*, 2020] Alice Cezanne, Janelle Lauer, Anastasia Solomatina, Ivo F Sbalzarini, and Marino Zerial, "A non-linear system patterns Rab5 GTPase on the membrane.," *eLife*, 9:2019.12.17.880203, jun 2020.

[Chavrier *et al.*, 1990] Philippe Chavrier, Robert G. Parton, Hans Peter Hauri, Kai Simons, and Marino Zerial, "Localization of low molecular weight GTP binding proteins to exocytic and endocytic compartments," *Cell*, 62(2):317–329, jul 1990.

[Chen *et al.*, 2014] Pin-I Chen, Kristine Schauer, Chen Kong, Andrew R. Harding, Bruno Goud, and Philip D. Stahl, "Rab5 Isoforms Orchestrate a "Division of Labor" in the Endocytic Network; Rab5C Modulates Rac-Mediated Cell Motility," *PLoS ONE*, 9(2):e90384, feb 2014.

[Cheng *et al.*, 2004] Kwai Wa Cheng, John P. Lahad, Wen Lin Kuo, Anna Lapuk, Kyosuke Yamada, Nelly Auersperg, Jinsong Liu, Karen Smith-McCune, Karen H. Lu, David Fishman, Joe W. Gray, and Gordon B. Mills, "The RAB25 small GTPase determines aggressiveness of ovarian and breast cancers," *Nature Medicine*, 10(11):1251–1256, 2004.

[Cherfils and Zeghouf, 2013] Jacqueline Cherfils and Mahel Zeghouf, "Regulation of small GTPases by GEFs, GAPs, and GDIs.," *Physiological reviews*, 93(1):269–309, 2013.

[Chiaruttini *et al.*, 2015] Nicolas Chiaruttini, Lorena Redondo-Morata, Adai Colom, Frédéric Humbert, Martin Lenz, Simon Scheuring, and Aurélien Roux, "Relaxation of Loaded ESCRT-III Spiral Springs Drives Membrane Deformation.," *Cell*, 163(4):866–79, nov 2015.

[Chin *et al.*, 2009] Harvey F. Chin, Yiying Cai, Shekar Menon, Susan Ferro-Novick, Karin M. Reinisch, and Enrique M. De La Cruz, "Kinetic Analysis of the Guanine Nu-

cleotide Exchange Activity of TRAPP, a Multimeric Ypt1p Exchange Factor," *Journal of Molecular Biology*, 389(2):275–288, jun 2009.

[Chotard *et al.*, 2010] Laëtitia Chotard, Ashwini K Mishra, Marc-André Sylvain, Simon Tuck, David G Lambright, and Christian E Rocheleau, "TBC-2 regulates RAB-5/RAB-7-mediated endosomal trafficking in Caenorhabditis elegans.," *Molecular biology of the cell*, 21(13):2285–96, jul 2010.

[Chou and Jahn, 2000] Judy H. Chou and Reinhard Jahn, "Binding of Rab3A to synaptic vesicles," *Journal of Biological Chemistry*, 275(13):9433–9440, 2000.

[Christoforidis *et al.*, 1999] Savvas Christoforidis, Heidi M. McBride, Robert D. Burgoyne, and Marino Zerial, "The Rab5 effector EEA1 is a core component of endosome docking.," *Nature*, 397(6720):621–5, feb 1999.

[Chung *et al.*, 2018] Jean K. Chung, Young Kwang Lee, John-Paul Denson, William K. Gillette, Steven Alvarez, Andrew G. Stephen, and Jay T. Groves, "K-Ras4B Remains Monomeric on Membranes over a Wide Range of Surface Densities and Lipid Compositions.," *Biophysical journal*, 114(1):137–145, jan 2018.

[Collins, 2003] Ruth N. Collins, ""Getting it on"–GDI displacement and small GTPase membrane recruitment.," *Molecular cell*, 12(5):1064–6, nov 2003.

[Coyle, 2016] Scott M. Coyle, "Reverse engineering GTPase programming languages with reconstituted signaling networks," *Small GTPases*, 1248(May):1–5, 2016.

[Coyle and Lim, 2016] Scott M. Coyle and Wendell A. Lim, "Mapping the functional versatility and fragility of Ras GTPase signaling circuits through in vitro network reconstitution.," *eLife*, 5:1–34, 2016.

[Csete and Doyle, 2002] Marie E. Csete and John C. Doyle, "Reverse engineering of biological complexity," *Science*, 295(5560):1664–1669, 2002.

[D'Adamo *et al.*, 1998] Patrizia D'Adamo, Andrea Menegon, Cristiana Lo Nigro, Marina Grasso, Massimo Gulisano, Filippo Tamanini, Thierry Bienvenu, Agi K. Gedeon, Ben Oostra, Shih-Kwang Wu, Anurag Tandon, Flavia Valtorta, William E. Balch, Jamel Chelly, and Daniela Toniolo, "Mutations in GDI1 are responsible for X-linked non-specific mental retardation," *Nature Genetics*, 19(2):134–139, jun 1998.

[Dehnen *et al.*, 2020] Lena Dehnen, Maren Janz, Jitender Kumar Verma, Olympia Ekaterini Psathaki, Lars Langemeyer, Florian Fröhlich, Jürgen J. Heinisch, Heiko Meyer, Christian Ungermann, and Achim Paululat, "A trimeric metazoan Rab7 GEF complex is crucial for endocytosis and scavenger function.," *Journal of cell science*, 133(13), jul 2020.

[Del Conte-Zerial *et al.*, 2008] Perla Del Conte-Zerial, Lutz Brusch, Jochen C. Rink, Claudio Collinet, Yannis Kalaidzidis, Marino Zerial, and Andreas Deutsch, "Membrane identity and GTPase cascades regulated by toggle and cut-out switches.," *Molecular systems biology*, 4(206):206, 2008.

[Delprato and Lambright, 2007] Anna Delprato and David G Lambright, "Structural basis for Rab GTPase activation by VPS9 domain exchange factors.," *Nature structural & molecular biology*, 14(5):406–12, may 2007.

[Delprato *et al.*, 2004] Anna Delprato, Eric Merithew, and David G. Lambright, "Structure, exchange determinants, and family-wide Rab specificity of the tandem helical bundle and Vps9 domains of Rabex-5," *Cell*, 118(5):607–617, 2004.

[Deneke and Di Talia, 2018] Victoria E. Deneke and Stefano Di Talia, "Chemical waves in cell and developmental biology.," *The Journal of cell biology*, 217(4):1193–1204, apr 2018.

[Di Fiore *et al.*, 2003] Pier Paolo Di Fiore, Simona Polo, and Kay Hofmann, "When ubiquitin meets ubiquitin receptors: a signalling connection.," *Nature reviews. Molecular cell biology*, 4(6):491–7, jun 2003.

[Dirac-Svejstrup *et al.*, 1997] A. Barbara Dirac-Svejstrup, Tomoyuki Sumizawa, and Suzanne R. Pfeffer, "Identification of a GDI displacement factor that releases endosomal Rab GTPases from Rab-GDI.," *The EMBO journal*, 16(3):465–72, feb 1997.

[Drin and Antonny, 2010] Guillaume Drin and Bruno Antonny, "Amphipathic helices and membrane curvature.," *FEBS letters*, 584(9):1840–7, may 2010.

[Duellberg *et al.*, 2016] Christian Duellberg, Nicholas I. Cade, David Holmes, and Thomas Surrey, "The size of the EB cap determines instantaneous microtubule stability.," *eLife*, 5(APRIL2016):1–23, apr 2016.

[Ferrell and Ha, 2014a] James E. Ferrell and Sang Hoon Ha, "Ultrasensitivity part I: Michaelian responses and zero-order ultrasensitivity," *Trends in Biochemical Sciences*, 39(10):496–503, 2014.

[Ferrell and Ha, 2014b] James E. Ferrell and Sang Hoon Ha, "Ultrasensitivity part II: multisite phosphorylation, stoichiometric inhibitors, and positive feedback.," *Trends in biochemical sciences*, 39(11):556–69, nov 2014.

[Ferrell and Ha, 2014c] James E. Ferrell and Sang Hoon Ha, "Ultrasensitivity part III: cascades, bistable switches, and oscillators.," *Trends in biochemical sciences*, 39(12):612–8, dec 2014.

[Ferrell and Xiong, 2001] James E. Ferrell and Wen Xiong, "Bistability in cell signaling: How to make continuous processes discontinuous, and reversible processes irreversible.," *Chaos (Woodbury, N.Y.)*, 11(1):227–236, mar 2001.

[Fitzgerald *et al.*, 2006] Daniel J. Fitzgerald, Philipp Berger, Christiane Schaffitzel, Kazuhiro Yamada, Timothy J. Richmond, and Imre Berger, "Protein complex expression by using multigene baculoviral vectors.," *Nature methods*, 3(12):1021–32, dec 2006.

[Fletcher, 2011] Daniel A. Fletcher, "To model or not to model?," *Molecular biology of the cell*, 22(7):909–10, apr 2011.

[Fletcher, 2016] Daniel A. Fletcher, "Bottom-Up Biology: Harnessing Engineering to Understand Nature," *Developmental Cell*, 38(6):587–589, 2016.

[Franke *et al.*, 2019] Christian Franke, Urska Repnik, Sandra Segeletz, Nicolas Brouilly, Yannis Kalaidzidis, Jean-Marc Verbavatz, and Marino Zerial, "Correlative single-molecule localization microscopy and electron tomography reveals endosome nanoscale domains," *Traffic*, 20(8):601–617, aug 2019.

[Frasa *et al.*, 2012] Marieke a. M. Frasa, Katja T. Koessmeier, M. Reza Ahmadian, and Vania M. M. Braga, "Illuminating the functional and structural repertoire of human TBC/RABGAPs," *Nature Reviews Molecular Cell Biology*, 13(2):476–476, 2012.

[Gallager, 2013] Robert G. Gallager, "Poisson processes," In *Stochastic Processes*, volume 53, pages 72–104. Cambridge University Press, dec 2013.

[Ganzinger and Schwille, 2019] Kristina A Ganzinger and Petra Schwille, "More from less - bottom-up reconstitution of cell biology.," *Journal of cell science*, 132(4), feb 2019.

[Gardner *et al.*, 2000] TS Gardner, CR Cantor, and JJ Collins, "Construction of a genetic toggle switch in Escherichia coli," *Nature*, 403:339–342, 2000.

[Gavriljuk *et al.*, 2012] Konstantin Gavriljuk, Emerich-Mihai Gazdag, Aymelt Itzen, Carsten Kötting, Roger S. Goody, and Klaus Gerwert, "Catalytic mechanism of a mammalian Rab·RabGAP complex in atomic detail.," *Proceedings of the National Academy of Sciences of the United States of America*, 109(52):21348–53, 2012.

[Gavriljuk *et al.*, 2013] Konstantin Gavriljuk, Aymelt Itzen, Roger S. Goody, Klaus Gerwert, and Carsten Kötting, "Membrane extraction of Rab proteins by GDP dissociation inhibitor characterized using attenuated total reflection infrared spectroscopy.," *Proceedings of the National Academy of Sciences of the United States of America*, 110(33):13380–5, aug 2013.

[Gibson *et al.*, 2009] Daniel G Gibson, Lei Young, Ray-Yuan Chuang, J Craig Venter, Clyde A Hutchison, and Hamilton O Smith, "Enzymatic assembly of DNA molecules up to several hundred kilobases.," *Nature methods*, 6(5):343–345, 2009.

[Gierer and Meinhardt, 1972] A Gierer and H Meinhardt, "A theory of biological pattern formation," *Kybernetik*, 12(1):30–39, dec 1972.

[Gillingham *et al.*, 2014] Alison K. Gillingham, Rita Sinka, Isabel L. Torres, Kathryn S. Lilley, and Sean Munro, "Toward a comprehensive map of the effectors of rab GTPases.," *Developmental cell*, 31(3):358–73, nov 2014.

[Goehring and Grill, 2013] Nathan W. Goehring and Stephan W. Grill, "Cell polarity: mechanochemical patterning," *Trends in Cell Biology*, 23(2):72–80, 2013.

[Goldbeter and Koshland, 1984] A. Goldbeter and D. E. Koshland, "Ultrasensitivity in biochemical systems controlled by covalent modification. Interplay between zero-order and multistep effects," *Journal of Biological Chemistry*, 259(23):14441–14447, 1984.

[Gomez *et al.*, 2019] Rachel C Gomez, Paulina Wawro, Pawel Lis, Dario R Alessi, and Suzanne R Pfeffer, "Membrane association but not identity is required for LRRK2 activation and phosphorylation of Rab GTPases.," *The Journal of cell biology*, oct 2019.

[Gomez-Uribe *et al.*, 2007] Carlos Gomez-Uribe, George C. Verghese, and Leonid A. Mirny, "Operating Regimes of Signaling Cycles: Statics, Dynamics, and Noise Filtering," *PLoS Computational Biology*, 3(12):e246, 2007.

[Goody and Hofmann-Goody, 2002] Roger Goody and Waltraud Hofmann-Goody, "Exchange factors, effectors, GAPs and motor proteins: common thermodynamic and kinetic principles for different functions," *European Biophysics Journal*, 31(4):268–274, jul 2002.

[Goody, 2014] Roger S. Goody, "How not to do kinetics: Examples involving GTPases and guanine nucleotide exchange factors," *FEBS Journal*, 281(2):593–600, 2014.

[Göpfrich *et al.*, 2018] Kerstin Göpfrich, Ilia Platzman, and Joachim P. Spatz, "Mastering Complexity: Towards Bottom-up Construction of Multifunctional Eukaryotic Synthetic Cells," *Trends in Biotechnology*, 36(9):938–951, 2018.

[Gorvel *et al.*, 1991] Jean-Pierre Gorvel, Philippe Chavrier, Marino Zerial, and Jean Gruenberg, "rab5 controls early endosome fusion in vitro.," *Cell*, 64(5):915–25, mar 1991.

[Goryachev and Leda, 2017] Andrew B. Goryachev and Marcin Leda, "Many roads to symmetry breaking: molecular mechanisms and theoretical models of yeast cell polarity," *Molecular Biology of the Cell*, 28(3):370–380, 2017.

[Goryachev and Leda, 2019] Andrew B. Goryachev and Marcin Leda, "Autoactivation of small GTPases by the GEF–effector positive feedback modules," *F1000Research*, 8:1676, sep 2019.

[Groves, 1997] Jay T Groves, "Micropatterning Fluid Lipid Bilayers on Solid Supports," *Science*, 275(5300):651–653, jan 1997.

[Groves and Kuriyan, 2010] Jay T Groves and John Kuriyan, "Molecular mechanisms in signal transduction at the membrane.," *Nature structural & molecular biology*, 17(6):659–65, jun 2010.

[Guimaraes *et al.*, 2013] Carla P Guimaraes, Martin D Witte, Christopher S Theile, Gunes Bozkurt, Lenka Kundrat, Annet E M Blom, and Hidde L. Ploegh, "Site-specific N-terminal and internal loop labeling of proteins using sortase-mediated reactions.," *Nature protocols*, 8(9):1787–99, sep 2013.

[Guo *et al.*, 2013] Zhong Guo, Xiaomin Hou, Roger S. Goody, and Aymelt Itzen, "Intermediates in the guanine nucleotide exchange reaction of Rab8 protein catalyzed by guanine nucleotide exchange factors Rabin8 and GRAB," *Journal of Biological Chemistry*, 288(45):32466–32474, 2013.

[Haas *et al.*, 2005] Alexander K Haas, Evelyn Fuchs, Robert Kopajtich, and Francis A. Barr, "A GTPase-activating protein controls Rab5 function in endocytic trafficking.," *Nature cell biology*, 7(9):887–93, sep 2005.

[Halatek *et al.*, 2018] J. Halatek, F. Brauns, and E. Frey, "Self-organization principles of intracellular pattern formation," *Philosophical Transactions of the Royal Society B: Biological Sciences*, 373(1747):20170107, may 2018.

[Hanahan and Weinberg, 2011] Douglas Hanahan and Robert a. Weinberg, "Hallmarks of cancer: The next generation," *Cell*, 144(5):646–674, 2011.

[Hansen *et al.*, 2019] Scott D. Hansen, William Y. C. Huang, Young Kwang Lee, Peter Bieling, Sune M. Christensen, and Jay T. Groves, "Stochastic geometry sensing and polarization in a lipid kinase–phosphatase competitive reaction," *Proceedings of the National Academy of Sciences*, page 201901744, 2019.

[Hartwell *et al.*, 1999] Leland H. Hartwell, John J. Hopfield, Stanislas Leibler, and Andrew W. Murray, "From molecular to modular cell biology," *Nature*, 402(S6761):C47–C52, dec 1999.

[He *et al.*, 2017] Kangmin He, Robert Marsland Iii, Srigokul Upadhyayula, Eli Song, Song Dang, Benjamin R. Capraro, Weiming Wang, Wesley Skillern, Raphael

Gaudin, Minghe Ma, and Tom Kirchhausen, "Dynamics of phosphoinositide conversion in clathrin-mediated endocytic traffic.," *Nature*, dec 2017.

[Heinrich *et al.*, 2002] Reinhart Heinrich, Benjamin G. Neel, and Tom A. Rapoport, "Mathematical models of protein kinase signal transduction," *Molecular Cell*, 9(5):957–970, 2002.

[Hicke, 2001] Linda Hicke, "Protein regulation by monoubiquitin.," *Nature reviews. Molecular cell biology*, 2(3):195–201, mar 2001.

[Hirakawa *et al.*, 2015] Hidehiko Hirakawa, Suguru Ishikawa, and Teruyuki Nagamune, "Ca2+ -independent sortase-A exhibits high selective protein ligation activity in the cytoplasm of Escherichia coli.," *Biotechnology journal*, 10(9):1487–92, sep 2015.

[Horiuchi *et al.*, 1995] H Horiuchi, Oliver Ullrich, Cecilia Bucci, and Marino Zerial, "Purification of posttranslationally modified and unmodified Rab5 protein expressed in Spodoptera frugiperda cells.," *Methods in enzymology*, 257:9–15, 1995.

[Horiuchi *et al.*, 1997] Hisanori Horiuchi, Roger Lippé, Heidi M. McBride, Mariantonietta Rubino, Philip Woodman, Harald Stenmark, Vladimir Rybin, Matthias Wilm, Keith Ashman, Matthias Mann, and Marino Zerial, "A novel Rab5 GDP/GTP exchange factor complexed to Rabaptin-5 links nucleotide exchange to effector recruitment and function.," *Cell*, 90(6):1149–59, sep 1997.

[Hsu *et al.*, 2018] FoSheng Hsu, Stephanie Spannl, Charles Ferguson, Anthony A Hyman, Robert G Parton, and Marino Zerial, "Rab5 and Alsin regulate stress-activated cytoprotective signaling on mitochondria.," *eLife*, 7:1–37, feb 2018.

[Huang and Ferrell, 1996] C Y Huang and J E Ferrell, "Ultrasensitivity in the mitogen-activated protein kinase cascade.," *Proceedings of the National Academy of Sciences of the United States of America*, 93(19):10078–83, sep 1996.

[Huang *et al.*, 2019] William Y C Huang, Steven Alvarez, Yasushi Kondo, Young Kwang Lee, Jean K Chung, Hiu Yue Monatrice Lam, Kabir H Biswas, John Kuriyan, and Jay T Groves, "A molecular assembly phase transition and kinetic proofreading modulate Ras activation by SOS.," *Science (New York, N.Y.)*, 363(6431):1098–1103, 2019.

[Huang *et al.*, 2016] William Y. C. Huang, Qingrong Yan, Wan-Chen Lin, Jean K. Chung, Scott D. Hansen, Sune M. Christensen, Hsiung-Lin Tu, John Kuriyan, and Jay T. Groves, "Phosphotyrosine-mediated LAT assembly on membranes drives kinetic bifurcation in recruitment dynamics of the Ras activator SOS," *Proceedings of the National Academy of Sciences*, 113(29):8218–8223, jul 2016.

[Huotari and Helenius, 2011] Jatta Huotari and Ari Helenius, "Endosome maturation.," *The EMBO journal*, 30(17):3481–500, aug 2011.

[Hutagalung and Novick, 2011] Alex H Hutagalung and Peter J Novick, "Role of Rab GTPases in membrane traffic and cell physiology.," *Physiological reviews*, 91(1):119–49, 2011.

[Hutt *et al.*, 2000] Darren M. Hutt, Lance F. Da-Silva, Li Hsin Chang, Derek C. Prosser, and Johnny K. Ngsee, "PRA1 inhibits the extraction of membrane-bound Rab GTPase by GDI1," *Journal of Biological Chemistry*, 275(24):18511–18519, 2000.

[Itoh *et al.*, 2006] Takashi Itoh, Megumi Satoh, Eiko Kanno, and Mitsunori Fukuda, "Screening for target Rabs of TBC (Tre-2/Bub2/Cdc16) domain-containing proteins based on their Rab-binding activity.," *Genes to cells : devoted to molecular & cellular mechanisms*, 11(9):1023–37, sep 2006.

[Iversen *et al.*, 2014] Lars Iversen, Hsiung-lin Tu, Wan-chen Lin, Sune M Christensen, Steven M Abel, Jeff Iwig, Hung-jen Wu, Jodi Gureasko, Christopher Rhodes, Rebecca S Petit, Scott D Hansen, Peter Thill, Cheng-han Yu, Dimitrios Stamou, Arup K Chakraborty, John Kuriyan, and Jay T Groves, "Molecular kinetics. Ras activation by SOS: allosteric regulation by altered fluctuation dynamics.," *Science (New York, N.Y.)*, 345(6192):50–4, jul 2014.

[Jacobson *et al.*, 2019] Ken Jacobson, Ping Liu, and B. Christoffer Lagerholm, "The Lateral Organization and Mobility of Plasma Membrane Components," *Cell*, 177(4):806–819, may 2019.

[Janosi *et al.*, 2012] Lorant Janosi, Zhenlong Li, John F. Hancock, and Alemayehu A. Gorfe, "Organization, dynamics, and segregation of Ras nanoclusters in membrane domains," *Proceedings of the National Academy of Sciences*, 109(21):8097–8102, may 2012.

[Jean and Kiger, 2012] Steve Jean and Amy a. Kiger, "Coordination between RAB GTPase and phosphoinositide regulation and functions," *Nature Reviews Molecular Cell Biology*, 13(7):463–470, 2012.

[Jékely, 2003] Gáspár Jékely, "Small GTPases and the evolution of the eukaryotic cell," *BioEssays*, 25(11):1129–1138, 2003.

[Jilkine *et al.*, 2011] Alexandra Jilkine, Sigurd B. Angenent, Lani F. Wu, and Steven J. Altschuler, "A density-dependent switch drives stochastic clustering and polarization of signaling molecules.," *PLoS computational biology*, 7(11):e1002271, nov 2011.

[Jongsma *et al.*, 2020] Marlieke LM Jongsma, Jeroen Bakker, Birol Cabukusta, Nalan Liv, Daphne Elsland, Job Fermie, Jimmy LL Akkermans, Coenraad Kuijl, Sabina Y Zanden, Lennert Janssen, Denise Hoogzaad, Rik Kant, Ruud H Wijdeven, Judith Klumperman, Ilana Berlin, and Jacques Neefjes, "<scp>SKIP</scp> - <scp>HOPS</scp> recruits <scp>TBC</scp> 1D15 for a Rab7-to-Arl8b identity switch to control late endosome transport," *The EMBO Journal*, 39(6):1–25, mar 2020.

[Jovic *et al.*, 2010] Marko Jovic, Mahak Sharma, Juliati Rahajeng, and Steve Caplan, "The early endosome: A busy sorting station for proteins at the crossroads," *Histology and Histopathology*, 25(1):99–112, 2010.

[Juniper *et al.*, 2018] Michael P. N. Juniper, Marian Weiss, Ilia Platzman, Joachim P. Spatz, and Thomas Surrey, "Spherical network contraction forms microtubule asters in confinement," *Soft Matter*, 14(6):901–909, 2018.

[Kajiho *et al.*, 2003] Hiroaki Kajiho, Kota Saito, Kyoko Tsujita, Kenji Kontani, Yasuhiro Araki, Hiroshi Kurosu, and Toshiaki Katada, "RIN3: a novel Rab5 GEF interacting with amphiphysin II involved in the early endocytic pathway.," *Journal of cell science*, 116(Pt 20):4159–68, 2003.

[Kälin *et al.*, 2016] Simone Kälin, Dominik P Buser, and Martin Spiess, "A fresh look at the function of Rabaptin5 on endosomes.," *Small GTPases*, 7(1):34–7, 2016.

[Kälin *et al.*, 2015] Simone Kälin, David T. Hirschmann, Dominik P. Buser, and Martin Spiess, "Rabaptin5 is recruited to endosomes by Rab4 and Rabex5 to regulate endosome maturation," *Journal of Cell Science*, 128(22):4126–4137, 2015.

[Kalinin *et al.*, 2001] Alexandr Kalinin, Nicolas H. Thomä, Andrei Iakovenko, Ines Heinemann, Elena Rostkova, Alexandru T. Constantinescu, and Kirill Alexandrov, "Expression of mammalian geranylgeranyltransferase type-II in Escherichia coli and its application for in vitro prenylation of Rab proteins.," *Protein expression and purification*, 22(1):84–91, jun 2001.

[Kapust *et al.*, 2001] Rachel B Kapust, J Tözsér, Jeffrey D Fox, D Eric Anderson, Scott Cherry, Terry D Copeland, and David S Waugh, "Tobacco etch virus protease: mechanism of autolysis and rational design of stable mutants with wild-type catalytic proficiency.," *Protein engineering*, 14(12):993–1000, dec 2001.

[Karsenti, 2008] Eric Karsenti, "Self-organization in cell biology: a brief history," *Nature Reviews Molecular Cell Biology*, 9(3):255–262, mar 2008.

[Kawasaki *et al.*, 2005] Masato Kawasaki, Kazuhisa Nakayama, and Soichi Wakatsuki, "Membrane recruitment of effector proteins by Arf and Rab GTPases.," *Current opinion in structural biology*, 15(6):681–9, dec 2005.

[Kholodenko *et al.*, 2010] Boris N. Kholodenko, John F. Hancock, and Walter Kolch, "Signalling ballet in space and time," *Nature Reviews Molecular Cell Biology*, 11(6):414–426, jun 2010.

[Kimura *et al.*, 2006] Toshihiro Kimura, Toshiaki Sakisaka, Takeshi Baba, Tomohiro Yamada, and Yoshimi Takai, "Involvement of the Ras-Ras-activated Rab5 guanine nucleotide exchange factor RIN2-Rab5 pathway in the hepatocyte growth factor-induced endocytosis of E-cadherin," *Journal of Biological Chemistry*, 281(15):10598–10609, 2006.

[Kinchen and Ravichandran, 2010] Jason M. Kinchen and Kodi S. Ravichandran, "Identification of two evolutionarily conserved genes regulating processing of engulfed apoptotic cells.," *Nature*, 464(7289):778–82, apr 2010.

[Kiontke *et al.*, 2017] Stephan Kiontke, Lars Langemeyer, Anne Kuhlee, Saskia Schuback, Stefan Raunser, Christian Ungermann, and Daniel Kümmel, "Architecture and mechanism of the late endosomal Rab7-like Ypt7 guanine nucleotide exchange factor complex Mon1–Ccz1," *Nature Communications*, 8:14034, jan 2017.

[Kiral *et al.*, 2018] Ferdi Ridvan Kiral, Friederike Elisabeth Kohrs, Eugene Jennifer Jin, and Peter Robin Hiesinger, "Rab GTPases and Membrane Trafficking in Neurodegeneration," *Current Biology*, 28(8):R471–R486, 2018.

[Kirsten *et al.*, 2013] Marie L Kirsten, Rudi a Baron, Miguel C Seabra, and Oscar Ces, "Rab1a and Rab5a preferentially bind to binary lipid compositions with higher stored curvature elastic energy.," *Molecular membrane biology*, 30(4):303–14, 2013.

[Kitano, 2002] Hiroaki Kitano, "Systems Biology: A Brief Overview," *Science*, 295(5560):1662–1664, mar 2002.

[Kitano *et al.*, 2008] Masahiro Kitano, Michio Nakaya, Takeshi Nakamura, Shigekazu Nagata, and Michiyuki Matsuda, "Imaging of Rab5 activity identifies essential regulators for phagosome maturation.," *Nature*, 453(7192):241–5, may 2008.

[Klöpper *et al.*, 2012] Tobias H. Klöpper, Nickias Kienle, Dirk Fasshauer, and Sean Munro, "Untangling the evolution of Rab G proteins: implications of a comprehensive genomic analysis," *BMC Biology*, 10(1):71, 2012.

[Klumperman and Raposo, 2014] Judith Klumperman and Graça Raposo, "The complex ultrastructure of the endolysosomal system.," *Cold Spring Harbor perspectives in biology*, 6(10):a016857, oct 2014.

[Kondo and Miura, 2010] Shigeru Kondo and Takashi Miura, "Reaction-diffusion model as a framework for understanding biological pattern formation," *Science*, 329(5999):1616–1620, 2010.

[Koshland *et al.*, 1982] Daniel E. Koshland, Albert Goldbeter, and Jeffry B. Stock, "Amplification and adaptation in regulatory and sensory systems.," *Science (New York, N.Y.)*, 217(4556):220–5, jul 1982.

[Köster *et al.*, 2016] Darius Vasco Köster, Kabir Husain, Elda Iljazi, Abrar Bhat, Peter Bieling, R. Dyche Mullins, Madan Rao, and Satyajit Mayor, "Actomyosin dynamics drive local membrane component organization in an in vitro active composite layer," *Proceedings of the National Academy of Sciences*, 113(12):E1645–E1654, mar 2016.

[Kramer and Fussenegger, 2005] Beat P Kramer and Martin Fussenegger, "Hysteresis in a synthetic mammalian gene network.," *Proceedings of the National Academy of Sciences of the United States of America*, 102(27):9517–22, jul 2005.

[Kulakowski *et al.*, 2018] Guillaume Kulakowski, Hugo Bousquet, Jean-Baptiste Manneville, Patricia Bassereau, Bruno Goud, and Lena K. Oesterlin, "Lipid packing defects and membrane charge control RAB GTPase recruitment," *Traffic*, 19(7):536–545, jul 2018.

[Kuriyan and Eisenberg, 2007] John Kuriyan and David Eisenberg, "The origin of protein interactions and allostery in colocalization," *Nature*, 450(7172):983–990, dec 2007.

[Landeros *et al.*, 2018] Alfonso Landeros, Timothy Stutz, Kevin L. Keys, Alexander Alekseyenko, Janet S. Sinsheimer, Kenneth Lange, and Mary E. Sehl, "BioSimulator.jl: Stochastic simulation in Julia.," *Computer methods and programs in biomedicine*, 167:23–35, dec 2018.

[Langemeyer *et al.*, 2020] Lars Langemeyer, Ann-Christin Borchers, Eric Herrmann, Nadia Füllbrunn, Yaping Han, Angela Perz, Kathrin Auffarth, Daniel Kümmel, and Christian Ungermann, "A conserved and regulated mechanism drives endosomal Rab transition," *eLife*, 9:1–20, may 2020.

[Langemeyer *et al.*, 2014] Lars Langemeyer, Ricardo Nunes Bastos, Yiying Cai, Aymelt Itzen, Karin M. Reinisch, and Francis A. Barr, "Diversity and plasticity in Rab GTPase nucleotide release mechanism has consequences for Rab activation and inactivation.," *eLife*, 3(3):e01623, 2014.

[Langemeyer *et al.*, 2018] Lars Langemeyer, Angela Perz, Daniel Kümmel, and Christian Ungermann, "A guanine nucleotide exchange factor (GEF) limits Rab GTPase-

driven membrane fusion.," *The Journal of biological chemistry*, 293(2):731–739, jan 2018.

[Lauer *et al.*, 2019] Janelle Lauer, Sandra Segeletz, Alice Cezanne, Giambattista Guaitoli, Francesco Raimondi, Marc Gentzel, Vikram Alva, Michael Habeck, Yannis Kalaidzidis, Marius Ueffing, Andrei N Lupas, Christian Johannes Gloeckner, and Marino Zerial, "Auto-regulation of Rab5 GEF activity in Rabex5 by allosteric structural changes, catalytic core dynamics and ubiquitin binding.," *eLife*, 8:562504, 2019.

[Lebar *et al.*, 2014] Tina Lebar, Urban Bezeljak, Anja Golob, Miha Jerala, Lucija Kadunc, Boštjan Pirš, Martin Stražar, Dušan Vučko, Uroš Zupančič, Mojca Benčina, Vida Forstnerič, Rok Gaber, Jan Lonzarić, Andreja Majerle, Alja Oblak, Anže Smole, and Roman Jerala, "A bistable genetic switch based on designable DNA-binding domains.," *Nature communications*, 5:5007, sep 2014.

[Leduc, 1912] S Leduc, *La biologie synthétique*, Leduc, Stéphane, 1853-. Etudes de biophysique. A. Poinat, 1912.

[Lee *et al.*, 2004] Il Kyu Lee, Kyung-Soo Kim, Hongtae Kim, Joo Yong Lee, Chung Hun Ryu, Heung Jae Chun, Kyoung-Uk Lee, Young Lim, Young Hoon Kim, Pil-Woo Huh, Kweon-Haeng Lee, Sang-Ick Han, Tae-Youn Jun, and Hyoung Kyun Rha, "MAP, a protein interacting with a tumor suppressor, merlin, through the run domain.," *Biochemical and biophysical research communications*, 325(3):774–83, dec 2004.

[Lee *et al.*, 2006] Sangho Lee, Yien Che Tsai, Rafael Mattera, William J Smith, Michael S Kostelansky, Allan M Weissman, Juan S Bonifacino, and James H Hurley, "Structural basis for ubiquitin recognition and autoubiquitination by Rabex-5.," *Nature structural & molecular biology*, 13(3):264–271, 2006.

[Lee *et al.*, 2019] Yerim Lee, Carey Phelps, Tao Huang, Barmak Mostofian, Lei Wu, Ying Zhang, Kai Tao, Young Hwan Chang, Philip JS Stork, Joe W Gray, Daniel M Zuckerman, and Xiaolin Nan, "High-throughput single-particle tracking reveals nested membrane domains that dictate KRasG12D diffusion and trafficking," *eLife*, 8, nov 2019.

[Leung *et al.*, 2007] Ka Fai Leung, Rudi Baron, Bassam R. Ali, Anthony I. Magee, and Miguel C. Seabra, "Rab GTPases containing a CAAX motif are processed post-

geranylgeranylation by proteolysis and methylation.," *The Journal of biological chemistry*, 282(2):1487–97, jan 2007.

[Li *et al.*, 2015] Dong Li, Lin Shao, B.-C. Chen, X. Zhang, Mingshu Zhang, Brian Moses, Daniel E. Milkie, Jordan R. Beach, John A. Hammer, Mithun Pasham, Tomas Kirchhausen, Michelle A. Baird, Michael W. Davidson, Pingyong Xu, and Eric Betzig, "Extended-resolution structured illumination imaging of endocytic and cytoskeletal dynamics," *Science*, 349(6251):aab3500–aab3500, aug 2015.

[Li *et al.*, 2014] Fu Li, Long Yi, Lei Zhao, Aymelt Itzen, Roger S. Goody, and Yao-Wen Wu, "The role of the hypervariable C-terminal domain in Rab GTPases membrane targeting.," *Proceedings of the National Academy of Sciences of the United States of America*, 111(7):2572–7, feb 2014.

[Lin *et al.*, 2001] Jialing Lin, Zhimin Liang, Zhi Zhang, and Guangpu Li, "Membrane topography and topogenesis of prenylated Rab acceptor (PRA1).," *The Journal of biological chemistry*, 276(45):41733–41, nov 2001.

[Lippe *et al.*, 2001] Roger Lippe, Hisanori Horiuchi, Anja Runge, and Marino Zerial, "Expression, purification, and characterization of Rab5 effector complex, Rabaptin-5/Rabex-5," *Regulators And Effectors Of Small Gtpases, Pt E*, 329(1992):132–145, 2001.

[Lippé *et al.*, 2001] Roger Lippé, Marta Miaczynska, Vladimir Rybin, Anja Runge, and Marino Zerial, "Functional synergy between Rab5 effector Rabaptin-5 and exchange factor Rabex-5 when physically associated in a complex.," *Molecular biology of the cell*, 12(7):2219–28, 2001.

[Liu and Fletcher, 2009] Allen P Liu and Daniel a Fletcher, "Biology under construction: in vitro reconstitution of cellular function.," *Nature reviews. Molecular cell biology*, 10(9):644–50, sep 2009.

[Loose *et al.*, 2008] Martin Loose, Elisabeth Fischer-Friedrich, Jonas Ries, Karsten Kruse, and Petra Schwille, "Spatial regulators for bacterial cell division self-organize into surface waves in vitro.," *Science (New York, N.Y.)*, 320(5877):789–92, may 2008.

[Loose *et al.*, 2011] Martin Loose, Karsten Kruse, and Petra Schwille, "Protein self-organization: lessons from the min system.," *Annual review of biophysics*, 40:315–336, 2011.

[Loose and Mitchison, 2014] Martin Loose and Timothy J. Mitchison, "The bacterial cell division proteins FtsA and FtsZ self-organize into dynamic cytoskeletal patterns.," *Nature cell biology*, 16(1):38–46, jan 2014.

[Loose and Schwille, 2009] Martin Loose and Petra Schwille, "Biomimetic membrane systems to study cellular organization," *Journal of Structural Biology*, 168(1):143–151, 2009.

[Lord *et al.*, 2019] Nathan D Lord, Thomas M Norman, Ruoshi Yuan, Somenath Bakshi, Richard Losick, and Johan Paulsson, "Stochastic antagonism between two proteins governs a bacterial cell fate switch.," *Science (New York, N.Y.)*, 366(6461):116–120, 2019.

[Mattera *et al.*, 2003] Rafael Mattera, Cecilia N. Arighi, Robert Lodge, Marino Zerial, and Juan S. Bonifacino, "Divalent interaction of the GGAs with the Rabaptin-5-Rabex-5 complex.," *The EMBO journal*, 22(1):78–88, jan 2003.

[Mattera and Bonifacino, 2008] Rafael Mattera and Juan S Bonifacino, "Ubiquitin binding and conjugation regulate the recruitment of Rabex-5 to early endosomes.," *The EMBO journal*, 27(19):2484–2494, 2008.

[McLauchlan *et al.*, 1998] Hilary McLauchlan, Jane Newell, Nick Morrice, Andrew Osborne, Michele West, and Elizabeth Smythe, "A novel role for Rab5-GDI in ligand sequestration into clathrin-coated pits.," *Current biology : CB*, 8(1):34–45, jan 1998.

[Mendoza *et al.*, 2014] Pablo Mendoza, Jorge Díaz, Patricio Silva, and Vicente A. Torres, "Rab5 activation as a tumor cell migration switch.," *Small GTPases*, 5(1):e28195, 2014.

[Mishra *et al.*, 2010] Ashwini Mishra, Sudharshan Eathiraj, Silvia Corvera, and David G. Lambright, "Structural basis for Rab GTPase recognition and endosome tethering by the C2H2 zinc finger of Early Endosomal Autoantigen 1 (EEA1).," *Pro-*

ceedings of the National Academy of Sciences of the United States of America, 107(24):10866–71, jun 2010.

[Misteli, 2001] Tom Misteli, "The concept of self-organization in cellular architecture," *Journal of Cell Biology*, 155(2):181–186, oct 2001.

[Mitchison and Kirschner, 1984] Tim Mitchison and Marc Kirschner, "Dynamic instability of microtubule growth," *Nature*, 312(5991):237–242, nov 1984.

[Mizuno-Yamasaki *et al.*, 2012] Emi Mizuno-Yamasaki, Felix Rivera-Molina, and Peter Novick, "GTPase networks in membrane traffic.," *Annual review of biochemistry*, 81:637–59, 2012.

[More *et al.*, 2020] Kira More, Christen M. Klinger, Lael D. Barlow, and Joel B. Dacks, "Evolution and Natural History of Membrane Trafficking in Eukaryotes," *Current Biology*, 30(10):R553–R564, may 2020.

[Mosesson *et al.*, 2008] Yaron Mosesson, Gordon B Mills, and Yosef Yarden, "Derailed endocytosis: an emerging feature of cancer.," *Nature reviews. Cancer*, 8(11):835–50, 2008.

[Mossman, 2005] K. D. Mossman, "Altered TCR Signaling from Geometrically Repatterned Immunological Synapses," *Science*, 310(5751):1191–1193, 2005.

[Mottola, 2014] Giovanna Mottola, "The complexity of Rab5 to Rab7 transition guarantees specificity of pathogen subversion mechanisms.," *Frontiers in cellular and infection microbiology*, 4(December):180, 2014.

[Mottola *et al.*, 2014] Giovanna Mottola, Nicolas Boucherit, Virginie Trouplin, Abdoulaye Oury Barry, Philippe Soubeyran, Jean-Louis Mege, and Eric Ghigo, "Tropheryma whipplei, the agent of Whipple's disease, affects the early to late phagosome transition and survives in a Rab5- and Rab7-positive compartment.," *PloS one*, 9(2):e89367, 2014.

[Müller and Goody, 2017] Matthias P. Müller and Roger S. Goody, "Molecular control of Rab activity by GEFs, GAPs and GDI," *Small GTPases*, 1248:1–17, 2017.

[Müller *et al.*, 2020] Paul M Müller, Juliane Rademacher, Richard D Bagshaw, Celina Wortmann, Carolin Barth, Jakobus van Unen, Keziban M Alp, Girolamo Giudice, Rebecca L Eccles, Louise E Heinrich, Patricia Pascual-Vargas, Marta Sanchez-Castro, Lennart Brandenburg, Geraldine Mbamalu, Monika Tucholska, Lisa Spatt, Maciej T Czajkowski, Robert-william Welke, Sunqu Zhang, Vivian Nguyen, Trendelina Rrustemi, Philipp Trnka, Kiara Freitag, Brett Larsen, Oliver Popp, Philipp Mertins, Anne-claude Gingras, Frederick P Roth, Karen Colwill, Chris Bakal, Olivier Pertz, Tony Pawson, Evangelia Petsalaki, and Oliver Rocks, "Systems analysis of RhoGEF and RhoGAP regulatory proteins reveals spatially organized RAC1 signalling from integrin adhesions," *Nature Cell Biology*, mar 2020.

[Murray *et al.*, 2016] David H. Murray, Marcus Jahnel, Janelle Lauer, Mario J. Avellaneda, Nicolas Brouilly, Alice Cezanne, Hernán Morales-Navarrete, Enrico D. Perini, Charles Ferguson, Andrei N. Lupas, Yannis Kalaidzidis, Robert G. Parton, Stephan W. Grill, and Marino Zerial, "An endosomal tether undergoes an entropic collapse to bring vesicles together.," *Nature*, 537(7618):107–111, sep 2016.

[Nagano *et al.*, 2019] Makoto Nagano, Junko Y. Toshima, Daria Elisabeth Siekhaus, and Jiro Toshima, "Rab5-mediated endosome formation is regulated at the trans-Golgi network," *Communications Biology*, 2(1):419, dec 2019.

[Nguyen *et al.*, 2016] Mai Khanh Nguyen, Cha Yeon Kim, Jin Man Kim, Byung Ouk Park, Sangkyu Lee, Hyerim Park, and Won Do Heo, "Optogenetic oligomerization of Rab GTPases regulates intracellular membrane trafficking," *Nature Chemical Biology*, 12(6):431–436, 2016.

[Nguyen *et al.*, 2015] Phuong A. Nguyen, Christine M. Field, Aaron C. Groen, Timothy J. Mitchison, and Martin Loose, "Using supported bilayers to study the spatiotemporal organization of membrane-bound proteins.," *Methods in cell biology*, 128:223–41, 2015.

[Nguyen *et al.*, 2014] Phuong A Nguyen, Aaron C Groen, Martin Loose, Keisuke Ishihara, Martin Wühr, Christine M Field, and Timothy J Mitchison, "Spatial organization of cytokinesis signaling reconstituted in a cell-free system.," *Science (New York, N.Y.)*, 346(6206):244–7, oct 2014.

[Nielsen *et al.*, 1999] Erik Nielsen, Ffedor Severin, Jonathan M. Backer, Anthony A. Hyman, and Marino Zerial, "Rab5 regulates motility of early endosomes on microtubules.," *Nature cell biology*, 1(6):376–82, oct 1999.

[Nottingham and Pfeffer, 2009] Ryan M. Nottingham and Suzanne R. Pfeffer, "Defining the boundaries: Rab GEFs and GAPs.," *Proceedings of the National Academy of Sciences of the United States of America*, 106(34):14185–6, 2009.

[Nottingham and Pfeffer, 2014] Ryan M Nottingham and Suzanne R Pfeffer, "Mutant enzymes challenge all assumptions.," *eLife*, 3(3):e02171, 2014.

[Oesterlin *et al.*, 2012] Lena K. Oesterlin, Roger S. Goody, and Aymelt Itzen, "Post-translational modifications of Rab proteins cause effective displacement of GDP dissociation inhibitor.," *Proceedings of the National Academy of Sciences of the United States of America*, 109(15):5621–6, apr 2012.

[Ohya *et al.*, 2009] Takeshi Ohya, Marta Miaczynska, Unal Coskun, Barbara Lommer, Anja Runge, David Drechsel, Yannis Kalaidzidis, and Marino Zerial, "Reconstitution of Rab- and SNARE-dependent membrane fusion by synthetic endosomes.," *Nature*, 459(7250):1091–7, jun 2009.

[Ong *et al.*, 2014] Seow Theng Ong, Michael Freeley, Joanna Skubis-Zegadło, Mobashar Hussain Urf Turabe Fazil, Dermot Kelleher, Friedrich Fresser, Gottfried Baier, Navin Kumar Verma, and Aideen Long, "Phosphorylation of Rab5a protein by protein kinase C is crucial for T-cell migration.," *The Journal of biological chemistry*, 289(28):19420–34, jul 2014.

[Penengo *et al.*, 2006] Lorenza Penengo, Marina Mapelli, Andrea G. Murachelli, Stefano Confalonieri, Laura Magri, Andrea Musacchio, Pier Paolo Di Fiore, Simona Polo, and Thomas R. Schneider, "Crystal Structure of the Ubiquitin Binding Domains of Rabex-5 Reveals Two Modes of Interaction with Ubiquitin," *Cell*, 124(6):1183–1195, 2006.

[Peter *et al.*, 1995] F Peter, C Nuoffer, I Schalk, and W E Balch, "Expression and purification of recombinant His6-tagged guanine nucleotide dissociation inhibitor and formation of its Rab1 complex.," *Methods in enzymology*, 257(1993):80–3, 1995.

[Peurois *et al.*, 2018] François Peurois, Gérald Peyroche, and Jacqueline Cherfils, "Small GTPase peripheral binding to membranes: Molecular determinants and supramolecular organization," *Biochemical Society Transactions*, 47(1):13–22, 2018.

[Peurois *et al.*, 2017] François Peurois, Simon Veyron, Yann Ferrandez, Ilham Ladid, Sarah Benabdi, Mahel Zeghouf, Gérald Peyroche, and Jacqueline Cherfils, "Characterization of the activation of small GTPases by their GEFs on membranes using artificial membrane tethering," *Biochemical Journal*, 474(7):1259–1272, 2017.

[Pfeffer *et al.*, 1995] S R Pfeffer, A B Dirac-Svejstrup, and T Soldati, "Rab GDP dissociation inhibitor: putting rab GTPases in the right place.," *The Journal of biological chemistry*, 270(29):17057–9, jul 1995.

[Pfeffer, 2005] Suzanne Pfeffer, "Filling the Rab GAP," *Nature Cell Biology*, 7(9):856–857, sep 2005.

[Pfeffer and Aivazian, 2004] Suzanne Pfeffer and Dikran Aivazian, "Targeting Rab GTPases to distinct membrane compartments.," *Nature reviews. Molecular cell biology*, 5(11):886–896, 2004.

[Pfeffer, 2013] Suzanne R. Pfeffer, "Rab GTPase regulation of membrane identity," *Current Opinion in Cell Biology*, 25(4):414–419, 2013.

[Pomerening *et al.*, 2003] Joseph R. Pomerening, Eduardo D. Sontag, and James E. Ferrell, "Building a cell cycle oscillator: hysteresis and bistability in the activation of Cdc2.," *Nature cell biology*, 5(4):346–51, apr 2003.

[Popp *et al.*, 2007] Maximilian W. Popp, John M. Antos, Gijsbert M. Grotenbreg, Eric Spooner, and Hidde L. Ploegh, "Sortagging: a versatile method for protein labeling.," *Nature chemical biology*, 3(11):707–8, nov 2007.

[Poteryaev *et al.*, 2010] Dmitry Poteryaev, Sunando Datta, Karin Ackema, Marino Zerial, and Anne Spang, "Identification of the switch in early-to-late endosome transition.," *Cell*, 141(3):497–508, apr 2010.

[Pucadyil and Schmid, 2008] Thomas J. Pucadyil and Sandra L. Schmid, "Real-Time Visualization of Dynamin-Catalyzed Membrane Fission and Vesicle Release," *Cell*, 135(7):1263–1275, dec 2008.

[Pylypenko *et al.*, 2006] Olena Pylypenko, Alexey Rak, Thomas Durek, Susanna Kushnir, Beatrice E. Dursina, Nicolas H. Thomae, Alexandru T. Constantinescu, Luc Brunsveld, Anja Watzke, Herbert Waldmann, Roger S. Goody, and Kirill Alexandrov, "Structure of doubly prenylated Ypt1:GDI complex and the mechanism of GDI-mediated Rab recycling.," *The EMBO journal*, 25(1):13–23, jan 2006.

[Qian, 2012] Hong Qian, "Cooperativity in Cellular Biochemical Processes: Noise-Enhanced Sensitivity, Fluctuating Enzyme, Bistability with Nonlinear Feedback, and Other Mechanisms for Sigmoidal Responses," *Annual Review of Biophysics*, 41(1):179–204, 2012.

[Rana *et al.*, 2015] M. Rana, J. Lachmann, and C. Ungermann, "Identification of a Rab GAP cascade that controls recycling of the Rab5 GTPase Vps21 from the vacuole," *Molecular Biology of the Cell*, 26(13):2535–49, 2015.

[Rapali *et al.*, 2017] Péter Rapali, Romain Mitteau, Craig Braun, Aurèlie Massoni-Laporte, Caner Ünlü, Laure Bataille, Floriane Saint Arramon, Steven P. Gygi, and Derek McCusker, "Scaffold-mediated gating of Cdc42 signalling flux.," *eLife*, 6:1–18, 2017.

[Remorino *et al.*, 2017] Amanda Remorino, Simon De Beco, Fanny Cayrac, Fahima Di Federico, Gaetan Cornilleau, Alexis Gautreau, Maria Carla Parrini, Jean-Baptiste Masson, Maxime Dahan, and Mathieu Coppey, "Gradients of Rac1 Nanoclusters Support Spatial Patterns of Rac1 Signaling," *Cell Reports*, 21(7):1922–1935, nov 2017.

[Rink *et al.*, 2005] Jochen Rink, Eric Ghigo, Yannis Kalaidzidis, and Marino Zerial, "Rab conversion as a mechanism of progression from early to late endosomes.," *Cell*, 122(5):735–49, sep 2005.

[Rivera-Molina and Novick, 2009] Félix E. Rivera-Molina and Peter J. Novick, "A Rab GAP cascade defines the boundary between two Rab GTPases on the secretory pathway.," *Proceedings of the National Academy of Sciences of the United States of America*, 106(34):14408–13, 2009.

[Rives and Galitski, 2003] Alexander W. Rives and Timothy Galitski, "Modular organization of cellular networks," *Proceedings of the National Academy of Sciences*, 100(3):1128–1133, feb 2003.

[Rybin *et al.*, 1996] V Rybin, O Ullrich, M Rubino, K Alexandrov, I Simon, M C Seabra, R Goody, and M Zerial, "GTPase activity of Rab5 acts as a timer for endocytic membrane fusion.," *Nature*, 383(6597):266–9, sep 1996.

[Saleem *et al.*, 2015] Mohammed Saleem, Sandrine Morlot, Annika Hohendahl, John Manzi, Martin Lenz, and Aurélien Roux, "A balance between membrane elasticity and polymerization energy sets the shape of spherical clathrin coats," *Nature Communications*, 6(1):6249, may 2015.

[Samoilov *et al.*, 2005] Michael Samoilov, Sergey Plyasunov, and Adam P. Arkin, "Stochastic amplification and signaling in enzymatic futile cycles through noise-induced bistability with oscillations.," *Proceedings of the National Academy of Sciences of the United States of America*, 102(7):2310–5, feb 2005.

[Sasaki *et al.*, 1990] T Sasaki, A. Kikuchi, S Araki, Y Hata, M Isomura, S Kuroda, and Y. Takai, "Purification and characterization from bovine brain cytosol of a protein that inhibits the dissociation of GDP from and the subsequent binding of GTP to smg p25A, a ras p21-like GTP-binding protein.," *The Journal of biological chemistry*, 265(4):2333–7, feb 1990.

[Sato *et al.*, 2005] Miyuki Sato, Ken Sato, Paul Fonarev, Chih-Jen Huang, Willisa Liou, and Barth D. Grant, "Caenorhabditis elegans RME-6 is a novel regulator of RAB-5 at the clathrin-coated pit," *Nature Cell Biology*, 7(6):559–569, jun 2005.

[Schmidt *et al.*, 2013] Thomas G.M. Schmidt, Lilia Batz, Lidia Bonet, Uwe Carl, Gerd Holzapfel, Klaus Kiem, Kamila Matulewicz, Dennis Niermeier, Isabel Schuchardt, and Kristian Stanar, "Development of the Twin-Strep-tag® and its application for purification of recombinant proteins from cell culture supernatants," *Protein Expression and Purification*, 92(1):54–61, 2013.

[Scholz *et al.*, 2013] Judith Scholz, Hüseyin Besir, Claudia Strasser, and Sabine Suppmann, "A new method to customize protein expression vectors for fast, efficient and background free parallel cloning.," *BMC biotechnology*, 13:12, 2013.

[Schweizer *et al.*, 2012] Jakob Schweizer, Martin Loose, Mike Bonny, Karsten Kruse, Ingolf Mönch, and Petra Schwille, "Geometry sensing by self-organized protein patterns.," *Proceedings of the National Academy of Sciences of the United States of America*, 109(38):15283–8, sep 2012.

[Semerdjieva *et al.*, 2008] Sophia Semerdjieva, Barry Shortt, Emma Maxwell, Sukhdeep Singh, Paul Fonarev, Jonathan Hansen, Giampietro Schiavo, Barth D. Grant, and Elizabeth Smythe, "Coordinated regulation of AP2 uncoating from clathrin-coated vesicles by rab5 and hRME-6.," *The Journal of cell biology*, 183(3):499–511, nov 2008.

[Shahinian and Silvius, 1995] S. Shahinian and J. R. Silvius, "Doubly-lipid-modified protein sequence motifs exhibit long-lived anchorage to lipid bilayer membranes.," *Biochemistry*, 34(11):3813–22, mar 1995.

[Shapiro and Pfeffer, 1995] A D Shapiro and S R Pfeffer, "Quantitative analysis of the interactions between prenyl Rab9, GDP dissociation inhibitor-alpha, and guanine nucleotides.," *The Journal of biological chemistry*, 270(19):11085–90, may 1995.

[Sherwood and Roy, 2013] Racquel Kim Sherwood and Craig R. Roy, "A Rab-Centric Perspective of Bacterial Pathogen-Occupied Vacuoles," *Cell Host & Microbe*, 14(3):256–268, sep 2013.

[Shin *et al.*, 2017] Donghyuk Shin, Wooju Na, Ji-Hyung Lee, Gyuhee Kim, Jiseok Baek, Seok Hee Park, Cheol Yong Choi, and Sangho Lee, "Site-specific monoubiquitination downregulates Rab5 by disrupting effector binding and guanine nucleotide conversion.," *eLife*, 6:1–26, 2017.

[Shinde and Maddika, 2016] Swapnil Rohidas Shinde and Subbareddy Maddika, "A modification switch on a molecular switch: Phosphoregulation of Rab7 during endosome maturation.," *Small GTPases*, 7(3):164–7, 2016.

[Shinde and Maddika, 2018] Swapnil Rohidas Shinde and Subbareddy Maddika, "Post translational modifications of Rab GTPases.," *Small GTPases*, 9(1-2):49–56, 2018.

[Simon *et al.*, 1996a] Iris Simon, Marino Zerial, and Roger S. Goody, "Kinetics of interaction of Rab5 and Rab7 with nucleotides and magnesium ions," *Journal of Biological Chemistry*, 271(34):20470–20478, 1996.

[Simon *et al.*, 1996b] Iris Simon, Marino Zerial, and Roger S. Goody, "Kinetics of interaction of Rab5 and Rab7 with nucleotides and magnesium ions," *Journal of Biological Chemistry*, 271(34):20470–20478, 1996.

[Sims and Allbritton, 2007] Christopher E. Sims and Nancy L. Allbritton, "Analysis of single mammalian cells on-chip," *Lab on a Chip*, 7(4):423, 2007.

[Sivars *et al.*, 2005] Ulf Sivars, Dikran Aivazian, and Suzanne Pfeffer, "Purification and properties of Yip3/PRA1 as a Rab GDI displacement factor," *Methods in Enzymology*, 403(05):348–356, 2005.

[Sivars *et al.*, 2003] Ulf Sivars, Dikran Aivazian, and Suzanne R Pfeffer, "Yip3 catalyses the dissociation of endosomal Rab-GDI complexes.," *Nature*, 425(6960):856–9, oct 2003.

[Solinger *et al.*, 2020] Jachen A Solinger, Harun-Or Rashid, Cristina Prescianotto-Baschong, and Anne Spang, "FERARI is required for Rab11-dependent endocytic recycling," *Nature Cell Biology*, jan 2020.

[Sönnichsen *et al.*, 2000] Birte Sönnichsen, Stefano De Renzis, Erik Nielsen, Jens Rietdorf, and Marino Zerial, "Distinct membrane domains on endosomes in the recycling pathway visualized by multicolor imaging of Rab4, Rab5, and Rab11.," *The Journal of cell biology*, 149(4):901–14, may 2000.

[Spano *et al.*, 2011] S. Spano, Xiaoyun Liu, and J. E. Galan, "Proteolytic targeting of Rab29 by an effector protein distinguishes the intracellular compartments of human-adapted and broad-host Salmonella," *Proceedings of the National Academy of Sciences*, 108(45):18418–18423, nov 2011.

[Stalder and Antonny, 2013] Danièle Stalder and Bruno Antonny, "Arf GTPase regulation through cascade mechanisms and positive feedback loops.," *FEBS letters*, 587(13):2028–35, 2013.

[Stalder *et al.*, 2011] Danièle Stalder, Hélène Barelli, Romain Gautier, Eric Macia, Catherine L. Jackson, and Bruno Antonny, "Kinetic studies of the Arf activator Arno on model membranes in the presence of Arf effectors suggest control by a positive feedback loop.," *The Journal of biological chemistry*, 286(5):3873–83, feb 2011.

[Steele-Mortimer *et al.*, 1993] Olivia Steele-Mortimer, Jean Gruenberg, and Michael J. Clague, "Phosphorylation of GDI and membrane cycling of rab proteins.," *FEBS letters*, 329(3):313–8, aug 1993.

[Stein *et al.*, 2012] Mary-Pat Stein, Matthias P. Müller, and Angela Wandinger-Ness, "Bacterial Pathogens Commandeer Rab GTPases to Establish Intracellular Niches," *Traffic*, 13(12):1565–1588, dec 2012.

[Stenmark, 2009] Harald Stenmark, "Rab GTPases as coordinators of vesicle traffic.," *Nature reviews. Molecular cell biology*, 10(8):513–25, 2009.

[Stenmark *et al.*, 1994] Harald Stenmark, Robert G. Parton, Olivia Steele-Mortimer, A. Lütcke, Jean Gruenberg, and Marino Zerial, "Inhibition of rab5 GTPase activity stimulates membrane fusion in endocytosis.," *The EMBO journal*, 13(6):1287–96, mar 1994.

[Stenmark *et al.*, 1995] Harald Stenmark, Gaetano Vitale, Oliver Ullrich, and Marino Zerial, "Rabaptin-5 is a direct effector of the small GTPase Rab5 in endocytic membrane fusion.," *Cell*, 83(3):423–32, nov 1995.

[Su *et al.*, 2016] Xiaolei Su, Jonathon A Ditlev, Enfu Hui, Wenmin Xing, Sudeep Banjade, Julia Okrut, David S. King, Jack Taunton, Michael K. Rosen, and Ronald D. Vale, "Phase separation of signaling molecules promotes T cell receptor signal transduction.," *Science (New York, N.Y.)*, 352(6285):595–9, apr 2016.

[Su *et al.*, 2007] Xiong Su, Chen Kong, and Philip D. Stahl, "GAPex-5 Mediates Ubiquitination, Trafficking, and Degradation of Epidermal Growth Factor Receptor," *Journal of Biological Chemistry*, 282(29):21278–21284, jul 2007.

[Sweet *et al.*, 1984] Raymond W. Sweet, Shiro Yokoyama, Tohru Kamata, James R. Feramisco, Martin Rosenberg, and Mitchell Gross, "The product of ras is a GTPase

and the T24 oncogenic mutant is deficient in this activity.," *Nature*, 311(5983):273–5, 1984.

[Tall *et al.*, 2001] Gregory G. Tall, M.Alejandro Barbieri, Philip D. Stahl, and Bruce F. Horazdovsky, "Ras-Activated Endocytosis Is Mediated by the Rab5 Guanine Nucleotide Exchange Activity of RIN1," *Developmental Cell*, 1(1):73–82, jul 2001.

[Tan *et al.*, 2020] Tzer Han Tan, Jinghui Liu, Pearson W Miller, Melis Tekant, Jörn Dunkel, and Nikta Fakhri, "Topological turbulence in the membrane of a living cell," *Nature Physics*, mar 2020.

[Tarantino *et al.*, 2014] Nadine Tarantino, Jean Yves Tinevez, Elizabeth Faris Crowell, Bertrand Boisson, Ricardo Henriques, Musa Mhlanga, Fabrice Agou, Alain Israël, and Emmanuel Laplantine, "Tnf and il-1 exhibit distinct ubiquitin requirements for inducing NEMO-IKK supramolecular structures," *Journal of Cell Biology*, 204(2):231–245, 2014.

[Thomas and Fromme, 2016] Laura L Thomas and J Christopher Fromme, "GTPase cross talk regulates TRAPPII activation of Rab11 homologues during vesicle biogenesis.," *The Journal of cell biology*, 215(4):499–513, nov 2016.

[Thomas *et al.*, 2019] Laura L. Thomas, Solveig A. van der Vegt, and J. Christopher Fromme, "A Steric Gating Mechanism Dictates the Substrate Specificity of a Rab-GEF.," *Developmental cell*, 48(1):100–114.e9, jan 2019.

[Tinevez *et al.*, 2017] Jean-Yves Tinevez, Nick Perry, Johannes Schindelin, Genevieve M. Hoopes, Gregory D. Reynolds, Emmanuel Laplantine, Sebastian Y. Bednarek, Spencer L. Shorte, and Kevin W. Eliceiri, "TrackMate: An open and extensible platform for single-particle tracking.," *Methods (San Diego, Calif.)*, 115:80–90, 2017.

[Tjørve and Tjørve, 2017] Kathleen M C Tjørve and Even Tjørve, "The use of Gompertz models in growth analyses, and new Gompertz-model approach: An addition to the Unified-Richards family.," *PloS one*, 12(6):e0178691, 2017.

[Topp *et al.*, 2004] Justin D. Topp, Noah W. Gray, Robert D. Gerard, and Bruce F. Horazdovsky, "Alsin Is a Rab5 and Rac1 Guanine Nucleotide Exchange Factor," *Journal of Biological Chemistry*, 279(23):24612–24623, jun 2004.

[Touchot *et al.*, 1987] Nicolas Touchot, Pierre Chardin, and Armand Tavitian, "Four additional members of the ras gene superfamily isolated by an oligonucleotide strategy: molecular cloning of YPT-related cDNAs from a rat brain library.," *Proceedings of the National Academy of Sciences of the United States of America*, 84(23):8210–4, dec 1987.

[Traut, 1994] Thomas W. Traut, "Physiological concentrations of purines and pyrimidines," *Molecular and Cellular Biochemistry*, 140(1):1–22, 1994.

[Tsyganov *et al.*, 2012] Mikhail A. Tsyganov, Walter Kolch, and Boris N. Kholodenko, "The topology design principles that determine the spatiotemporal dynamics of G-protein cascades.," *Molecular bioSystems*, 8(3):730–43, mar 2012.

[Turing, 1952] A. M. Turing, "The chemical basis of morphogenesis," *Philosophical Transactions of the Royal Society of London. Series B, Biological Sciences*, 237(641):37–72, 1952.

[Tyson *et al.*, 2003] John J. Tyson, Katherine C. Chen, and Bela Novak, "Sniffers, buzzers, toggles and blinkers: Dynamics of regulatory and signaling pathways in the cell," *Current Opinion in Cell Biology*, 15(2):221–231, 2003.

[Vale *et al.*, 1985] R D Vale, T S Reese, and M P Sheetz, "Identification of a novel force-generating protein, kinesin, involved in microtubule-based motility.," *Cell*, 42(1):39–50, aug 1985.

[Vale *et al.*, 1996] Ronald D Vale, Takashi Funatsu, Daniel W. Pierce, Laura Romberg, Yoshie Harada, and Toshio Yanagida, "Direct observation of single kinesin molecules moving along microtubules," *Nature*, 380(6573):451–453, apr 1996.

[Vartak and Bastiaens, 2010] Nachiket Vartak and Philippe Bastiaens, "Spatial cycles in G-protein crowd control," *EMBO Journal*, 29(16):2689–2699, 2010.

[Vetter and Wittinghofer, 2001] Ingrid R. Vetter and Alfred Wittinghofer, "The guanine nucleotide-binding switch in three dimensions.," *Science (New York, N.Y.)*, 294(5545):1299–304, nov 2001.

[Walther *et al.*, 2003] Diego J. Walther, Jens Uwe Peter, Sandra Winter, Markus Höltje, Nils Paulmann, Maik Grohmann, Jakob Vowinckel, Victor Alamo-Bethencourt, Claudia S. Wilhelm, Gudrun Ahnert-Hilger, and Michael Bader, "Serotonylation of Small GTPases Is a Signal Transduction Pathway that Triggers Platelet α-Granule Release," *Cell*, 115(7):851–862, 2003.

[Wenzel *et al.*, 2018] Eva Maria Wenzel, Sebastian Wolfgang Schultz, Kay Oliver Schink, Nina Marie Pedersen, Viola Nähse, Andreas Carlson, Andreas Brech, Harald Stenmark, and Camilla Raiborg, "Concerted ESCRT and clathrin recruitment waves define the timing and morphology of intraluminal vesicle formation," *Nature Communications*, 9(1):2932, dec 2018.

[Wittinghofer, 2014a] Alfred Wittinghofer, *Ras Superfamily Small G Proteins: Biology and Mechanisms 1*, Springer Vienna, Vienna, 2014.

[Wittinghofer, 2014b] Alfred Wittinghofer, *Ras Superfamily Small G Proteins: Biology and Mechanisms 2*, Springer International Publishing, Cham, 2014.

[Wittinghofer and Vetter, 2011] Alfred Wittinghofer and Ingrid R. Vetter, "Structure-function relationships of the G domain, a canonical switch motif.," *Annual review of biochemistry*, 80(1):943–71, 2011.

[Wu *et al.*, 2010] Yao-Wen Wu, Lena K. Oesterlin, Kui-Thong Tan, Herbert Waldmann, Kirill Alexandrov, and Roger S. Goody, "Membrane targeting mechanism of Rab GTPases elucidated by semisynthetic protein probes.," *Nature chemical biology*, 6(7):534–40, jul 2010.

[Wu *et al.*, 2007] Yao-Wen Wu, Kui-Thong Tan, Herbert Waldmann, Roger S. Goody, and Kirill Alexandrov, "Interaction analysis of prenylated Rab GTPase with Rab escort protein and GDP dissociation inhibitor explains the need for both regulators.," *Proceedings of the National Academy of Sciences of the United States of America*, 104(30):12294–9, jul 2007.

[Yoshimura *et al.*, 2010] Shin Ichiro Yoshimura, Andreas Gerondopoulos, Andrea Linford, Daniel J. Rigden, and Francis A. Barr, "Family-wide characterization of the DENN domain Rab GDP-GTP exchange factors," *Journal of Cell Biology*, 191(2):367–381, 2010.

[Zeigerer *et al.*, 2012] Anja Zeigerer, Jerome Gilleron, Roman L Bogorad, Giovanni Marsico, Hidenori Nonaka, Sarah Seifert, Hila Epstein-Barash, Satya Kuchimanchi, Chang Geng Peng, Vera M Ruda, Perla Del Conte-Zerial, Jan G Hengstler, Yannis Kalaidzidis, Victor Koteliansky, and Marino Zerial, "Rab5 is necessary for the biogenesis of the endolysosomal system in vivo.," *Nature*, 485(7399):465–70, 2012.

[Zerial and McBride, 2001] Marino Zerial and Heidi McBride, "Rab proteins as membrane organizers.," *Nature reviews. Molecular cell biology*, 2(2):107–17, feb 2001.

[Zhang *et al.*, 2014] Zhe Zhang, Tianlong Zhang, Shanshan Wang, Zhou Gong, Chun Tang, Jiangye Chen, and Jianping Ding, "Molecular mechanism for Rabex-5 GEF activation by Rabaptin-5.," *eLife*, 3:1–19, jun 2014.

[Zheng *et al.*, 2011] Xiu-Deng Zheng, Xiao-Qian Yang, and Yi Tao, "Bistability, Probability Transition Rate and First-Passage Time in an Autoactivating Positive-Feedback Loop," *PLoS ONE*, 6(3):e17104, mar 2011.

[Zhu *et al.*, 2004] Guangyu Zhu, Peng Zhai, Jian Liu, Simon Terzyan, Guangpu Li, and Xuejun C Zhang, "Structural basis of Rab5-Rabaptin5 interaction in endocytosis.," *Nature structural & molecular biology*, 11(10):975–983, 2004.

[Zhu *et al.*, 2009] Huaiping Zhu, Zhimin Liang, and Guangpu Li, "Rabex-5 is a Rab22 effector and mediates a Rab22-Rab5 signaling cascade in endocytosis.," *Molecular biology of the cell*, 20(22):4720–9, nov 2009.

[Zhu *et al.*, 2010] Huaiping Zhu, Hong Qian, and Guangpu Li, "Delayed onset of positive feedback activation of Rab5 by Rabex-5 and Rabaptin-5 in endocytosis.," *PloS one*, 5(2):e9226, 2010.

[Zhu *et al.*, 2007] Huaiping Zhu, Guangyu Zhu, Jay Liu, Zhimin Liang, Xuejun C Zhang, and Guangpu Li, "Rabaptin-5-independent membrane targeting and Rab5

activation by Rabex-5 in the cell.," *Molecular biology of the cell*, 18(10):4119–28, oct 2007.

A Appendix 1

A.1 Amino acid sequences of purified protein components

Displayed are protein sequences of polypeptide components which were used in *in vitro* reconstitution assays after isolation and protease digestion of the purification peptide (if applicable).

A.1.1 GDI

```
  1 GADEEYDVIV LGTGLTECIL SGIMSVNGKK VLHMDRNPYY GGESSSITPL
 51 EELYKRFDMA DGPPESMGRG RDWNVDLIPK FLMANGQLVK MLLYTEVTRY
101 LDFKVIEGSF VYKGGKIYKV PSTETEALAS NLMGMFEKRR FRKFLVFVAN
151 FDENDPKTFE GVDPMDTNMR DVYKKFDLGQ DVIDFTGHAL ALYRTDDYLD
201 QPCLETINRI KLYSESLARY GKSPYLYPLY GLGELPQGFA RLSAIYGGTY
251 MLNKSVDEIV MEKGTVVGVK SEGEVARCKQ LICDPSYVPD RVHKAGQVIR
301 VICILNHPIK NTNDANSCQI IIPQNQVNRK SDIYVCMISY AHNVAAQGKY
351 IAIVSTTVET AEPEKEIEPA LELLEPIEQK FMAISDLYES TEDGTESQIF
401 CSRSYDATTH FETTCNDIKD IYKRMTGTDF DFENMKRKQN DVFGEDEQ
```

A.1.2 His_{10}-Ub

```
  1 MKHHHHHHHH HHSAGLEVLF QGPQIFVKTL TGKTITLEVE PSDTIENVKA
 51 KIQDKEGIPP DQQRLIFAGK QLEDGRTLSD YNIQKESTLH LVLRLRGG
```

A.1.3 PRA1

```
  1 GGGGGAGKNG DDFSDVAEEG PGGILNKMFP KMITQTAAKD WINRRRAHIR
 51 PWRNFVDQRR FSRPPNFGEL CKRMTRNVEH FQSNYIFIFL GLILYCIITS
101 PMLLIALAVF FGGCYIIYLR TLESKMVLFG RELSTANQYG LAGAVSFPFF
151 WLAGAGAAVF WVIGATLVVI GSHASFHEIE GEVEELQMEP V
```

A.1.4 Rab5

```
  1 GGGGGANRGG ATRPNGPNAG NKICQFKLVL LGESAVGKSS LVLRFVKGQF
 51 HEFQESTIGA AFLTQTVCLD DTTVKFEIWD TAGQERYHSL APMYYRGAQA
101 AIVVYDITNE ESFARAKNWV KELQRQASPN IVIALSGNKA DLSTKRAVDF
151 QEAQAYADDN SLLFMETSAK TSVNVNEIFM AIAKKLPKTE PQAGASNTIR
201 GRGVDLTETA QPTKSQCCSN
```

A.1.5 Rab5Q80L-His_{10}

```
  1 GGGGGANRGG ATRPNGPNAG NKICQFKLVL LGESAVGKSS LVLRFVKGQF
 51 HEFQESTIGA AFLTQTVCLD DTTVKFEIWD TAGLERYHSL APMYYRGAQA
101 AIVVYDITNE ESFARAKNWV KELQRQASPN IVIALSGNKA DLSTKRAVDF
151 QEAQAYADDN SLLFMETSAK TSVNVNEIFM AIAKKLPKTE PQAGASNTIR
201 GRGVDLTETA QPTKSQHHHH HHHHHH
```

A.1.6 Rabaptin5

```
  1 GAAEPGSVVQ PDATLQQRVQ ELERDNAEFL RTKQLLEQEF NQKRAKFKEL
 51 YLSKEEDLKH QQAVIQVAQE EIVQLNIKLS QAQAEMENIK AVATVSENTK
101 QEAIDEVKKQ WQEEVASHQA IMKETVREYE LQFHHRLEQE RAQWGQYRES
151 VEREIAELRR RLSEGQQEEN LENDMKKAQE DAEKLRSVVM PMEKEIGTLK
201 EKLTEAEEKI KDLEASKMKE MNHYLEAEKS CRTDLEMYVA VLNTQKSVLQ
251 EDAEKLRKEL HEVCHLLEQE RQQHNQLKHT WQKANDQFLE SQRLMMQDMK
301 RMEAVLTTEQ LRQVEESKKK NQVEEQRTRK RKEKETVQKE EECRKVILEE
351 SLPNLKQEEL LNSSHSSIHS LDTDIMLHEG DSFNKQEDLF KDGLRRAQSS
401 DSLGASGPLQ TKTLGYNNKA KSAGNLDESD FGPLVGADSV SENFDTSSLG
451 SLHMPSGFML TKDQEKAIKA MTPEQEETAS LLSSVTQTLE CTYVPPSDYR
501 LVSETEWNLL QKEVQTAGNK LGRRCDMCSN YEKQLQVIQT QEAEIRDQVK
551 KLQTMLRQVN DQLEKTLKDK KDLEDYMKQN TEETSTQIST LTLRINQSET
601 LLADLQQAFH TGKRNIQDQM AVLMHSREQV SEELLRLQRD NESLQGKHSL
651 HVSLQQSEIF NLPETSEELQ NLVLKYREDI ISVRTATDHL EEKLKAEILF
701 LKEQIQAEQC QKENIEETLQ IEIENCKEEM ASTSSLQLEL DRIKAEREQL
751 EVSLQEKTQE LQNLQTLKDS LENQLKKETG SKASLEQLAF EEKNKAQRLQ
801 TELDVSEQVQ RDFVKLSQML QVQLERIRQT ESLETIRAIL NDTKLTDINQ
851 LPET
```

A.1.7 Rabex5

```
  1 GGGGGSLKTE RRGIHVDQSE LLCKKGCGYY GNPAWQGFCS KCWREEYQKA
 51 RQKQIQEDWE FAERLQREEE EAYASSQGAQ AGPQSLTFSK FEEKKSNEKT
101 RKVTTVKKFF TASSKSLPKK DIKEAKSPSP SLSRQFSLET DRVSKDFIEF
151 LKTYQKAGHD VYKLSKIFLE AMHHKRESNI DEQSEFTQDF YQNTADKLQM
201 YWKVSPDKVE KVMDQIERFI MTRLYKHVFC PETTDDEKKD LTVQKRIRAL
251 HWVTLQMLCV PVNEDIAEVS DMVVKAITDI IEMDSKRIPR DKLACITRCS
301 KHIFNAIKIT KNEPASADDF LPTLIYIVLK ANPPRLQSNI QYITRFCNPS
351 RLMTGEDGYY FTNLCCAVAF IEKLDGQSLN LSEEEFSRYM SGQASPKKQD
401 LENWPEDTCT GVKQMHRNLD LLTQLSKRQE HIVNGAKKLE KDLIDWTDEV
451 TKEVKDIVEK YPLNIKTASQ ALAALESENV EDDNLPPPLQ PQVYAG
```

A.1.8 Rabex5(D314A)

```
  1 GGGGGSLKTE RRGIHVDQSE LLCKKGCGYY GNPAWQGFCS KCWREEYQKA
 51 RQKQIQEDWE FAERLQREEE EAYASSQGAQ AGPQSLTFSK FEEKKSNEKT
101 RKVTTVKKFF TASSKSLPKK DIKEAKSPSP SLSRQFSLET DRVSKDFIEF
151 LKTYQKAGHD VYKLSKIFLE AMHHKRESNI DEQSEFTQDF YQNTADKLQM
201 YWKVSPDKVE KVMDQIERFI MTRLYKHVFC PETTDDEKKD LTVQKRIRAL
251 HWVTLQMLCV PVNEDIAEVS DMVVKAITDI IEMDSKRIPR DKLACITRCS
301 KHIFNAIKIT KNEPASADDF LPTLIYIVLK ANPPRLQSNI QYITRFCNPS
351 RLMTGEDGYY FTNLCCAVAF IEKLDGQSLN LSEEEFSRYM SGQASPKKQD
401 LENWPEDTCT GVKQMHRNLD LLTQLSKRQE HIVNGAKKLE KDLIDWTDEV
451 TKEVKDIVEK YPLNIKTASQ ALAALESENV EDDNLPPPLQ PQVYAG
```

A.1.9 RabGAP-5

```
  1 GPSGSYTPSP GGPFSALTAS MWPQDILAKY TQKEQTVEQP EFRYDEFGFR
 51 VDKEDGAEPN SSKLLGIPLT EDPQQRLRWQ AHLEFTHNHD VGDLTWDKID
101 VTLPHSDKLR SLVLAGIPHS MRPQLWMRLS GALQKKQNSE MTYKDIGRNS
151 SNDDTLAAKQ IEKDLLRTMP SNACFSNLQS VGVPRLRRVL RGLAWLFPDI
201 GYCQGTGMVA ACLLLFLEEE DAFWMMAAIV EDLVPVSYFN TTLVGVQTDQ
251 RVLRHLIVQY LPRLDKLLQE HDIELSLITL HWFLTAFASV VHIKLLLRIW
301 DFFFYQGSLV LFQTTLGMLK MKEEELIQSE NSASIFNTLS DIPSQIEEAD
351 VLLREAMLIS GTLTEVMIEA QRRKHLAYLI ADQGQLLNST AAVANLSKIM
401 RRQSQRRKSA ITTLLFGDDN FEALKSKNIK QTALVADLRE AILQVARHFQ
451 YTDPKNCSID LTPDYTMESH QRDHENYVSC SQSRRRRAKA LLDFERHDDD
501 ELGFRKNDII TIISQKDEHC WVGELNGLRG WFPAKFVDIL DERSKEYSVA
551 GDDSVTEGIT DLIRGTLSPS IKSIFEHGLK KPSLLGGPCH PWLFIEEAAS
601 REVERDFDSV YSRLVLCKTY RLDEDGKVLT PEELLYRGVQ SVNVSHDAAH
651 AQMDVKLRSL ISIGLNEQVL HLWLEVLCSS LPTVEKWYQP WSFLRSPGWV
701 QIKCELRVLS KFAFSLSPDW ELPVKREDKE KKPLKEGVQD MLVKHHLFSW
751 DIDG
```

A.1.10 ΔRabex5

```
  1 GGGGGSLETD RVSKDFIEFL KTYQKAGHDV YKLSKIFLEA MHHKRESNID
 51 EQSEFTQDFY QNTADKLQMY WKVSPDKVEK VMDQIERFIM TRLYKHVFCP
101 ETTDDEKKDL TVQKRIRALH WVTLQMLCVP VNEDIAEVSD MVVKAITDII
151 EMDSKRIPRD KLACITRCSK HIFNAIKITK NEPASADDFL PTLIYIVLKA
201 NPPRLQSNIQ YITRFCNPSR LMTGEDGYYF TNLCCAVAFI EKLDGQSLNL
251 SEEEFSRYMS GQASPKKQDL ENWPEDTCTG VKQMHRNLDL LTQLSKRQEH
301 IVNGAKKLEK DLIDWTDEVT KEVKDIVEKY PLNIKTASQA LAALESENVE
351 DDNLPPPLQP QVYAG
```

A.1.11 Δ_{RBD}Rabaptin5

```
  1 GAAEPGSVVQ PDATLQQRVQ ELERDNAEFL RTKQLLEQEF NQKRAKFKEL
 51 YLSKEEDLKH QQAVIQVAQE EIVQLNIKLS QAQAEMENIK AVATVSENTK
101 QEAIDEVKKQ WQEEVASHQA IMKETVREYE LQFHHRLEQE RAQWGQYRES
151 VEREIAELRR RLSEGQQEEN LENDMKKAQE DAEKLRSVVM PMEKEIGTLK
201 EKLTEAEEKI KDLEASKNQV EEQRTRKRKE KETVQKEEEC RKVILEESLP
251 NLKQEELLNS SHSSIHSLDT DIMLHEGDSF NKQEDLFKDG LRRAQSSDSL
301 GASGPLQTKT LGYNNKAKSA GNLDESDFGP LVGADSVSEN FDTSSLGSLH
351 MPSGFMLTKD QEKAIKAMTP EQEETASLLS SVTQTLECTY VPPSDYRLVS
401 ETEWNLLQKE VQTAGNKLGR RCDMCSNYEK QLQVIQTQEA EIRDQVKKLQ
451 TMLRQVNDQL EKTLKDKKDL EDYMKQNTEE TSTQISTLTL RINQSETLLA
501 DLQQAFHTGK RNIQDQMAVL MHSREQVSEE LLRLQRDNES LQGKHSLHVS
551 LQQSEIFNLP ETSEELQNLV LKYREDIISV RTATDHLEEK LKAEILFLKE
601 QIQAEQCQKE NIEETLQIEI ENCKEEMAST SSLQLELDRI KAEREQLEVS
651 LQEKTQELQN LQTLKDSLEN QLKKETGSKA SLEQLAFEEK NKAQRLQTEL
701 DVS
```